FINAL REPORT

FHWA/IN/JTRP-2001/10-I-2

FATIGUE BEHAVIOR OF BEAM DIAPHRAGM CONNECTIONS WITH INTERMITTENT FILLET WELDS

PART I, VOLUME 2: LABORATORY FATIGUE EVALUATION

By

Amy S. Grider
Graduate Research Assistant

and

Mark D. Bowman
Professor of Civil Engineering

Purdue University
School of Civil Engineering

Joint Transportation Research Project
Project No: C-36-56KK
File No: 7-4-37
SPR-2113

Prepared in Cooperation with the
Indiana Department of Transportation and
the U.S. Department of Transportation
Federal Highway Administration

Purdue University
West Lafayette, IN 47907-1284
March 2002

TECHNICAL REPORT STANDARD TITLE PAGE

1. Report No.	2. Government Accession No.	3. Recipient's Catalog No.
FHWA/IN/JTRP-2001/10-I-2		

4. Title and Subtitle	5. Report Date
Fatigue Behavior of Beam Diaphragm Connections With Intermittent Fillet Welds Part I, Volume 2: Laboratory Fatigue Evaluation	March 2002
	6. Performing Organization Code
7. Author(s) Amy S. Grider and Mark D. Bowman	8. Performing Organization Report No. FHWA/IN/JTRP-2001/10-I-2
9. Performing Organization Name and Address Joint Transportation Research Program 1284 Civil Engineering Building Purdue University West Lafayette, Indiana 47907-1284	10. Work Unit No.
	11. Contract or Grant No. SPR-2113
12. Sponsoring Agency Name and Address Indiana Department of Transportation State Office Building 100 North Senate Avenue Indianapolis, IN 46204	13. Type of Report and Period Covered Final Report
	14. Sponsoring Agency Code

15. Supplementary Notes

Prepared in cooperation with the Indiana Department of Transportation and Federal Highway Administration.

16. Abstract

This report is the second of a two-part, three volume final report presenting the findings of the research work that was undertaken to evaluate the behavior of Indiana highway bridges with diaphragm members welded directly to the web of the primary beams and girders. Fatigue cracks have been observed at several bridges that utilize the welded diaphragm connection. The seriousness of the cracking and the corresponding potential risk on the integrity of the bridge superstructure were assessed. Inspection and repair guidelines for bridges with the welded diaphragm connections were also developed as part of the research effort. This volume presents the results of laboratory fatigue tests that were conducted to evaluate the cyclic life of staggered and non-staggered diaphragm connections. The performance of three different repair and retrofit procedures on the cyclic life of the welded diaphragm connection was also studied. Analytical models of the cracked diaphragm connection were developed to study the expected response under field loading conditions. Recommendation for implementation of inspection, repair, and retrofit procedures are presented.

The titles of the three volumes (Report Number in parentheses) are listed:

Part I, Volume 1: Field Evaluation (FHWA/IN/JTRP-2001/10-I-1)
Part I, Volume 2: Laboratory Fatigue Evaluation (FHWA/IN/JTRP-2001/10-I-2)
Part II: Brittle Fracture Examination of the I-64 Blue River (FHWA/IN/JTRP-2001/10-II)

17. Key Words	18. Distribution Statement
bridge, connection, diaphragm, welded connection, fatigue, cracking, secondary bending, displacement-induced cracking, load-testing, inspection, retrofit, repair	No restrictions. This document is available to the public through the National Technical Information Service, Springfield, VA 22161

19. Security Classif. (of this report)	20. Security Classif. (of this page)	21. No. of Pages	22. Price
Unclassified	Unclassified	307	

Form DOT F 1700.7 (8-69)

ACKNOWLDGEMENTS

The funding from the Indiana Department of Transportation and the Federal Highway Administration is greatly appreciated.

The advice and input of the study advisory committee members throughout the course of the study is appreciated. The study advisory committee consisted of William Dittrich, James Karr, and Joseph Torkos from the Indiana Department of Transportation and Tom Saad of the Federal Highway Administration.

The assistance of those who helped with the experimental phase of this study is gratefully acknowledged: Charlie Crow, Jeff Lynch, Harry Tidrick, and Brian Malone. The authors would also like to acknowledge Beth Webster for her assistance with ANSYS.

INDOT Research

TECHNICAL *Summary*

Technology Transfer and Project Implementation Information

TRB Subject Code: 25-01 Bridge Design and Performance *March 2002*
Publication No.: FHWA/IN/JTRP-2001/10-I-2 *Final Report*

Fatigue Behavior of Beam Diaphragm Connections with Intermittent Fillet Welds: Part I, Volume 2, Laboratory Fatigue Evaluation

Introduction

Fatigue cracks have been observed in several bridges at the intermittent welds used to connect hot-rolled diaphragm sections to the web of steel beam members. The consequence of this type of cracking was studied for two different diaphragm configurations: staggered and back-to-back. The work in Part I of the study consisted of two portions: field testing (Vol. 1) to determine typical stress levels for the connection detail and laboratory testing (Vol. 2) to establish the fatigue behavior and resistance of the diaphragm connection.

Findings

Experimental tests were performed in order to determine the fatigue resistance of the welded diaphragm-to-beam connections and to evaluate repair and retrofit methods. Two diaphragm configurations were studied: one with the diaphragms positioned back-to-back and one with staggered diaphragms. The experimental results indicate that non-staggered diaphragms distribute the load laterally more than staggered diaphragm connections. Many of the intermittent web welds and flange welds connecting the diaphragm to the beam fractured for non-staggered diaphragms, which resulted in decreased load transfer. Horizontal cracking also developed in the beam webs but did not affect the fatigue strength of the beam. In the staggered diaphragm tests, cracks perpendicular to the primary stress field developed in the beam webs at the toe of one of the bottom flange welds. One repair and two retrofit methods were investigated also. The following repair/retrofit procedures were studied: remove the diaphragm and drill holes at the beam crack tips, remove the diaphragm by flame cutting and air hammer peen the bottom flange weld toes, and leave the diaphragm intact and peen the bottom flange weld toes.

A comparison was made between the beam stresses in the experimental tests and computed stresses for typical bridge beam members. Two representative type bridges were analyzed for several truck loadings: HS20, Fatigue, Michigan 5, Michigan 8, and a special 19 axle 2135 kN (480-kip) vehicle. The stresses developed during the experimental tests are significantly higher than the calculated stresses for the two bridges. The stresses from the analyzed bridges fall below the AASHTO Category D endurance limit while the experimental stresses lie just above the endurance limit.

Implementation

Based on the experimental and analytical results of this study, it is believed that detrimental fatigue cracking, if it occurs at all, will initiate in the beam web at the toe of a lower flange connection weld. It is recommended, therefore, that the welded connections in the maximum positive moment regions be closely examined at the lower flange welds; the upper flange welds should be examined for connections in the negative moment regions (near the piers of continuous structures). If fatigue crack initiation is to be avoided, then air-hammer peening of the lower flange welds can be performed to significantly extend the cyclic life. This is not necessary for most structures, however, since the service level stresses are quite low and fatigue crack initiation is often not likely to occur.

If a beam web crack is detected at the toe of a lower flange or upper diaphragm flange weld, the crack dimensions should be determined. The fatigue crack propagation program can be used to estimate the time needed to propagate the crack to a specific length for a given load history and ADTT. Although a crack may be present in a beam member, the stresses are often quite low such that rapid crack growth is not likely to occur and an immediate repair is often not necessary.

In order to repair a beam member that has developed cracks in the beam web, then holes should be drilled at the beam crack tips to arrest crack growth. The holes should be sized based upon the anticipated stress level and the effective crack length. The diaphragms should not be removed during beam repair unless the welded connection is completely fractured.

Contact

For more information:

Prof. Mark D. Bowman
Principal Investigator
School of Civil Engineering
Purdue University
West Lafayette IN 47907
Phone: (765) 494-2220
Fax: (765) 496-1105

Indiana Department of Transportation
Division of Research
1205 Montgomery Street
P.O. Box 2279
West Lafayette, IN 47906
Phone: (765) 463-1521
Fax: (765) 497-1665

Purdue University
Joint Transportation Research Program
School of Civil Engineering
West Lafayette, IN 47907-1284
Phone: (765) 494-9310
Fax: (765) 496-1105

TABLE OF CONTENTS

Page

Page

Page

LIST OF TABLES

LIST OF FIGURES

Figure Page

Figure Page

Figure Page

Figure Page

Figure Page

Figure Page

Figure Page

Figure Page

CHAPTER 1

INTRODUCTION

1.1 Problem Statement

Diaphragms are commonly used in multigirder bridges to provide lateral stability and to distribute loads laterally among the bridge girders. Diaphragm members are usually connected to the steel girders through vertical connection plates that are often cut short of the tension flange thus creating a small unstiffened gap. However, a common diaphragm-to-beam connection used in Indiana utilizes a rolled beam member for the diaphragm which is welded directly to the web of the longitudinal beam members at midheight. Intermittent fillet welds are used to connect the diaphragm web to the beam web. A short fillet weld is used to attach the top side of the top and bottom flanges of the diaphragm to the beam web. An illustration of the welded Indiana diaphragm-to-beam connection is shown in Fig. 1.1.

Cracks have been observed in the welds that connect the diaphragm to the beam web. The cracks, which were found during visual inspection, have been detected in the bottom flange welds and the intermittent web welds. The cracks have only sheared the welds and have not been observed to propagate into the beam web.

The fatigue strength of this particular detail is necessary in order to properly assess the long-term performance of the detail and the longitudinal member. Much of the

research on diaphragm-to-beam connections has focused on diaphragms attached to a connection plate which was welded to the beam web. Little research data exists for diaphragm members welded directly to the beam member.

1.2 Objectives and Scope

The purpose of this study is to understand the behavior of the welded diaphragm-to-beam connection and evaluate repair methods. There are two major parts to the present study: an experimental phase and an analytical phase. The main objectives of the experimental phase are:

1. evaluate the number of loading cycles required to cause failure of the beam with welded diaphragms,
2. examine the failure modes, and
3. evaluate methods to repair and retrofit steel beams with the welded diaphragm connection that developed cracks.

Nine steel beams with welded diaphragms were tested under constant amplitude cyclic loading. The repair and retrofit methods investigated were:

1. flame cut diaphragm and drill holes at the beam crack tips,
2. flame cut diaphragm and air hammer peen the bottom flange weld areas, and
3. leave diaphragm in place and air hammer peen the bottom flange weld areas.

The main objective of the analytical phase is to accurately evaluate the fatigue strength of the diaphragm-to-beam welded connection. Finite element analyses were conducted to determine to stresses near the welded detail and a computer program was developed to compute the propagation life of cracked beam members.

A review of literature on distortion-induced fatigue cracking is presented in Chapter 2. Case studies of fatigue cracking are discussed as well as experimental and analytical work.

Chapter 3 discusses the experimental testing program. The experimental results are presented in Chapter 4. A discussion of the crack growth and static measurements as well as comparisons between the tests is provided in Chapter 4.

In Chapter 5 a comparison is made between the measured experimental stresses and calculated stresses from a bridge analysis for several truck configurations.

An analytical model to predict the fatigue life of cracked bridge members with the welded diaphragm connection is presented in Chapter 6.

The conclusions and recommendations for the study are presented in Chapter 7.

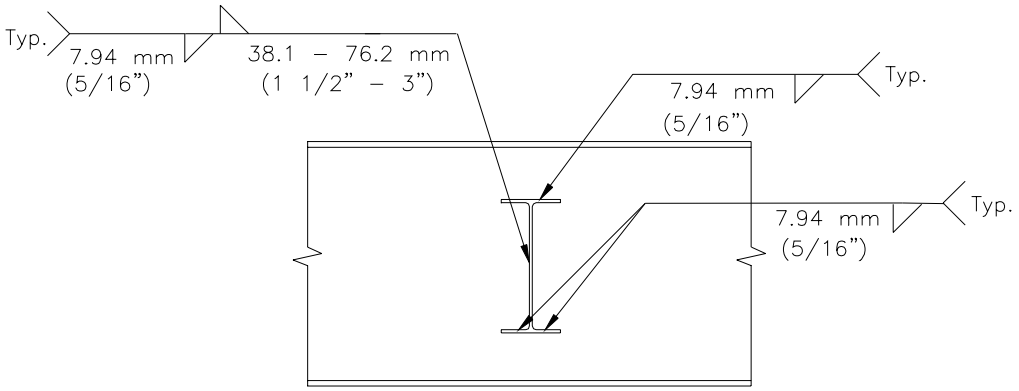

Figure 1.1 Welded diaphragm-to-beam connection used in Indiana

CHAPTER 2

LITERATURE REVIEW

The literature survey presented in this chapter focuses mainly on the fatigue behavior of transverse bridge members that are attached to a vertical stiffener which in turn is welded to the longitudinal girder web. Little research data exists for diaphragm members which are directly welded to the beam web at midheight. Although both connections involve the development of fatigue cracks in the beam web, the behavior of the two connections is quite different. Research that models the geometry of the welded diaphragm-to-beam connection must be conducted.

The literature review includes case studies of bridges with diaphragms and floor beams which are attached to vertical stiffeners that have experienced fatigue cracking, as well as analytical and experimental studies on the fatigue behavior at diaphragm connection details.

2.1 Case Studies

2.1.1 Cracking in Diaphragm Connection Plates in Multigirder Bridges

Diaphragms have commonly been used in multigirder steel bridges to provide lateral stability and to distribute loads laterally among the bridge girders. The diaphragms

range from rolled beam shapes to built up crossframes. Usually, diaphragm members are connected to the steel girders through vertical connection plates. The connection plates are welded to the web, sometimes welded to the compression flange, and often cut short of the tension flange thus creating a small unstiffened gap.

Adjacent bridge girders deflect differing amounts with vehicle loading thus producing an out-of-plane deformation in the web gap at the connection plate ends that are not connected to the beam flange. The magnitude of this out-of-plane movement depends on the girder spacing, skew, and type of diaphragm. Due to relatively high stress levels in the web gap region from out-of-plane distortion, fatigue cracking at susceptible details can occur. Following are several case studies which illustrate this type of fatigue cracking.

A welded plate girder bridge on Route 95 in Providence, Rhode Island developed several cracks near midspan in the webs of the girders and one crack in the web and lower flange of an outside girder (Pullaro 1990). The bridge girders are crossbraced with K-type diaphragms and bottom lateral bracing composed of angles. The midspan diaphragms are welded plate girders which are rigidly attached to a partial height stiffener and top and bottom gusset plates which were shop welded to the girder web (see Fig. 2.1). There is a 76.2 mm (3 in.) gap between the diaphragm flange and girder tension flange. A fractographic observation showed that the crack which severed the lower flange and extended up the web initiated at two crack-like porosity defects at the junction between the web surface and the end of the diaphragm plate weld. In order to "soften" the diaphragm connection, a circular portion of the diaphragm web, horizontal gusset plate,

and a portion of the vertical stiffener was removed. A short bolted field splice was placed at all locations where cracks had been found.

Fatigue cracks developed at the diaphragm to girder connections in the Belle Fourche River Bridge near Belle Fourche, South Dakota and the Chamberlain Bridge near Chamberlain, South Dakota (Fisher 1984). For each of these bridges, the crossframe diaphragms were welded to transverse stiffeners, which were welded to the girder web. Cracks were found along the web-to-flange weld toe, in the girder web at the end of the stiffener, and in the vertical weld that connected the stiffener to the girder as shown in Fig. 2.2. Because the fatigue cracks were parallel to the longitudinal axes of the main girders, they were also parallel to the primary bending stresses in the web. To arrest further crack growth, holes were drilled at the tips of existing cracks and a positive welded attachment was made between the transverse stiffener and the girder flanges.

A similar type of crack pattern occurred in the negative moment regions of the continuous span Beaver Creek Bridge on I-80 in Clarion County, Pennsylvania (Fisher, Kaufmann, et. al. 1987). All intermediate stiffeners and diaphragm connection plates on the girder webs were cut one inch short of the tension flanges; the diaphragm connection plates were fitted to the compression flange. Cracks were found at three locations: along the weld toe between the tension flange and web, at the toe of the end weld attaching the diaphragm connection plate to the web, and along the weld between the connection plate and web. A direct attachment of the connection plate to the top tension flange was made with a bolted set of channels to reduce the out-of-plane bending.

Diaphragm connection cracks in the girder web were also discovered in the I-79 Bridge 2680 over Big Sandy Creek (Fisher, Yen, and Wagner 1987 and Kulicki, Murphy, et. al. 1986). The diaphragm connection plate is welded to the girder web, but is not connected to the top or bottom flange. Small horizontal cracks were commonly found in pairs on opposite sides of the same girder web. On one side of the web, the crack was located at the toe of the top flange to web weld. On the other side of the web, the crack occurred at the termination of the connection plate to web weld. The cracks developed as a result of cyclic, secondary bending stresses that occurred as the girder web was bent into double curvature due to lateral translation and rotation of the connection plates with respect to the top flange as shown in Fig. 2.3.

Another structure which experienced cracks at a diaphragm connection plate was a bridge along the Washington Metropolitan Area Transit Authority railroad (Mertz 1984). The cracks were located at the lower end of transverse crossframe diaphragm connection plates which were welded to the girder web but cut short from the tension flange. The cracks exhibited the characteristics associated with web deformations in the small web gap at the end of the transverse connection plate. The cracking developed after little more than two years of service for the structure. The structure was retrofitted by providing a positive attachment using a structural tee bolted to the connection plate and flange.

Girder web cracking was found in steel box girder bridges in which the transverse stiffeners were cut short of both the top and bottom flange plates (Wilson, Duncan and Fisher 1989). The cracks were found in the positive moment regions as well as areas adjacent to solid diaphragms near expansion joints and the piers. The retrofit included

drilling holes to arrest the crack growth and providing a positive attachment between the stiffeners and flanges. The retrofit for the top corners of the intermediate crossframes and pier diaphragms was made difficult by the presence of the existing concrete deck as the partial removal of the deck in areas to be retrofitted was considered too costly and disruptive. Therefore, high-strength studs in drilled and tapped holes were used to provide a stiff attachment to the top flange plate as seen in Fig. 2.4.

Fatigue cracking occurred in hundreds of diaphragm to girder connections on multi-girder steel bridges in Birmingham, Alabama (Stallings and Cousins 1997). The original welded connection was repaired with a bolted connection angle that developed fatigue cracks within two years of service. The cracks initiated at the outside surface of the angle in front of the bottom bolt as shown in Fig. 2.5. The gap between the leg of the connection angle and girder web resulted from fit-up error, the installation procedure, and yielding of the angle due to heavy truck loads. The original angle (L152 x 152 x 9.5 mm x 0.483 m long) was replaced with an alternate connection angle (L203 x 152 x 13 mm x 0.483 m long) and the bolts on the girder web were tightened first in order to minimize the gap between the angle and girder web.

A survey of web gap cracking in the webs of approximately 50 multigirder bridges in Iowa was reported by Brakke (Fisher, Kaufmann, et. al. 1987). Some observations that were drawn include:

1. The cracks occur at the upper end of diaphragm connection plates whether they are tight fit or cut short of the top flange (which is rigidly held by the deck slab). Most cracks are horizontal and are located at the toe of fillet weld joining the web to top flange. Vertical or diagonal cracks can occur at the ends of the vertical fillet welds attaching the connection plate to the girder web.

2. The cracks can occur at the bottom of the connection plate which is cut short from the bottom flange when the bridge is skewed.

3. The cracks can develop in both exterior and interior girders.

4. Web cracks can occur at connection plates for both rolled section type and truss type diaphragms. Some indications suggest that the potential for web cracks at "K" type truss diaphragms is considerably less than at "X" (cross) type truss or rolled section diaphragms.

5. The potential for these cracks is greater on skewed bridges, although many cracks have been found in the negative moment regions of non-skewed bridges.

6. The minimum time for the cracks to develop in bridges carrying less than 3,000 trucks per day is about 10 years and in most cases considerably longer.

2.1.2 Cracking in Floor Beam Connection Plates

Small unstiffened portions of girder webs in floor beam girder bridges are also susceptible to girder web cracking. In these bridges, the girder web is constrained above by the longitudinal girder flanges embedded in concrete and constrained below by the floor beam connection plate. Unlike the diaphragms in multigirder bridges, the floor beams are designed as load carrying members. Under normal traffic loading, the floor beam will deflect and develop end moments as well as cause out-of-plane bending moments in the webs of longitudinal girders as seen in Fig. 2.6.

Extensive cracking has been observed in the small gap regions in the Poplar Street Bridge approaches in East St. Louis, Illinois, the Polk County Bridge near Des Moines, Iowa, and the Woodrow Wilson Bridge in Washington D.C. (Fisher 1984 and Mertz 1984). Fatigue cracks developed in the web gap region between the flange of the main girder and floor beam connecting plate, in the vertical weld joining the connection plate

to the main girder, and in the longitudinal web to flange weld. The repair procedures consisted of drilling holes, providing positive attachments between the connection plates and girder flanges in the regions at the piers, and removing the top portion of the connection plate in the negative moment regions away from the piers.

Cracks were found in floor beam webs at a stringer to floor beam connection on a truss bridge (Lai 1996). The stringers are framed into the floor beam webs with the bottom flange and part of the web welded to the floor beam web; the stringer top flanges are connected with a welded tie plate passing over the floor beam top flange. The stringer bottom flange is located near midheight of the floor beam. The cracks are typically located at the weld toes of the stringer bottom flange and form a smiling face pattern. In order to reduce the stiffness of the connection, two holes 51 mm (2 in.) in diameter were drilled at the crack tips with a 25 mm (1 in.) saw cut between them. However, the crack reinitiated at a drilled hole. The connection was then stiffened by bolting an angle (L152 x 152 x 19 mm) to the stringer bottom flange and floor beam web on each side of the floor beam web.

The Lehigh Canal Bridges in Pennsylvania had several fatigue cracks in tie plates which connected the floor beams to outrigger cantilever brackets (Fisher, Yen, and Daniels 1976). All of the cracks started at the edge of the tie plates from a tack weld that was used to connect the tie plates to the outrigger bracket during fabrication. An investigation was conducted to evaluate the effect of tie plate geometry and the influence of the connection tie plate to the main longitudinal girder. It was found that the stress range in the tie plates decreased when narrow tie plates were used and when the tie plate

was unbolted from the main girder. It was also found that changes in plate thickness did not alter the magnitude of the stress range in the tie plates.

Cracked tie plates were also found in the Edison Bridge on Route 9 over the Raritan River in New Jersey (Fisher, et. al. 1995). Field testing to determine the live load stress levels showed that the in-plane bending of the tie plates was the principal cause of the fatigue cracking. Three cracked tie plates were removed and it was found that the fatigue cracking initiated at flame cut plate edges.

2.1.3 Lateral Gusset Plate Gaps

Lateral bracing is used in bridges to resist lateral forces and lateral movement due to wind or live loading. The horizontal gusset plates which connect the lateral members to the girder web are often welded or bolted to the girder web and may be welded or bolted to the transverse stiffener or cut free of the stiffener. Often, the gusset plate is coped to fit around the stiffener to avoid the problem of intersecting welds which have often resulted in cracking from lack of fusion weld discontinuities.

One of the first bridges to exhibit this type of cracking was the Lafayette Street Bridge over the Mississippi River at St. Paul, Minnesota (Fisher, Pense, and Roberts 1977). The primary problem was a large defect in the weld attaching the lateral connection plate to the transverse stiffener. A detailed study indicated that the crack originated in the weld between the gusset plate and the transverse stiffener as a consequence of a large lack of fusion discontinuity in the welded connection. The intersecting welds permitted the crack to penetrate into the girder web.

Cracking in web plates at the lateral gusset plate gaps developed both in the I-79 Bridge 2682 over Big Sandy Creek near Charleston, West Virginia and in the Canoe Creek Bridge on I-80 in Pennsylvania (Fisher, Yen, and Wagner 1987 and Fisher, Kaufmann, et. al. 1987). The horizontal web gaps between the transverse stiffener and lateral gusset plate varies from 6.4 mm to 25.4 mm (1/4 in. to 1 in.) for Bridge 2682 and measures 38.1 mm (1-1/2 in.) in the Canoe Creek Bridge. Strain measurements at the details revealed that double curvature out-of-plane bending developed in the web gap. The lateral connection plate was forced to rotate as well as deflect out of plane. The rotations reduced the stress at one weld toe, but elevated the stress at another thus causing cracking. For Bridge 2682 the lateral bracing system, including connection plates and welds, was removed in order to eliminate the displacement induced stresses (Kulicki, Murphy, et. al. 1986). Retrofit for the Canoe Creek Bridge included increasing the horizontal web gap length by removing the welded tab and installing a bolted gusset connection angle to connect the bracing system to the girder web.

Vertical girder web cracks were found on a two girder bridge in the horizontal web gap between the floor beam connection plate and the horizontal lateral gusset plate (Kulicki and Mertz 1987). The lateral gusset plate was coped around the floor beam connection plate. Due to inadequate space on the lateral gusset plate for a bolted connection and anticipated difficulties in a welded connection, the lateral bracing system was removed from the structure and holes were drilled at the crack tips.

The I-64 Bridges over Maury River and Kerr's Creek in Rockbridge County, Virginia also developed cracks in the girder webs at the diaphragm and lateral bracing connection locations (Albrecht, Brown, and Wright 1992). The K-type diaphragms were

bolted to the vertical stiffener which is fillet welded to the girder web and welded to the top flange in the positive moment regions and to the bottom flange in the negative moment regions. The vertical stiffener penetrates the horizontal gusset plate which is groove welded to the girder web. The cracks initiated at the weld toe on the inner end of the longitudinal weld connecting the gusset plate to the web. The cracks propagated in a vertical plane and then began to curve off the vertical away from the vertical stiffener. Prior to complete removal of the lateral bracing system, the bracing was removed from three adjacent spans and strain measurements were taken to determine if any unforeseen problems arose (Wright, Nelson, and Chase 1991). The measurements showed a change in the distribution of live load stresses between the interior and exterior girders. The stress range increased about 30% in the exterior girder with a corresponding decrease in the interior girder.

2.2 Analytical and Experimental Studies

Fisher, Fisher, and Kostem (1979) analyzed a multigirder skewed railroad bridge with intermediate diaphragms using the SAP IV finite element program in order to examine the causes of cracking and the consequences of changes in stiffener configuration. The structure was loaded with a six axle locomotive with 288 kN axle loads. Three web gaps were examined: no gap with the stiffener attached to the flanges at each end, and web gaps of 50 mm and 100 mm. With the stiffener welded to each flange, no significant out-of-plane web bending stresses developed. For the two web gap configurations, the computed web bending stresses were 155 MPa for the 50 mm gap and 334 MPa for the 100 mm gap. For this skewed structure, the results indicated that the

out-of-plane web bending stresses increased as the gap between the end of the transverse connection plate and the girder flange increased.

Another finite element study done by Castiglioni, Fisher, and Yen (1988) studied the effect of the ratio of web gap length to girder web thickness on the web gap behavior. From their analysis it was found that varying the gap length does not influence the transverse web displacement at the diaphragm; however, increasing the web thickness does cause a reduction of the transverse displacement. The horizontal components of the diaphragm member forces are not influenced by variations in web thickness and gap length, but they sharply increase if the gap length is cut to zero.

An analytical study which included a comparison with field measurements of stress distribution at web gap regions was conducted by Mertz (1984). Finite element modeling techniques were developed to determine the out-of-plane displacement induced stresses in web gaps. Stresses obtained by finite element analyses and field measurements were compared in order to identify factors contributing to displacement induced fatigue cracking and to study various alternative details. This study concluded that a positive attachment between the connection plate and flange assured adequate fatigue performance; whereas, an increase in the web gap length was not a reliable solution.

Lee (1987) used a finite element program to examine the influence of global geometry on local out-of-plane stresses in webs at diaphragm connection plate gaps and to develop fatigue strength curves. The results demonstrated that the S-N curves for out-of-plane bending are close to the Category C fatigue strength line of AASHTO and provide a lower bound for experimental data of details with out-of-plane distortion.

Only a few experimental studies have been conducted to examine the influence of girder web cracking at diaphragm connection details. The primary studies include: Fisher, Hausammann, et. al. (1979) on out-of-plane displacements at cut short stiffeners; Keating and Fisher (1987) and Fisher, et. al. (1993) on girders loaded near the fatigue limit; Zwerneman, et. al. (1989 and 1993) on diaphragm cracking at bolted connections; and Fisher, et. al. (1990) on distortion induced cracking due to secondary bending stresses at a vertical stiffener and at a web gap in a lateral gusset plate. Kennedy and Grace (1983) studied the influence of diaphragms on the transverse load distribution in composite bridges, while Kennedy, Grace, and Soliman (1989) compared the effects of welded and bolted steel I-beam diaphragms on the transverse load distribution in composite bridges.

NCHRP Report 206 (Fisher, Hausammann, et. al. 1979) discusses an early experimental test on out-of-plane displacements in web gaps. Five welded built-up full scale girder specimens with a total of 48 vertical stiffeners were tested. The stiffeners were terminated in the web, short of the tension flange, and resulted in a small gap between the stiffener and the tension flange. The gap lengths at the end of the transverse stiffeners varied from 1.25 to 20 times the web thickness. The web gaps were displaced out-of-plane by a small jack as shown in Fig. 2.7. After cracks formed, the web gaps were retrofitted by drilling holes at the crack tips. The retrofitted beams were then subjected to cyclic in-plane loading to test the retrofit with no further out-of-plane displacement occurring. The test simulated a field condition that caused cracks to develop during shipping and handling.

Experimental tests on plate girders with connection plate web gaps are reported by Keating and Fisher (1987) and Fisher, et. al. (1993). A diaphragm was bolted at one end to the connection plate with the opposite end supported against vertical motion at the test frame column. The bottom flange of the test girder was restrained against horizontal motion by a rolled section strut which simulated a flange embedded in a concrete deck or the restraint at a support (see Fig. 2.8). As the load was applied, the in-plane vertical deflection of the test girder caused the connection plate to be forced out-of-plane by the resisting moment developed at the diaphragm connection. The experimental setup modeled the differential displacement of bridge girders and the resulting distortion at diaphragm locations in the negative and positive moment regions. Distortion-induced fatigue cracks developed at both the toe of the web to flange fillet weld and at the weld toe of the connection plate end. The web gap cracking was retrofitted by drilling holes at the crack tips; however, the out-of-plane motion of the diaphragm caused the stress levels to remain high and cracks quickly redeveloped. The diaphragms were removed during the test to prevent further distortion-induced cracking, but cracks continued to develop and propagate since the stress levels were already high.

NCHRP Report 336 (Fisher, et. al 1990) contains the results of a laboratory testing program that focused on distortion-induced fatigue cracking in bridges. Eighteen full size welded girders were tested under cyclic loading. Twelve girders with transverse connection plates attached to the girder were tested in pairs in order to impose out-of-plane distortion in the web gap. The other six girders, also tested in pairs, had transverse connection plates and lateral gusset plates attached to the girder webs. The tension flanges of the girders were restrained from rotating or translating out of the plane of the

web plate by clamping large sections to the flanges, producing a condition similar to the restraint the concrete deck provides in the negative moment region of a girder. Adjustable steel rods were used to impose out-of-plane distortion as shown in Fig. 2.9. The rod length and angle could be changed to control the magnitude of the out-of-plane distortion. Each rod was gaged and calibrated to allow the measurement of the cyclic rod force being introduced in the girder by the vertical deflection from the hydraulic jacks. Since the driving rods reacted directly against the hydraulic jack loads, measured girder stresses were necessary to control the experiments. The girders with transverse connection plates were subjected to two levels of stress range: 41.4 MPa and 82.7 MPa (6 ksi and 12 ksi). The girders with gusset plates were all subjected to a stress range of 41.4 MPa (6 ksi).

The pairs of girders were cycled until a crack was detected or until at least ten million cycles of loading had been applied. Cracks were allowed to propagate through the web thickness before being retrofitted with the initial retrofit being done when the crack lengths exceeded 50.8 mm (2 in.). Cracks developed along the weld toe of the web to flange weld or along the toe of the connection plate weld.

Retrofit procedures consisted of drilling one or two holes at the crack tips, providing a bolted attachment between the connection plate and the bottom flange, or removing a part of the connection plate to increase the web gap flexibility. Drilling holes at the crack tips was found to be effective when the in-plane bending stress range was 41.4 MPa (6 ksi) and the distortion-induced cyclic stresses were less than 103.4 MPa (15 ksi). Details that have higher distortion-induced cyclic stresses require a positive attachment between the connection plate and the girder flange to stop the crack growth

and reduce the out-of-plane web bending stress. Removing a portion of the connection plate was found to reduce the cyclic stress and crack growth rate as long as the increased gap size is twenty times the web plate thickness.

Zwerneman, West, and Lim (1989 and 1993) conducted field measurements and experimental tests to determine the cause of cracking and a method of repair for a coped diaphragm bolted to the girder web. Strain gages were placed on three diaphragms in an existing bridge. The bridge was loaded with a tank truck and strain measurements were collected for lane and shoulder loading conditions. Dynamic strain measurements were also taken as the truck moved across the bridge at 20, 30, and 35 mph in the inside traffic lane. Strains produced by the truck were insignificant when the truck was on the spans preceding and following the span containing the instrumented diaphragms, even though the girders are continuous across these spans. For most cases, the measured strains were low even when the truck was on the instrumented span. Strains typically peaked when the truck was directly over the instrumented diaphragms. There was a slight tendency for peak strain to increase as the velocity increased.

The experimental test specimens consisted of a tee-shaped section with a gusset plate welded to each side of the web and diaphragms bolted to each gusset plate. The diaphragm on one side of the girder was attached to the test frame, while the other side was attached to a hydraulic actuator used to apply the cyclic loading. The original bolted diaphragm detail (Fig. 2.10) and four modifications were tested. The modifications were no cope in the bottom flange, tapered cope (Fig. 2.11), bolts removed from the bottom two bolt holes, and adding an auxiliary flange (Fig. 2.12). Not coping the bottom flange produced the greatest improvement in fatigue life. The performance of the specimens

with bottom bolts removed was more consistent than the performance of the specimens with tapered copes or with auxiliary flanges.

Kennedy and Grace (1983) studied the influences of the number of diaphragms, aspect ratio, skew, and cracking of the concrete deck on the transverse load distribution in continuous composite bridges using orthotropic plate theory and experimental tests. The experimental tests utilized two 1/8 scale models of a two-span continuous composite bridge with rigidly connected steel I-beams for diaphragms. The results indicate that rigidly connected steel I-beam diaphragms enhance the transverse load distribution and provide a reduction in the design load for longitudinal girders. The effectiveness of the diaphragms in distributing the load was found to increase with a decrease in the aspect ratio of the bridge (i.e. a wider bridge) as well as an increase in skew angle.

A comparison of welded and bolted steel I-beam diaphragms in composite bridges was made by Kennedy, Grace, and Soliman (1989). The experimental models represented to 1/5 scale a single span two-lane composite highway bridge. The steel framework consisted of 5 longitudinal beams connected by I-diaphragm beams at the two ends, midspan, and at the quarter-spans. All beams were W6x15. In one experimental model, the diaphragms were bolted to back-to-back angles which were welded to the web of the longitudinal beam. In the other model, the diaphragms were welded to the flanges and to the web of the longitudinal beam using 1/4 inch fillet and groove welds. The results show that the concrete slab plays a more important role in the transverse load distribution in bolted diaphragm than in welded diaphragm composite bridges. Welded diaphragm composite bridges were found to be stiffer and stronger than bolted diaphragm bridges.

2.3 Specifications

The current Standard Specifications for Highway Bridges (AASHTO 1996) classifies the toe of transverse stiffener welds on girder webs or flanges as a Category C detail. The allowable stress range is 82.7 MPa (12 ksi) for over 2,000,000 cycles on a redundant load path structure and it is 75.8 MPa (11 ksi) on a nonredundant load path structure. The base metal adjacent to fillet welded details with the weld length in the direction of stress between 50.8 mm and 101.6 mm (2 in. to 4 in.) corresponds to a Category D detail. The allowable stress range is 48.3 MPa (7 ksi) for a redundant load path structure and 34.5 MPa (5 ksi) for a nonredundant load path structure for more than 2,000,000 cycles. The shear stress on the throat of fillet welds is classified as a Category F detail. For a redundant load path structure the allowable stress range is 55.2 MPa (8 ksi) for over 2,000,000 cycles and for a nonredundant load path structure the allowable stress range is 41.4 MPa (6 ksi).

The specification requires that diaphragms or crossframes be placed at each support with intermediate diaphragms or crossframes placed in all bays and spaced at intervals no greater than 7620 mm (25 ft.). Diaphragms for rolled beams are required to be at least 1/3 and preferably 1/2 the beam depth; and for plate girders shall be at least 1/2 and preferably 3/4 the girder depth.

2.4 Summary and Conclusions

In multigirder steel bridges, diaphragms contribute to the lateral load distribution among the bridge girders and provide lateral stability during construction and

rehabilitation. Usually the diaphragms are connected to transverse stiffeners which are welded to the girder web. These stiffeners are usually not attached to the girder tension flange, and are sometimes not attached to either flange. Since adjacent beams deflect differing amounts, an out-of-plane deformation is produced in the web gap at the stiffener ends that are not connected to the beam flange. The magnitude of the out-of-plane movement depends on girder spacing, bridge skew, and type of diaphragm.

Repair of distortion-induced fatigue cracking can be accomplished through the use of several retrofit procedures. If the distortion is caused by the interaction of the longitudinal girder and the diaphragm, increasing the flexibility of the gap region through the use of drilled holes or removal of a portion of the connection plate will usually be sufficient to reduce the bending stresses that are driving the crack. Details that have higher distortion-induced cyclic stresses, such as girder-floor beam connections, require a positive attachment between the connection plate and the girder flange to stop the crack growth and reduce the out-of-plane web bending stress.

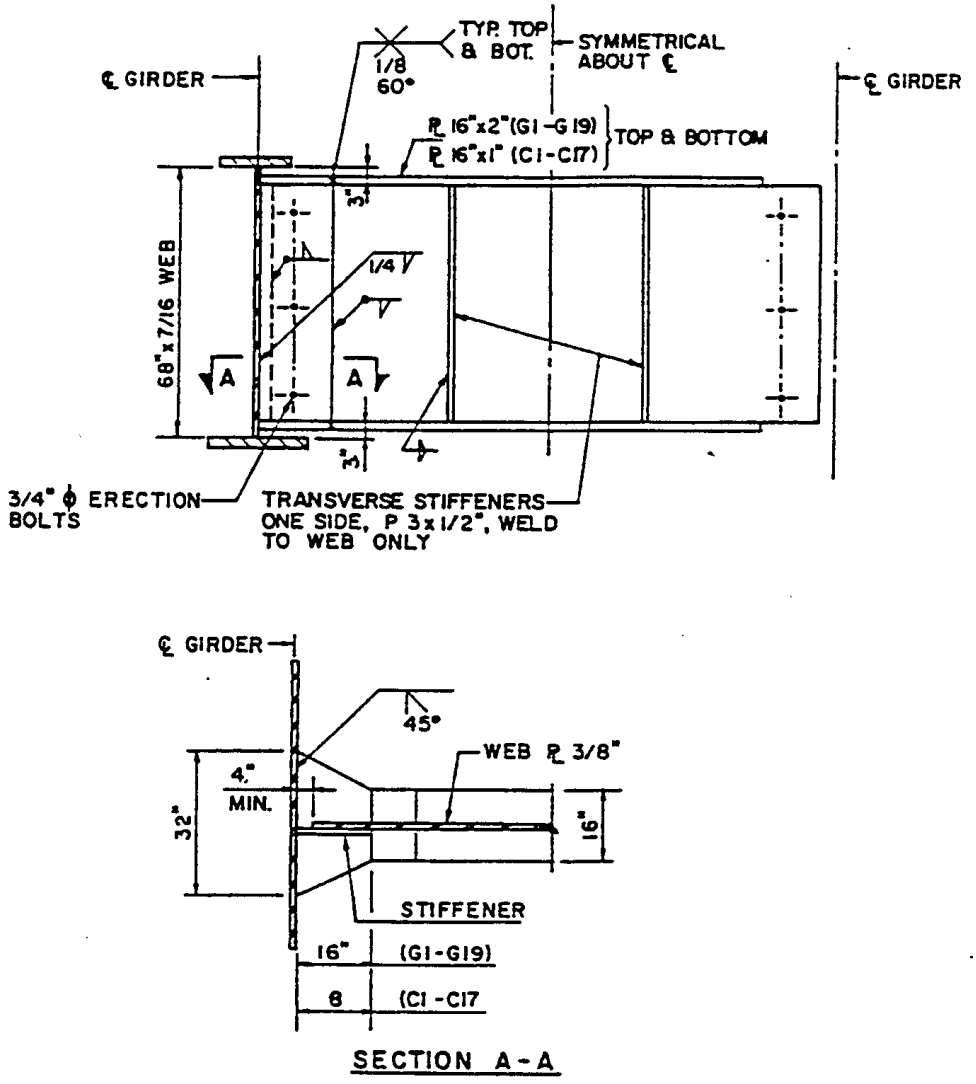

Figure 2.1 Midspan diaphragm-to-beam connection on Route 95 (Pullaro 1990)

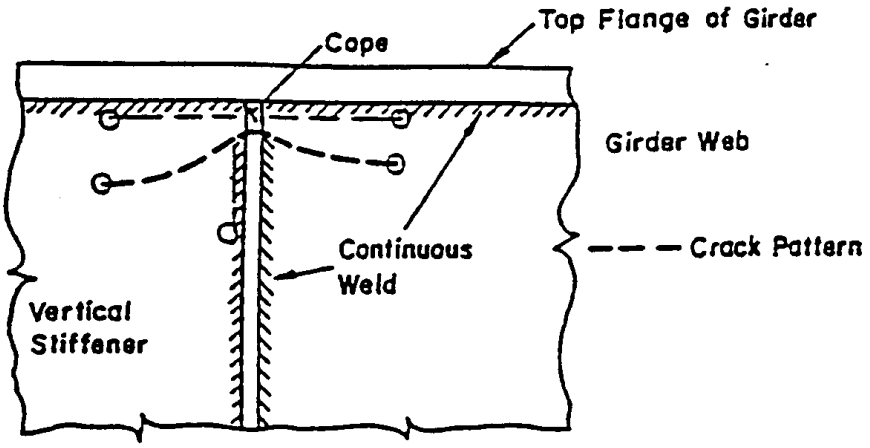

(a) Belle Fourche River Bridge

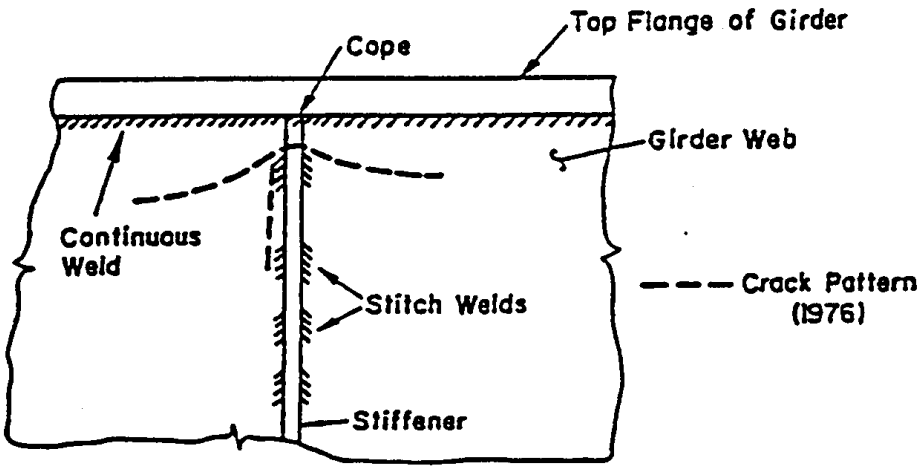

(b) Chamberlain Bridge

Figure 2.2 Schematic showing weld details and crack pattern for (a) Belle Fourche River Bridge and (b) Chamberlain Bridge (Fisher 1984)

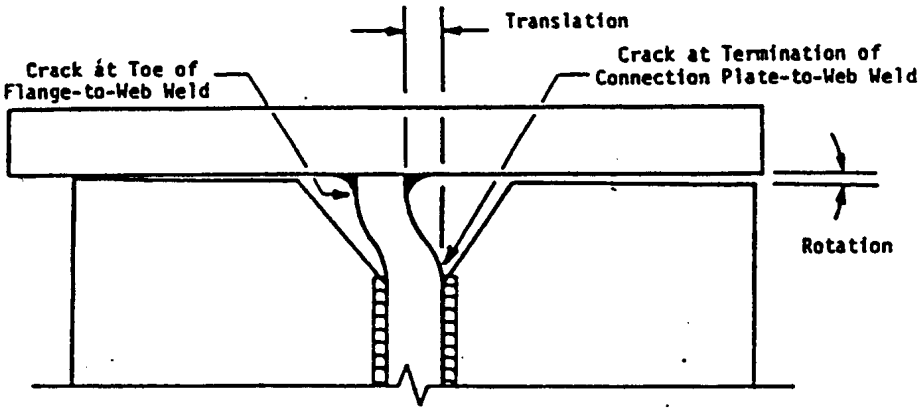

Figure 2.3 Double curvature in girder web of Bridge 2682
(Kulicki, Murphy, et.al. 1986)

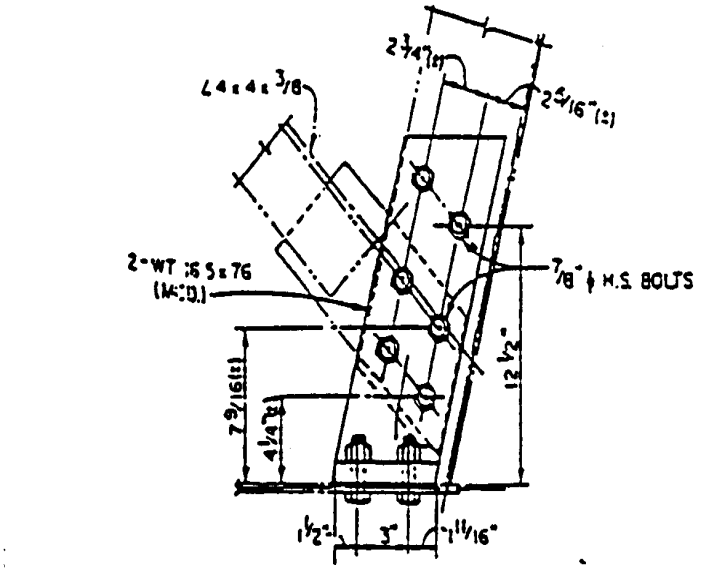

(a) Bottom corner retrofit detail

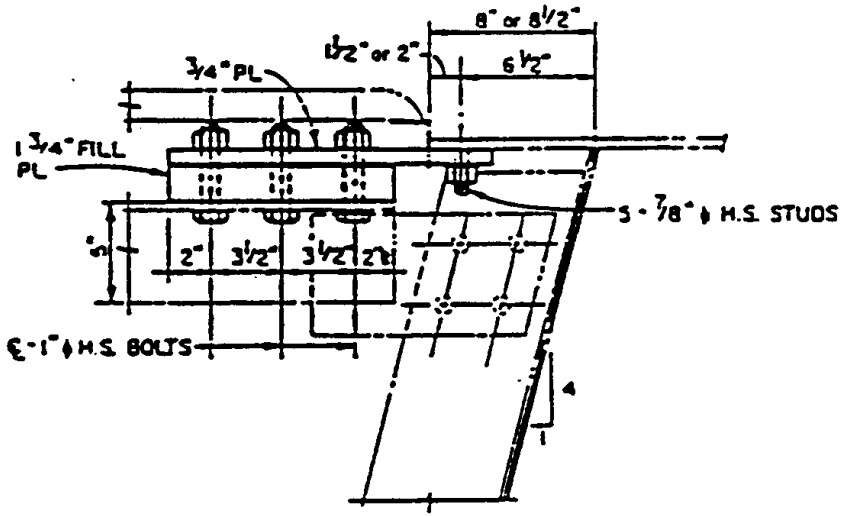

(b) Top corner retrofit detail

Figure 2.4 Retrofit details at (a) bottom corner and (b) top corner of an intermediate crossframe (Wilson, Duncan, and Fisher 1989)

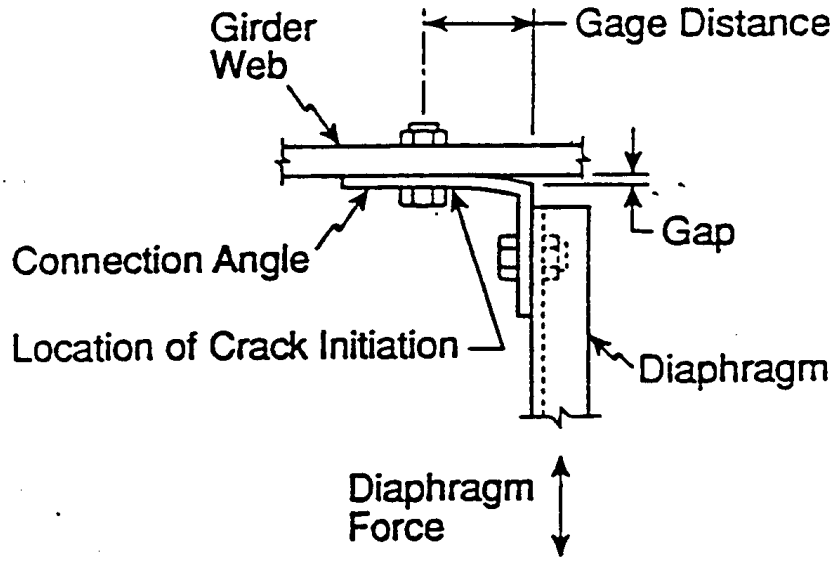

Figure 2.5 Section through connection angle (looking down)
(Stallings and Cousins 1997)

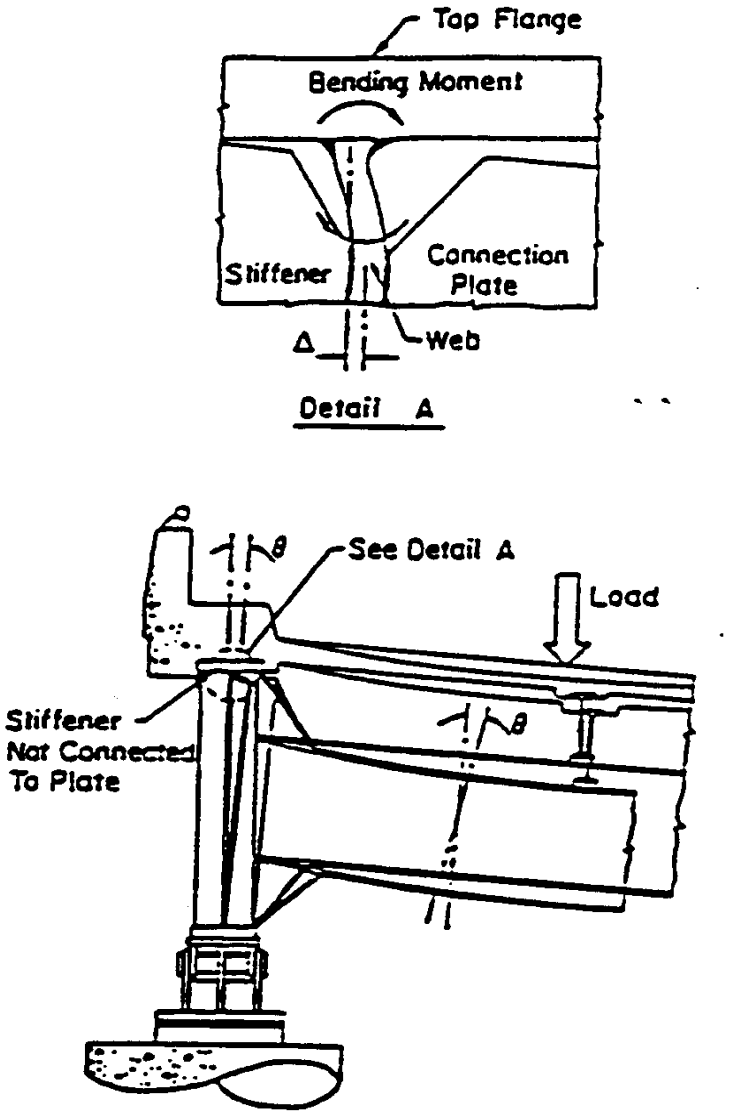

Figure 2.6 Representation of floor beam end rotation and web behavior (Fisher, Yen, and Wagner 1987)

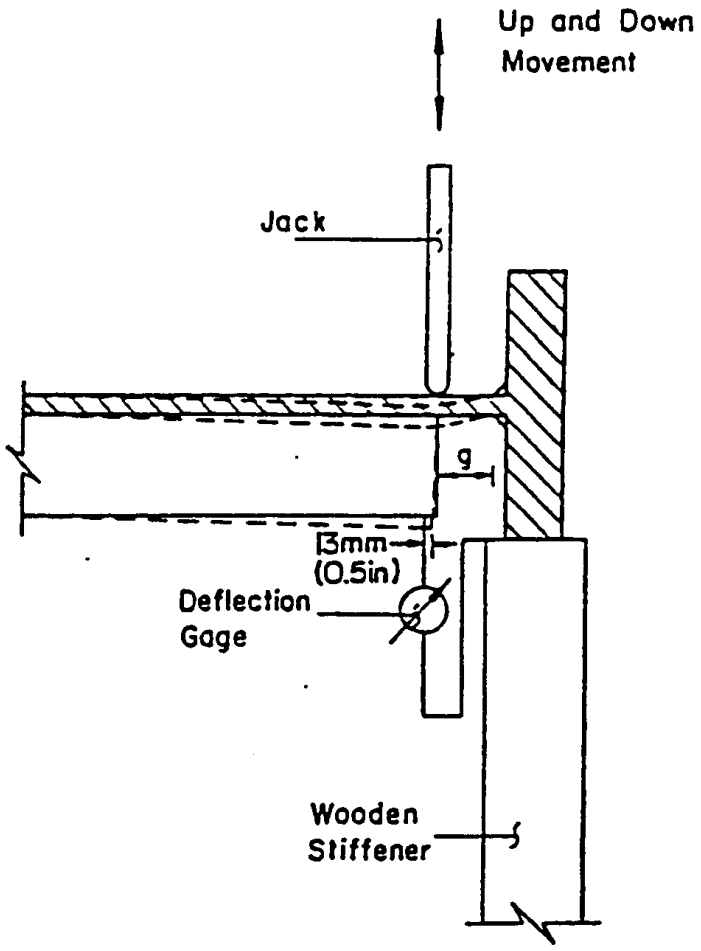

Figure 2.7 Schematic showing out-of-plane movement used for experimental test in NCHRP 206 (Fisher, Hausammann, et.al. 1979)

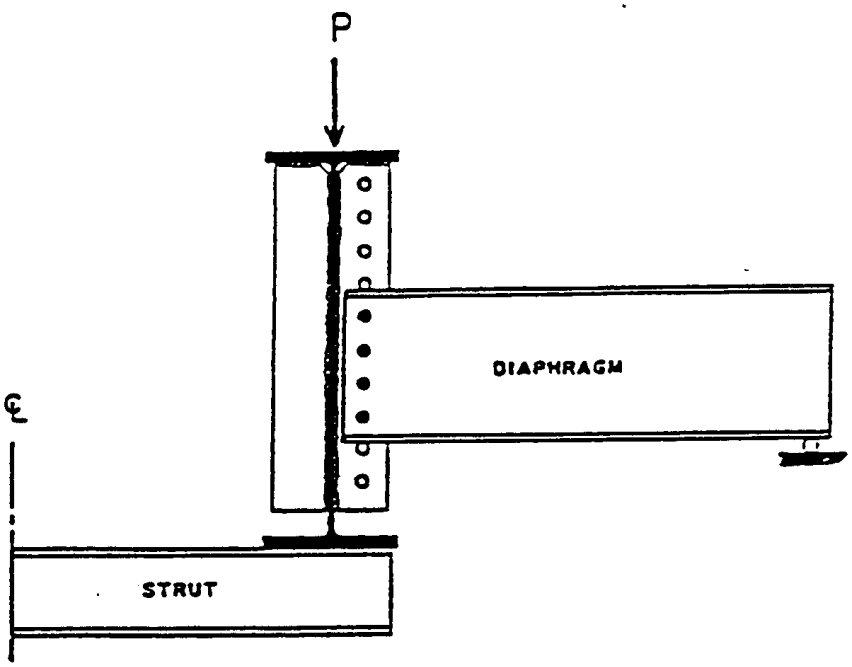

Figure 2.8 Test setup for distortion-induced web gap cracking
(Keating and Fisher 1987)

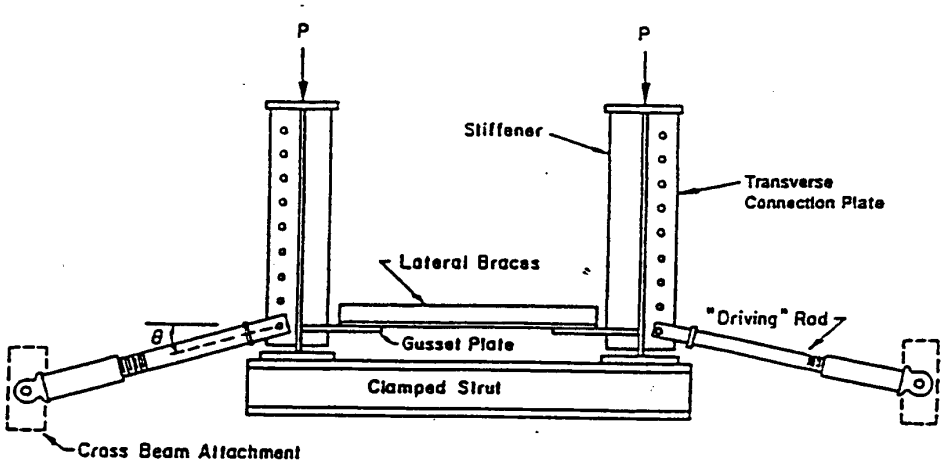

Figure 2.9 Test setup for distortion-induced fatigue cracking in NCHRP 336 (Fisher, et.al. 1990)

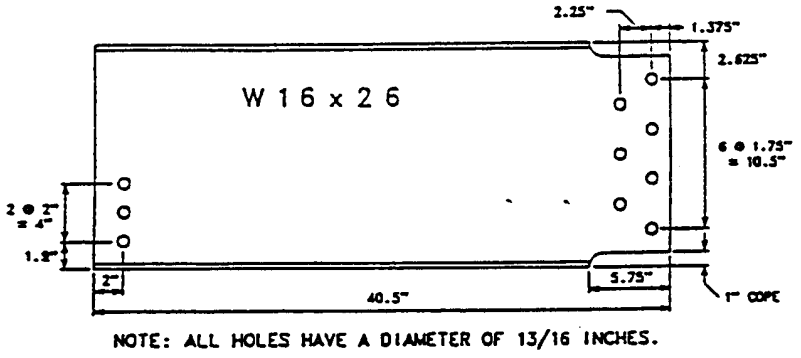

Figure 2.10 Test specimen for original bolted diaphragm detail (Zwerneman, West, and Lim 1989)

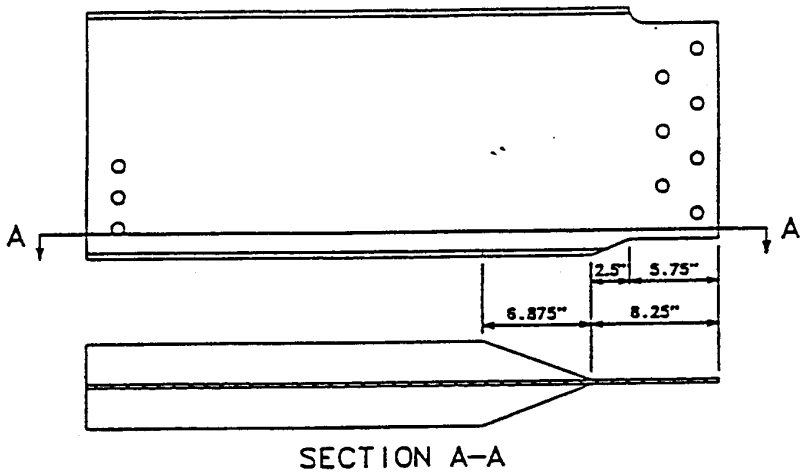

Figure 2.10 Test specimen for tapered cope diaphragm modification
(Zwerneman, West, and Lim 1989)

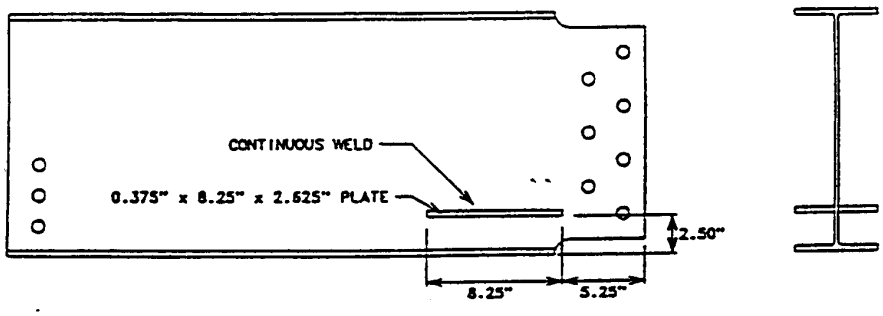

Figure 2.10 Test specimen for addition of an auxiliary flange for diaphragm modification (Zwerneman, West, and Lim 1989)

CHAPTER 3

EXPERIMENTAL PROGRAM

The main objectives of the experimental study were to evaluate the number of loading cycles required to cause failure of the beam with welded diaphragms, to examine the failure modes, and to evaluate repair methods. Nine steel beams with welded diaphragms were tested under constant amplitude cyclic loading. The experimental program showing the various types of tests conducted can be seen in Table 3.1. Six of the steel beams were cycled with no repairs being performed. Three additional tests were conducted to evaluate the effectiveness of the following repair and retrofit methods: flame cut diaphragm and drill holes at the beam crack tips; flame cut diaphragm and peen bottom flange weld areas; and leave diaphragm in place and peen bottom flange weld areas.

3.1 Design Variables

The design variables for this part of the study were the stagger condition of the diaphragm, the magnitude of the applied load, and the repair method performed.

3.1.1 Stagger Condition

Two diaphragm-to-beam configurations were examined. In one case the

diaphragms were directly opposite of each other, while in the other configuration the diaphragms were offset 1219 mm (4 ft). The staggered diaphragm configuration is typical when the bridge is skewed. With the staggered diaphragms, the load was applied at a location that was either centered between the diaphragms or applied at one of the staggered diaphragms (Fig. 3.1).

3.1.2 Load Magnitude

A test load was desired that would be large enough to cause cracks in the welded connection, but not so large that the load was unrealistic. A weigh in motion study was undertaken on six steel bridges in Michigan to determine the distribution of truck axle weights (Nowak, et. al. 1994). The bridges ranged from 2 spans to 4 spans and the instrumented spans were all entrance spans with span lengths ranging from 9906 mm to 23,927 mm (32.5 ft. to 78.5 ft.). A summary of the axle weight statistics for each of the six bridges can be seen in Table 3.2. The average of the mean axle weight for the bridges is approximately 49 kN (11,000 lbs.). An HS20 truck has an axle weight of 142 kN (32,000 lbs.) as provided in AASHTO. The Michigan study shows that the average truck axle weight is much lower than the design truck axle weight.

A distribution of the truck axle weights can be plotted from the Michigan statistics. The kurtosis is a measure of the skewness of the distribution curve; a normal distribution has a kurtosis of zero. A positive kurtosis value indicates long tails to the right. The bridges studied have an average kurtosis of 2.7, which indicates a normal distribution would not adequately represent the axle weight frequency. A lognormal

distribution has a skewed shape and was therefore chosen to represent the truck frequency as shown in Fig. 3.2. The lognormal model has a long tail to the right indicating a small probability of heavy truck axle weights.

The load for the first two experimental tests was 133 kN (30,000 lbs.). The load was applied as a single point load to the test beam. A load of 133 kN (30,000 lbs.) is located in the right tail of the lognormal plot in Fig. 3.2. Indiana Department of Transportation engineers have observed an increasing number of special-permit overload trucks for which a wheel load of 133 kN (30,000 lbs.) is not uncommon.

The remaining seven experimental tests were conducted with an applied load of 200 kN (45,000 lbs.). The load was increased in order to shorten the experimental time. The 200 kN (45,000 lb.) load encompasses most truck weights the bridge is likely to experience since this load is much further out in the right tail of the frequency plot.

3.1.3 Repair and Retrofit Methods

The repair method investigated was to flame cut the diaphragm and drill holes at the beam crack tips. This repair was performed on a staggered diaphragm configuration. Previous work (Fisher et. al. 1980, 1990, 1993) has shown that holes drilled at the crack tips can be an effective method of arresting crack growth. It is important that the crack tip is contained within the hole otherwise the stress concentration due to the hole may accelerate crack propagation. If the hole contains the crack tip, the stress intensity factor at the crack tip is reduced since the crack tip radius now equals the radius of the drilled hole.

The drilled hole should satisfy the following relationship to prevent re-initiation (Fisher et. al. 1980, 1990, 1993):

$$\frac{\Delta K}{\rho} < 10.5\sqrt{\sigma_y} \quad \text{for } \sigma_y \text{ in MPa}$$

$$\frac{\Delta K}{\rho} < 4\sqrt{\sigma_y} \quad \text{for } \sigma_y \text{ in ksi} \tag{3.1}$$

where ΔK is the stress intensity factor, ρ is the radius of the drilled hole, and σ_y is the yield stress. The stress intensity factor is calculated using the in-plane bending stress and the relationship:

$$\Delta K = \Delta\sigma\sqrt{\pi a_r} \tag{3.2}$$

where $\Delta\sigma$ is the in-plane bending stress range and a_r is the effective crack length as illustrated in Fig. 3.3.

For this study 38.1 mm (1.5 in.) diameter holes were drilled at the crack tips, which corresponds to an equivalent crack length of 50.8 mm (2 in.). The welded end of the diaphragm was flame cut to a length of 229 mm (9 in.) and the bolted end was disconnected; the diaphragm was then removed. Figure 3.4 shows the repair for this study.

The retrofit method involved the use of air hammer peening the bottom flange weld toes. Figure 3.5 shows the areas around the weld toes that were peened. Peening was performed before any cracks were detectable in the beam since peening is only effective for shallow depth cracks. Air hammer peening was performed using a hardened tool and a pneumatic hammer operated at 0.28 MPa (40 psi). A total of six complete passes were performed around the weld toe, with each successive pass causing additional

deformation in the base metal along the toe.

The peening retrofit was performed on a no stagger configuration as well as a staggered one. In each of the tests, the specimens were cycled for 385,100 cycles under a constant amplitude load range of 200 kN (45,000 lbs.) prior to peening. Although no cracks were detected after this precycle, the loading was conducted to simulate a significant service loading. During the peening process, a 22 kN (5,000 lb.) load was applied to the test beam which corresponds to a maximum stress of 13.8 MPa (2 ksi) at the bottom flange of the beam.

3.2 Test Arrangement

The specimen configuration and testing arrangement consists of three parallel beam members as shown in Figs. 3.6 and 3.7. Photographs of the test setups are shown in Figs. 3.8 through 3.10. Figure 3.8 shows a back-to-back diaphragm arrangement using the 1468 kN (330 kip) linear actuator and Fig. 3.9 is a staggered diaphragm arrangement using the 1468 kN (330 kip) linear actuator. Figure 3.10 is a nonstaggered diaphragm configuration using the 979 kN (220 kip) linear actuator. The primary member of the test set-up was the middle beam. The outside beams were reused for several tests. Diaphragm members were welded to the test beam and bolted to the outside beam members as shown in Figs. 3.11 and 3.12. Figure 3.13 shows a welded connection from one of the experimental tests. The longitudinal beams spanned 4877 mm (16.0 ft.) between supports with a total length of 5029 mm (16.5 ft.). The diaphragm members were 1372 mm (4.5 ft.) in length. The beam members were W24 x 55 hot-rolled shapes

and the diaphragms were W14 x 26 sections; all steel was ASTM A572 Gr. 50. The test beams were from three different heats of steel and the diaphragms were all of the same heat. The chemical composition and mechanical properties are provided in Appendix A for all of the steel used in the tests.

In order to simulate a concrete deck and to provide lateral support, six 76.2 mm x 76.2 mm x 7.9 mm (3 in. x 3 in. x 5/16 in.) angles were attached to the top flanges of the three beam system. The angles were bolted to the outside beam members and clamped to the test beam using heavy duty C-clamps. The angles were placed over each end support and evenly spaced over the remaining beam length. Figure 3.8 illustrates the lateral support angles attached to the top flanges of the beam members.

3.3 Fabrication of Welds

The diaphragm to test beam welds were deposited by an American Welding Society certified welder in the Kettelhut Structural Engineering Laboratory. The welding procedures were intentionally conducted in a manner similar to those used in actual bridge construction. The welding was performed downhand using shielded metal arc welding - DC reversed (approximately 90 Amps) with a Miller Electric Dialarc 250 AC/DC Arc Welding Power Source. Although no preheat was used, the welding was conducted in the laboratory at room temperature. The welds were 6.4 mm (0.25 in.) fillet welds placed with 3.2 mm (0.125 in.) diameter E6010 electrodes. No tests were performed to determine the weld electrode mechanical properties; however, the American Welding Society requirements for this electrode type are provided in Appendix A.

The welder first placed a tack weld on each corner of the top flange while sitting on a plank placed across the longitudinal beams. He then sat on the diaphragm to place the remaining welds in the following order (refer to Fig. 3.11):

- top flange,
- intermittent welds on one side of the diaphragm web,
- bottom flange on same side,
- intermittent welds on other side of diaphragm web, and
- bottom flange on second side.

Figures 3.14 through 3.16 illustrate the welding procedure as follows:

1. mark the weld placement,
2. place the weld while sitting on the diaphragm, and
3. chip the slag from the weld.

3.4 Test Procedure

The test procedure involved the application of loading cycles along with periodic interruptions to monitor the response of the system. Two separate test set-ups were used during the testing. The load was applied to the test beam using an MTS 1,468 kN (330 kip) capacity servo-hydraulic actuator in one set-up (Fig. 3.6), while a 979 kN (220 kip) actuator was used in the other set-up (Fig. 3.7). The load was applied at midspan of the test beam through a 102 mm x 229 mm (4 in. x 9 in.) bearing plate which was bolted to the head of the actuator.

The first few static load measurements consisted of loading the beam from the

low value to the high value and adding the angles in pairs to determine the load transferred to the outside beams through the angles. These initial measurements were used to evaluate the load carried by the test beam, the load transferred to the outside beams, and the strains developed at the gage locations before any fatigue cracks developed. The beam was then subjected to a sine-wave shaped cyclic loading, with an R-ratio of 0.10, at a frequency of 1 - 2 Hz. At regular intervals the cyclic loading was interrupted and static load measurements were performed. Visual inspections were performed during cyclic loading to detect the onset of fatigue cracking in the welds connecting the diaphragm to the test beam or in the web of the test beam. A 10X magnifying glass was used for the visual inspections.

3.5 Data Collection

A variety of information was gathered during the test. For the tests conducted using the 1,468 kN (330 kip) loading actuator (Fig. 3.6), 1,334 kN (300 kip) Eaton fatigue-rated load cells were placed at each end of the test beam in order to determine the total load carried by the test beam. The load applied to the system from the actuator as well as the actuator stroke were also monitored. Schaevitz linear variable differential transformers (LVDTs) with a range of ±25.4 mm (±1 in.) were located at midspan of each longitudinal beam when the diaphragms were not staggered. When the diaphragms were staggered, the LVDTs were placed at the diaphragm locations on each of the outside longitudinal beams and at midspan of the test beam. A total of fourteen longitudinal strain gages and two strain rosettes were attached to the beams and diaphragms as shown in Fig.

3.17 for the diaphragms which were not staggered. Fourteen gages and two rosettes were also used for the test configurations where the diaphragms were staggered as seen in Fig. 3.18. The output signals from the instrumentation were collected using a 200 channel Megadac data acquisition system.

For the tests performed with the 979 kN (220 kip) loading actuator, ten longitudinal strain gages were attached to the beams and diaphragms as shown in Fig. 3.19. The output signals were collected using a Measurements Group P3500 strain indicator in conjunction with a switch and balance unit. The actuator load and stroke were also monitored.

Table 3.1 Experimental Program

No. of tests	Stagger	Load	No repair	Flame cut diaph. and drill hole	Flame cut diaph. and peen	Leave diaph. and peen
4	NS	200 (45)	2	-	1	-
		133 (30)	1	-	-	-
1	SL	200 (45)	1	-	-	-
4	SC	200 (45)	1	1	-	1
		133 (30)	1	-	-	-

Notes:

- NS = No stagger in diaphragm location
- SL = Stagger in diaphragm location with load applied at one of the diaphragms
- SC = Stagger in diaphragm location with load centered between the diaphragms
- Load = Net test load applied to the system, kN (kip)
- Flame cut diaph. and drill hole = Flame cut diaphragm to a length of 229 mm (9 in.) when there is a crack present in the beam and drill holes at the crack tips
- Flame cut diaph. and peen = Flame cut diaphragm to a length of 229 mm (9 in.) and peen the bottom flange welds before a crack is present in the beam
- Leave diaph. and peen = Leave the diaphragm in place and peen the bottom flange welds before a crack is present in the beam

Table 3.2 Axle Weight Statistics for all Truck Axles from Michigan Study (Nowak, et. al. 1994)

Bridge	Maximum Axle Weight (kN) *(kip)*	Mean Axle Weight (kN) *(kip)*	Median Axle Weight (kN) *(kip)*	Standard Deviation	Kurtosis
23/HR (92)	199.7 *(44.9)*	48.2 *(10.84)*	43.1 *(9.7)*	4.49	3.348
23/HR (91)	261.1 *(58.7)*	50.3 *(11.30)*	46.7 *(10.5)*	4.33	5.787
23/SR	181.5 *(40.8)*	54.8 *(12.31)*	48.0 *(10.8)*	5.58	0.707
94/PR (93)	241.5 *(54.3)*	50.6 *(11.38)*	46.7 *(10.5)*	4.13	3.313
94/PR (91)	121.4 *(27.3)*	50.3 *(11.30)*	47.4 *(10.65)*	3.89	-0.257
14/NY	198.4 *(44.6)*	54.4 *(12.24)*	48.0 *(10.8)*	5.68	2.548
WY/94	141.5 *(31.8)*	45.5 *(10.22)*	42.7 *(9.6)*	3.88	2.315
94/JR	233.5 *(52.5)*	52.2 *(11.73)*	44.9 *(10.1)*	5.15	3.840
Average	197.5 *(44.4)*	50.7 *(11.4)*	45.8 *(10.3)*	4.64	2.70

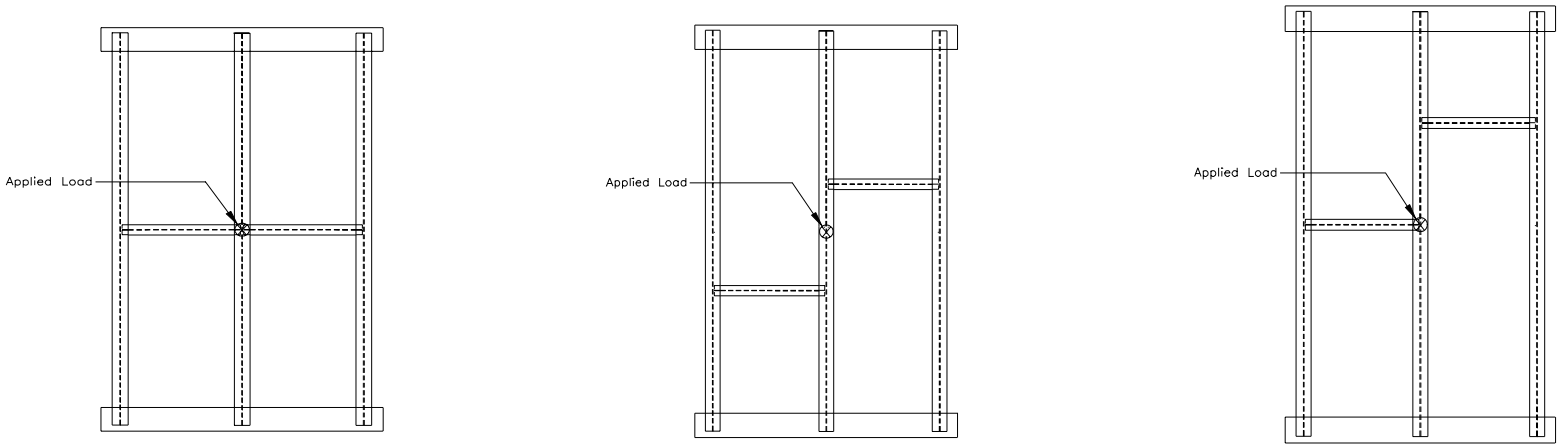

(a) No stagger

(b) Stagger with load centered between diaphragms

(c) Stagger with load at one of diaphragms

Figure 3.1 Stagger configurations studied in experimental tests

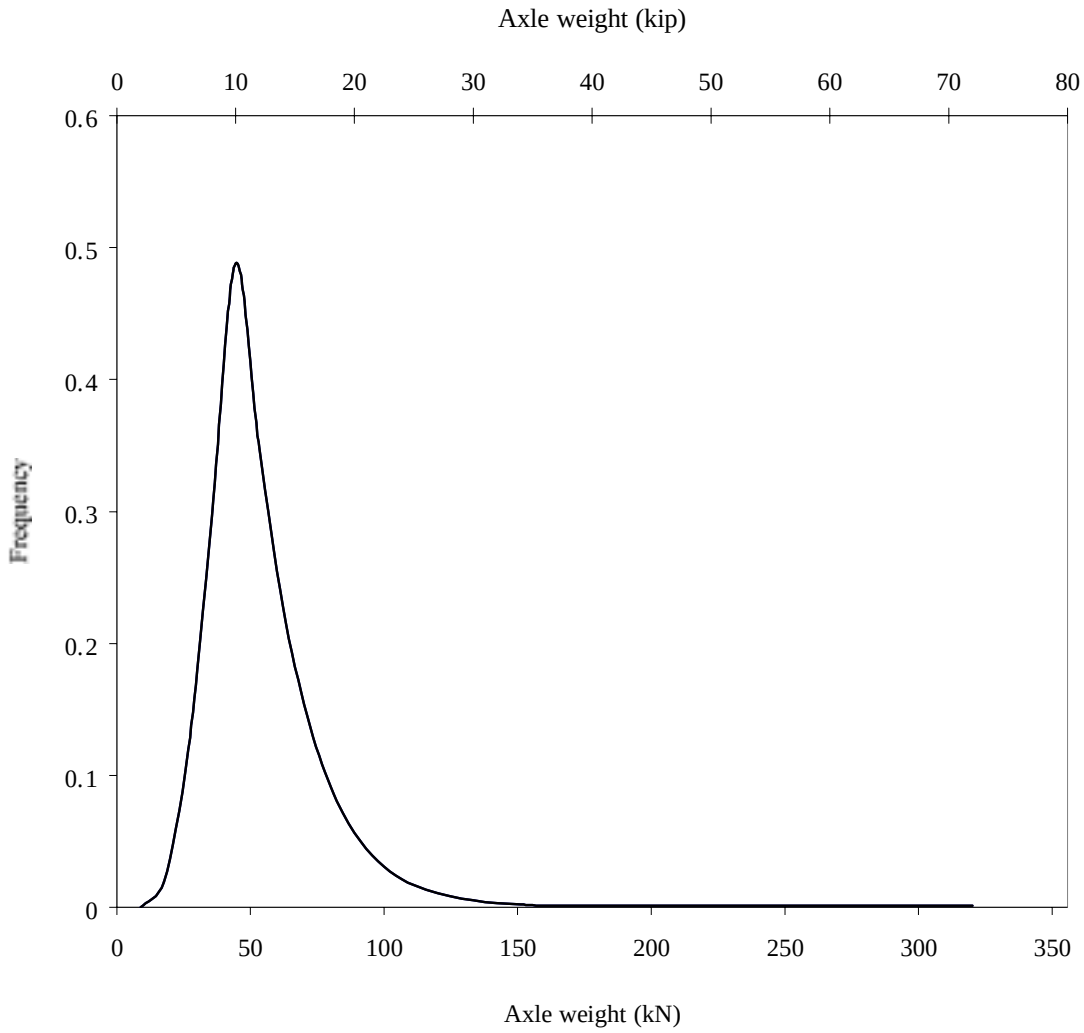

Figure 3.2 Lognormal distribution of truck axle weights from Michigan study

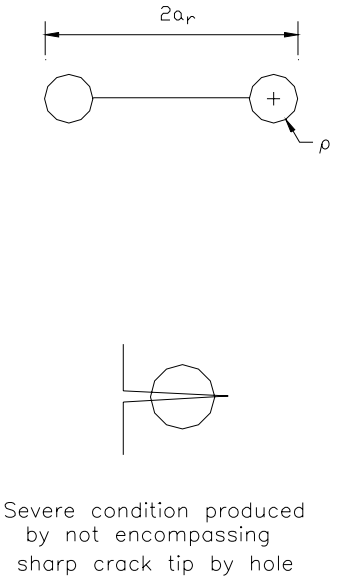

Figure 3.3 Effective crack length

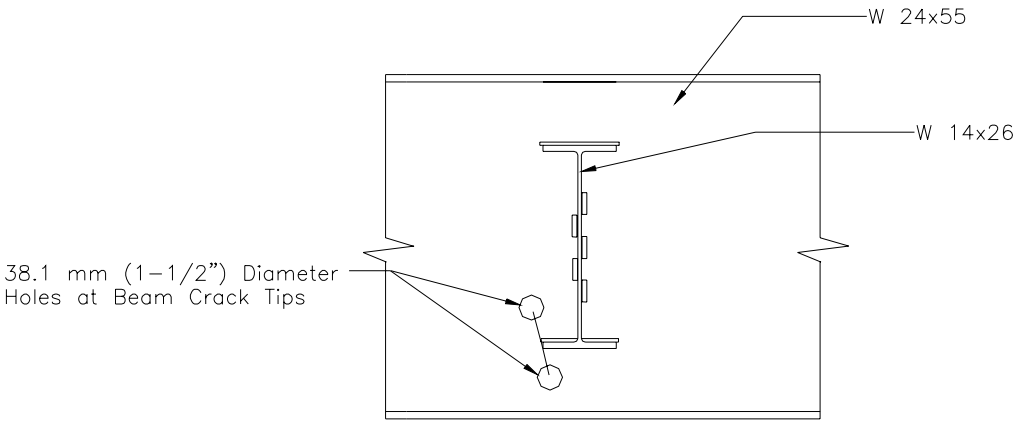

Figure 3.4 Flame cut diaphragm and drill hole repair

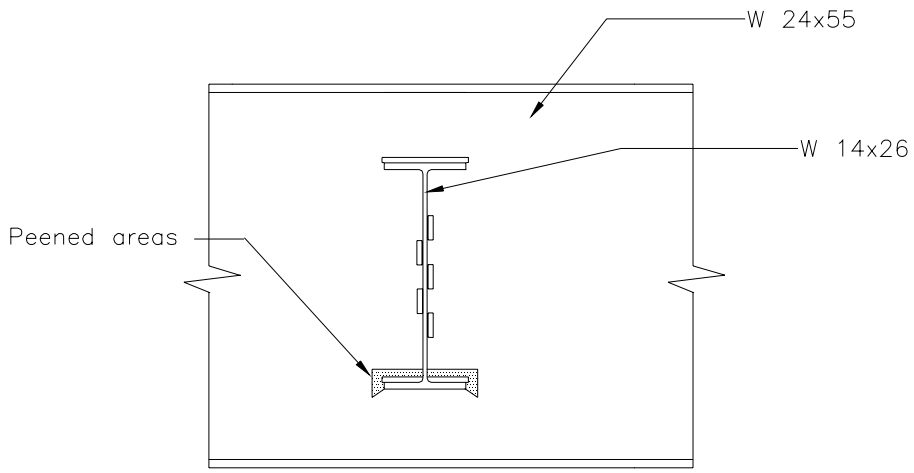

Figure 3.5 Peened areas around bottom flange weld toes

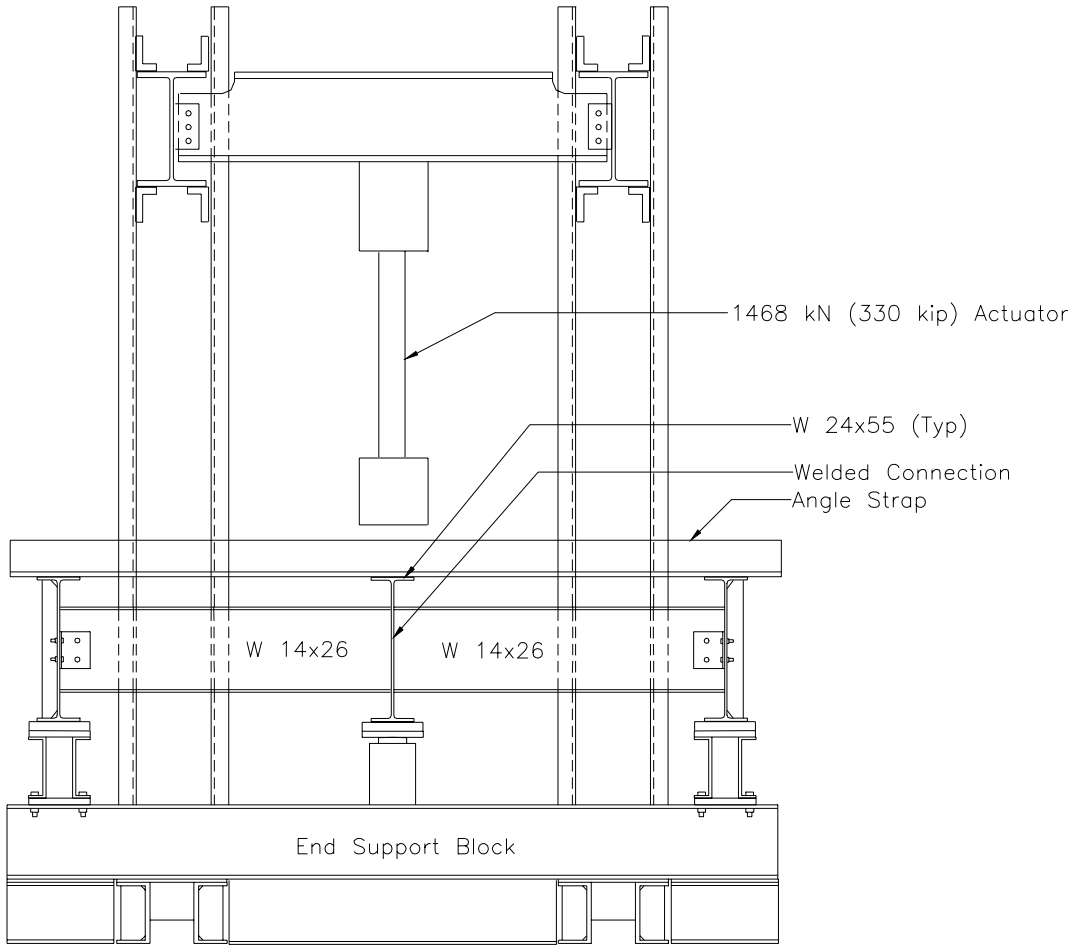

Figure 3.6 Test setup with 1468 kN (330 kip) linear actuator

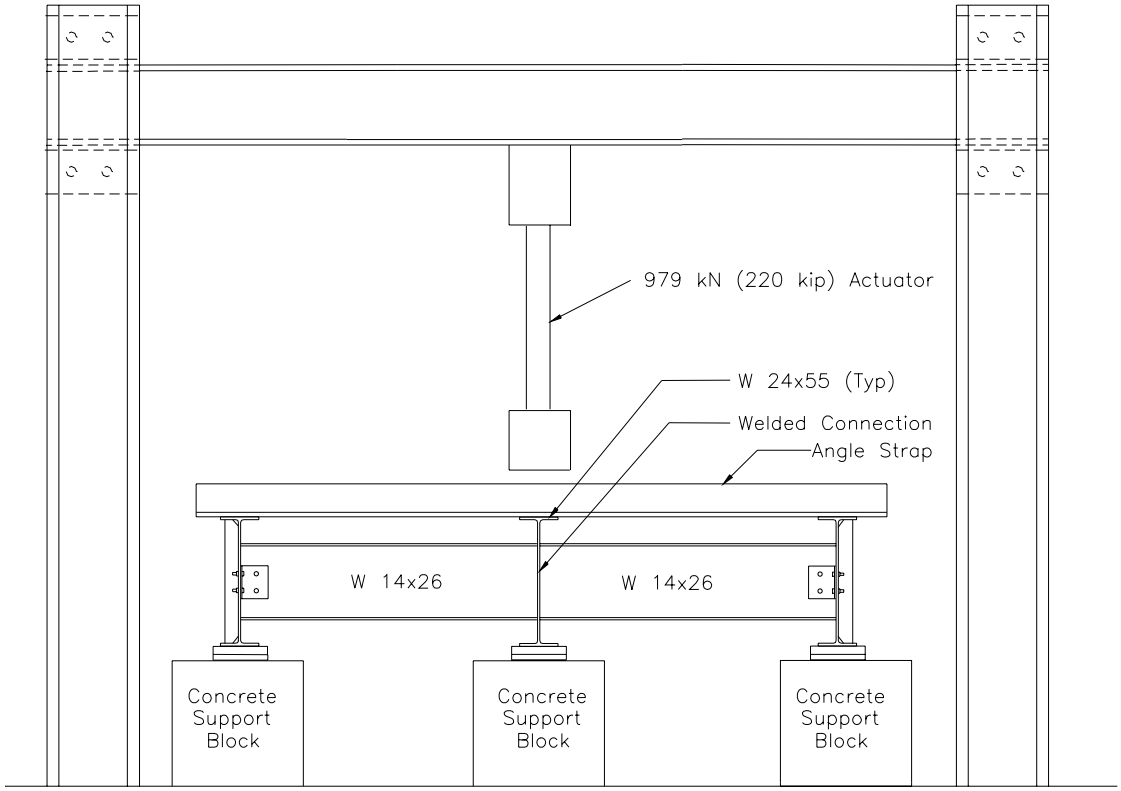

Figure 3.7 Test setup with 979 kN (220 kip) linear actuator

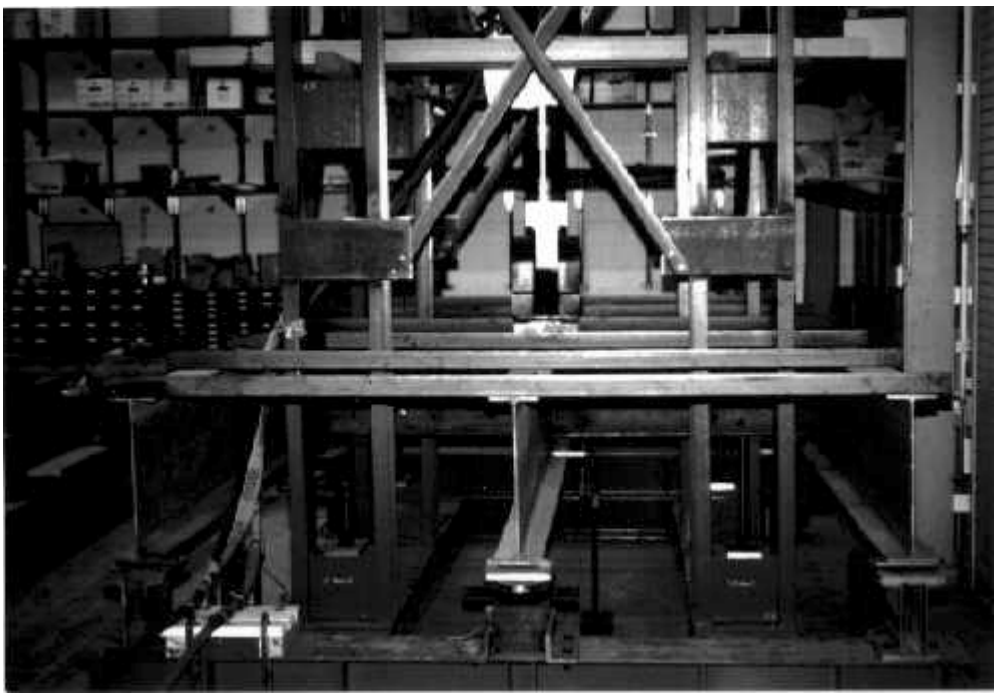

Figure 3.8 Laboratory setup with back-to-back diaphragms using the 1468 kN (330 kip) linear actuator

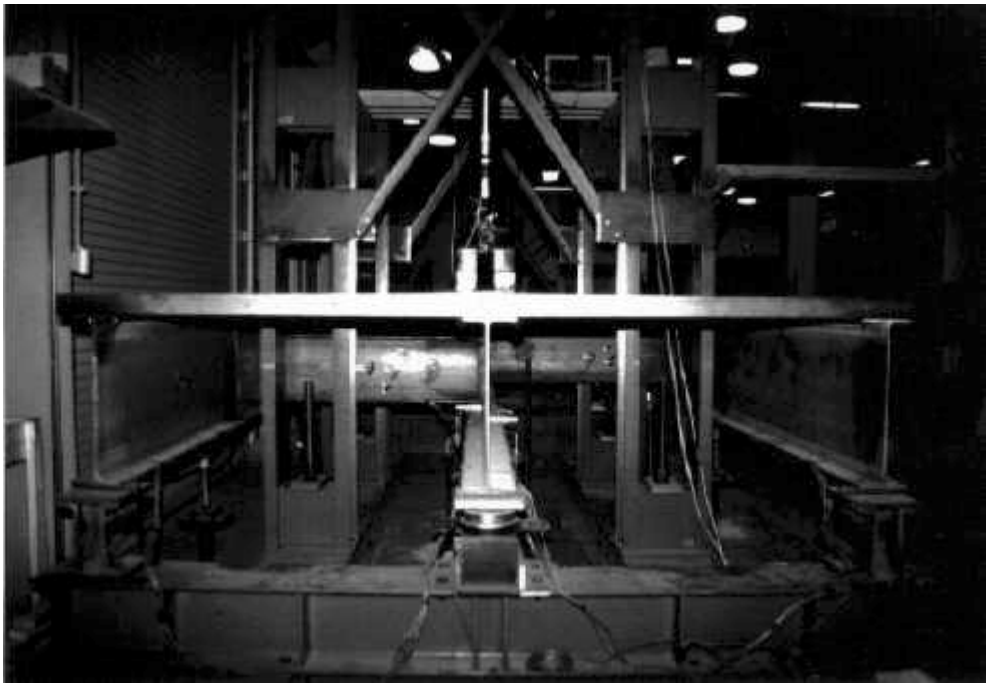

Figure 3.9 Laboratory setup with staggered diaphragms using the 1468 kN (330 kip) linear actuator

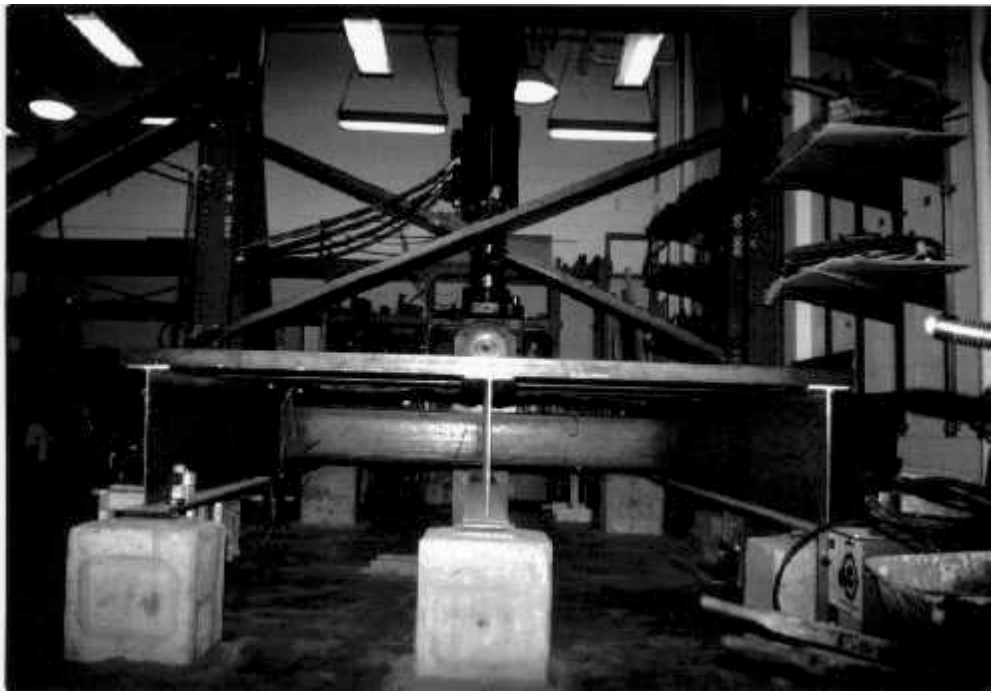

Figure 3.10 Laboratory setup with back-to-back diaphragms using the 979 kN (220 kip) linear actuator

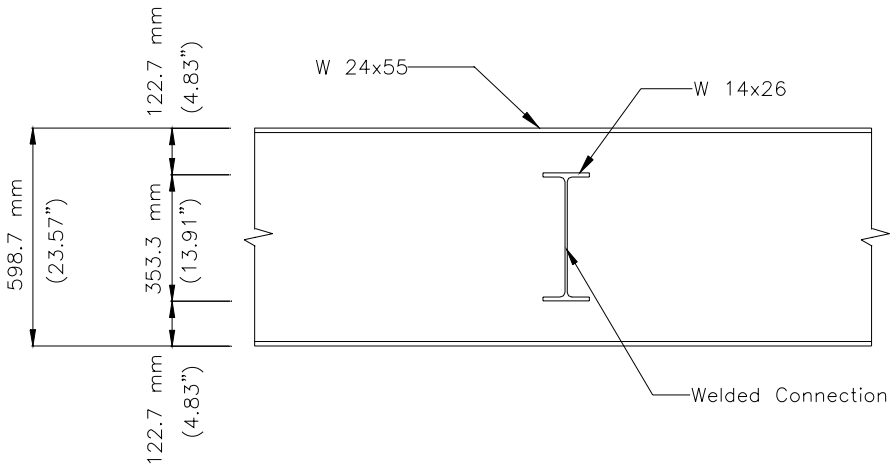

(a) Plan view of test beam

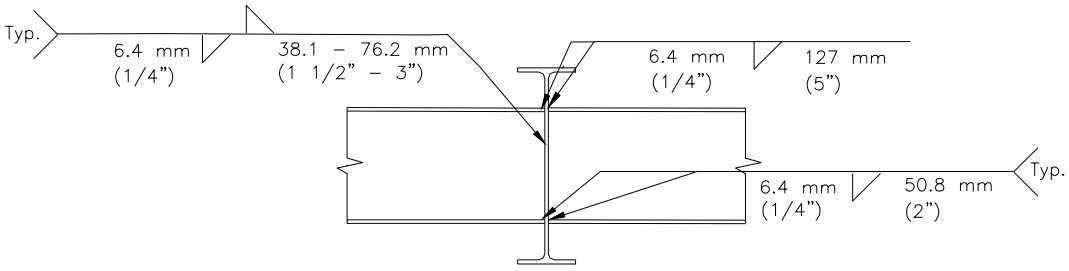

(b) Cross sectional view of test beam

Figure 3.11 Welded diaphragm-to-test beam connection

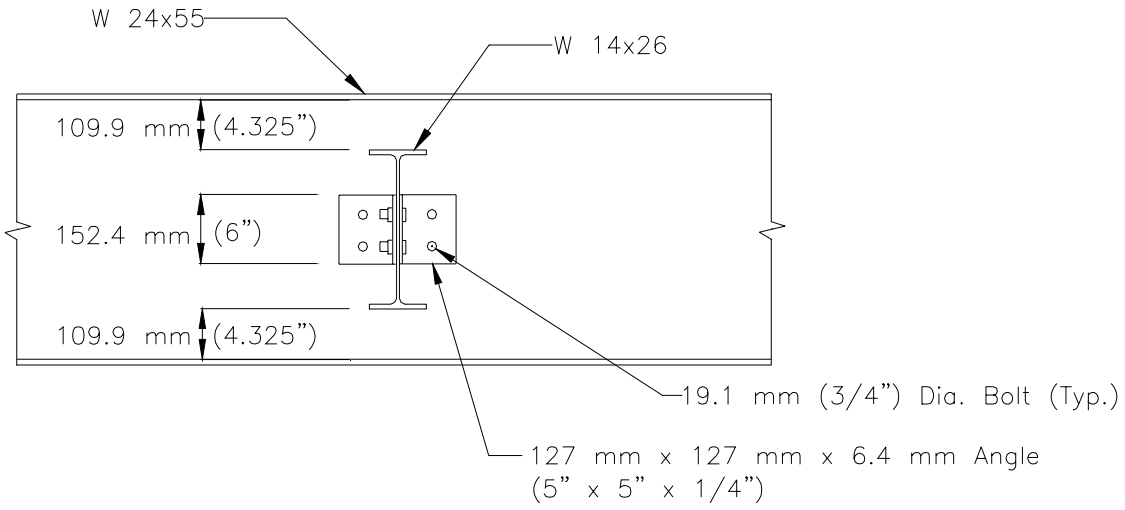

(a) Plan view of outside beam

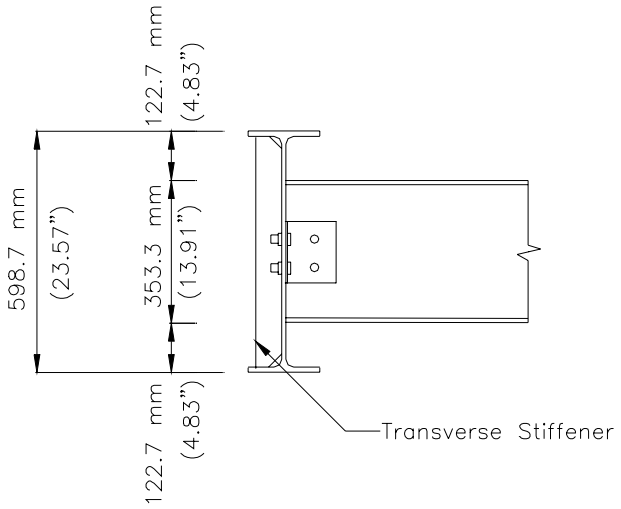

(b) Cross sectional view of outside beam

Figure 3.12 Bolted diaphragm-to-outside beam connection

Figure 3.13 Welded connection from experimental test

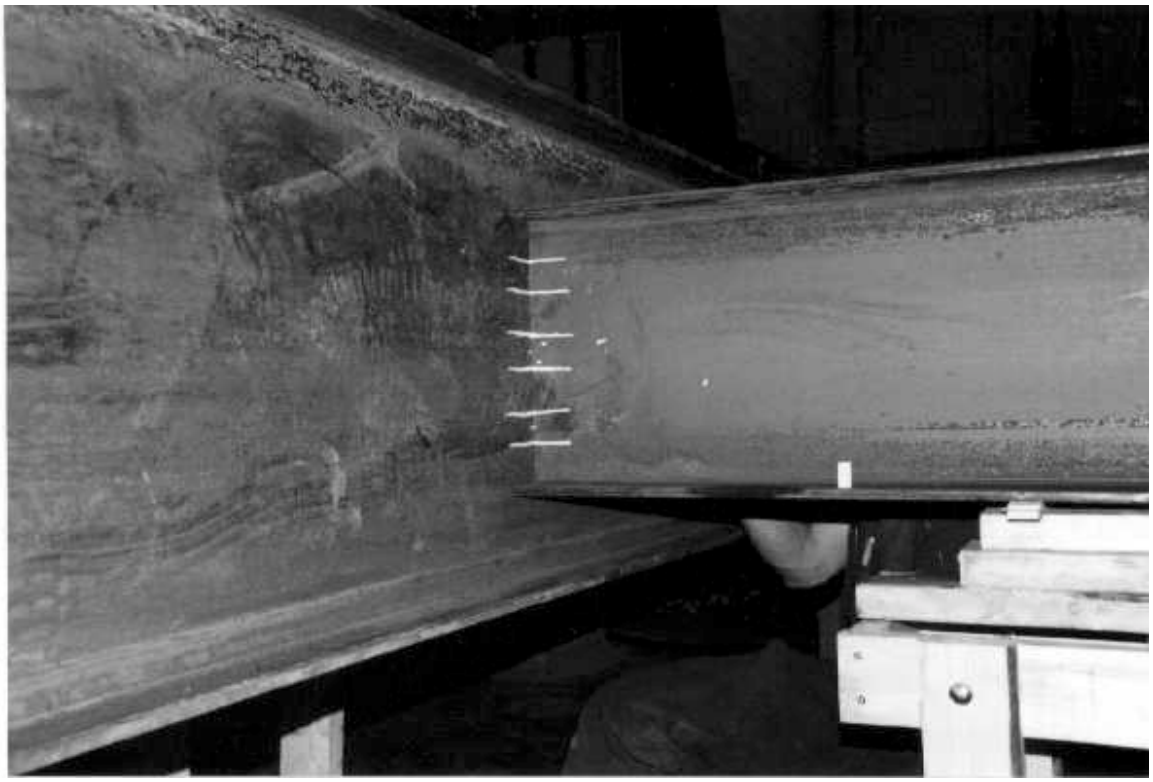

Figure 3.14 First step in weld procedure: mark the weld placement

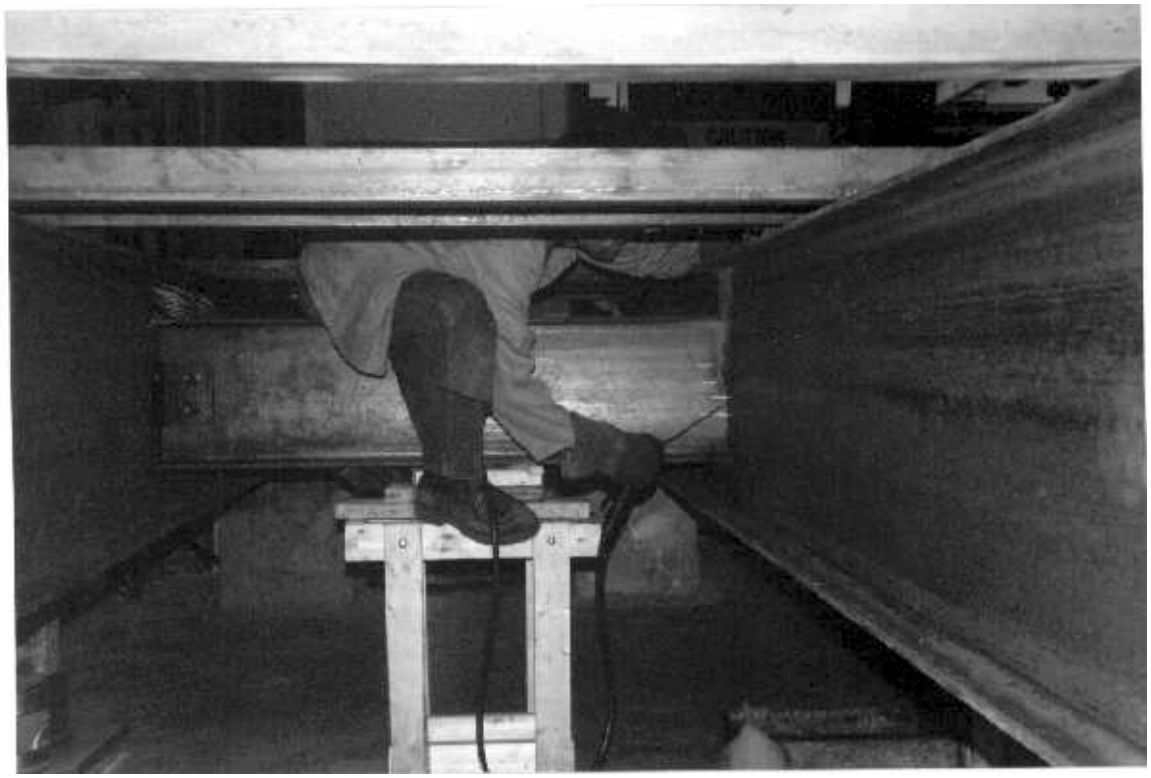

Figure 3.15 Second step in weld procedure: place the weld

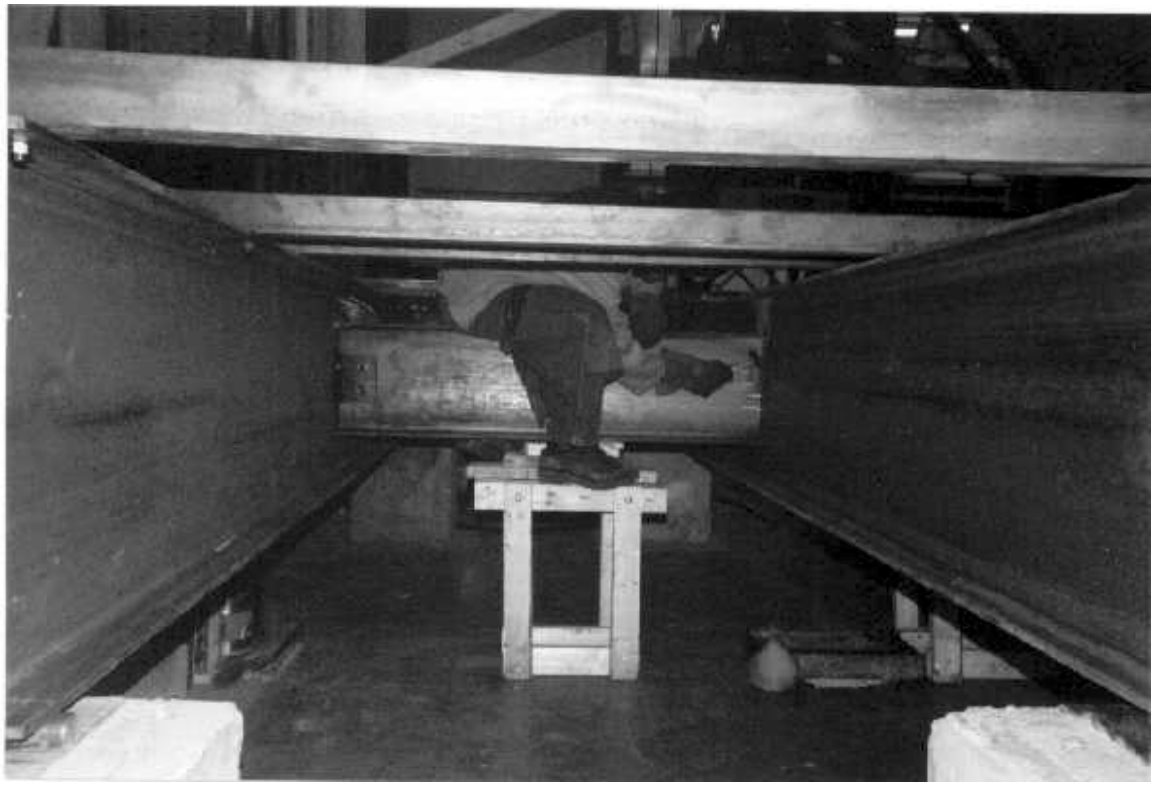

Figure 3.16 Third step in weld procedure: chip the slag from the weld

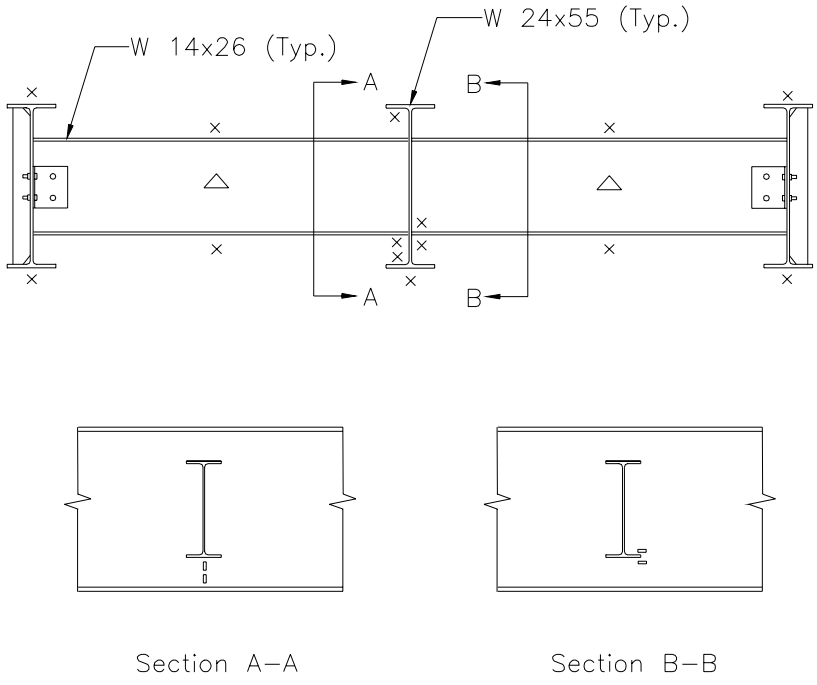

Figure 3.17 Strain gage layout for non-staggered diaphragms for tests with 1468 kN (330 kip) actuator

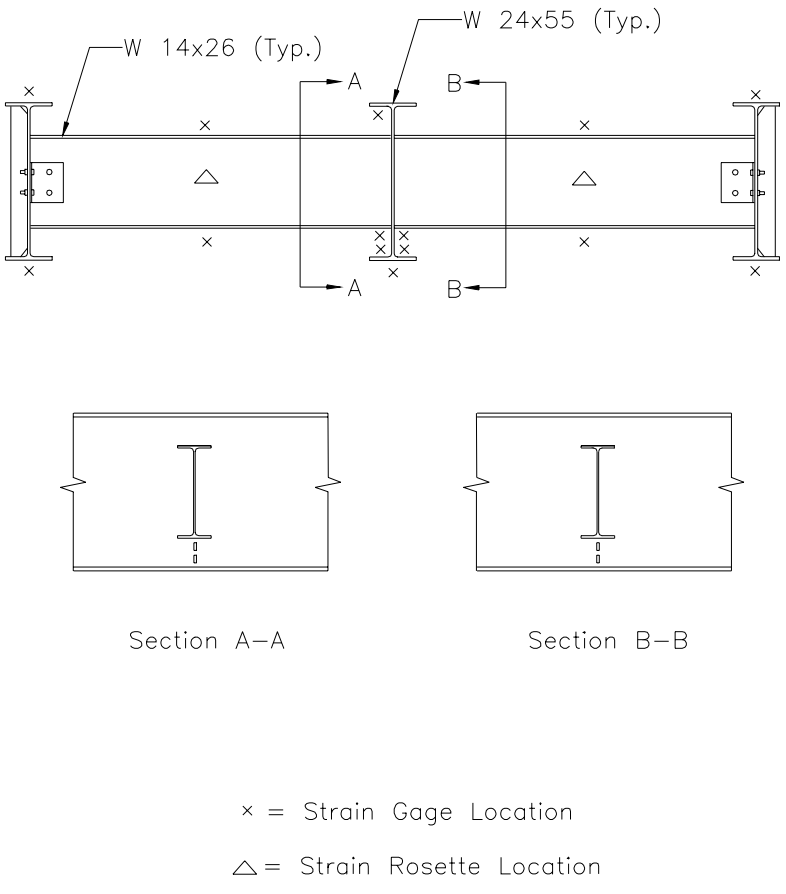

Figure 3.18 Strain gage layout for staggered diaphragms
for tests with 1468 kN (330 kip) actuator

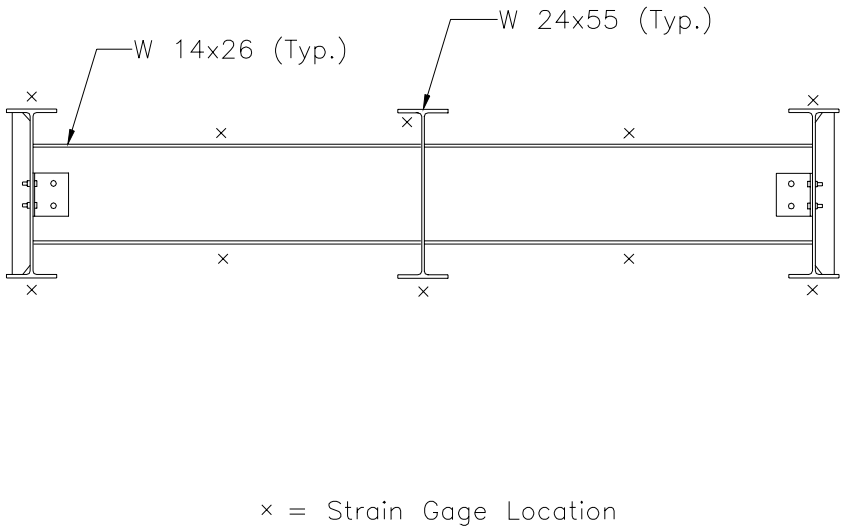

Figure 3.19 Strain gage layout for tests with 979 kN (220 kip) actuator

CHAPTER 4

EXPERIMENTAL RESULTS

The specimen identification consists of two pairs of letters and a number. The first pair of letters indicates the stagger condition of the diaphragms: *NS* = no stagger, *SC* = stagger with applied load centered between the diaphragms, *SL* = stagger with load applied at one of the diaphragm locations. The second pair of letters indicates the repair or retrofit technique: *NR* = no repair, *FH* = flame cut diaphragm and drill holes at beam crack tips, *FP* = flame cut diaphragm and peen bottom flange weld areas, and *LP* = leave diaphragm in place and peen bottom flange weld areas. The number in parentheses corresponds to the range of applied load in kips.

A summary of the crack history and measurement results is provided below for the experimental tests. The transverse stresses presented were calculated using the longitudinal strains in the beam and a Poisson's ratio value of 0.3. The weld measurements are provided in Appendix B for all of the tests. A detailed summary of the measured crack sizes and number of loading cycles sustained for each test specimen is given in Appendix C. Appendix D contains all of the static measurements for the tests.

4.1 NS-NR(30)

The test was performed using the 1468 kN (330 kip) actuator. The diaphragms were located at midspan and were not staggered. The test load range was 133 kN (30,000 lbs.) applied at a frequency of 2 Hz; the load was applied at midspan and varied from 14.8 kN to 148 kN (3,333 lbs. to 33,333 lbs.). The test was stopped, prior to failure, at 8 million cycles.

4.1.1 Crack History

A crack was observed in the east bottom flange weld of the south connection (SE) at 200,000 cycles. It was 25.4 mm (1 in.) long and was located along the throat of the weld. There was also a 6.4 mm (0.25 in.) crack at the toe of this weld along the diaphragm leg. At 300,000 cycles, a 6.4 mm crack was detected in the throat of the bottom west web weld for the south connection. The web weld fractured at 602,200 cycles. The cracks in the SE bottom flange weld were 31.8 mm (1.25 in.) along the throat and 15.9 mm (0.625 in.) along the toe. The crack along the toe extended toward the diaphragm fillet area.

A 6.4 mm crack was observed in the bottom west web weld of the north connection (NW) at 705,200 cycles. The bottom flange weld at the SW connection fractured at 1,597,000 cycles. The bottom NW web weld was 12.7 mm (0.5 in.) at this stage.

Numerous welds were severed at 1,640,844 cycles: all web welds of the N connection, top web weld at SW, and bottom web weld on the SE.

Beam cracks parallel to the stress field were observed after 3,007,000 cycles. The cracks were located approximately 343 mm (13.5 in.) from the top of the beam and were 12.7 mm on the west side of the north connection and 25.4 mm on the east side of the south connection.

A weld crack was found in the NW bottom flange at 3,590,000 cycles. At 6,184,200 cycles both of the bottom flange welds severed for the north connection. The beam cracks were 66.7 mm (2.625 in.) NE side, 92 mm (3.625 in.) NW side, 50.8 mm (2 in.) SE side, and 34.9 mm (1.375 in.) SW side. The test was stopped, prior to failure, at 8,000,000 cycles as the beam cracks had not changed after the north bottom flange welds fractured. Figure 4.1 shows the locations of the weld cracks and the beam cracks.

The uncracked web welds on the south diaphragm and the bottom flange welds of the north diaphragm may have caused the horizontal crack in the test beam. The welds act as fixed points that pull the beam web out of plane. An illustration of the undeformed web and the deformed web may be seen in Fig. 4.2. As load is applied to the test beam, the welds that are not severed act as fixed points pulling the beam web and creating areas of tension. The beam web is bent into double curvature with the fixed points being the top flange welds, south middle web welds, and north bottom flange welds. The deformation of the web causes out-of-plane bending stresses to develop which then caused a crack to form in the beam. When the north bottom flange welds severed at 6,184,200 cycles, the beam web was no longer bent into double curvature thus the beam cracks did not continue to grow.

4.1.2 Static Measurements

A graphical summary of the static load cell measurements can be seen in Fig. 4.3. The static load measurements indicate the test beam carried approximately 64% of the applied load (93 kN of 148 kN applied) before the onset of fatigue cracks. The readings show a slight increase in the test beam load up to 1.5 million cycles. The static load cell measurement at 1,597,000 cycles shows an increased load carried by the test beam which corresponds with both bottom flange welds being severed for the south diaphragm. There was a significant increase in the load carried by the test beam at 1,640,884 cycles when numerous welds were severed for both the north and south diaphragm connections. After this point the load in the test beam was approximately 85% of the applied load (126 kN of 148 kN applied). When the north bottom flange welds fractured at 6,184,200 cycles, the load carried by the test beam increased again.

Before the welded connections developed cracks, the diaphragms distributed load to the two outside beams. The strain gages on the beams and diaphragms clearly illustrate the decreased load transfer when the welded connections fractured (shown in Figs. D.3 and D.4).

Figure 4.4 illustrates the out-of-plane stresses that were calculated from the gages located in the beam web gap region between the bottom flange of the diaphragm and beam. The stresses indicate the gap region is being bent in double curvature up to 1,640,844 cycles. Between 1,640,844 and 6,184,200 the web gap is in single curvature bending as shown in Fig. 4.4. After the north bottom flange welds sever at 6,184,200, the web gap goes back into double curvature bending.

4.2 NS-NR(45) #1

For this test the diaphragms were not staggered and were located at midspan of the test beam. The test load range was 200 kN (45,000 lbs.) applied at a frequency of 1.25 Hz. The load was applied at midspan of the beam using the 979 kN (220 kip) actuator and varied between 22.2 kN and 222 kN (5,000 lbs. and 50,000 lbs.). The test was stopped at 5,660,000 cycles.

4.2.1 Crack History

Weld cracks formed in the all of the web welds and bottom flange welds in the south connection. After 27,000 cycles, the bottom flange welds had fractured as well as the west web welds and the bottom east web weld. By 32,000 cycles, all the web welds were fractured at the south connection. No cracks were observed in the welds for the north connection.

A 60.3 mm (2.375 in.) beam crack parallel to the stress field was observed after 1,704,800 cycles. The crack developed approximately 127 mm (5 in.) from the top flange of the beam. The north diaphragm was approximately 25.4 mm lower than the south diaphragm. The beam crack that developed parallel to the stress field was located along the toe of the top flange weld of the north diaphragm.

Beam cracks perpendicular to the stress field developed at the toe of each of the bottom flange welds for the north diaphragm. The crack on the east side of the north diaphragm was first observed after 1,806,700 cycles of loading with a crack length of 19

mm (0.75 in.). The crack on the west side was observed after 1,914,000 cycles when it was 3 mm (0.125 in.) long.

Figure 4.5 shows the location of the weld cracks and the beam cracks at the end of the test. The test was stopped at 5,660,000 cycles due to mechanical difficulty. The horizontal beam crack was 238 mm (9.375 in.). The NE crack was 264 mm (10.375 in.) and extended to the base of the beam fillet and the NW crack was 79 mm (3.125 in.).

4.2.2 Static Measurements

Figure 4.6 shows a graphical summary of the static beam strain measurements for the test beam and the two outside beams. One of the welded connections fractured quickly and the test beam strain jumped from 436 με to 620 με. The strain in both outside beams dropped from 119 με to 15 με. Although the welds in the north connection did not fracture, the load transferred through this diaphragm dropped when the south connection fractured.

The test beam strains began increasing at approximately 2.5 million cycles. The strain increase correlates with significant crack propagation in the beam. The crack in the beam on the east side of the diaphragm at the north connection began propagating towards the tension flange of the test beam.

4.3 NS-NR(45) #2

For this test the diaphragms were located at midspan and were not staggered. The test load range was 200 kN (45,000 lbs.) and was applied at a frequency of 1.0 Hz. The

load was applied at midspan of the test beam using the 979 kN (220 kip) actuator and varied between 22.2 kN and 222 kN (5,000 lbs. and 50,000 lbs.). The test was stopped at 6,000,000 cycles.

4.3.1 Crack History

The east bottom flange weld for the south connection severed by 8300 cycles and the west bottom flange weld severed by 11,000 cycles. All of the web welds for the south connection were severed by 19,000 cycles. At 1,500,000 cycles the top flange weld on the south connection was found cracked and the diaphragm was removed from the setup. No cracks were observed in the welds for the north connection.

A beam crack parallel to the stress field was observed after 1,747,500 cycles when it was 137 mm (5.375 in.) long. The crack developed approximately 127 mm (5 in.) from the top flange of the beam along the toe of the top flange weld. The crack propagated to a length of 203 mm (8 in.) and did not prove detrimental to the beam.

A beam crack perpendicular to the stress field developed at the toe of the east bottom flange weld for the north diaphragm. The crack was 6.4 mm when it was first observed after 2,430,600 cycles. The crack was 92 mm (3.625 in.) at the end of the test.

Figure 4.7 illustrates the weld cracks and beam cracks at the end of the test. The test was stopped, prior to failure, at 6,000,000 cycles since the beam crack appeared to be non-propagating.

4.3.2 Static Measurements

A graphical summary of the static beam strain measurements can be seen in Fig. 4.8. As in the previous NS tests, the test beam strain increased (435 με to 640 με) when one of the welded connections split. There is a slight change in the measured strain values at 1,500,000 cycles when the south top flange weld fractured.

4.4 NS-FP(45)

The diaphragms were not staggered and were located at midspan of the test beam. The test load was applied at midspan of the test beam using the 979 kN (220 kip) actuator and varied between 22.2 kN and 222 kN (5,000 lbs. and 50,000 lbs.) at a frequency of 1 Hz. The test was retrofitted at 385,300 cycles and was stopped at 4,476,794 cycles due to equipment difficulty.

The goal of this test was to evaluate the retrofit method of flame cutting the diaphragm and peening the bottom flange weld areas. Based on the results of the previous nonstaggered diaphragms where horizontal cracks developed along the toe of the top flange welds, it was decided to also peen the top flange weld area. The retrofit was performed after the welds were severed, but before cracks were present in the test beam. Peening was performed using a hardened tool and a pneumatic hammer operated at 0.28 MPa (40 psi). Six complete passes were performed around the weld, with each successive pass causing additional deformation in the base metal and along the weld toe. Figure 4.9 shows the areas around the welds that were peened. Figures 4.10 and 4.11 are photographs of the top and bottom weld areas that were peened. During the peening

process, a 22.2 kN (5,000 lb.) load was applied to the beam which corresponds to a maximum stress of 13.8 MPa (2 ksi) at the bottom flange of the beam.

4.4.1 Crack History

The west bottom flange weld of the south connection was found severed at 6,300 cycles. At 14,130 cycles the east bottom flange weld and all of the web welds were severed for the south connection. No cracks were observed in the welds for the north connection.

This test was performed after a similar repair test with staggered diaphragms where the bottom flange weld areas were peened and the diaphragm was left in place. For the staggered diaphragm test, the bottom flange weld areas were peened at 385,300 cycles. It was decided to retrofit the nonstaggered diaphragms at the same number of cycles.

Cyclic loading was resumed after the south diaphragm was removed and the welded flange areas were peened at both connections. The test was stopped at 4,476,794 cycles (more than 4 million cycles after retrofit) due to equipment difficulties. No cracks were evident in the beam web at the end of the test.

4.4.2 Static Measurements

A summary of the static beam strain measurements can be seen in Fig. 4.12. The vertical dashed line represents the time of the retrofit. The graph shows that the load distribution to both outside beams changed drastically when the welds fractured at the

south connection. Although no welds fractured for the north connection, the load transferred to the north outside beam also dropped. The static strain measurements remained nearly constant after the retrofit.

4.5 SC-NR(30)

The diaphragms were offset 1219 mm (4 ft.) and the test load was applied at midspan of the test beam using the 1468 kN (330 kip) actuator. For this test, the diaphragms were each 610 mm (2 ft.) away from the applied load. The load range was 133 kN (30,000 lbs.) at a frequency of 2 Hz; the applied load varied between 14.8 kN and 148 kN (3,333 lbs. and 33,333 lbs.). The test ended at 8,772,046 cycles when the beam tension flange fractured.

4.5.1 Crack History

The only weld that developed a visible crack was the west bottom flange weld at the toe on the north diaphragm. It was detected at 3,555,000 cycles and only grew to 12.7 mm (0.5 in.).

Two beam cracks that were perpendicular to the stress field were also observed at 3,555,000 cycles at both the north and south connections. The crack at the NE connection was 41.2 mm (1.625 in.) and the SW crack was 66.7 mm (2.625 in.). Each of the beam cracks was located at the toe of one of the two bottom flange welds as seen in Fig. 4.13. An unexpected behavior was observed regarding the growth of the beam cracks. The cracks were propagating faster towards the neutral axis of the beam rather

than the bottom flange. It is suspected that this phenomenon is due to twisting of the test beam.

The test ended at 8,772,046 cycles when the west beam crack at the south connection fractured the bottom flange of the test beam. The beam crack at the north connection was 146 mm (5.75 in.).

4.5.2 Static Measurements

A graphical summary of the static load cell measurements is shown in Fig. 4.14. The static load cell measurements illustrate the test beam carried 93% of the applied load throughout the test. Although the welded connections did not fracture, very little of the applied load is transferred to the outside beams through the staggered diaphragms.

The transverse stresses in the web gap between the bottom flange of the diaphragm and bottom flange of the beam are shown in Fig. 4.15. The stresses at the south connection are of the same sense and indicate single curvature bending. However, those at the north connection go from single curvature to double curvature as the beam crack at the south connection grows. Once the beam crack reached the bottom fillet, the north connection web gap changed to single curvature bending again.

4.6 SC-NR(45)

The diaphragms were staggered 1219 mm (4 ft.) and the test load was applied at midspan of the test beam using the 1468 kN (330 kip) actuator. For this test, the diaphragms were each 610 mm (2 ft.) away from the applied load. The load range was

200 kN (45,000 lbs.) at a frequency of 1.5 Hz; the applied load varied between 22.2 kN and 222 kN (5,000 lbs. and 50,000 lbs.). The test ended at 4,182,467 cycles.

4.6.1 Crack History

No cracks were visible in the welds at the end of the test. This behavior is significantly different than the no-staggered tests where the intermittent web welds fractured rather quickly.

Two cracks were detected at 277,000 cycles around the toe of the bottom flange welds on the east side of the north diaphragm as well as the west side of the south diaphragm. At 510,700 cycles each of the cracks was observed to be in the beam. The crack at the bottom flange of the north diaphragm propagated more quickly than the south connection crack. The crack at the north connection fractured the bottom flange at 2,649,537 cycles. The crack at the south connection was 73 mm (2.875 in.) long at this stage.

In order to allow the crack to propagate at the south connection, a 27 mm (1.0625 in.) diameter hole was drilled in the beam web at the north connection crack tip. To repair the fractured flange, a bolted splice attachment that consisted of 11.1 mm (0.4375 in.) top plates and a 12.7 mm (0.5 in.) bottom plate was attached to the flange with twelve 22.2 mm (0.875 in.) diameter A325 high-strength bolts. The bolts were fully tightened by the turn-of-the-nut procedure to prevent significant deformation of the repaired region. A photograph of the repair is shown in Figure 4.16.

The crack at the south connection propagated until fracturing the flange at 4,182,467 cycles. Figure 4.17 shows the location of the beam cracks.

As in the previous test with staggered diaphragms, SC-NR(30), the beam cracks were propagating faster towards the neutral axis of the beam rather than the flange.

4.6.2 Static Measurements

The static measurements for this test, shown in Fig. 4.18, follow a similar pattern as SC-NR(30). The test beam carried 93% of the applied load throughout the test. The open symbols in the figures represent the measurements that were performed after the beam was repaired at the north connection. Little change occurred in the load distribution after the repair.

The transverse stresses in Fig. 4.19 also follow a similar trend as SC-NR(30). The out-of-plane stresses in the south connection web gap are changing as the beam crack grows at the north connection. As the north crack grows, the stress range in the south connection web gap changes and the web gap changes from single curvature to double curvature bending. During this time, the out-of-plane stresses in the north connection web gap remain nearly constant. When the crack is growing at the south connection later in the test, the north connection out-of-plane stresses are then changing.

4.7 SL-NR(45)

The diaphragms were staggered 1219 mm (4 ft.) with one of the diaphragms located at midspan of the test beam where the load was applied using the 1468 kN (330

kip) actuator. The applied load range was 200 kN (45,000 lbs.) at a frequency of 1.5 Hz; the load varied between 22.2 kN and 222 kN (5,000 lbs. and 50,000 lbs.). The test was stopped, prior to failure, at 6,550,000 cycles.

4.7.1 Crack History

No cracks were visible in any of the web or flange welds at the end of testing.

Two cracks around the toe of each of the bottom flange welds for the north diaphragm were detected at 615,900 cycles - see Fig. 4.20 for the location of the beam cracks. At 849,000 cycles, the crack was observed to be in the beam on the west side of the north diaphragm (NW). The crack on the east side of the north diaphragm (NE) was observed in the beam at 1,104,700 cycles at which time the NW crack was 19 mm (0.75 in.). The east crack propagated to 50.8 mm (2 in.) while the west crack grew to a length of 98.4 mm (3.875 in.) at the end of the test.

A 6.4 mm (0.25 in.) crack was detected at the toe of the west bottom flange of the south diaphragm (SW) at 4,138,000 cycles. At 5,545,900 cycles a 50.8 mm (2 in.) crack was found on the east side of the bottom flange of the south diaphragm (SE). The cracks had not changed in length at the end of the test.

4.7.2 Static Measurements

The load cell measurements are shown in Fig. 4.21. The distribution of load to the outside beams was similar to the case where each diaphragm was 610 mm (2 ft.) from the applied load. Although the north diaphragm was located at the point of load

application, the strains in the diaphragm were about the same as those in the south diaphragm – graphs shown in Appendix Figs. D.24 and D.25.

The out-of-plane stresses are shown in Fig. 4.22. The graph indicates some out-of-plane bending did occur.

4.8 SC-FH(45)

The diaphragms were each staggered 610 mm (2 ft) from the applied load. The test load was applied at midspan with a range of 200 kN (45,000 lbs.) at a frequency of 1.5 Hz using the 1468 kN (330 kip) actuator. The maximum applied load was 222 kN (50,000 lbs.) and the minimum was 22.2 kN (5,000 lbs.). The test was repaired at 1,785,100 cycles and was stopped at 6,000,000 cycles.

The purpose of this test was to evaluate the repair procedure in which the diaphragm is flame cut and holes are drilled at the beam crack tips. The welded end of the diaphragm was flame cut to a length of 229 mm (9 in.) and the bolted end was disconnected; the diaphragm was then removed. The holes drilled at the crack tips were sized according to work described previously to minimize the stress concentration. For this study 38.1 mm (1.5 in.) diameter holes are drilled at the beam crack tips which corresponds to a 50.8 mm (2 in.) crack. Figure 4.23 shows a sketch of the repair and Fig. 4.24 is a photograph of the laboratory repair.

4.8.1 Crack History

No cracks were detected in any of the welds at the end of the test.

Beam cracks developed at the toe of each of the bottom flange welds for both the north and south connections. Cracks were detected at the bottom flange welds of the south connection after 1,032,000 cycles. The SW crack was 12.7 mm (0.5 in.) long and the SE crack was 6.4 mm (0.25 in.) long. After 1,570,900 cycles a crack was detected at the east bottom flange weld of the north connection (NE) that was 9.5 mm (0.375 in.) in length.

The crack at the bottom flange on the west side of the south connection (SW) was repaired at 1,785,100 cycles; this was the only crack that was repaired. At this stage the crack was 60.3 mm (2.375 in.) long. The crack at both the east bottom flange of the south connection (SE) and the east bottom flange of the north connection (NE) was 9.5mm long.

A 9.5 mm crack was detected on the west bottom flange of the north connection (NW) at 2,186,400 cycles which was not repaired.

The test was stopped at 6,000,000 cycles (4.2 million cycles after the repair at the SW crack) at which time the SE crack was 47.6 mm (1.875 in.), the NE crack was 9.5 mm, and the NW crack was 57.2 mm (2.25 in.) (Fig. 4.25).

4.8.2 Static Measurements

A graph summarizing the static load cell measurements is shown in Fig. 4.26. The vertical dashed line represents the time of the repair. The graphs indicate a slight increase in the load carried by the test beam after the repair. The deflection and strain measurements are given in Appendix Figs. D.27 to D.31. The midspan deflection as well

as the beam deflection at the north diaphragm also increased after the repair at the south diaphragm connection. The strains in the north diaphragm and outside beam decreased after the south diaphragm was removed. Strain was still measured in the south outside beam, shown in Fig. D.30, after diaphragm removal because of the six angles across the top flanges of the three beams.

Fig. 4.27 illustrates the calculated stresses from the strain gages located in the web gap region between the bottom flange of the diaphragm and the bottom flange of the beam. The gages are positioned transverse to the primary bending stress in the beam thus measuring the out-of-plane strain in the beam web. The graph shows a reduction in the out-of-plane stresses in the web gap region at each diaphragm location after the repair. After the repair, the gap regions were being bent in double curvature; thus, cracks were able to continue to propagate at the weld toes. However, the stresses were low so the cracks were not propagating quickly.

4.9 SC-LP(45)

The diaphragms were each staggered 610 mm (2 ft.) from the applied load. The test load was applied at midspan using the 1468 kN (330 kip) actuator with a range of 200 kN (45,000 lbs.) at a frequency of 1.5 Hz. The maximum load was 222 kN (50,000 lbs.) and the minimum was 22.2 kN(5,000 lbs.). The test was stopped at 4,947,709 cycles due to mechanical difficulties.

The purpose of this test was to evaluate a retrofit procedure in which the diaphragms are left in place and the bottom flange weld areas are peened. Peening was

performed using the method described previously for the NS-FP(45) test. The peening area included the entire bottom flange weld area. The areas peened are shown in Fig. 4.28. During the peening process, a 22.2 kN (5,000 lb.) load was applied to the beam which corresponds to a maximum stress of 13.8 MPa (2 ksi) at the bottom flange of the beam.

4.9.1 Crack History

A beam crack 3.2 mm (0.125 in.) long was detected at the toe of the west bottom flange weld of the south connection (SW) at 385,300 cycles. Since peening is only effective for shallow depth cracks, the weld areas were peened at 385,300 cycles and the test was resumed.

Weld cracks were detected in the south connection at 1,419,300 cycles. The crack in the west bottom flange weld (SW) was 3.2 mm and the east bottom flange weld (SE) crack was 19.1 mm (0.75 in.). A 3.2 mm crack was detected in the east bottom flange weld of the north connection (NE) at 3,904,500 cycles. At the end of the test the NE weld crack was 3.2 mm, the SW weld crack was 9.5 mm and the SE weld crack was 28.6 mm. No cracks were evident in the beam web at the end of the test; the SW beam crack was arrested by peening. Figure 4.29 shows the crack locations at the end of the test which was 4.56 million cycles after retrofit.

4.9.2 Static Measurements

The load cell measurements are shown in Fig. 4.30. The vertical dashed line in the graph represents the time of the retrofit. As seen in the graph, very little change occurred in the measurements throughout the test.

The transverse stresses (shown in Fig. 4.31) indicate the web gap region was in single curvature bending throughout the test. The calculated stresses were tensile at both gages.

4.10 Discussion of Results

Figure 4.32 shows the stress range versus number of applied cycles at the end of the test for the beams tested. It should be noted that this is not an S-N curve since all of the beams did not fail. Only two of the beams failed - SC-NR(30) and SC-NR(45). There are two points plotted for SC-NR(45) since the beam failed at each of the diaphragm locations. The points marked with arrows indicate the test did not fail. It can be seen that most of the data points fall above a Category D detail and below a Category C.

4.10.1 Comparison of No Stagger Tests

4.10.1.1 NS-NR(30) and NS-NR(45)

For the diaphragms that are directly opposite, the tests indicate that load is transferred through the diaphragms to the outside beams. As the test progresses the

bottom flange welds are typically the first to fracture. Once the bottom flange welds fractured, the web welds severed soon thereafter. Figures 4.33 and 4.34 illustrate the fractured welds.

The back-to-back diaphragm connection behaves like a rigid connection. Diaphragms stiffen each side of the web and load is effectively transferred through the diaphragms. However, when the bottom flange welds and web welds sever, the rigidity of the connection no longer exists and the transferred load decreases through each of the diaphragms. Each of the no stagger tests indicates the decreased load transfer with the severing of one of the welded connections.

Each of the tests with back-to-back diaphragms experienced horizontal cracking in the beam web. The horizontal crack did not limit the fatigue life for the tests as the critical beam crack typically formed at the bottom flange weld toe. A photograph of a horizontal beam crack at the top flange is shown in Fig. 4.35.

4.10.1.2 Retrofit Method NS-FP(45)

The retrofit method investigated for the back-to-back diaphragms was effective in preventing beam cracks at both the top and bottom flange weld areas. Peening was performed before cracks were present in the beam. The test sustained approximately 4.1 million cycles of load after the retrofit without any evidence of cracks initiating in the beam.

4.10.2 Comparison of Stagger Tests

4.10.2.1 SC-NR(30), SC-NR(45) and SL-NR(45)

The tests with the staggered diaphragms behaved similarly. None of the welds fractured for any of the tests. Beam cracks typically developed at the toe of the bottom flange weld at each of the diaphragms as shown in Figure 4.36. The beam cracks grew towards the neutral axis of the beam as well as towards the tension flange. The crack growth rate between the SC tests and the SL test was different. The rate for the SL test was much slower than the SC tests and the cracks appeared to be non-propagating.

The static measurements for the tests show the test beam carried approximately 93% of the applied load and the diaphragms transfer little load to the adjacent beams. Even when one of the staggered diaphragms is located at the point of load application, little load is transferred to the outside girder.

4.10.2.2 Repair and Retrofit Methods SC-FH(45) and SC-LP(45)

The repair and retrofit methods investigated for the staggered diaphragms proved to be adequate in controlling the growth of beam cracks. In the previous tests with staggered diaphragms, cracks started in the beam at the toe of the bottom flange welds and eventually fractured the tension flange.

For the method of repair where holes are drilled at the beam crack tips, the beam crack was allowed to propagate to a length of 60.3 mm before the repair was performed.

The diaphragm was then flame cut and 38.1 mm diameter holes were drilled at the tips of the crack. Although this repair did not stop the propagation of cracks at other locations, the growth rate for the cracks at other locations was reduced. The drilled holes did arrest the fatigue crack that was repaired.

Peening the bottom flange weld toes proved to be an effective retrofit procedure in preventing the growth of beam cracks. In the test completed, peening was performed when the beam crack was still very small (3.2 mm) and before it propagated through the thickness of the beam web. Although some of the welds developed cracks after peening, the fatigue resistance of the beam was not affected. No cracks were present in the beam at the end of the test. The absence of cracks is quite significant because more than four million cycles were applied after the peening retrofit. In comparable tests where no retrofit was performed, four million cycles of loading was enough to fail the test beam.

4.10.3 Comparison of No Stagger and Stagger Tests

The diaphragms that are directly opposite act like a rigid connection and transfer load to the adjacent beams. The diaphragms stiffen each side of the beam web and act as a continuous member perpendicular to the loaded member. As long as the welded connection remains intact, the diaphragm transfers load through the system.

The staggered diaphragms do not stiffen the web, but instead pull the beam web out-of-plane. When load is applied to the beam, the diaphragms (being rigidly connected to the adjacent beam) cause the beam web to bend out-of-plane. Little load is transferred

through the staggered diaphragms since the system is able to deform with the load. Consequently, the welds for the staggered diaphragms seldom fractured.

Since the back-to-back setup is rigid, the welds are more prone to cracking. In fact, the welds for the no stagger setup often fractured rather quickly after a few thousand loading cycles. Moreover, the cracking resulted in the release in some rigidity at the connection. The bottom flange welds usually fractured first, followed by severing of the web welds. When one of the welded connections cracks, the no stagger setup behaves like a stagger setup and the load transfer through the uncracked connection decreases.

The stagger setup is likely to develop cracks in the beam at the toe of a bottom flange weld. The cracks propagate in two directions, both towards the beam neutral axis and towards the tension flange.

4.10.4 Comparison of Repair Methods

The repair methods can be divided into two categories: retrofit the beam to prevent crack initiation (SC-LP(45) and NS-FP(45)) and repair a crack present in the beam (SC-FH(45)). The staggered diaphragms cause a high out-of-plane bending stress in the beam web since the diaphragms pull the beam web out-of-plane. The back-to-back diaphragms do not produce as large an out-of-plane bending stress.

The staggered diaphragm configuration is more critical for beam crack initiation than the back-to-back setup. Cracks initiated in the beam webs for the stagger arrangements much earlier than the no stagger arrangements. The welded connections

fractured for the back-to-back setup, but this did not seriously affect the fatigue life of the beam members.

The retrofit performed for the offset diaphragms, peening of the bottom flange weld toes and leaving the diaphragms in place, was effective in preventing crack initiation in the beam. The SC-LP(45) test sustained more than 4 million load cycles after the repair with no beam cracks visibly detected at the end of the test. A similar peening retrofit was performed on the back-to-back diaphragm arrangement; however, one of the diaphragms was flame cut and removed from the system. The NS-FP(45) test also sustained more than 4 million load cycles with no visible beam cracks detected at the end of the test.

The staggered diaphragm configuration is the most critical in terms of cracks initiating in the beam. Since the retrofit of leaving the diaphragm in place and peening the bottom flange welds was effective in preventing crack initiation for the staggered case, diaphragm removal is not necessary.

When a crack is detected in the beam, holes should be drilled at the beam crack tips to reduce the crack tip concentration. The diaphragm, however, does not need to be removed.

4.11 Conclusions

Both beams with a test load range of 133 kN (30,000 lbs.) sustained more than 8 million cycles of load without failing. This is significant because the magnitude of the applied load is quite high compared with the axle weights (and wheel loads) typically observed

through field surveys. Moreover, this load magnitude resulted in a stress range at the diaphragm connection that is estimated to be higher than would typically occur in a bridge member in the field.

The experimental tests have shown that even though cracks may develop in the welds, the system does not fail immediately. When the diaphragms were directly opposite of each other, many of the web and flange welds connecting the diaphragms to the beam fractured. Horizontal cracking occurred in the beam webs but did not affect the fatigue resistance. When one of the welded connections fractured, the load transfer through the still-connected diaphragm decreased.

In the tests with the staggered diaphragms, cracks perpendicular to the stress field developed in the beam webs at the toe of a bottom flange weld. However, the beams did not fracture immediately. Very little load is transferred through the diaphragms when they are staggered.

The repair and retrofit methods investigated proved adequate to increase the fatigue life of the beam. Peening the flange areas before the onset of beam cracks did prevent cracks from forming for both the nonstaggered and staggered diaphragms. When a crack was present in the beam web, drilling holes at the crack tips did arrest the crack growth.

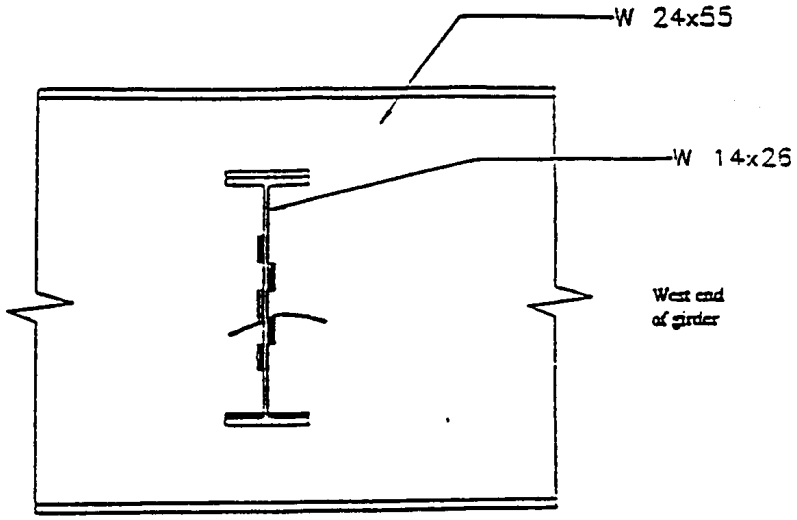

(a) North diaphragm connection

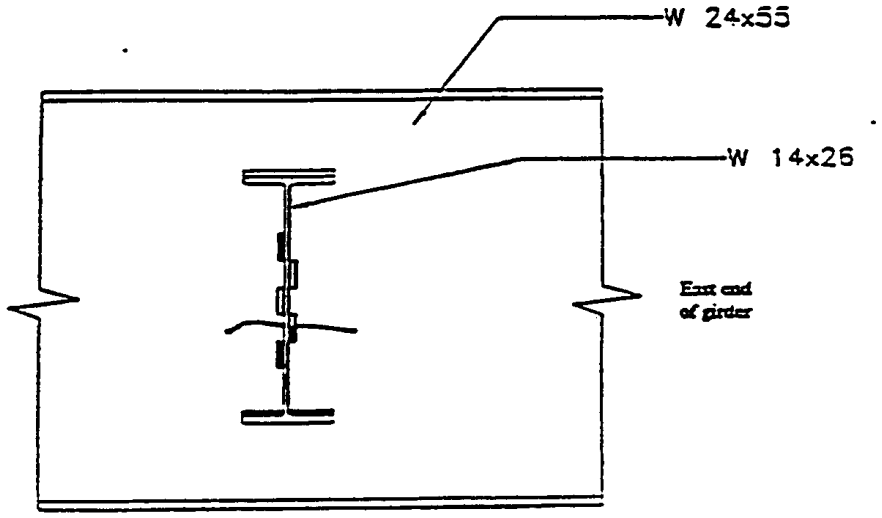

(b) South diaphragm connection

Figure 4.1 NS-NR(30) Crack locations

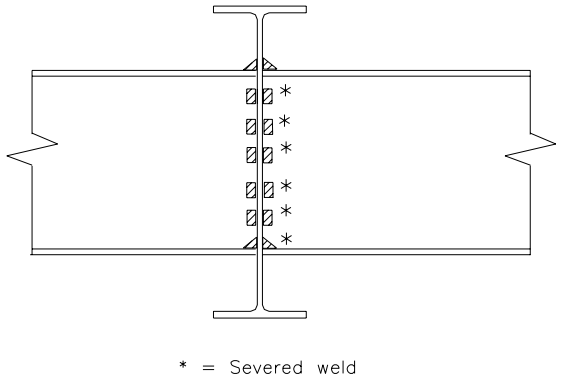

(a) Undeformed beam

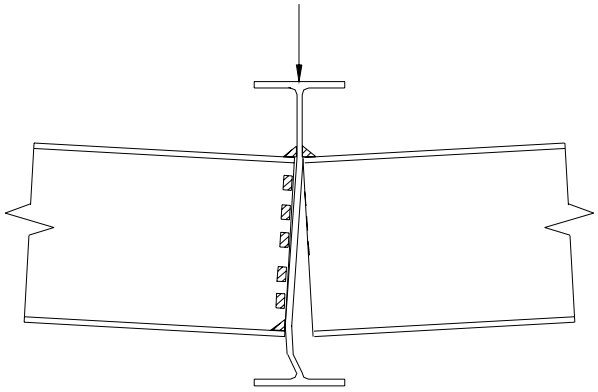

(b) Deformed beam (exaggerated)

Figure 4.2 Exaggerated illustration of NS-NR(30) beam web

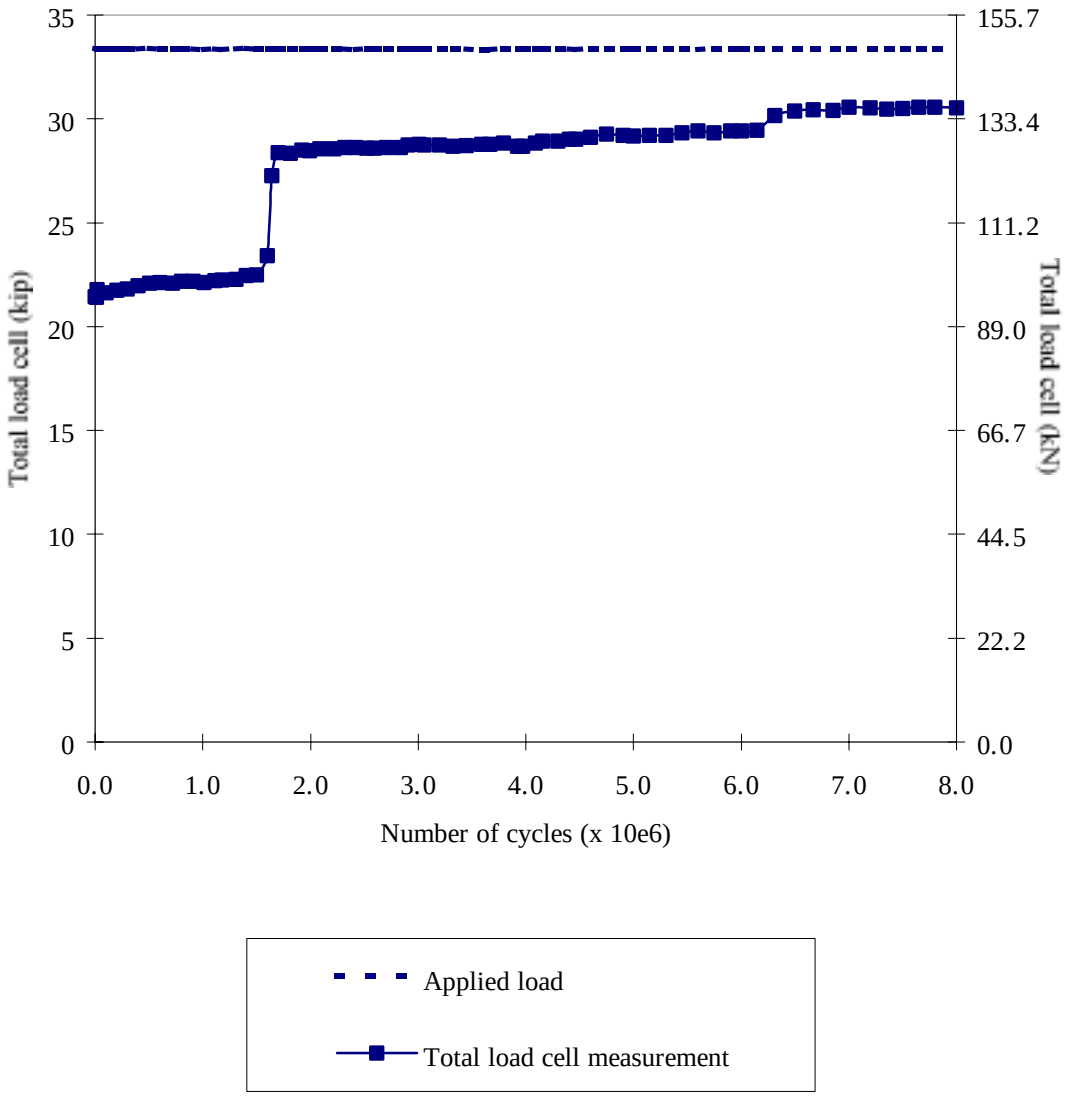

Figure 4.3 Static load cell measurements for NS-NR(30)

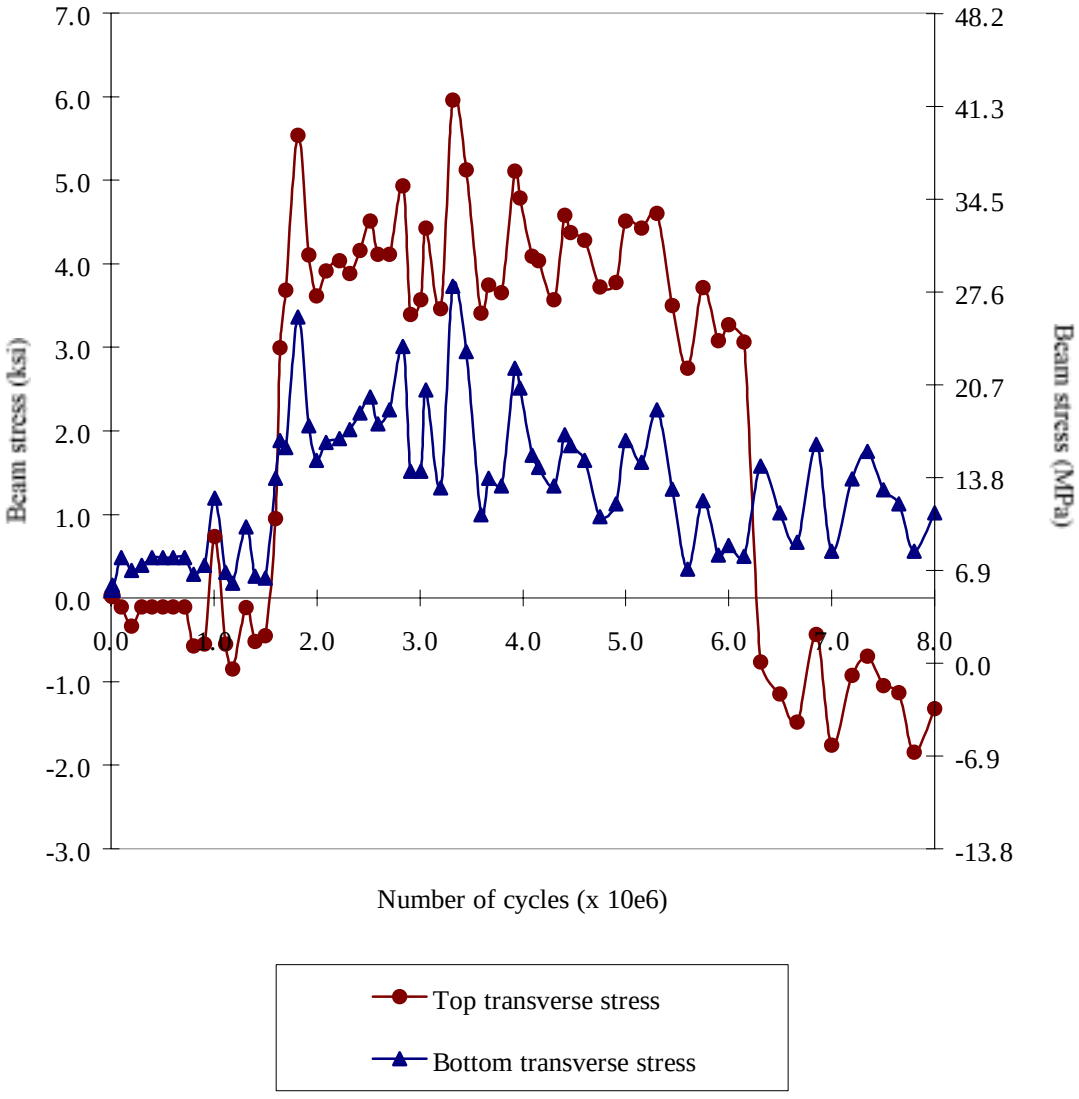

Figure 4.4 Transverse beam stresses in north web gap for NS-NR(30)

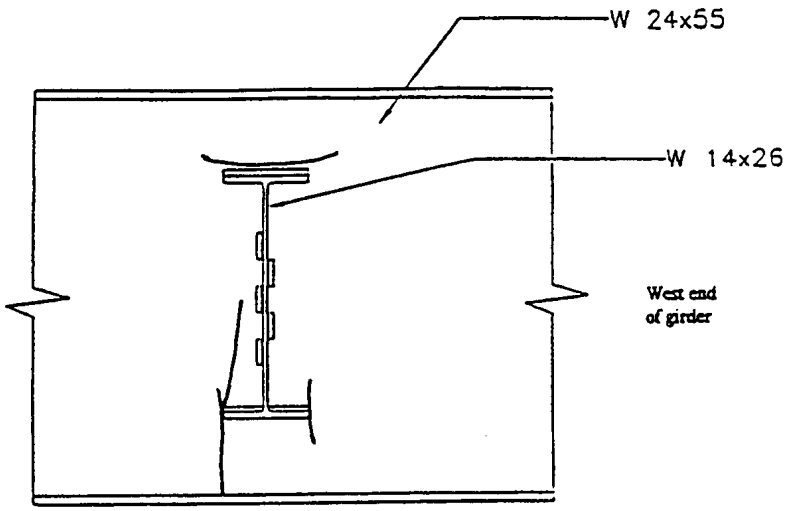

(a) North diaphragm connection

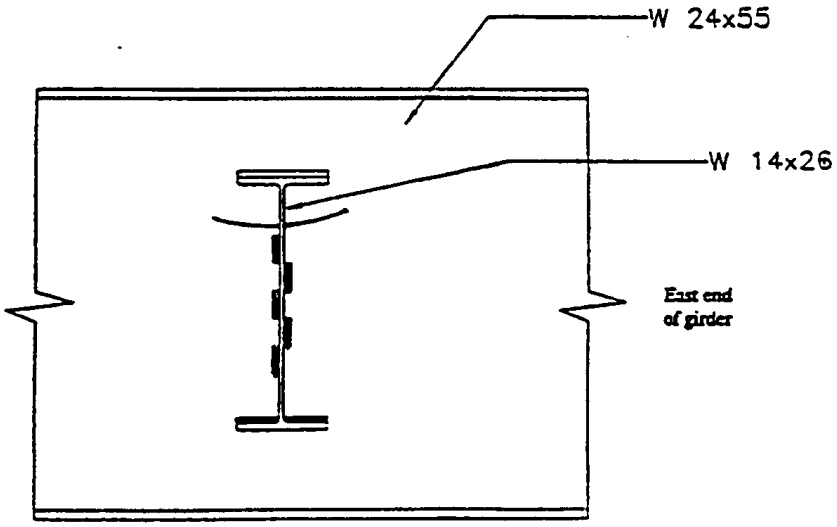

(b) South diaphragm connection

Figure 4.5 NS-NR(45) #1 Crack locations

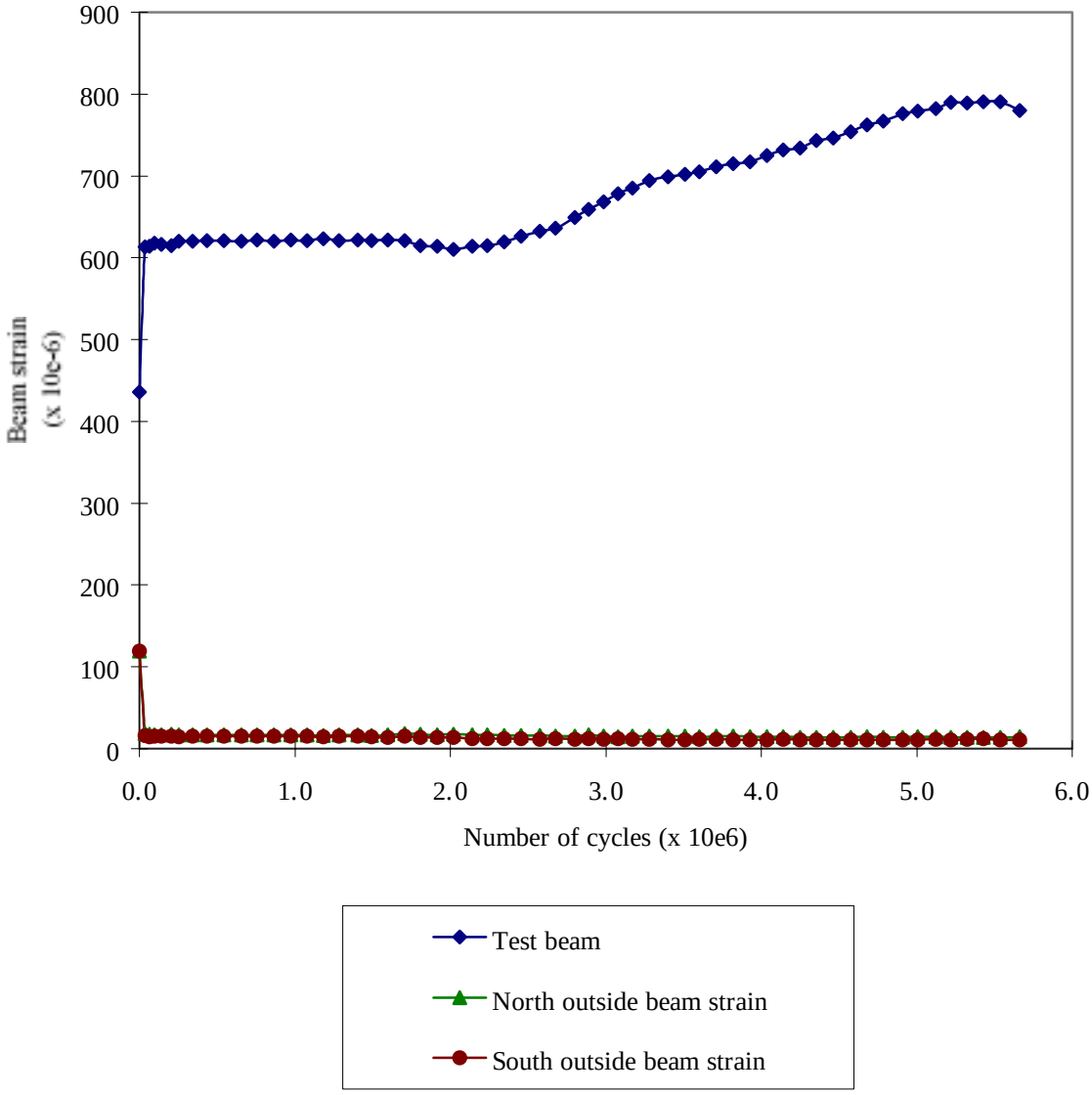

Figure 4.6 Longitudinal beam strain measurements for NS-NR(45) #1

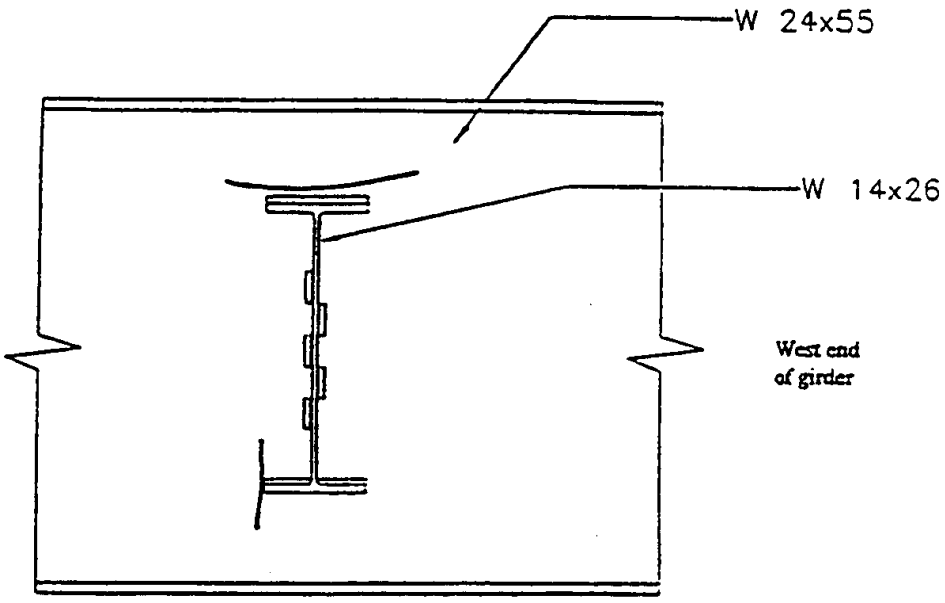

(a) North diaphragm connection

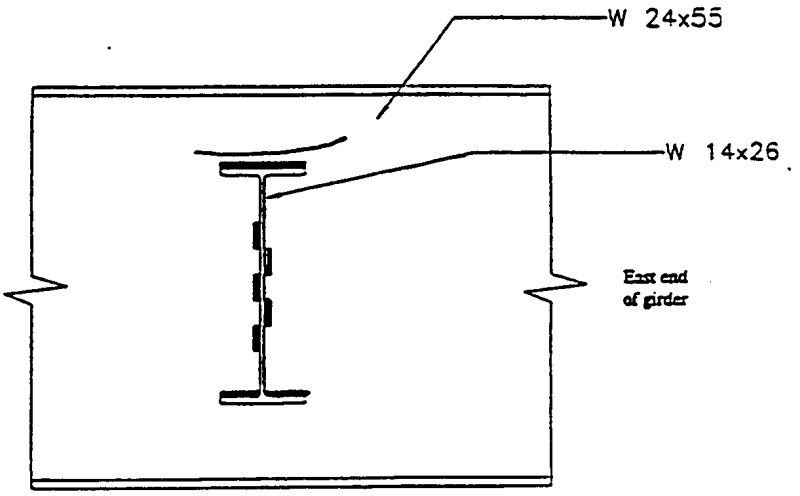

(b) South diaphragm connection

Figure 4.7 NS-NR(45) #2 Crack locations

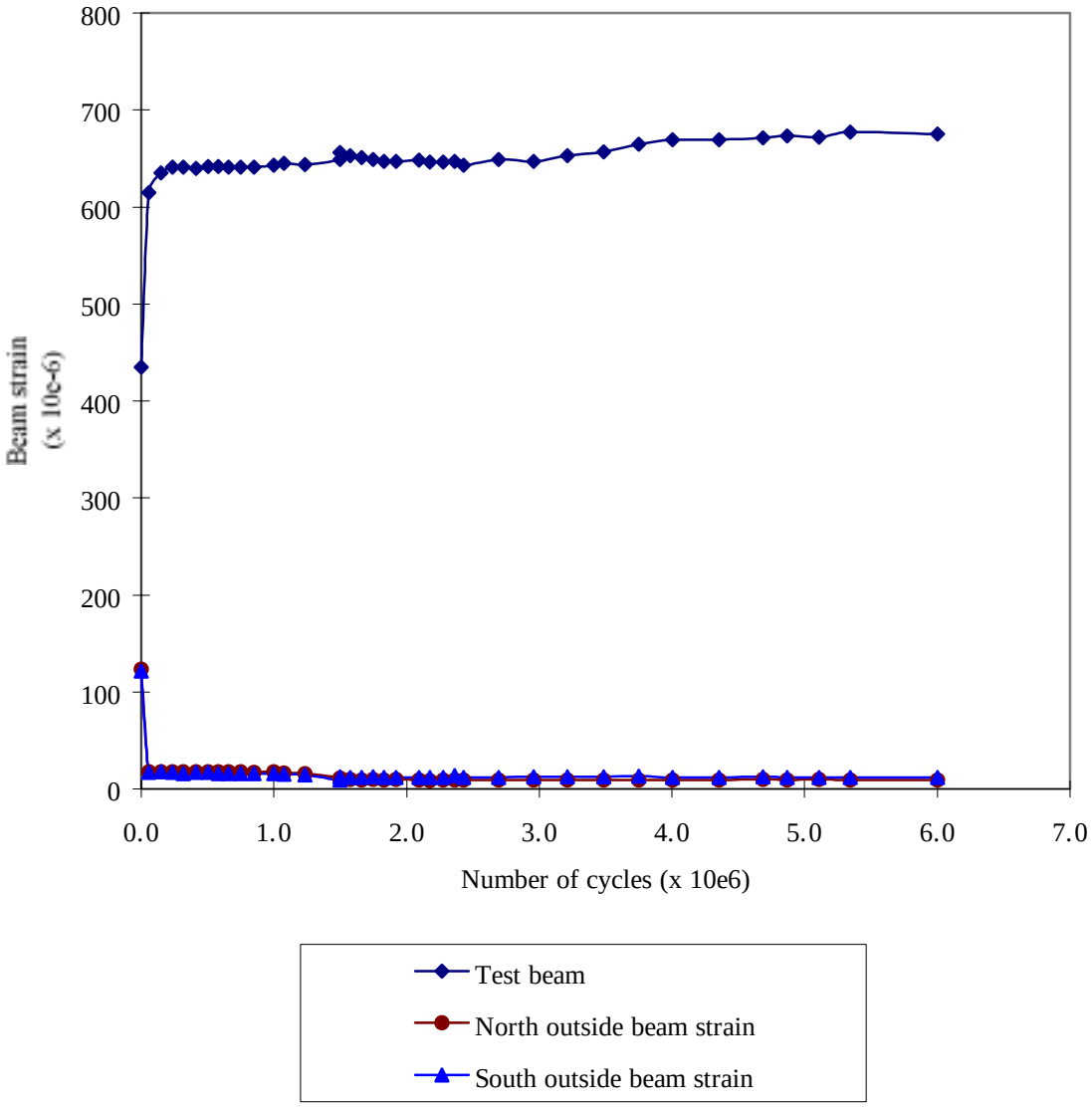

Figure 4.8 Longitudinal beam strain measurements for NS-NR(45) #2

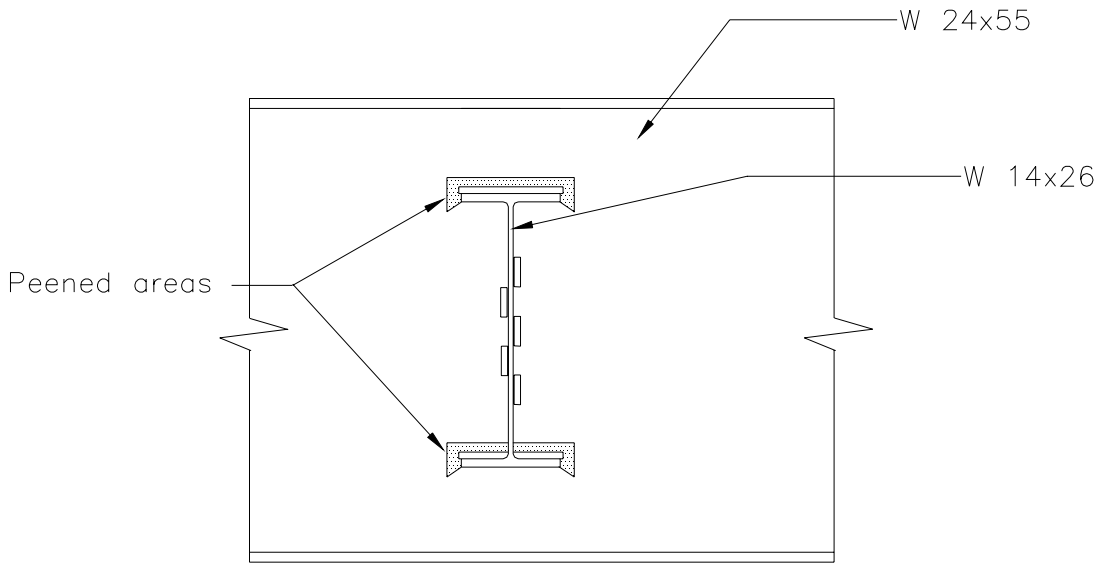

Figure 4.9 Repair method for NS-FP(45)

Figure 4.10 Photograph of the peened bottom flange weld area

Figure 4.11 Photograph of the peened top flange area

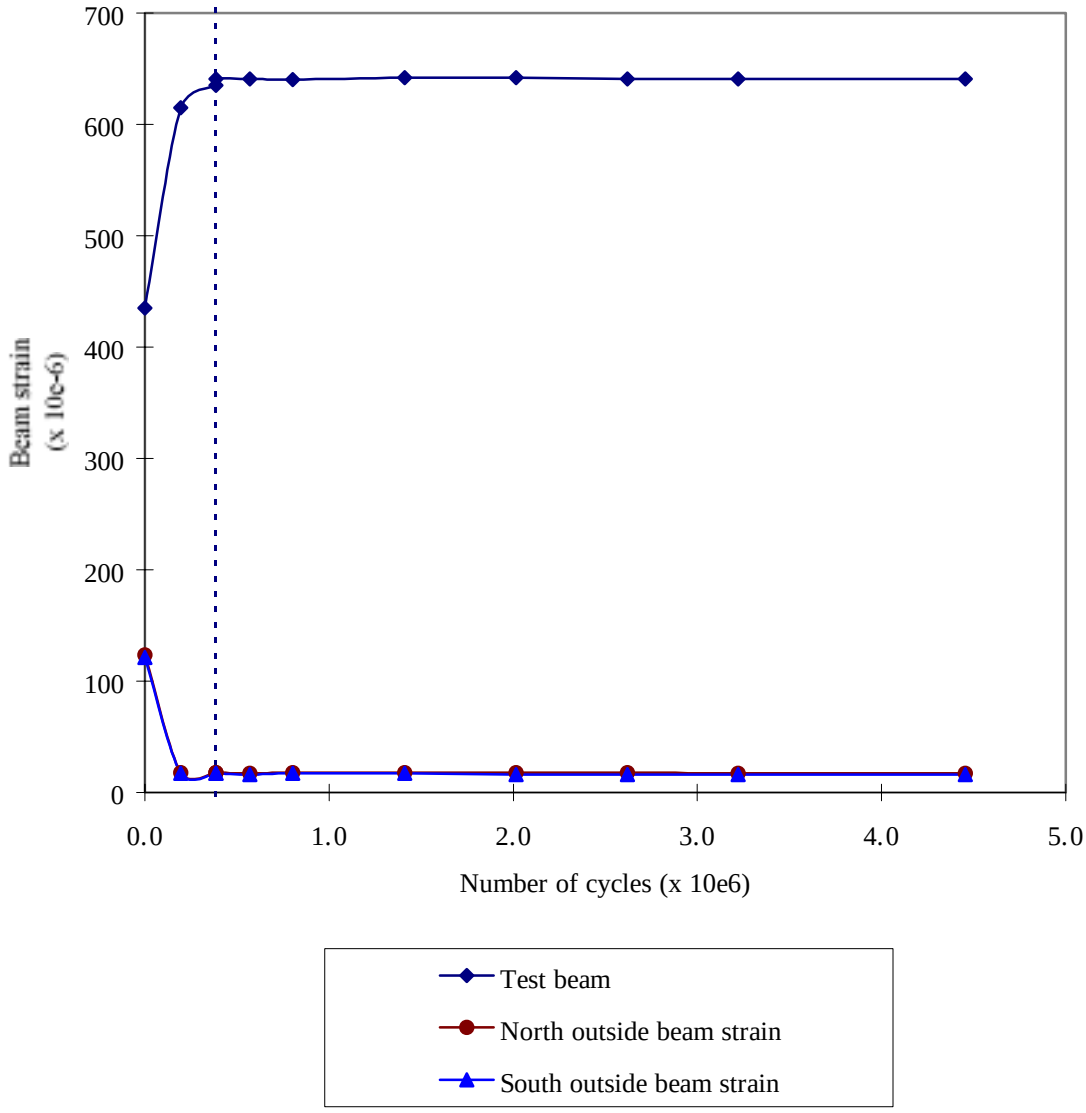

Figure 4.12 Longitudinal beam strain measurements for NS-FP(45)

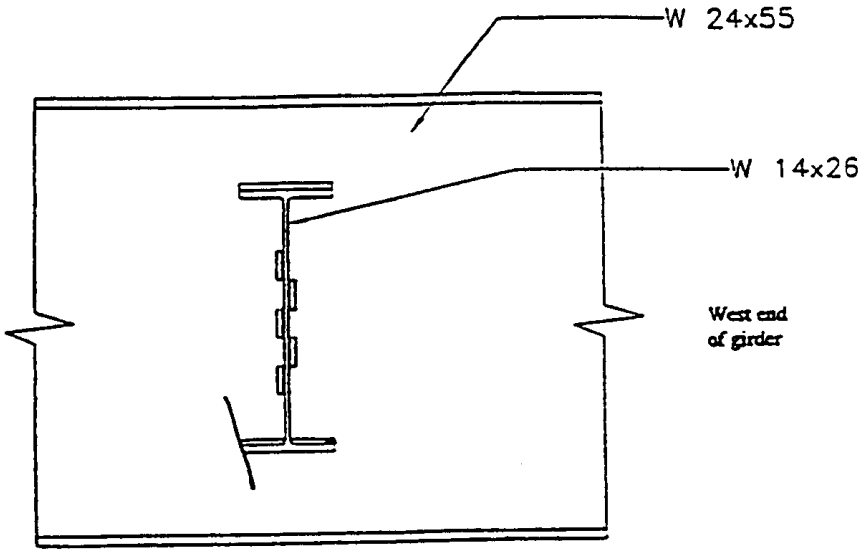

(a) North diaphragm connection

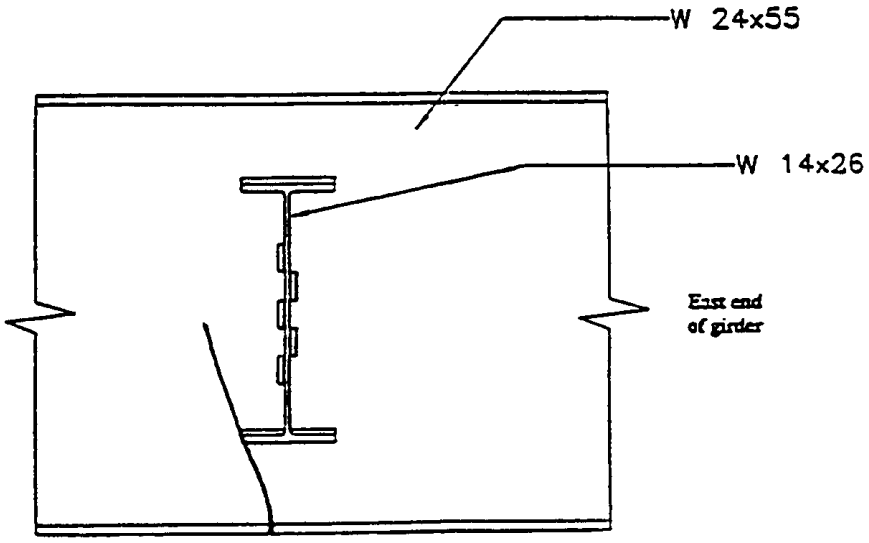

(b) South diaphragm connection

Figure 4.13 SC-NR(30) Crack locations

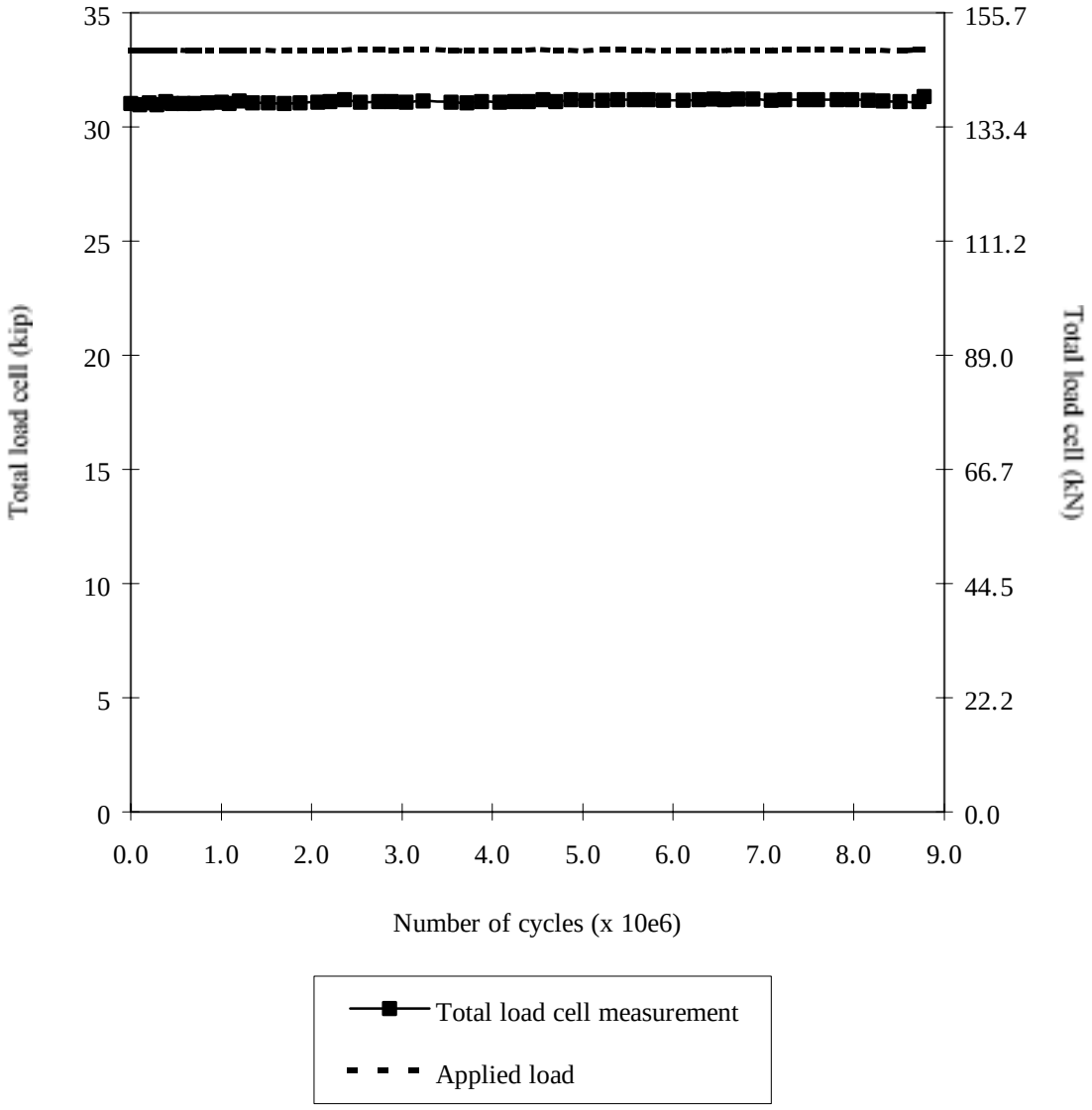

Figure 4.14 Static load cell measurements for SC-NR(30)

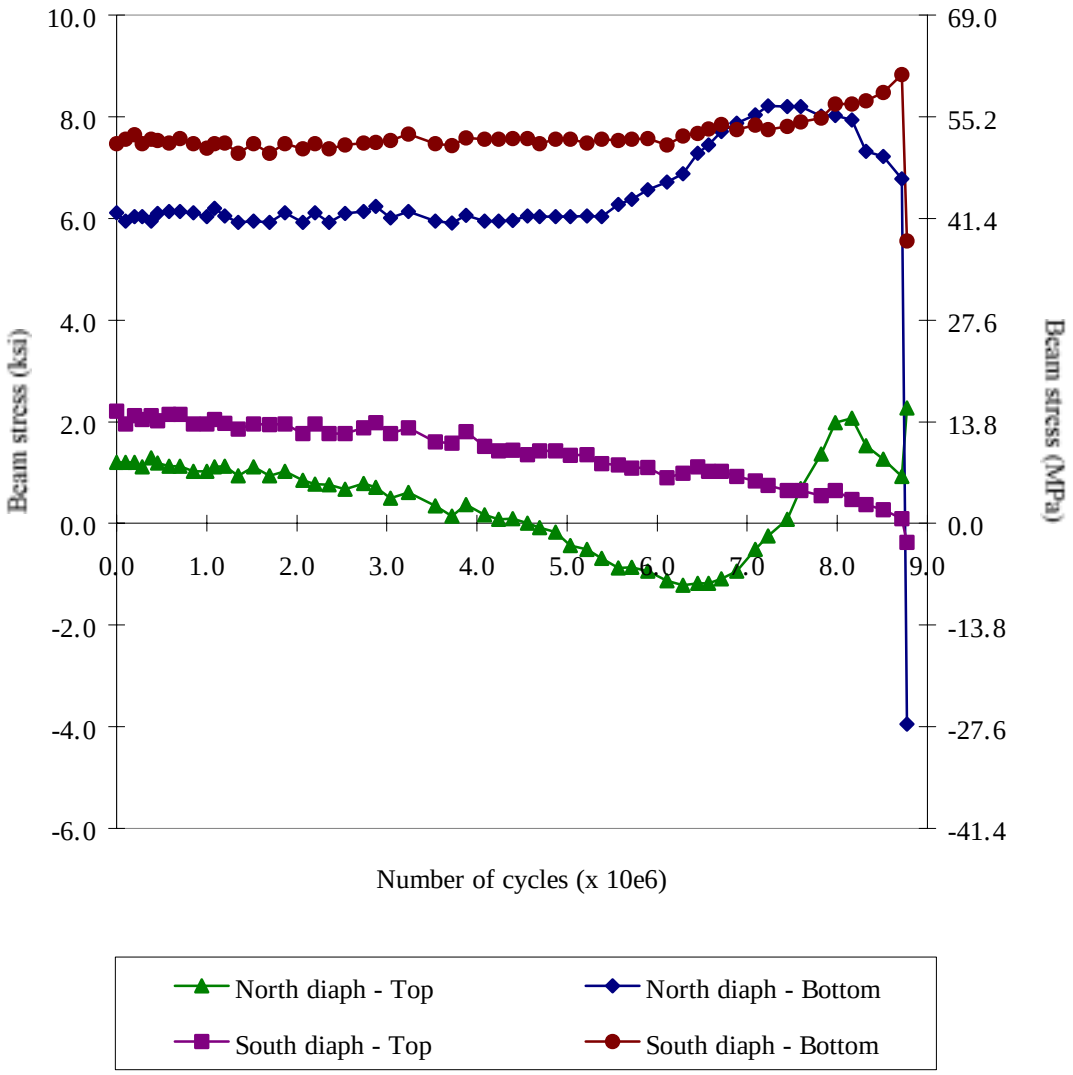

Figure 4.15 Transverse beam stresses in web gap for SC-NR(30)

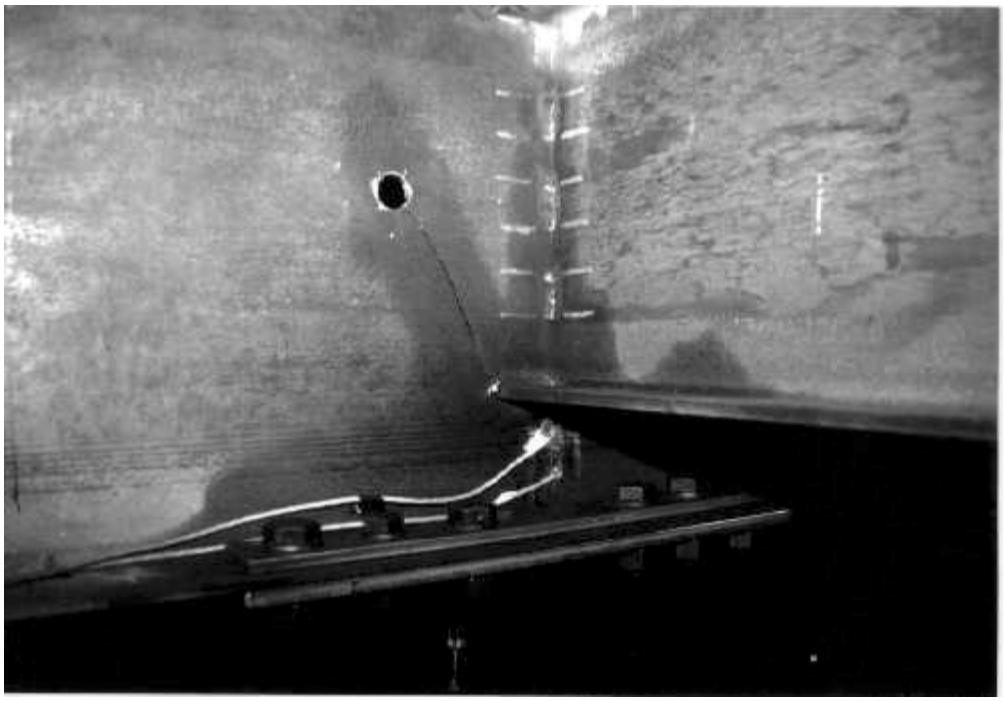

Figure 4.16 Bolted splice attachment used for SC-NR(45)

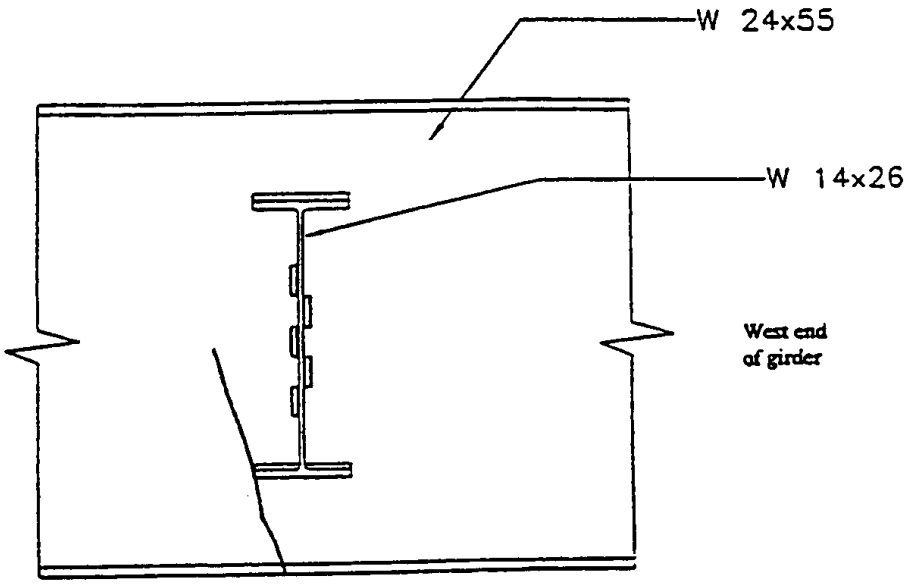

(a) North diaphragm connection

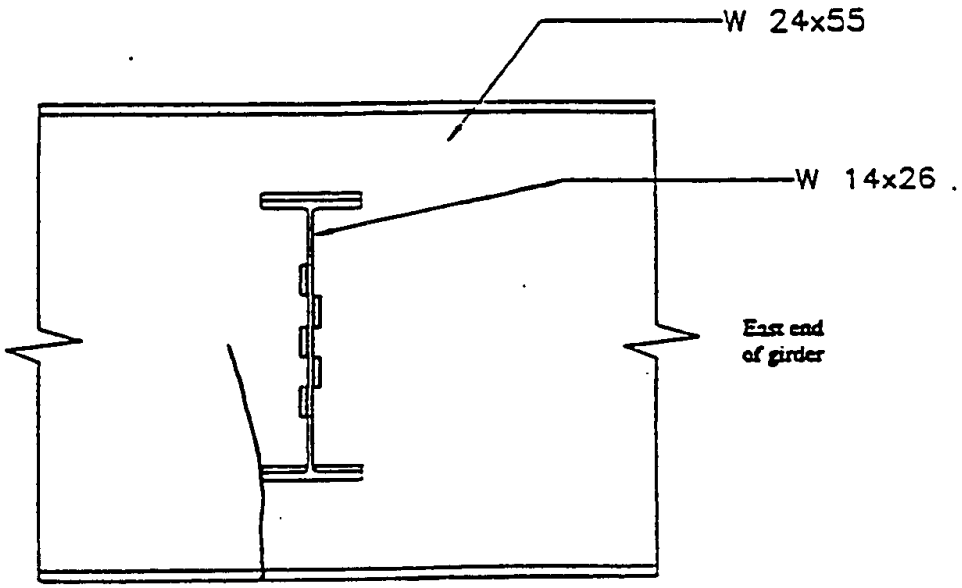

(b) South diaphragm connection

Figure 4.17 SC-NR(45) Crack locations

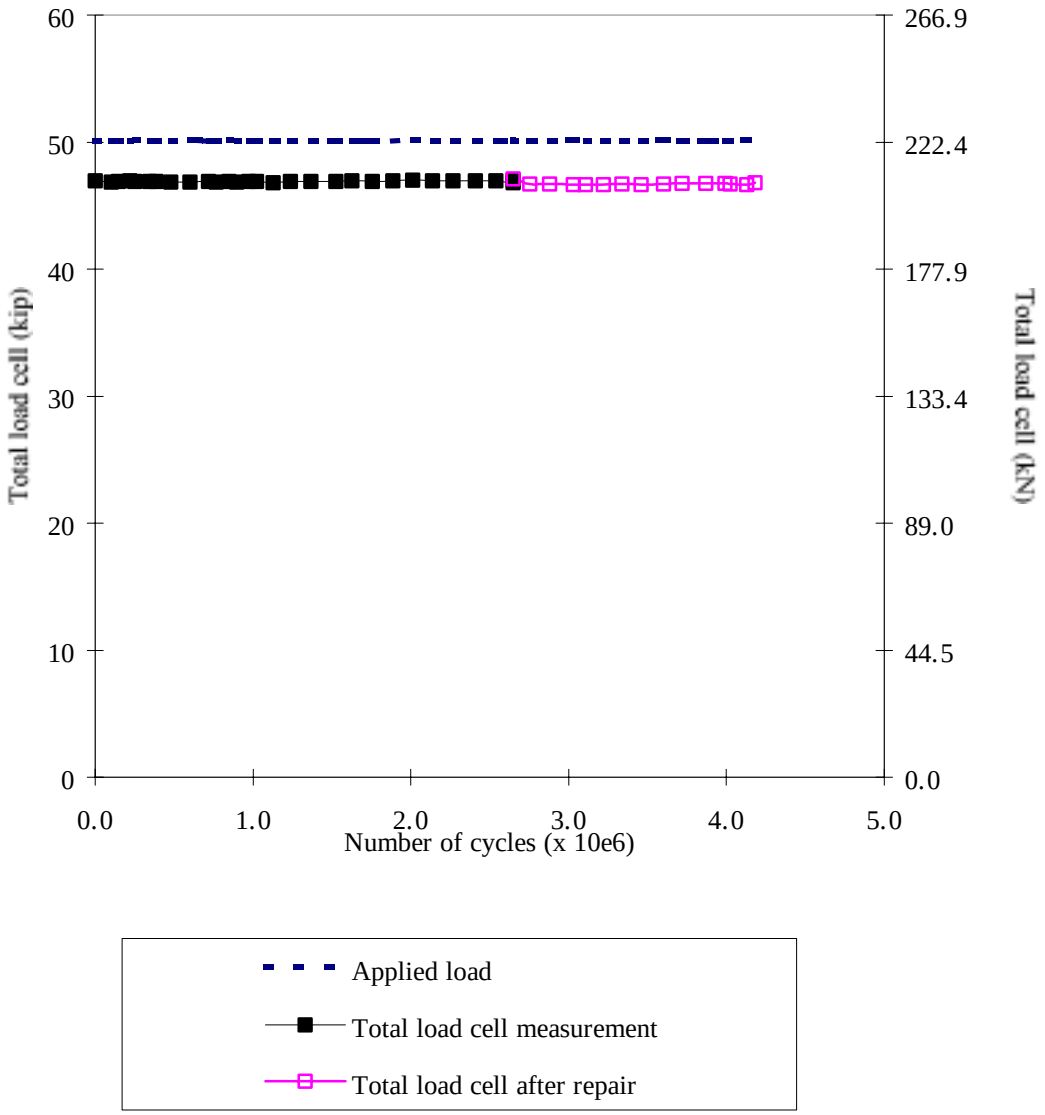

Figure 4.18 Static load cell measurements for SC-NR(45)

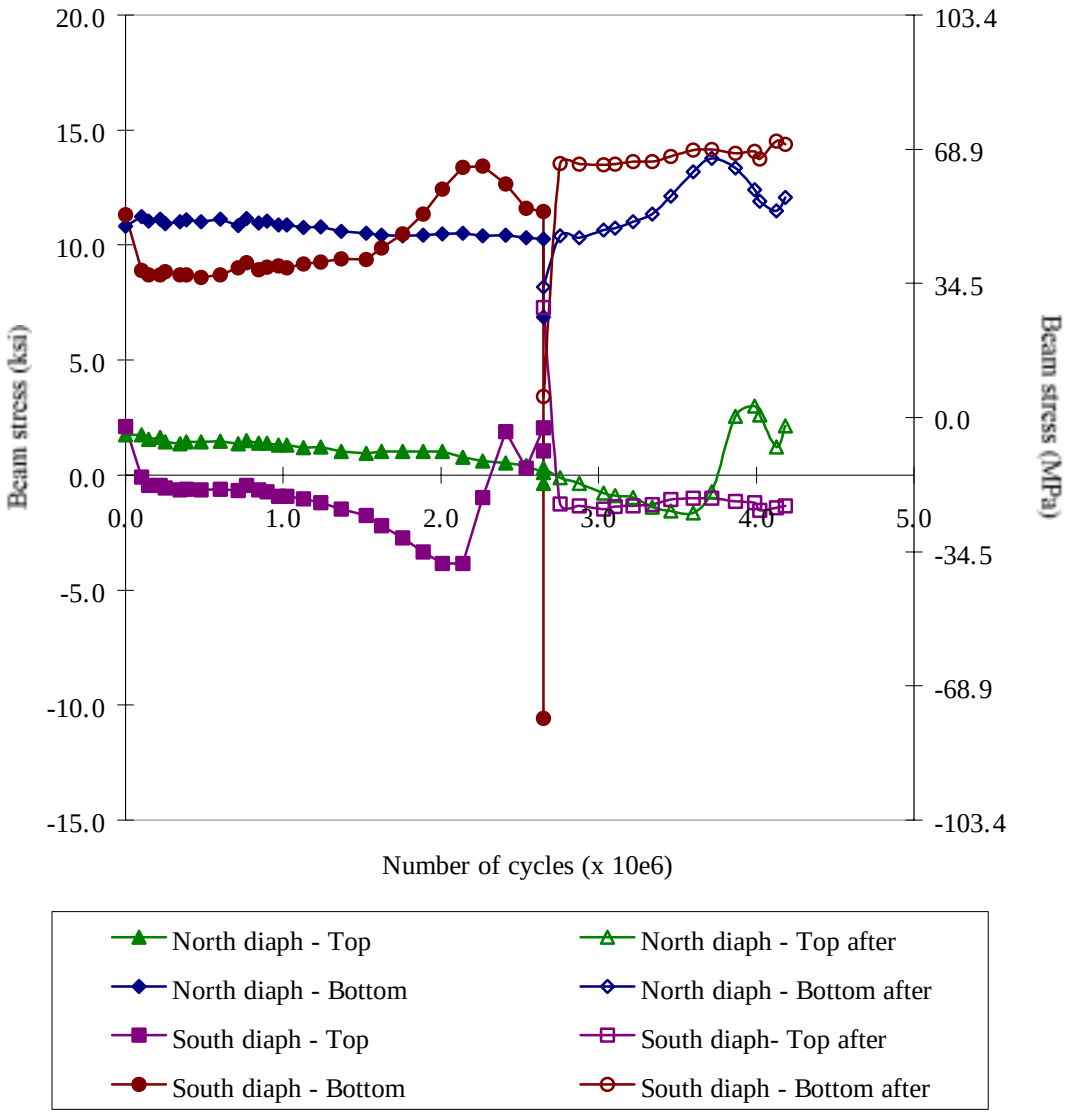

Figure 4.19 Transverse beam stresses in web gap for SC-NR(45)

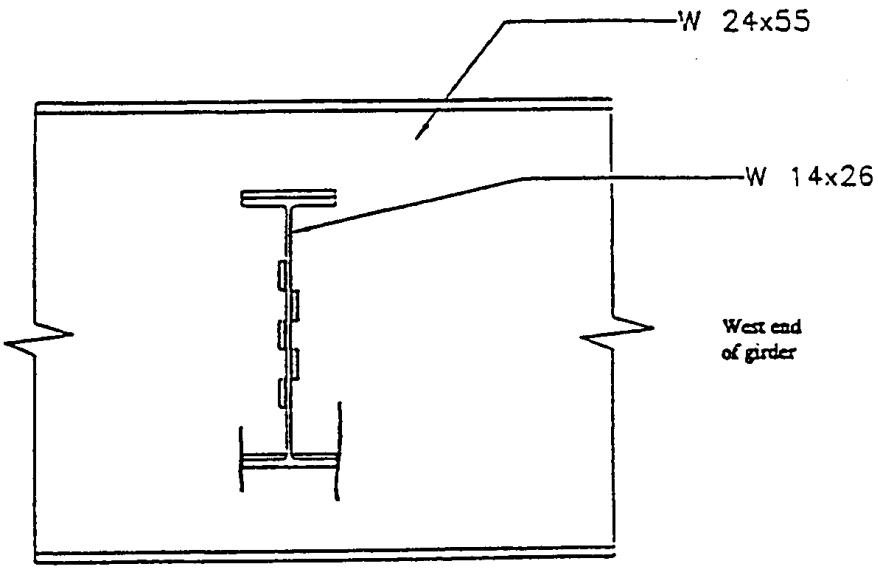

(a) North diaphragm connection

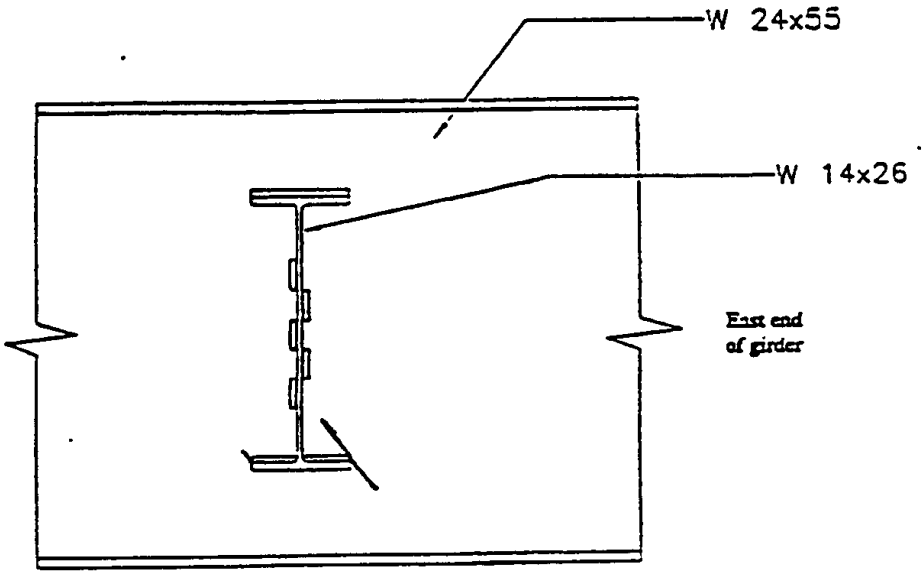

(b) South diaphragm connection

Figure 4.20 SL-NR(45) Crack locations

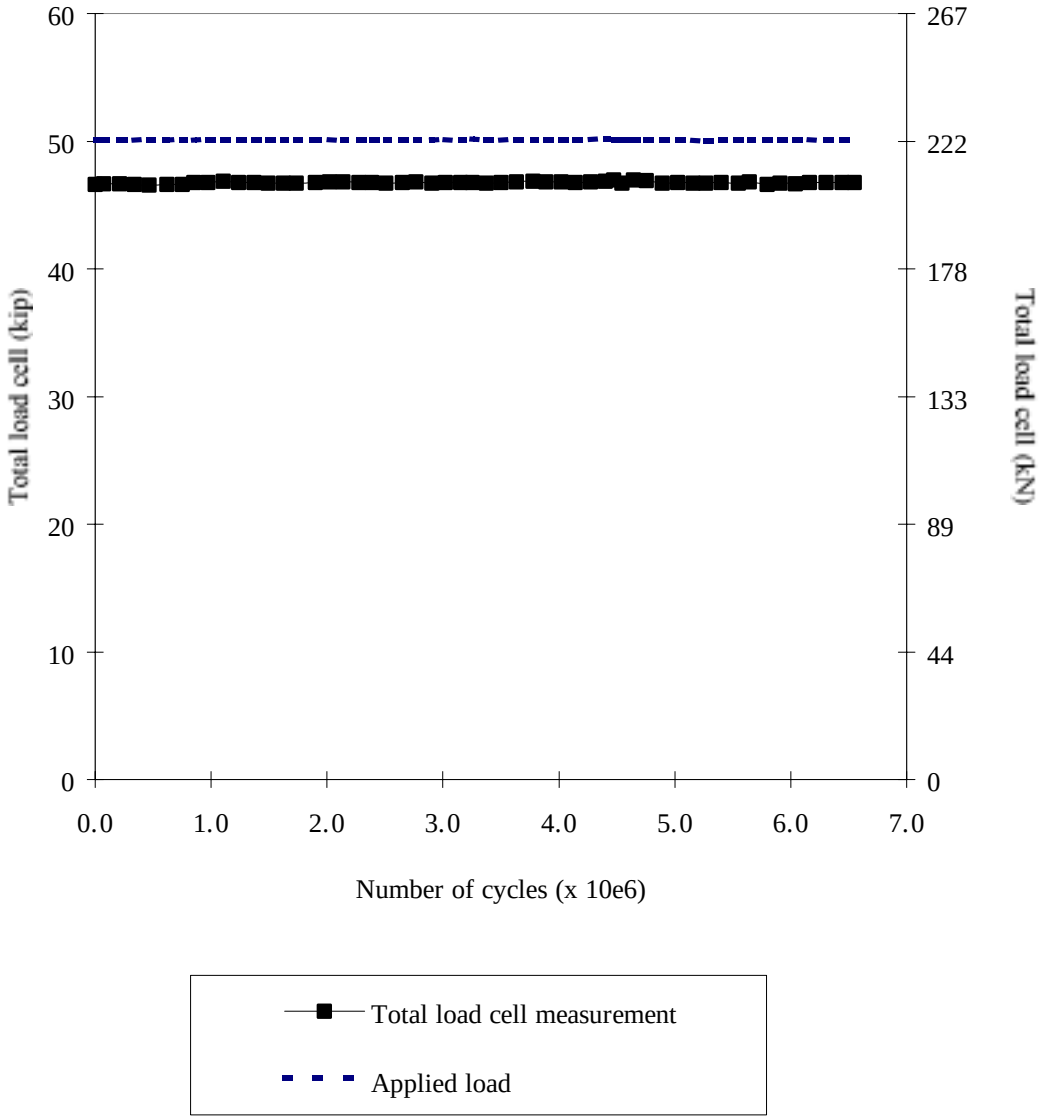

Figure 4.21 Static load cell measurements for SL-NR(45)

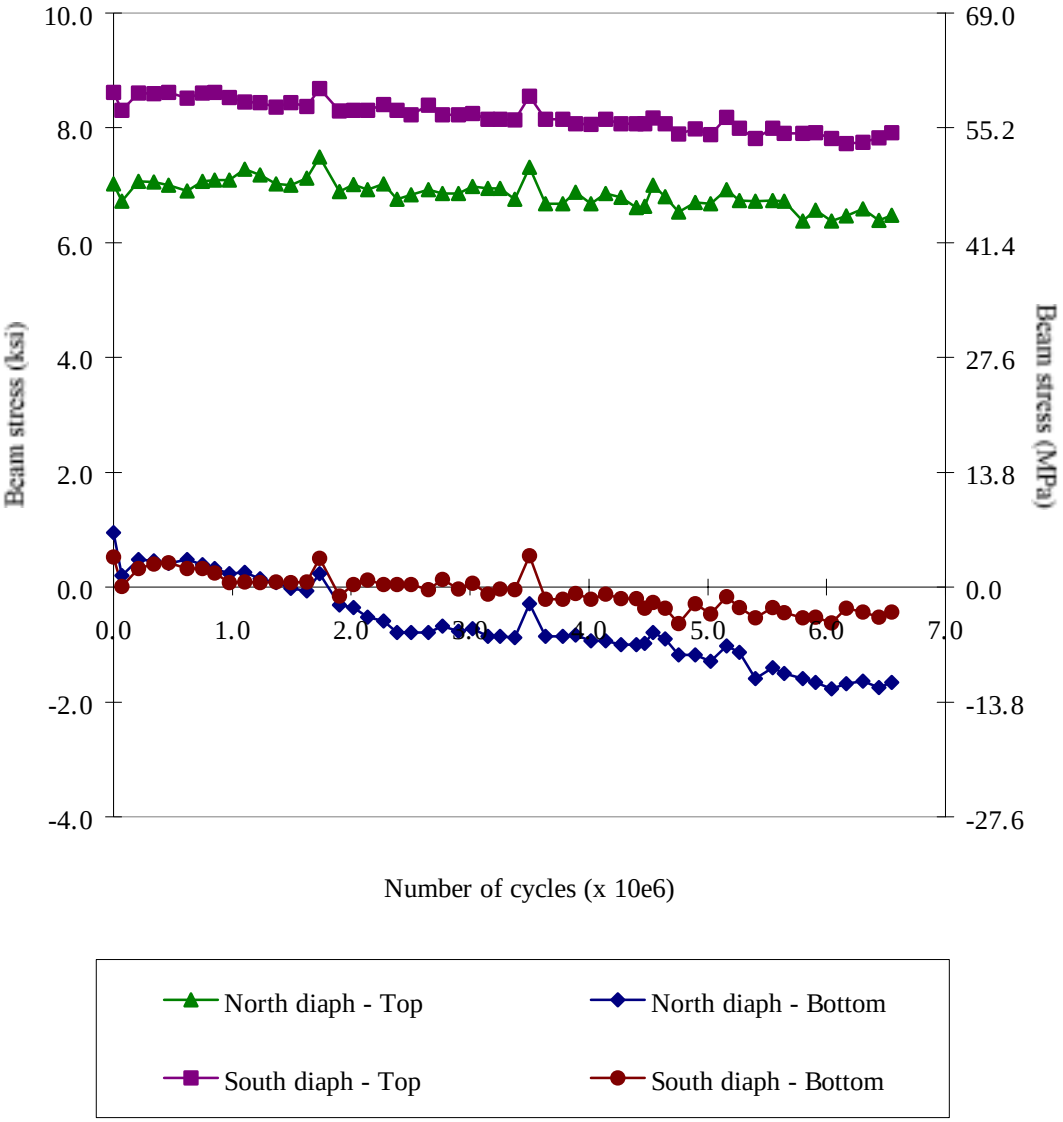

Figure 4.22 Transverse beam stresses in web gap for SL-NR(45)

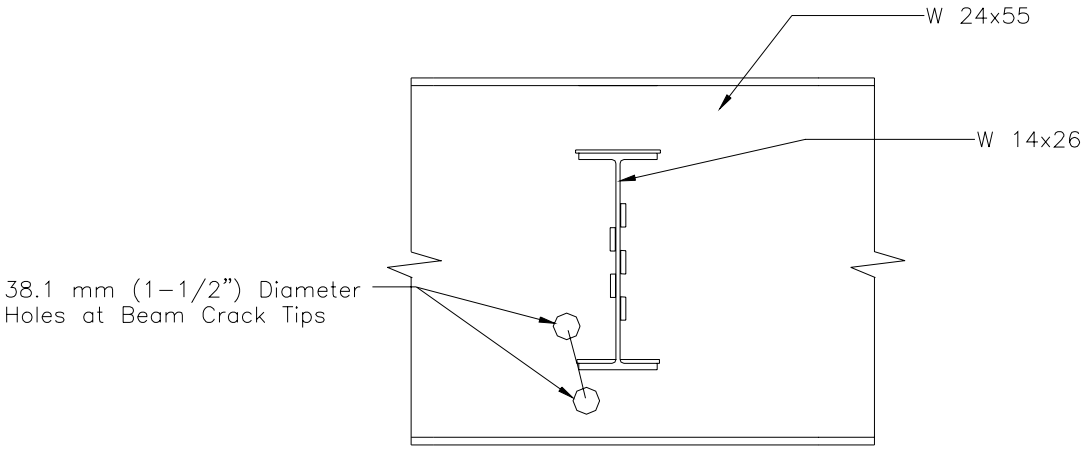

Figure 4.23 Repair method for SC-FH(45)

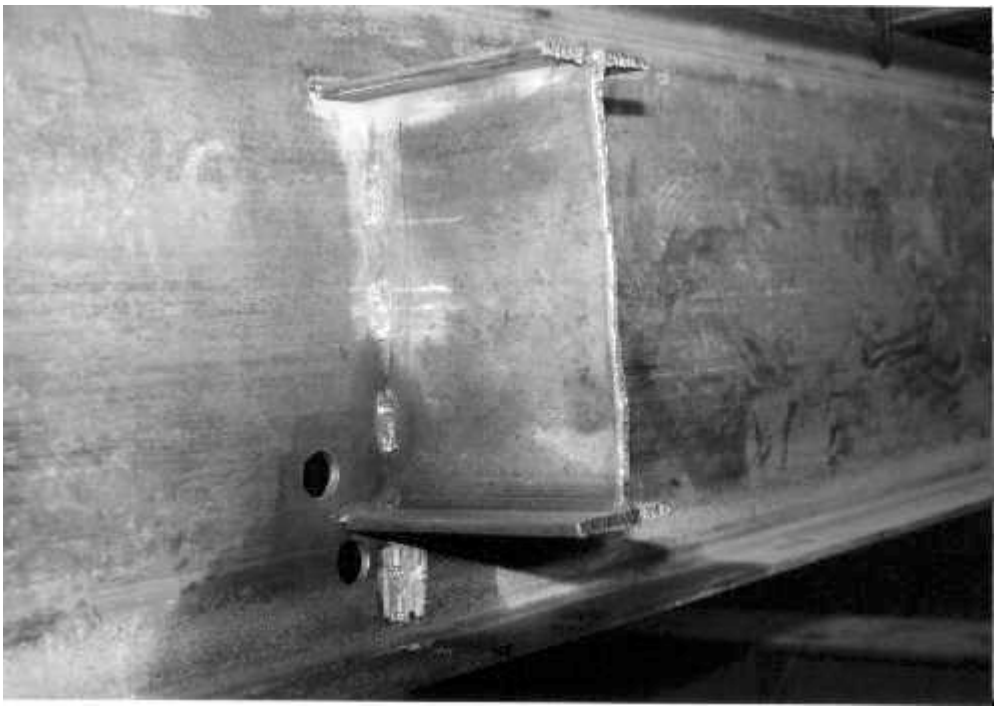

Figure 4.24 Photograph of repair for SC-FH(45)

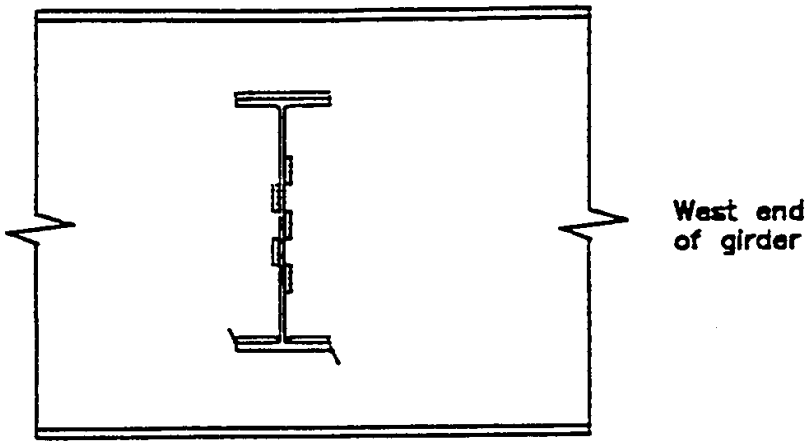

(a) North diaphragm connection

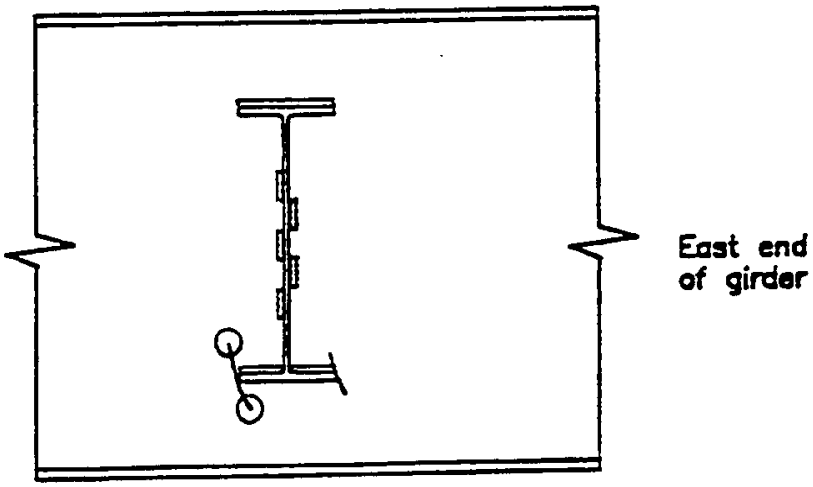

(b) South diaphragm connection

Figure 4.25 SC-FH(45) Crack locations

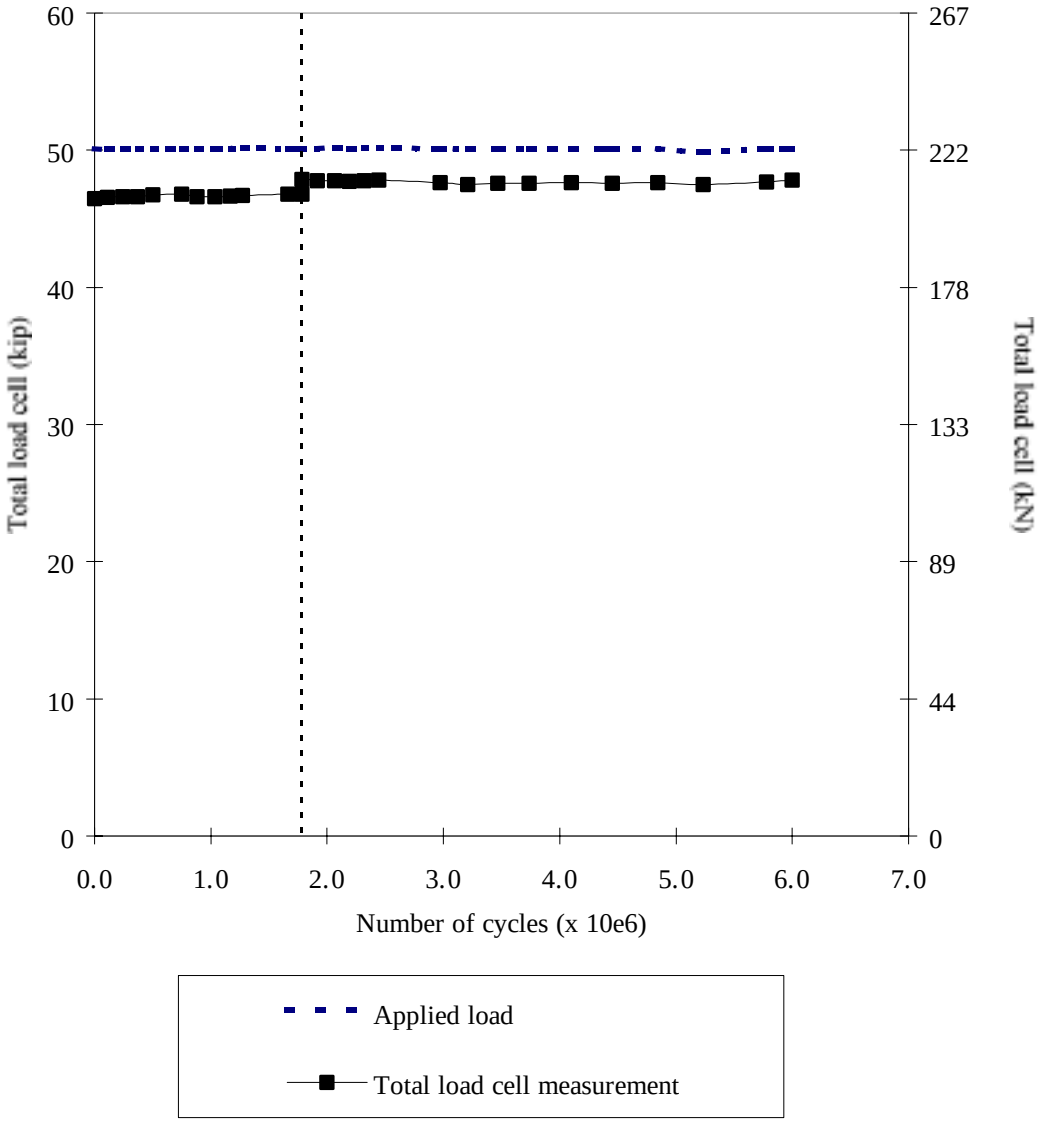

Figure 4.26 Static load cell measurements for SC-FH(45)

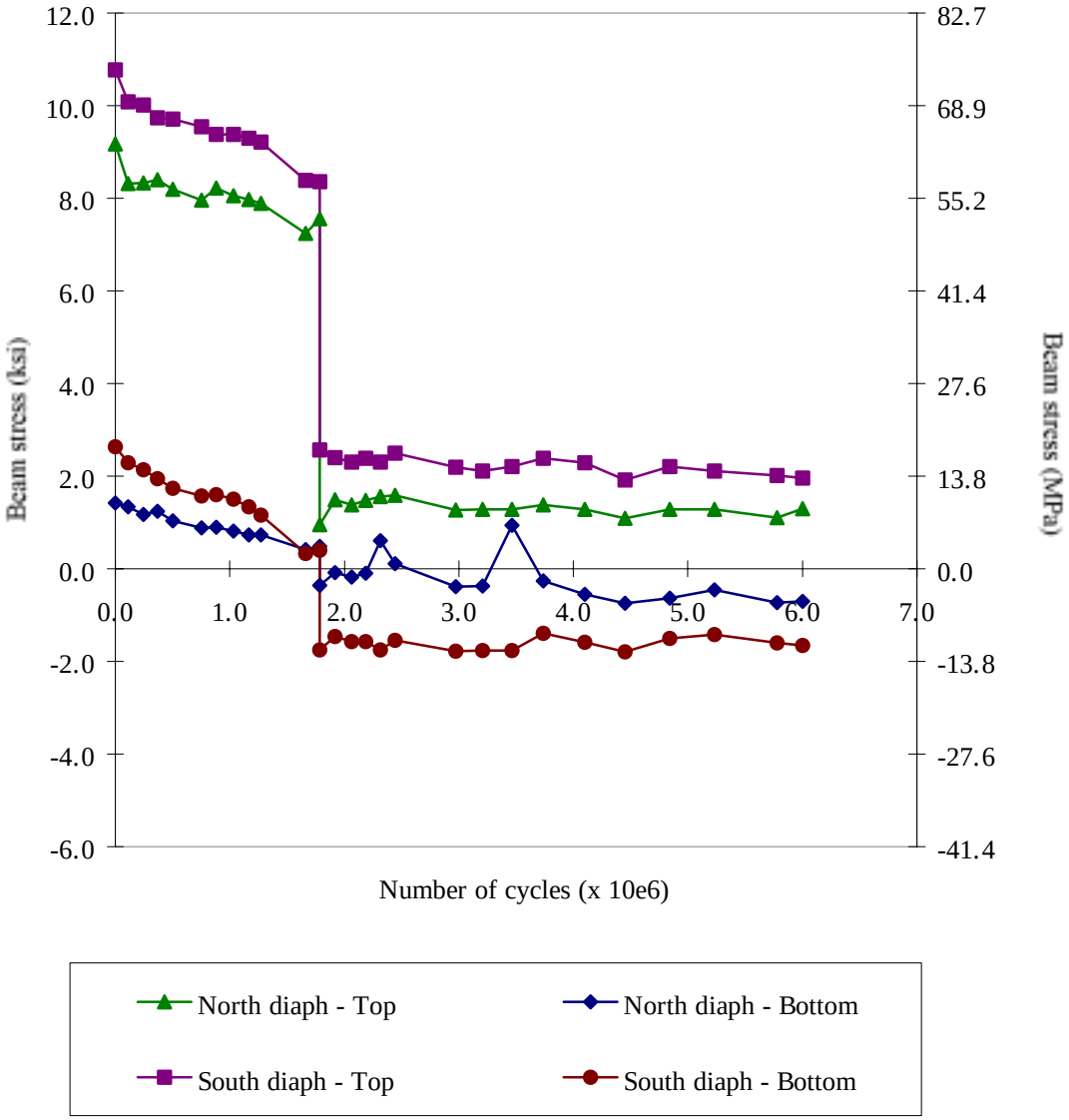

Figure 4.27 Transverse beam stresses in web gap for SC-FH(45)

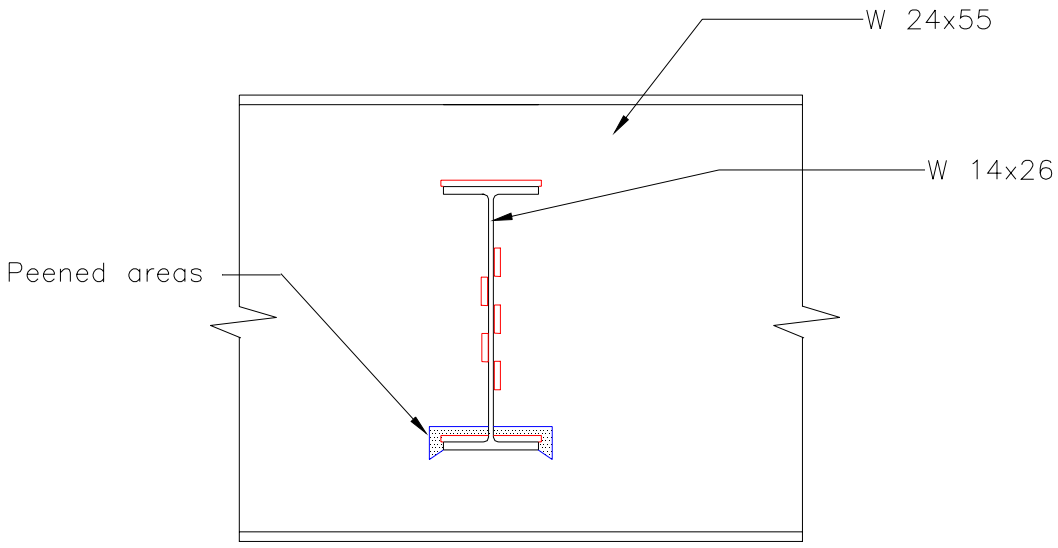

Figure 4.28 Repair method for SC-LP(45)

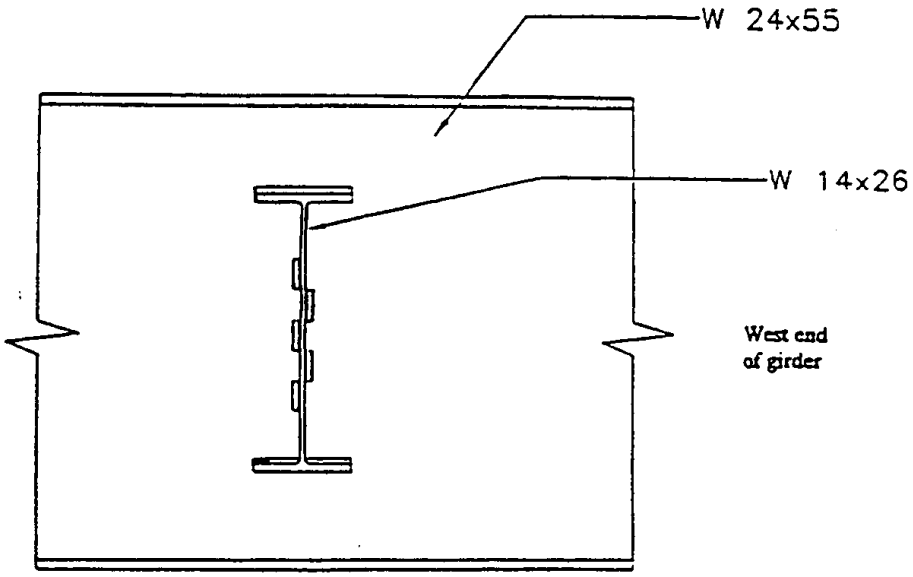

(a) North diaphragm connection

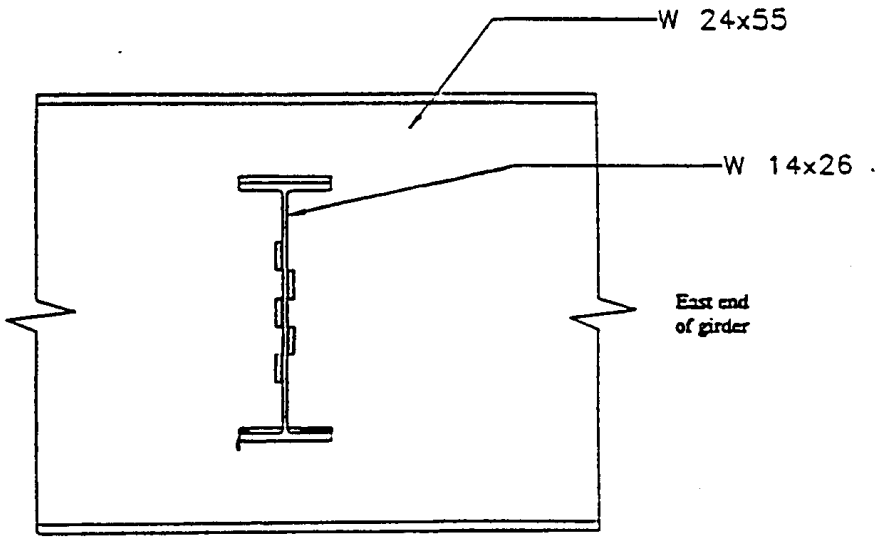

(b) South diaphragm connection

Figure 4.29 SC-LP(45) Crack locations

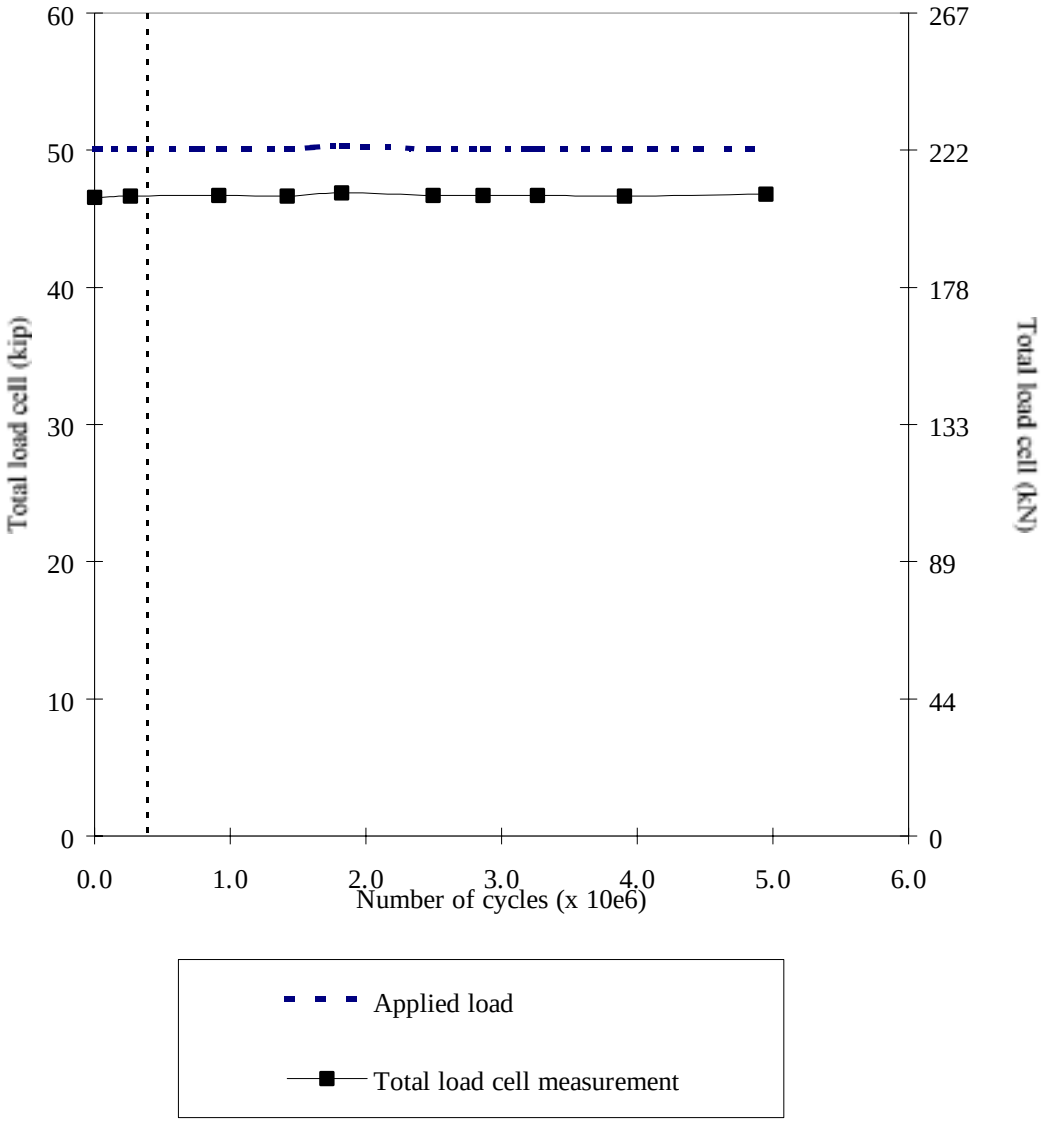

Figure 4.30 Static load cell measurements for SC-LP(45)

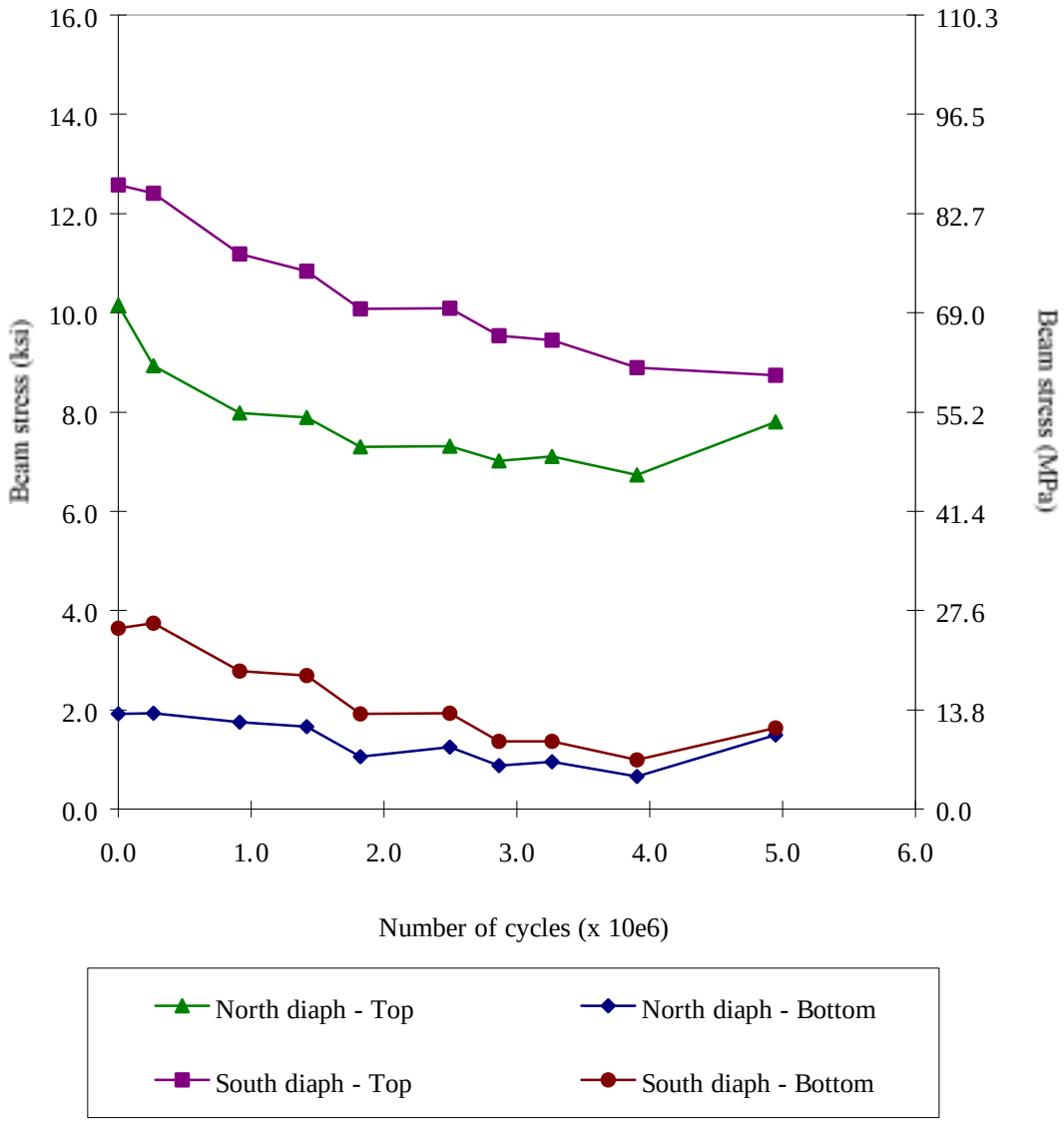

Figure 4.31 Transverse beam stresses in web gap for SC-LP(45)

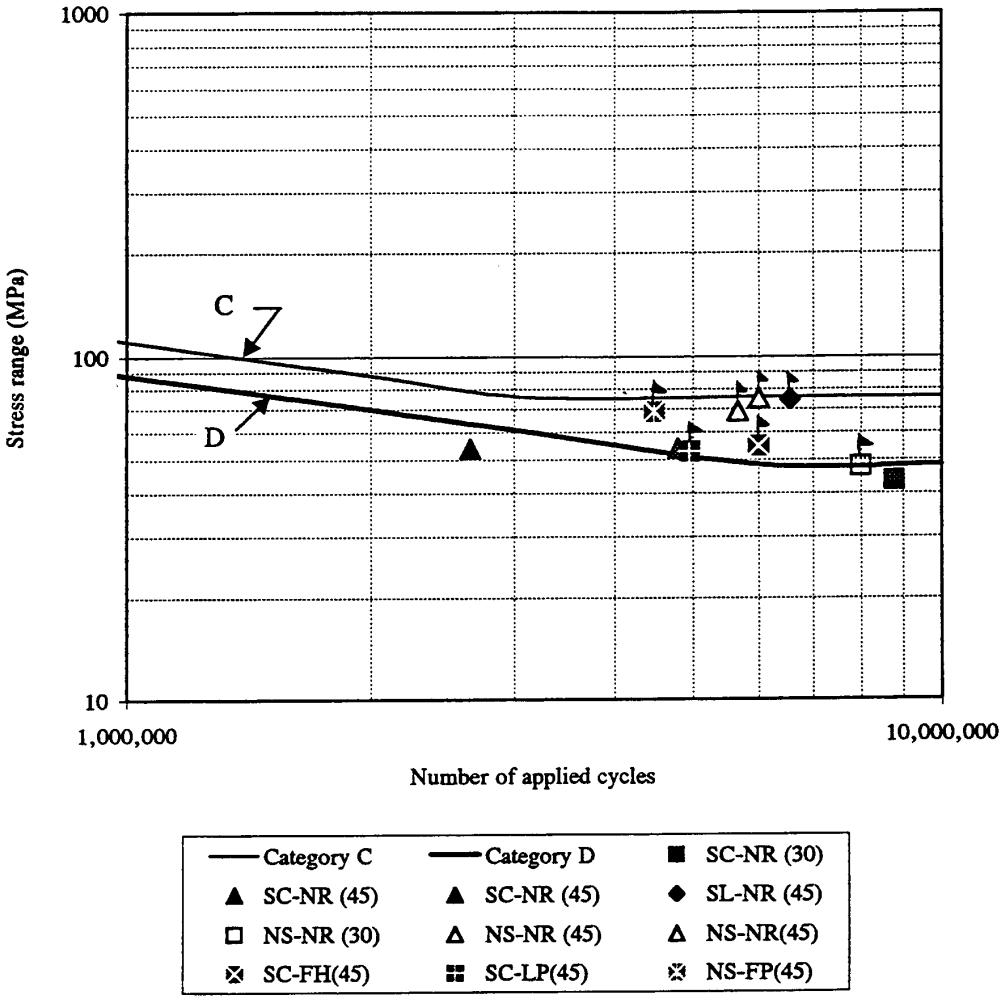

Note: 1 ksi = 6.89 MPa
Points with arrows indicate test did not fail

Figure 4.32 Stress range versus number of cycles for all tests

Figure 4.33 Typical fractured bottom weld in nonstaggered diaphragm tests

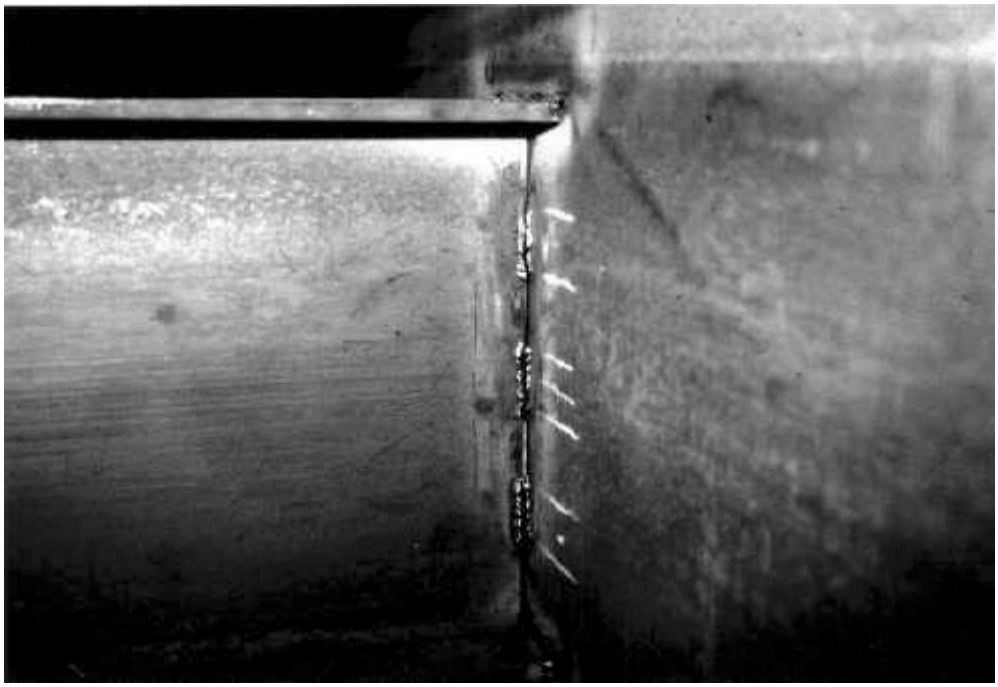

Figure 4.34 Typical fractured web welds in nonstaggered diaphragm tests

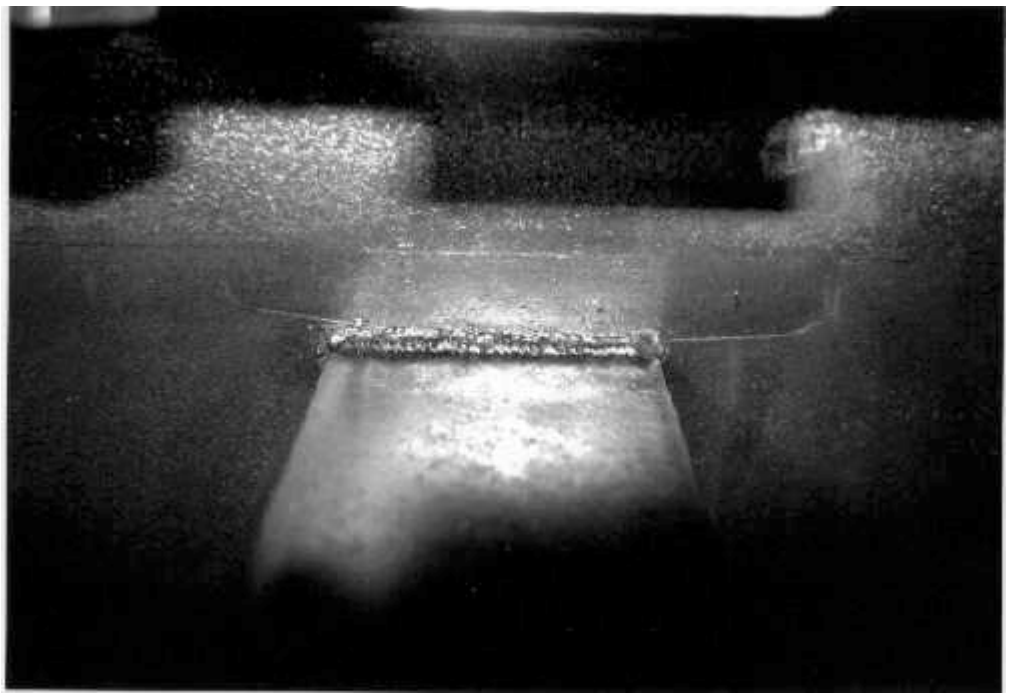

Figure 4.35 Typical horizontal beam crack located along top flange connection weld in nonstaggered diaphragm tests

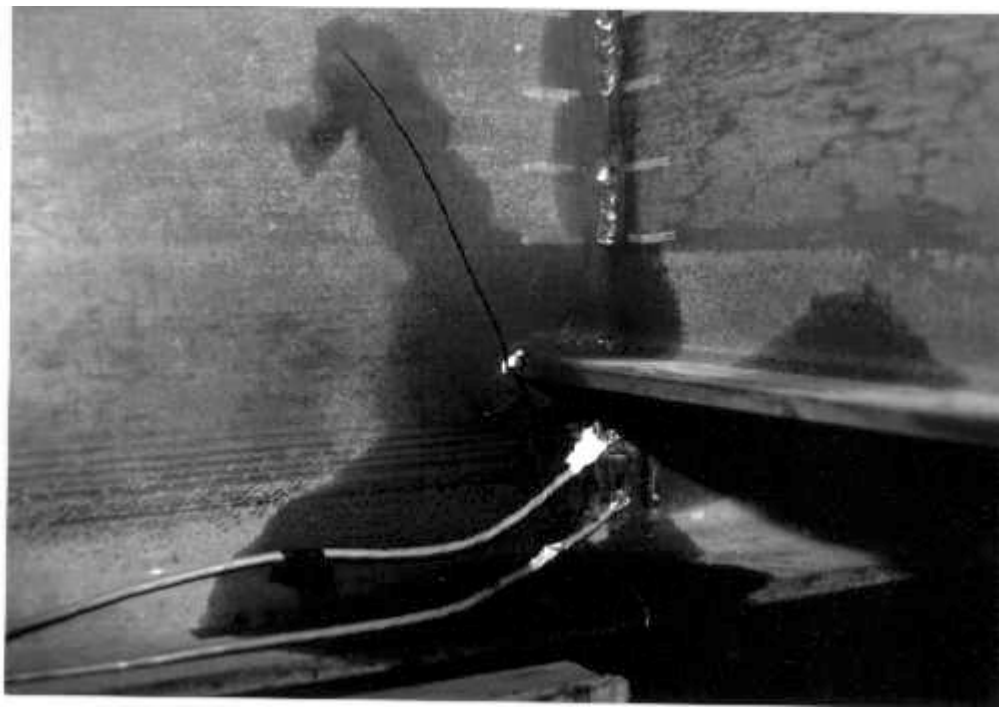

Figure 4.36 Typical vertical beam crack located along toe of lower flange connection weld in staggered diaphragm tests

CHAPTER 5

EXPERIMENTAL STRESS COMPARISON WITH BRIDGE STRESSES

The experimental tests were conducted with a constant amplitude stress range from a single concentrated load applied directly to the beam. However, an actual bridge has a concrete deck to distribute several wheel loads to adjacent beams. In order to compare the experimental stress values with actual bridge values, two bridges were analyzed for different truck configurations. The bridges analyzed were similar to bridges studied by Canna (1996) in which strains were measured for a known truck weight as well as random truck traffic.

5.1 Bridge Models

Two bridges were analyzed in order to compare the experimental stress values with values seen in typical highway bridge members. The bridges analyzed are not bridges in the field, but are similar in cross section to bridges studied by Canna (1996).

Cross sectional views of the bridges analyzed are shown in Figs. 5.1 and 5.2. The first bridge (Bridge 1) is a two span continuous steel bridge with W36x150 beam members and W18x46 diaphragms. The spans are each 27,432 mm (90 ft.) and the bridge has a 203 mm (8 in.) concrete deck. The beam spacing is 2438 mm (8 ft.) and the diaphragms are spaced at 6858 mm (22.5 ft.) and are not staggered. The second bridge

(Bridge 2) is a three span continuous bridge with W27x114 beams and W14x26 diaphragms. The spans are 12,192 mm (40 ft.) each and the concrete deck is 203 mm thick. The beam spacing varies from 1524 mm (5 ft.) for the exterior beams and 1829 mm (6 ft.) for the interior beams. The diaphragms are not staggered and are spaced at 6096 mm (20 ft.).

A three-dimensional model of each bridge was analyzed using SAP90 (1990) or SAP2000 (1996). The beams and diaphragms were modeled as frame elements using members from the program database. The diaphragm-to-beam welded connection was defined as a rigid attachment. Fixed supports were modeled by restraining translation in the x, y, and z directions. Roller supports restrained translation in the x and z directions.

Each bridge was analyzed for several truck loadings. The trucks investigated were: HS20, Fatigue, Michigan 5 (MI5), Michigan 8 (MI8), and a 19 axle 2135 kN (480 kip) vehicle. The truck dimensions and axle loads are illustrated in Figs. 5.3 to 5.7. The HS20 truck data was obtained from AASHTO (1996) and the Fatigue truck data was obtained from the *Guide Specifications for Fatigue Design of Steel Bridges* (1990). INDOT engineers provided the dimensions and axle loads for the MI5, MI8, and 19 axle trucks. Bridge member forces for the HS20 and Fatigue truck loadings were evaluated using SAP90. SAP2000 was used for the MI5, MI8, and 19 axle trucks.

5.2 Load Distribution

A two step method of distributing the wheel loads to individual beam members was developed to analyze the bridge structure. The method assumes that the longitudinal beam members act as linear springs supporting the concrete deck. The bridge is first

analyzed as a two-dimensional structure in order to determine the stiffness of the beam member. A concentrated force is applied to the structure and the deflection is obtained. The spring stiffness is then determined from $K=P/\delta$ where K is the spring stiffness, P is the applied load, and δ is the vertical deflection at the point of load application. The cross section of the bridge is then modeled with linear springs of stiffness K and a 305 mm (1 ft.) wide concrete deck that is 203 mm thick. Figure 5.8 illustrates the load distribution model for Bridge 1.

For each bridge, truck wheel loads were applied in the right traffic lane and in both traffic lanes (except the 19 axle truck). The spring forces from each loading were then used as the forces applied to the beams in the SAP bridge models.

5.2.1 Comparison with AASHTO Load Distribution

AASHTO (1996) specifies the wheel load distribution to longitudinal beam members as $S/5.5$ where S is the average girder spacing in feet. This means that all longitudinal beams have the same wheel distribution factor. The load distribution model presented earlier gives different distribution factors for each beam member. The beams located near the traffic lanes have a higher distribution than those beams near the exterior of the bridge. Tables 5.1 and 5.2 provide a comparison between the wheel distribution factors developed for trucks in one lane and both lanes with the values determined from AASHTO. The values are given for 4.4 kN (1 kip) wheel loads, which corresponds to 8.9 kN (2 kip) total axle load. When trucks are in both traffic lanes, the most heavily loaded member has a wheel distribution factor that is close to the AASHTO value. The values

determined using the AASHTO equation are conservative for beams away from the traffic lane.

5.3 Analysis Results

Each of the five trucks investigated was positioned on the bridges to develop the maximum positive moment in the beam members. The bending stress was then determined in the beam member by using the elastic flexure formula. The bending stress was calculated in the beam at the height of the diaphragm lower flange and at the outside of the beam tension flange. In order to determine the maximum stress at the diaphragm flange, it was assumed that a diaphragm was located at the point of maximum moment. However, in the analysis a diaphragm may not have been located there.

Table 5.3 presents a summary of the maximum beam stress calculated at the tension flange and at the diaphragm lower flange for each of the bridges with the five trucks. The maximum beam stress from the analyses is 64.8 MPa (9.4 ksi) for Bridge 1 and 57.2 MPa (8.3 ksi) for Bridge 2. These stresses correspond to 24.8 MPa and 24.1 MPa (3.6 ksi and 3.5 ksi) at the diaphragm level for Bridge 1 and 2, respectively. The maximum stress occurred with Michigan 8 trucks in both traffic lanes.

5.3.1 Analytical Comparison with Measured Field Values

Canna (1996) measured strains on beam and diaphragm members on two bridges for a truck of known weight and regular truck traffic. One bridge (US52) had back-to-back diaphragms and the other (I65) had staggered diaphragms.

The US52 structure is a six span bridge. The first span is a 9754 mm (32 ft.) concrete simple span, while the remaining spans are continuous steel spans at 28,042mm–32,918 mm–28,651 mm–30,785 mm–28,042 mm (92 ft.-108 ft.-94 ft.-101 ft.-92 ft.). The instrumented span was 28,042 mm and consists of eight beams (W36x150 before the construction joint and W36x230 after). The interior beams are spaced at 1829 mm (6 ft.) and the exterior beams at 1524 mm (5 ft.). The diaphragm members are W18x45 at a spacing of 7163 mm (23.5 ft.) with no stagger. The concrete deck is 190.5 mm (7.5 in.) thick and 13,106 mm (43 ft.) wide. Strain gages were attached to three diaphragms and two interior beams near the centerline of the span and under the outside traffic lane.

The I65 bridge is a two span steel bridge with a skew of approximately 35 degrees. The spans are each 26,975 mm (88.5 ft.) in length and consist of six beams (W36x150) spaced at 2438 mm (8 ft.). The diaphragms (W18x45) are spaced at 6706 mm (22 ft.) with a stagger of 1702 mm (5.583 ft.). The concrete deck is 209.6 mm (8.25 in.) thick and 13,056 mm (42.83 ft.) wide. Strains were measured in three beams and two diaphragms located near the centerline of the span. The members were located under the outside traffic lane.

The maximum measured beam strain values for the two bridges are given in Table 5.4 as well as the corresponding stresses (calculated assuming E=200 GPa (29,000 ksi)). Values are provided for static and dynamic loadings of the known truck weight, dynamic loading of a random eighteen wheel tractor trailer in the outside lane, and a dynamic loading of random tractor trailers in both traffic lanes. For the US52 bridge the maximum stress for a truck in the outside traffic lane was 24.8 MPa (3.6 ksi) and it was 21.4 MPa

(3.1 ksi) for the I65 bridge. Trucks in both traffic lanes produced stresses of 29.0 MPa (4.2 ksi) and 16.5 MPa (2.4 ksi) for the US52 and I65 bridge, respectively.

The maximum stresses from the field measurements are less than the maximum stresses from the two example bridges studied. The stresses from the field measurements compare closely to the bridge analyses performed with an HS20 truck in one lane and both lanes.

5.3.2 Bridge Comparison with Experimental Measurements

The experimental tests were conducted with a single concentrated load at midspan of a W24x55 test beam. The longitudinal test beams were 4877 mm (16 ft.) between supports and spaced at 1372 mm (4.5 ft.). The diaphragms were W14x26. The W14x26 diaphragm members were positioned back-to-back in four of the tests and were staggered 1219 mm (4 ft.) in the five other tests. The experimental setup had no concrete deck; however, angle straps were provided at frequent intervals along the beam length for lateral support.

Table 5.5 shows the maximum measured beam strains and corresponding stresses from the experimental tests. The stresses developed during the experimental tests are significantly higher than the calculated stresses for the two example bridges and the stresses determined from the field measurements. The largest beam stress from the analysis is 64.8 MPa (9.4 ksi) while the smallest experimental stress was 89.6 MPa (13 ksi). The largest beam stress determined from the field test was 29.0 MPa (4.2 ksi). Figure 5.9 shows the stress range versus number of cycles for the experimental tests and the example bridges analyzed. The points marked with the arrows indicate the test did

not fail. The number of cycles was assumed for the bridges analyzed in order to show the points on the graph. It can be seen that the stresses from the analyses fall below the Category D endurance limit while those from the experiments lie just above it.

The experimental test load is larger than the loads used in the SAP analyses and loads typically seen on highway bridges. The high test load was chosen in order to have a high stress at the welded connection to cause fatigue cracks. The endurance limit specified in AASHTO (1996) for the base metal adjacent to fillet welded details with the weld length in the direction of stress between 50.8 mm and 101.6 mm (2 in. and 4 in.) is 48.3 MPa (7 ksi), which corresponds to a Category D detail. Assuming a linear stress distribution and a stress of 7 ksi in the experimental test beam at the diaphragm lower flange, the beam stress at the extreme tension fiber is 81.8 MPa (11.9 ksi). Therefore, in order to cause fatigue cracks, the minimum stress at the tension flange of the test beam had to be 82 MPa (12 ksi). This stress is larger than the stresses usually measured and calculated on highway bridge members.

5.4 Conclusions

The stresses in the experimental tests are significantly larger than the measured field values and the analysis results for typical bridge structures. The experimental applied load encompasses most truck weights on bridges, as shown in Fig. 3.2. The experimental tests were designed to give a high stress at the diaphragm connection to represent a worst case for fatigue conditions.

Table 5.1 Load Distribution Configuration for Bridge 1

Bridge 1			
Beam Number	Distribution Method Truck in right lane	Distribution Method Trucks in both lanes	AASHTO
B1	-0.0266	-0.0642	1.45
B2	-0.0332	0.719	1.45
B3	0.3176	1.360	1.45
B4	1.0496	1.353	1.45
B5	0.7347	0.700	1.45
B6	-0.0421	-0.675	1.45

Table 5.2 Load Distribution Configuration for Bridge 2

Bridge 2			
Beam Number	Distribution Method Truck in right lane	Distribution Method Trucks in both lanes	AASHTO
B1	0.003	-0.075	1.091
B2	-0.018	0.297	1.091
B3	-0.036	0.913	1.091
B4	0.264	1.036	1.091
B5	0.916	1.006	1.091
B6	0.815	0.760	1.091
B7	0.112	0.124	1.091
B8	-.055	-0.060	1.091

Table 5.3 Stress Results from SAP Analysis

Truck	Bridge 1		Bridge 2	
	Tension flange (MPa) *(ksi)*	Diaph. level (MPa) *(ksi)*	Tension flange (MPa) *(ksi)*	Diaph. level (MPa) *(ksi)*
HS20	20.34 *(2.95)*	7.79 *(1.13)*	27.30 *(3.96)*	11.72 *(1.70)*
HS20 (both lanes)	33.78 *(4.90)*	13.03 *(1.89)*	34.27 *(4.97)*	14.69 *(2.13)*
Fatigue	15.24 *(2.21)*	5.86 *(0.85)*	20.55 *(2.98)*	8.83 *(1.28)*
MI8	34.13 *(4.95)*	13.10 *(1.90)*	40.61 *(5.89)*	17.44 *(2.53)*
MI8 (both lanes)	64.81 *(9.40)*	24.89 *(3.61)*	56.88 *(8.25)*	24.41 *(3.54)*
MI5	37.65 *(5.46)*	14.48 *(2.10)*	32.27 *(4.68)*	13.86 *(2.01)*
MI5 (both lanes)	59.09 *(8.57)*	22.68 *(3.29)*	44.54 *(6.46)*	19.10 *(2.77)*
19 axle	53.71 *(7.79)*	20.62 *(2.99)*	56.81 *(8.24)*	24.41 *(3.54)*

Table 5.4 Summary of Maximum Field Measurements (Canna 1996)

Load Condition	Bridge			
	US52		I65	
	Strain (με)	Stress (MPa) *(ksi)*	Strain (με)	Stress (MPa) *(ksi)*
Static - known truck	90.6	18.13 *(2.63)*	75.3	15.03 *(2.18)*
Dynamic - known truck	94.9	18.96 *(2.75)*	107.3	21.44 *(3.11)*
Dynamic - random trailer	125	25.03 *(3.63)*	84	16.82 *(2.44)*
Dynamic - random trailers (both lanes)	146	29.16 *(4.23)*	83	16.62 *(2.41)*

Table 5.5 Summary of Maximum Experimental Measurements

Experimental Test	Strain (με)	Stress (MPa) *(ksi)*
NS-NR(30)	482	96.5 *(14.0)*
NS-NR(45) #1	791	157.9 *(22.9)*
NS-NR(45) #2	677	135.1 *(19.6)*
NS-FP(45)	642	128.2 *(18.6)*
SC-NR(30)	450	89.6 *(13.0)*
SC-NR(45)	668	133.8 *(19.4)*
SL-NR(45)	706	141.3 *(20.5)*
SC-FH(45)	690	137.9 *(20.0)*
SC-LP(45)	674	134.4 *(19.5)*

Notes:

- NS = no stagger
- SC = stagger with load centered between diaphragms
- SL= stagger with load at one of diaphragms

- NR = no repair performed in test
- FP = diaphragm was flame cut and the lower flange connection weld toes were peened
- FH = diaphragm was flame cut and holes were drilled at the beam crack tips
- LP = diaphragm was left in place and the lower flange connection weld toes were peened

- (##) = range of applied load in kips

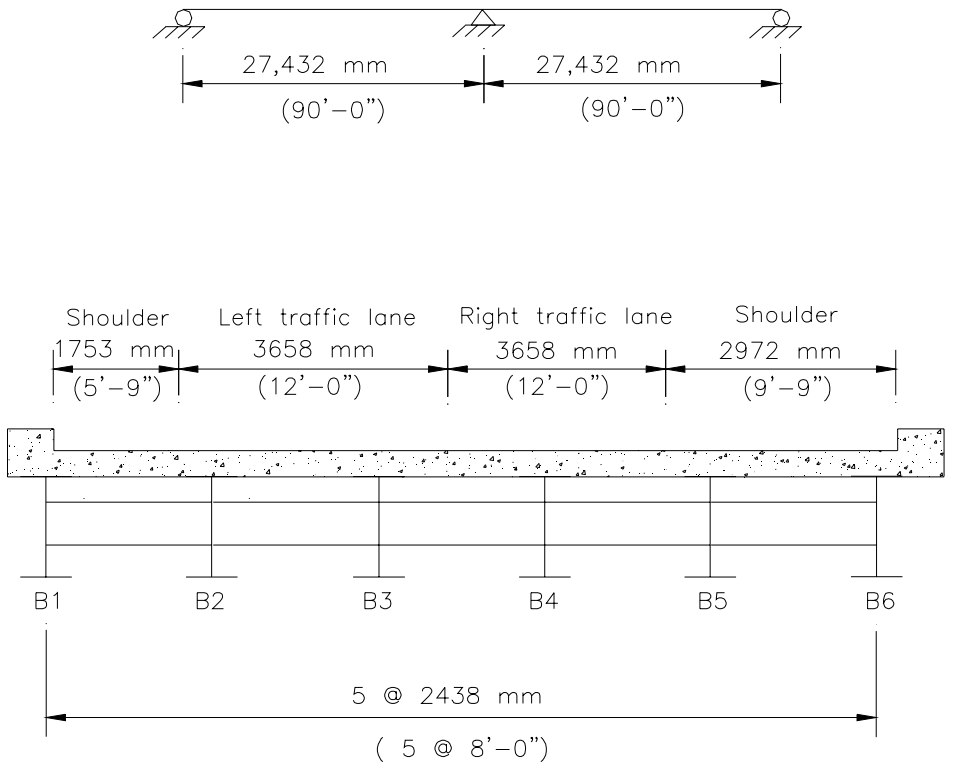

Figure 5.1 Example bridge 1

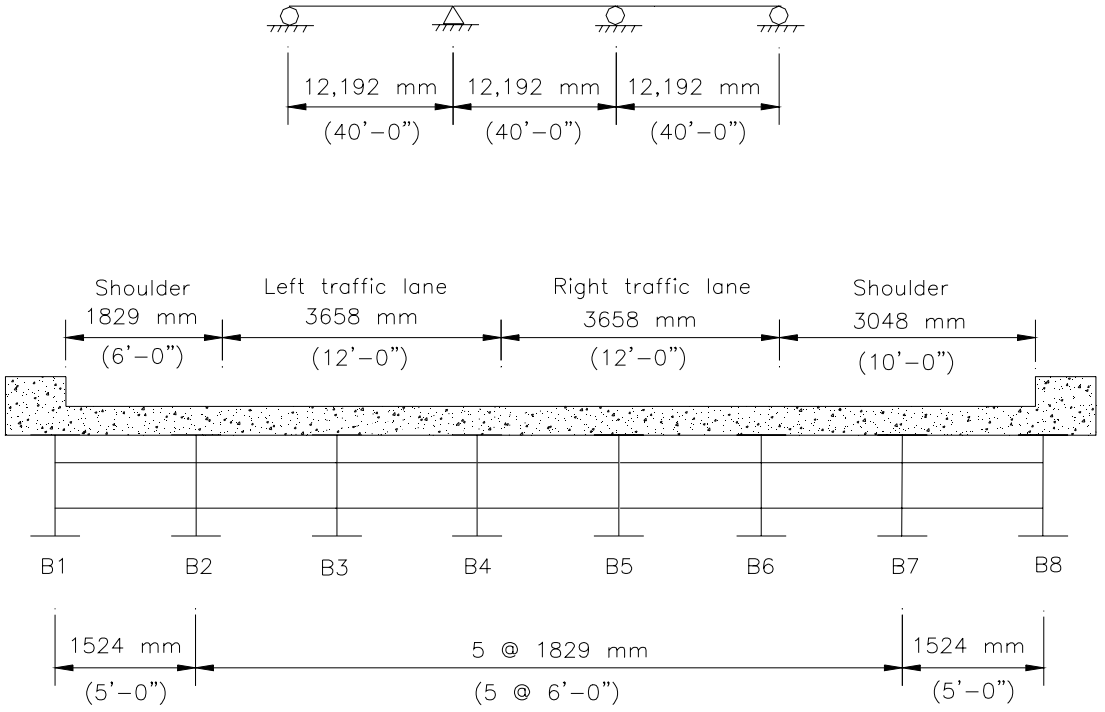

Figure 5.2 Example bridge 2

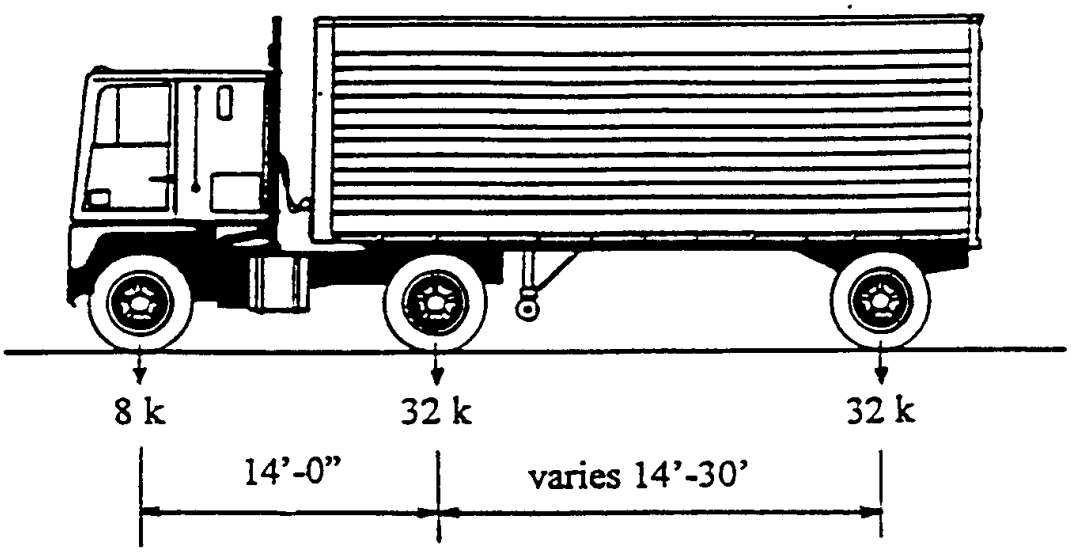

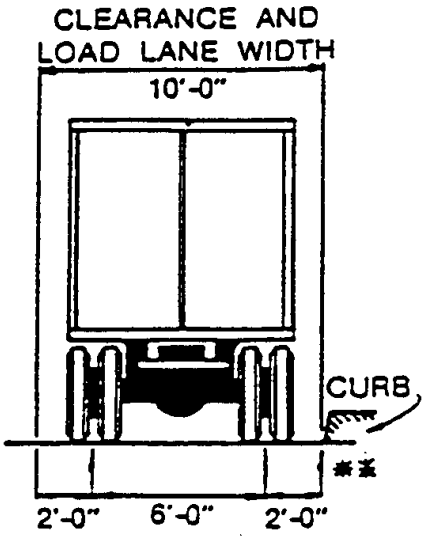

Standard HS truck
Gross weight 72,000 lbs.

Figure 5.3 HS20 truck

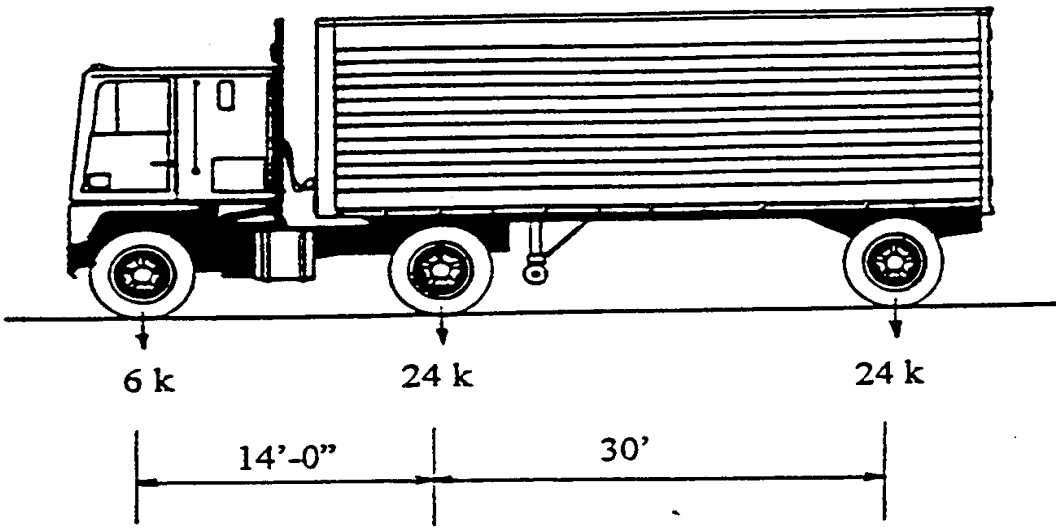

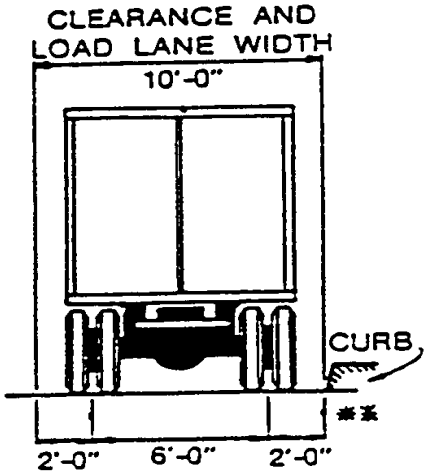

Fatigue truck
Gross weight 54,000 lbs.

Figure 5.4 Fatigue truck

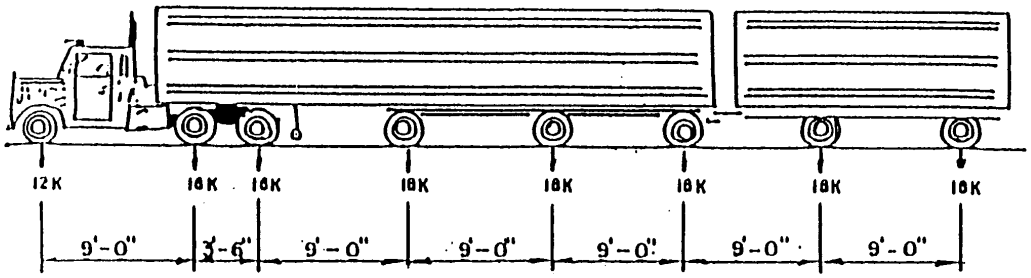

MICHIGAN TRAIN
TRUCK NUMBER 5

GROSS WEIGHT 134,000lbs.

Figure 5.5 Michigan 5 truck

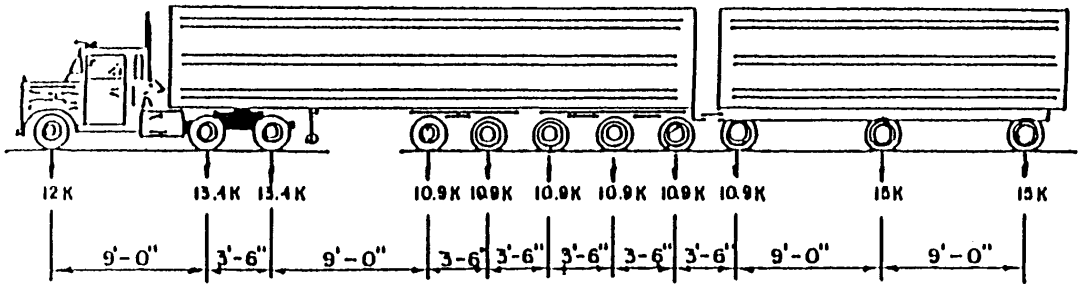

MICHIGAN TRAIN
MODIFIED TRUCK NUMBER 8

GROSS WEIGHT 134,200lbs.

Figure 5.6 Michigan 8 truck

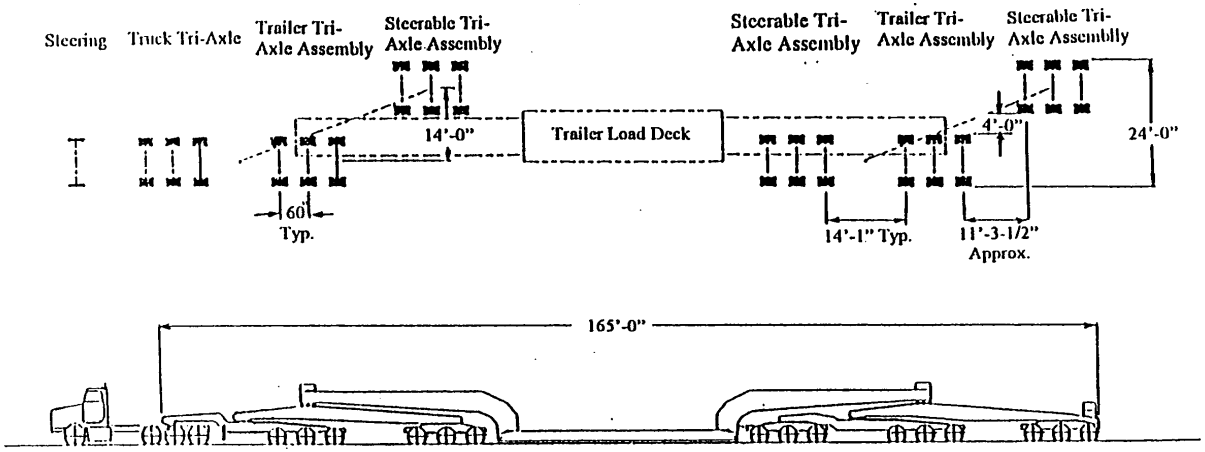

Axle	Wt. (kip)	Axle Spacing	Axle Width
1	12.99	12’-6”	8’
2	25.94	5’-0”	8’
3	25.94	5’-0”	8’
4	25.94	14’-1”	8’
5	25.94	5’-0”	10’
6	25.94	5’-0”	10’
7	25.94	14’-1”	10’
8	25.94	5’-0”	10’
9	25.94	5’-0”	10’
10	25.94	50’-0”	10’

Axle	Wt. (kip)	Axle Spacing	Axle Width
11	25.94	5’-0”	10’
12	25.94	5’-0”	10’
13	25.94	14’-1”	10’
14	25.94	5’-0”	10’
15	25.94	5’-0”	10’
16	25.94	14’-1”	10’
17	25.94	5’-0”	10’
18	25.94	5’-0”	10’
19	25.94	14’-1”	10’

Figure 5.7 19 axle 480 kip truck

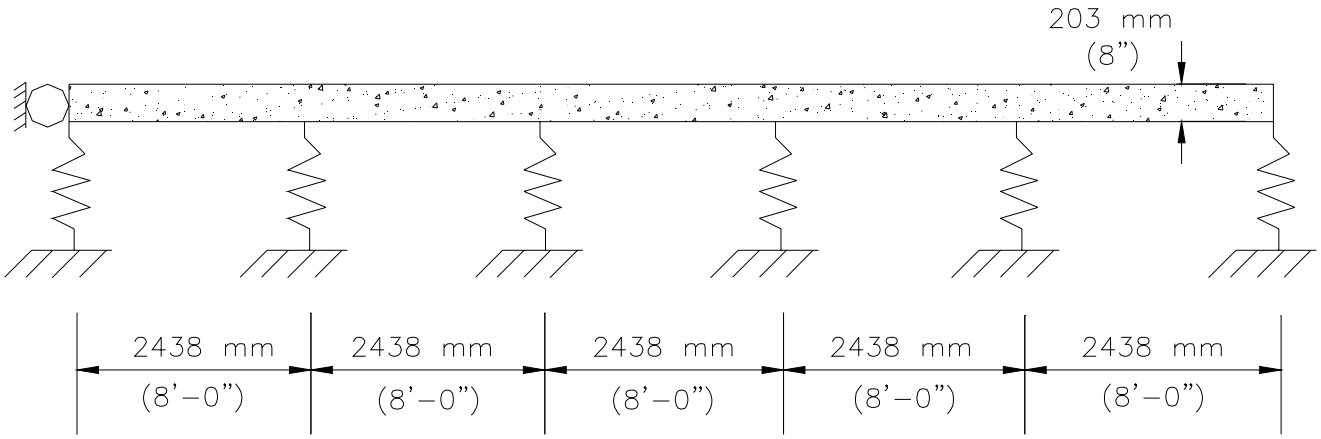

Figure 5.8 Load distribution model

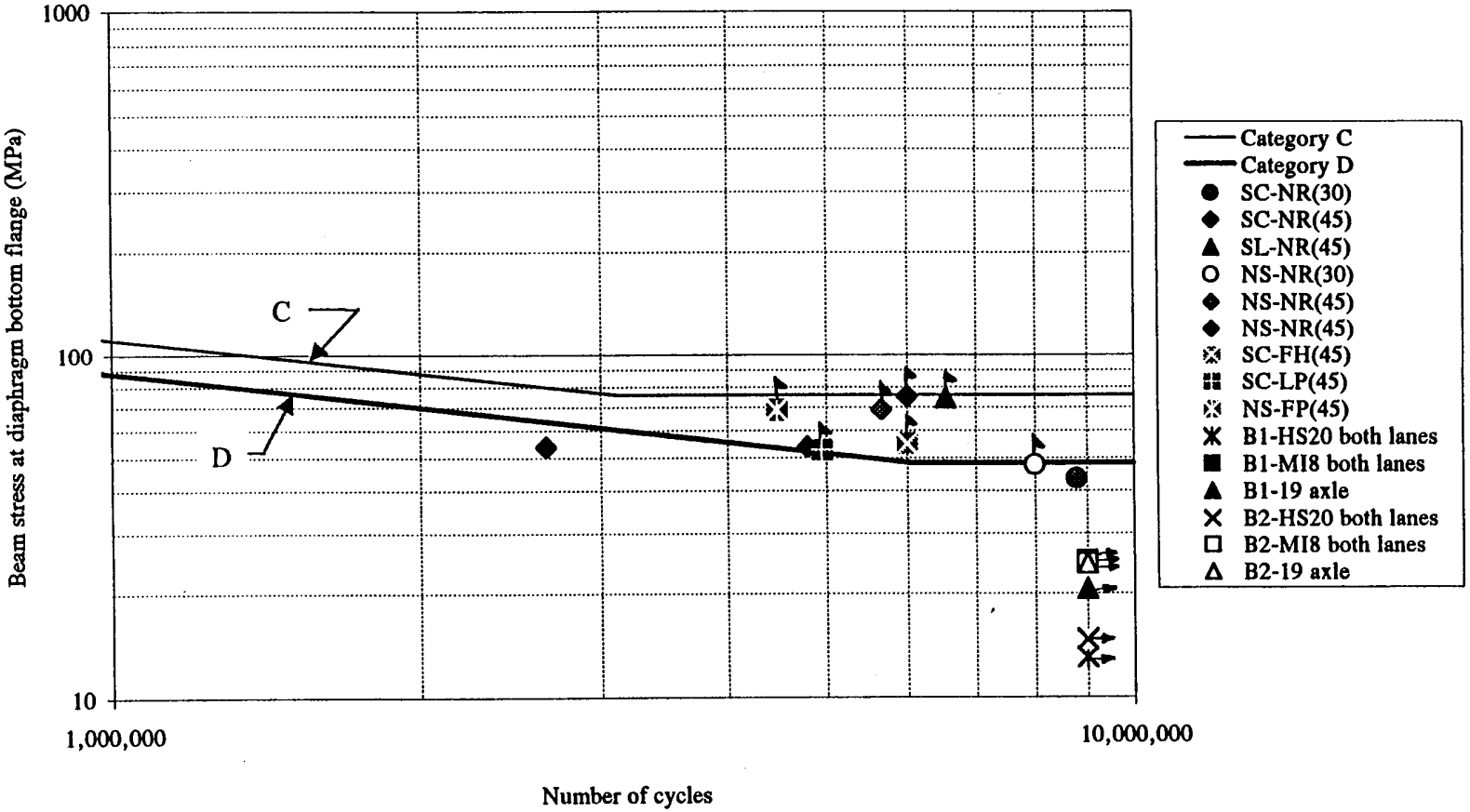

Note: 1 ksi = 6.89 MPa
Points with arrows indicate test did not fail

Figure 5.9 Stress range versus number of cycles for experimental tests and bridges analyzed

CHAPTER 6

ANALYTICAL PREDICTION OF CYCLIC LIFE

The purpose of the analytical work is to gain a more thorough understanding of the stresses that exist in the diaphragm-to-beam welded connection so that the fatigue strength and resistance of the detail can be evaluated accurately. The stress field near the welds is not simple to determine since it is caused by in-plane flexural bending stresses and out-of-plane distortion induced bending stresses. Finite element models of the welded diaphragm connection were developed in order to determine the stresses near the welds. The stresses were then used in a crack propagation model which predicts the life to propagate an initial crack to a specified length.

6.1 Stress Analysis

Finite element analyses were performed using ANSYS (1996), a general purpose finite element computer package. The analysis was conducted in two phases in order to determine the stress distribution along the toe of the diaphragm flange.

In the first phase, a three-dimensional model of the overall experimental setup was generated. The beams and diaphragms were modeled using 4 node elastic shell elements for the webs and flanges. The diaphragm was continuously connected to the beam web and the welds were not modeled. A view of a typical global mesh for a

staggered diaphragm configuration is shown in Fig. 6.1. A fixed support was modeled at one end of the beam by restraining translation at the lower flange nodes in the x, y, and z directions. A roller support was modeled at the opposite end by restraining movement in the x and z (vertical and lateral) directions at the lower flange nodes. Additionally, restraints were added at the angle strap locations in the lateral direction at the mid-top flange nodes. The load was applied at midspan of the center beam on the mid-flange node.

Global models were analyzed for each of the stagger conditions: no stagger (NS), stagger with load centered between the diaphragms (SC), and stagger with load at one of the diaphragms (SL). The load applied to the finite element model was the maximum load applied to the experimental test beam: 148 kN (33.3 kip) or 222 kN (50 kip). The nodal displacements from the global model were then used in the second step of the finite element model.

The second phase of the finite element modeling involved an independent, more finely meshed model of the area around the diaphragm-to-beam connection. The second phase was conducted so that a denser mesh could be obtained near the connection which was the primary area of interest.

The submodel utilized the cut-boundary displacement method. The boundary of the submodel represents a cut through the global coarse model. The boundary conditions of the submodel are the displacements calculated on the cut boundary of the global model. The displacements associated with the nodes of the denser mesh are interpolated from the nodal displacements in the global model.

The submodel was created by “zooming” into the diaphragm connection area. A distance of 610 mm (24 in.), approximately the height of the test beam, was taken on each side of the connection area, including along the diaphragm length. Figure 6.2 shows a typical submodel for the stagger condition SC. The submodel has a more refined mesh in the web gap area between the bottom flange of the diaphragm and the bottom flange of the beam. The model uses 4 node elastic shell elements for the webs and flanges of the beam and diaphragm. As in the global model, the diaphragm is continuously connected to the beam web so the welds themselves are not modeled. Within the cut boundary of the submodel, it was necessary to add a lateral restraint due to an angle strap falling within the region.

Submodels were analyzed for the same conditions as the global models: NS, SC, and SL with 148 kN and 222 kN applied loads. Figure 6.3 shows a 50X magnification of the deformed shape of the submodel SC from a 222 kN applied load. From this figure it can be seen that the beam web is bending out-of-plane during load application. Figure 6.4 shows the out-of-plane stress contours. Within the lower web gap, there is a change in the sign of the stress magnitude which indicates the web gap is in double curvature bending.

Illustrations of the global models and submodels, as well as the deformed shapes and stress contours for the two load magnitudes, for each of the stagger conditions can be found in Grider (1998).

The stress distribution in the beam along the toe of the diaphragm flange was obtained for each stagger configuration and load magnitude. The results are plotted in

Figs. 6.5 to 6.10. Also shown in these figures is the bending stress calculated from strength of materials formulas ($\sigma = M*y/I$). The horizontal dashed lines represent the diaphragm flange location. The plots indicate that there is a notable difference in stresses induced in the beam for the back-to-back diaphragm configuration and the staggered one. There is a significant stress concentration at the lower diaphragm flange for the staggered configuration that does not exist in the back-to-back configuration. In fact, for the staggered condition, the finite element stresses are elevated approximately 2.3 times the elastic flexural stresses. Moreover, it is likely that additional increases in stress at this location are due to residual stresses from welding. Residual stresses, however, are not included in the computed stresses. Beyond the bottom flange region, the longitudinal stress is very nearly the same as the bending stress calculated from basic mechanics. The welded connection has little effect on the longitudinal stress at the bottom beam flange for both nonstagger and stagger layouts.

6.2 Crack Propagation

A method of predicting the fatigue crack propagation life of the diaphragm-to-beam welded connection can be developed using linear elastic fracture mechanics concepts. A computer program was written to estimate the propagation life of steel members with fatigue cracks that develop in the beam web at the diaphragm connection. The time to initiate the crack was not considered. In order to calculate the propagation life, the following information is needed:

- nominal stress and stress concentration at the critical detail,

- stress intensity factor for the cracked detail,
- model to describe the crack growth rate for a given material,
- initial and final crack sizes.

6.2.1 Stress Intensity Factor

The stress intensity factor, *K*, characterizes the magnitude of the local stresses near the crack tip. The factor depends on loading, crack size, crack shape, and geometric boundaries. Exact determination of the stress intensity factor is often difficult to obtain. A simplified method of calculating the stress intensity factor for the crack opening mode (Mode I) was proposed by Albrecht and Yamada (1977). The basic stress intensity factor for a through crack in an infinite plate subjected to a uniform tensile stress is multiplied by several correction factors to give

$$K = F_E\ F_S\ F_W\ F_G\ \sigma\sqrt{\pi a} \tag{6.1}$$

where F_E, , F_S , F_W , and F_G account for elliptical crack shape, free surface, finite width, and nonuniform opening stress, respectively; σ is the remote stress; and a is the half crack length.

An empirical equation for the stress intensity factor for an elliptical surface crack under tension and bending loads was developed by Newman and Raju (1981). The equation is based on the stress intensity factors obtained from a three-dimensional, finite element analysis of semi-elliptical surface cracks in finite elastic plates subjected to tension or bending loads. The solution is presented in Grider (1998). The Newman and Raju model does not account for the nonuniform opening stress (such as those due to the

welded diaphragm connection), F_G , but does account for the other correction factors in the Albrecht and Yamada equation .

The geometrical stress concentration factor, F_G , can be expressed as

$$F_G = \frac{2}{\pi} \sum_{i=1}^{n} \frac{\sigma_{bi}}{\sigma} \left(\arcsin\left(\frac{b_{i+1}}{a}\right) - \arcsin\left(\frac{b_i}{a}\right) \right) \tag{6.2}$$

where σ_{bi} = normal stress in the finite element model of the structural detail where the crack is inserted,

σ = normal stress in the member uniformly distributed over the thickness of the plate and computed with strength of materials formulas,

b_i = increment of crack length, and

F_G = geometric correction factor which accounts for the structural detail.

It represents the ratio of the stress intensity factor for a nonuniform stress distribution along the line of the crack to the stress intensity factor for a uniformly distributed mean stress.

6.2.2 Propagation Model

One of the most widely accepted models for stable crack growth is the Paris equation:

$$\frac{da}{dN} = C\left(\Delta K\right)^m \tag{6.3}$$

where *da/dN* is the crack growth rate in mm/cycle, ΔK is the stress intensity range in MPa*mm$^{0.5}$, and *C* and *m* are material constants. Table 6.1 shows some common values of *C* and *m* for steel.

The number of cycles to propagate a crack to a specified length may then be calculated by:

$$N_P = \int_{a_i}^{a_f} \frac{da}{C\left(\Delta K\right)^m} \tag{6.4}$$

6.2.3 Initial and Final Crack Sizes

The initial and final crack sizes were obtained from the experimental portion of this study. In each test the crack lengths were obtained by visual inspection using a 10X magnifying glass. A crack depth to length ratio was assumed to obtain the initial crack depth required for calculation purposes. A number of ratios were examined for web and flange cracks in order to obtain propagation results that compared reasonably well with the experimental propagation results. Of the experimental tests conducted, SC-NR(45) was used for comparative purposes to obtain the appropriate depth to length ratios. This specimen provided two data points for cracks growing through the web thickness and fracturing the tension flange. The first fracture occurred 2,138,840 cycles after first detecting the crack and the second fracture occurred 3,671,770 cycles after first detection.

Four crack depth to length ratios were studied for elliptical web cracks ranging from elliptical cracks to penny shaped cracks: 1/20, 1/10, 1/4, and 1/2. For a given initial web crack length, four crack depths were calculated. The initial crack length seen in the SC-NR(45) test was 3 mm (0.125 in.). The crack depths examined were: 0.16 mm (0.00625 in.), 0.32 mm (0.00125 in.), 0.79 mm (0.03125 in.), and 1.59 mm (0.0625 in.) for the depth to length ratios 1/20, 1/10, 1/4, and 1/2 respectively.

The flange depth to length ratios studied were: 1/4, 1/3, and 1/2. In the computer program, a through web crack propagates down to the beam tension flange until it reaches the bottom of the beam. The crack then grows across the flange width as a through-thickness flange crack. Therefore, the crack depth is known to be the flange thickness (12.8 mm (0.505 in.) for W24x55) and the crack length is the variable studied. The crack lengths studied were: 51.3 mm (2.02 in.), 38.5 mm (1.515 in.), and 25.7 mm (1.01 in.) corresponding to the ratios 1/4, 1/3, and 1/2 respectively.

The life to fracture the beam tension flange was computed for each combination of web and flange ratios. The computed propagation life was then compared with the experimental propagation lives. The results are shown in Figs. 6.11 to 6.13 for an initial web crack length of 3.2 mm (0.125 in.). Each figure represents the computed lives for a specific flange ratio with each of the web ratios plotted in the graph. Lives were computed using each of the material properties in Table 6.1 with the following designation:

- Material 1: $C=2.18(10)^{-13}$ and $m=3.0$
- Material 2: $C=2.09(10)^{-14}$ and $m=3.3$
- Material 3: $C=1.52(10)^{-13}$ and $m=3.0$.

Material 1 corresponds to a conservative growth rate and is shown for comparative purposes only. The two horizontal lines refer to the observed experimental lives to propagate an initial crack to fracture the tension flange.

The small web depth ratios (1/20 and 1/10) do not predict the time to fracture the flange well for any of the flange ratios. The computed lives for these ratios are close to

the second fracture in the beam and do not compare well with the first fracture. The largest web ratio (1/2), which corresponds to a semi-circular crack, does not predict the propagation life well for the second fracture; however, the predicted life with the 1:2 ratio compares very well with the time to first fracture.

The predicted lives computed using a depth to length ratio of 1:4 for the web crack fall between the two experimental lives for materials 2 and 3 for all of the flange ratios studied. The computed propagation life does not vary greatly between the flange ratios for a specific web ratio. For a web ratio of 1:4, the computed life varies from 2,647,160 for a 1:4 flange ratio to 2,852,560 for a 1:2 flange ratio (for material 2).

In the experimental tests, the crack lengths on the top and bottom of the flange were measured when the crack was first observed to be through the flange thickness. The measured length to depth ratios were approximately 4. Therefore, a ratio of 4 was chosen for the flange length to depth ratio in all of the analytical predictions.

In conclusion, the depth to length ratio of 1:4 is used for both web cracks and flange cracks to determine the propagation life using the program developed. Also material 2 is used for the analytical predictions.

6.2.4 Model Algorithm

From the experimental tests it was determined that the critical location for crack initiation is at the toe of the lower flange of the welded diaphragm connection; the finite element results also show a high stress concentration at this location. Three stages are used to grow an elliptical web crack at the diaphragm to a position in the lower flange

that results in fracture of the beam tension flange. The first stage is the propagation of an elliptical web surface crack to a through thickness crack in the beam web. The through web thickness crack then propagates to the tension flange of the beam and reaches the bottom of the beam. The crack is then a through flange thickness crack and propagates across the flange until fracture. The program ends when the crack size reaches a specified size that the user inputs, the tension flange fractures, or when the stress intensity factor exceeds the toughness of the material.

When the stress intensity factor reaches a critical value, K_c, unstable fracture occurs. The critical value of the stress intensity factor is known as the fracture toughness of the material. The fracture toughness depends on the temperature, specimen thickness, and loading rate. If a combination of stress and crack size, represented by K, reaches the K_c value, then brittle fracture can occur.

The following sections describe the calculation procedure for each of the growth stages. The computer program is given in Appendix G along with a users guide.

6.2.4.1 Stage I Growth

The first stage in the propagation life is to propagate an elliptical surface web crack (that initiates in the beam at the diaphragm lower flange) through the beam web thickness. The stress distribution along the diaphragm flange line was computed from the finite element models described in Section 6.1. The Newman and Raju model for an elliptical surface crack is used to calculate the stress intensity factor for stage I. The finite element stress at the crack center is used for the propagating stress.

Two growth rates are calculated using the Newman and Raju stress intensity solution: one at the crack depth and one on the surface which represents the length. The crack is first grown an incremental amount through the web depth (*da=a/500*) and the corresponding number of cycles (*dN*) is determined using the depth growth rate. The change in crack length (*dc*) is calculated with the crack length growth rate using *dN* from the depth calculation.

The crack depth and length are updated with each program cycle. The end of the first stage occurs when the crack depth equals the beam web thickness or if the stress intensity factor exceeds the material fracture toughness. Some additional criteria are also checked to ensure the validity of the stress intensity factor solution by Newman and Raju:

1. Crack depth is less than half the crack length.
2. The crack length is less than half the plate width (in this case, the plate width is half the beam depth).

6.2.4.2 Stage II Growth

This stage of the crack growth corresponds to the propagation of the web crack from the size that corresponds to a through thickness crack to a size that reaches the tension flange of the beam. The stress intensity factor solution by Albrecht and Yamada is used with F_E = 1.0 and F_S = 1.0. F_G is calculated using Equation 6.2. The average bending stress along the crack length is used for the propagating stress. The finite width correction factor is taken to be

$$F_W = \sqrt{\frac{W}{\pi c} \tan\left(\frac{\pi c}{W}\right)} \tag{6.5}$$

where W is the plate width (half the beam depth for this case) and c is half the crack length.

The crack growth rate is then calculated from

$$\frac{dc}{dN} = C\left(F_W F_G \Delta\sigma \sqrt{\pi c}\right)^m \tag{6.6}.$$

The crack is grown an incremental amount ($dc=c/500$) and the corresponding number of cycles is determined. Stage II growth is completed when the crack length reaches the bottom of the tension flange or if the stress intensity factor is greater than the fracture toughness of the material.

6.2.4.3 Stage III Growth

The final growth stage is the propagation of a flange crack to fracture the tension flange. The stage II crack extended to the bottom of the flange so the flange crack is already through thickness. A length to depth ratio of 4 is used to determine the crack length in the flange.

The Albrecht and Yamada solution for the stress intensity factor is used with $F_E = 1.0$, $F_S = 1.0$, and $F_G = 1.0$. The geometric correction factor equals unity for this stage since the finite element stress at the bottom of the beam equals the bending stress calculated from simple bending theory. The welded connection has little effect on the stresses at the bottom flange. Equation 6.5 is used to calculate the finite width correction factor where W is the beam flange width.

The flange crack was grown by *c/500*, where *c* is half the flange crack width, and the number of cycles was determined from the growth rate. The program ends when the flange crack equals the flange width, which corresponds to the tension flange fracturing, or when the stress intensity factor exceeds the fracture toughness of the material.

6.3 Model Verification

The computer program predicts the fatigue crack propagation life of cracked steel members with welded diaphragms. Comparisons between the experimental test results and the corresponding program predictions are presented in this section. The number of cycles to first detect a beam crack in an experimental test was subtracted from the total cyclic life so that the experimental propagation life is compared with the analytical prediction.

The analytical results were obtained using a crack depth to length ratio of 1 to 4 for elliptical web cracks and a ratio of 1 to 4 for through flange cracks. The constants for mean propagation rates of ASTM A36 steel were used in the Paris growth law.

6.3.1 Stagger Specimens

Two experimental tests were conducted in the stagger diaphragm configuration with no repairs performed. The SC-NR(30) specimen was subjected to a 67.6 MPa (9.8 ksi) stress range at the beam tension flange on the cross-section where the diaphragm was attached while the SC-NR(45) specimen had a stress range of 98.6 MPa (14.3 ksi). A comparison between the experimental test lives and the corresponding predicted

analytical lives are presented in Table 6.2. The experimental life corresponds to tension flange fracture or the end of the test. The analytical life is either the time to fracture the flange or the time to propagate an initial crack to a final size measured from the experiments. The analytical predictions for specimen SC-NR(30) are generally conservative, while the results for the other test agree well with the experimental results.

The tension flange fractured at only one diaphragm location for the SC-NR(30) test. The initial crack lengths were fairly large for this test: 66.7 mm (2.625 in.) at the fractured flange location and 41.3 mm (1.625 in.) at the other diaphragm. Neither crack was through thickness when first observed. If a ratio of 1 to 4 is used to determine the initial web depth for these cracks, then the cracks would be through thickness. Since the cracks were not yet through the web when first observed, a ratio of 1 to 10 is used to predict the propagation time. With the large initial crack sizes, the program is conservative in predicting the propagation time.

The initial crack lengths were very small (3 mm at each location) for the SC-NR(45) specimen. The experimental propagation lives of this test were 2,138,840 cycles and 3,671,770 cycles for the two diaphragm locations. A web crack length to depth ratio of 4 predicts a life of 2,647,150 cycles, about midway between the two experimental values.

6.3.2 No Stagger Specimens

There were three experimental tests performed with no repair for the back-to-back diaphragm layout. However, the NS-NR(30) specimen did not develop vertical cracks at the diaphragm lower flange so no comparison can be made with this test.

The stress distribution along the toe of the diaphragm flange, as determined from the finite element analysis, is very different for the no stagger and stagger configurations. Specifically, the no stagger layout has little stress amplification at the diaphragm flange. The finite element distribution was computed with all welds intact. However, the welds fractured quickly in the experimental tests and the load distribution throughout the beam-diaphragm system changed significantly. The back-to-back layout behaved like a stagger layout once the welded connection fractured. Therefore, the analytical predictions were made using the stagger stress distribution developed in the finite element model.

Table 6.3 shows the comparison between the experimental tests and the predicted analytical life. The analytical predictions represent the time needed to propagate an initial web crack, with a depth to length ratio of 1 to 4, to the final size measured in the experiments since neither NS-NR(45) specimen fractured the tension flange. The stress range at the tension flange was 77.9 MPa (11.3 ksi) before the welds fractured and 117 MPa (17 ksi) after the welds fractured for each test.

From the comparison of lives it is apparent that the analytical model underestimates the lives, especially with large initial cracks. Two factors could be responsible for the significant difference in computed and observed lives: crack length to depth ratio and lateral restraint of the beam. For the first factor, accurate modeling of the

crack geometry is necessary to obtain a good estimate of the crack propagation life. For large crack widths, it appears that the depth of the crack may not be as deep as originally assumed. For example, in the prediction for specimen SC-NR(30), which also had a large initial crack size, a 1 to 10 ratio of the crack depth to length still provided a very conservative estimate. For the second factor, the stress distribution varies depending upon where the diaphragms are located. For each of the no stagger tests, the diaphragms were located at midspan where the load was applied. As noted in the experimental results, the staggered diaphragms twisted the test beam which amplified the stress at the detail. However, when one of the staggered diaphragms was located at the point of load application (SL-NR(45)), the beam did not undergo as much twisting; the point of load application offered some lateral resistance to the beam. The finite element stress distribution used in the program is based on the stagger centered configuration which produced the greatest stress amplification at the critical location for crack initiation. Therefore, the program provides conservative estimates for beams that have more lateral restraint.

6.4 Fatigue Life of Bridge Members

6.4.1 Model Development

The experimental tests were conducted with constant amplitude loading; however, the actual service loading of the bridge is variable amplitude. In order to estimate the life

of a bridge member with the welded diaphragm connection, a model is needed to relate variable amplitude loading with constant amplitude loading.

A linear damage rule developed by Palmgren and Miner, known as Miner's rule, is

$$D_i = \frac{\alpha_i}{N_i} N \tag{6.7}$$

where D_i is the damage fraction of the ith stress range, α_i and N_i are the frequency and fatigue life of the ith stress range respectively, and N is the service life in cycles of loading applied to the structural detail. Failure occurs when the summation of the damage fraction equals 1.0, or

$$\sum D_i = 1.0 \tag{6.8}$$

The service life of the detail can then be expressed as

$$N = \frac{1.0}{\sum \frac{\alpha_i}{N_i}} \tag{6.9}$$

The frequency of the loading in Equation 6.9 can be inferred if an accurate estimate of the service loading histograms can be constructed. The service loading histogram of the bridge can be determined through weigh-in-motion measurements or it can be estimated from traffic counts on similar types of highways.

The propagation program described previously can be used to predict the service life of bridge members. Weigh-in-motion measurements from Nowak, et. al. (1994)

were used as a typical bridge load histogram. To evaluate the cyclic life for this loading history, the histogram (shown in Fig. 3.2) is broken into 9 kN (2 kip) increments from 27 kN to 356 kN (6 kip to 80 kip). The lower limit chosen was arbitrary since smaller axle weights are unlikely to contribute to the fatigue damage of the structural detail. The life is determined at the middle of the increment range and the corresponding frequency is calculated using a lognormal distribution. The cyclic life of a cracked bridge member with the welded diaphragm connection is calculated using Equation 6.9. The yearly life can be calculated by knowing the average daily truck traffic (ADTT) and assuming a truck causes one stress cycle.

6.4.2 Bridge Member Lives

The fatigue propagation life of bridge members with the welded diaphragm connection can be predicted with the program. The propagation life of the middle size of each beam depth commonly used on Indiana bridges was computed for initial crack sizes ranging from 6 mm to 102 mm (0.25 in. to 4.0 in.). The results were obtained using a length to depth ratio of 4 for web cracks and 4 for flange cracks and the mean propagation constants for A36 steel. The fatigue life is also computed for average daily truck traffic values from 2,500 to 10,000.

The two example bridges discussed in Chapter 5 were at the two extremes of beam sizes:

- Bridge 1: 2 spans at 27,432 mm (90 ft.) with W36x150 beams
- Bridge 2: 3 spans at 12,192 mm (40 ft.) with W27x114 beams.

Each of these bridges was analyzed using SAP90 with an HS20 design truck positioned to cause the maximum positive moment. The maximum computed bending stress from this placement was 21 MPa (3 ksi) for Bridge 1 and 28 MPa (4 ksi) for Bridge 2. For calculation purposes for the program, it was assumed that a 142 kN (32 kip) axle (following axle weight for HS20 design truck) caused a stress of 24 MPa (3.5 ksi) at the beam tension flange for all the beam sizes studied.

A tabular format of the calculated bridge lives is provided in Table 6.4 and graphical summaries are presented in Figs. 6.14 to 6.17. Each figure represents the time to fracture the beam tension flange of a bridge member for a range of initial crack lengths and ADTT values. The results show that the bridge members, even with a high ADTT and large initial crack, should have lives exceeding the expected design life of the bridge.

For comparative purposes, a W36x160 beam with an ADTT of 5,000 was further studied. The spacing and number of beams on a bridge may cause the stress in the beam tension flange to increase from the 24 MPa stress used above. Figure 6.18 provides life estimates for stress ranges of 24 MPa, 34 MPa (5 ksi), and 69 MPa (10 ksi) at the beam tension flange. The life does decrease with the higher stress; however, the lives to fracture the tension flange are still very long.

6.5 Summary and Conclusions

A computer program has been developed to estimate the propagation life of cracked steel members with the welded diaphragm connection. The critical location for the initiation of cracks is at the lower flange weld of the diaphragm. Finite element

analyses were performed to obtain the stress distribution in the beam web along the toe of the diaphragm flange. Two regression equations were developed to represent the distribution above and below the diaphragm flange. The crack propagation program, which is written in FORTRAN, uses the Paris equation to determine the crack growth.

Comparisons were made between the experimental results and the analytical predictions. The propagation life computed for staggered diaphragms agree reasonably well with the experimental results. The analytical predictions are conservative, however, for the back-to-back diaphragms.

The crack propagation program can also be used to determine the life of bridge members subjected to varying load. Weigh-in-motion measurements from a study performed in Michigan (Nowak, et. al. 1994) can be used or the user can input values for the mean and standard deviation of the truck axle weights. The program uses a lognormal distribution to determine the frequency of axle weights and uses a linear damage model to determine the cyclic life. Results were presented for bridge beams commonly used in Indiana and it was shown that long lives are expected.

Table 6.1 Material Constants used in Crack Propagation

Material	C	m	Reference
Conservative growth rates for ferrite-pearlite steels	$2.18(10)^{-13}$ ($3.6(10)^{-10}$)	3.0	Barsom and Rolfe (1987)
Mean growth rates for ASTM A36 steel	$2.09(10)^{-14}$ ($1.0(10)^{-10}$)	3.3	Barsom and Rolfe (1987)
Mean growth rates for ferrite-pearlite steels	$1.52(10)^{-13}$ ($2.507(10)^{-10}$)	3.0	Yamada and Hirt (1982)

Note: English units are given in italics

Table 6.2 Propagation Results for Stagger Diaphragm Specimens

Test	Experimental	Analytical	Notes
SC-NR(30)	5,235,050	1,527,260	Tension flange fracture
	5,235,050	1,233,840	Crack growth from 41.3 mm to 146.1 mm with a_i=4.13 mm (*1.625 in. to 5.75 in. a_i = 0.1625 in.*)
SC-NR(45)	2,138,840	2,647,160	Tension flange fracture
	3,671,770	2,647,160	Tension flange fracture

Table 6.3 Propagation Results for No Stagger Diaphragm Specimens

Test	Experimental	Analytical	Notes
NS-NR(45) #1	3,955,200	541,260	Crack growth from 19.1 mm (*0.75 in.*) to mid-fillet
NS-NR(45) #2	3,569,400	1,276,720	Crack growth from 6.4 mm to 104.8 mm (*0.25 in. to 4.125 in.)*

Table 6.4 Bridge Member Lives

Beam Size	ADTT	Initial Web Crack (mm) (*in.*)					
		6.4 mm (*0.25 in.*)	12.7 mm (*0.50 in.*)	25.4 mm (*1.0 in.*)	50.8 mm (*2.0 in.*)	76.2 mm (*3.0 in.*)	101.6 mm (*4.0 in*)
W36x160	2,500	893	693	551	445	389	346
	5,000	446	347	275	222	195	173
	7,500	298	231	184	148	130	115
	10,000	223	173	138	111	97	87
W33x130	2,500	897	700	561	462	414	372
	5,000	449	350	281	231	207	186
	7,500	299	233	187	154	138	124
	10,000	224	175	140	116	104	93
W30x116	2,500	904	705	567	468	420	374
	5,000	452	353	283	234	210	187
	7,500	301	235	189	156	140	125
	10,000	226	176	142	117	105	94
W27x102	2,500	868	671	537	444	400	355
	5,000	434	336	269	222	200	177
	7,500	289	224	179	148	133	118
	10,000	217	168	134	111	100	89

Note: Values are given in number of years

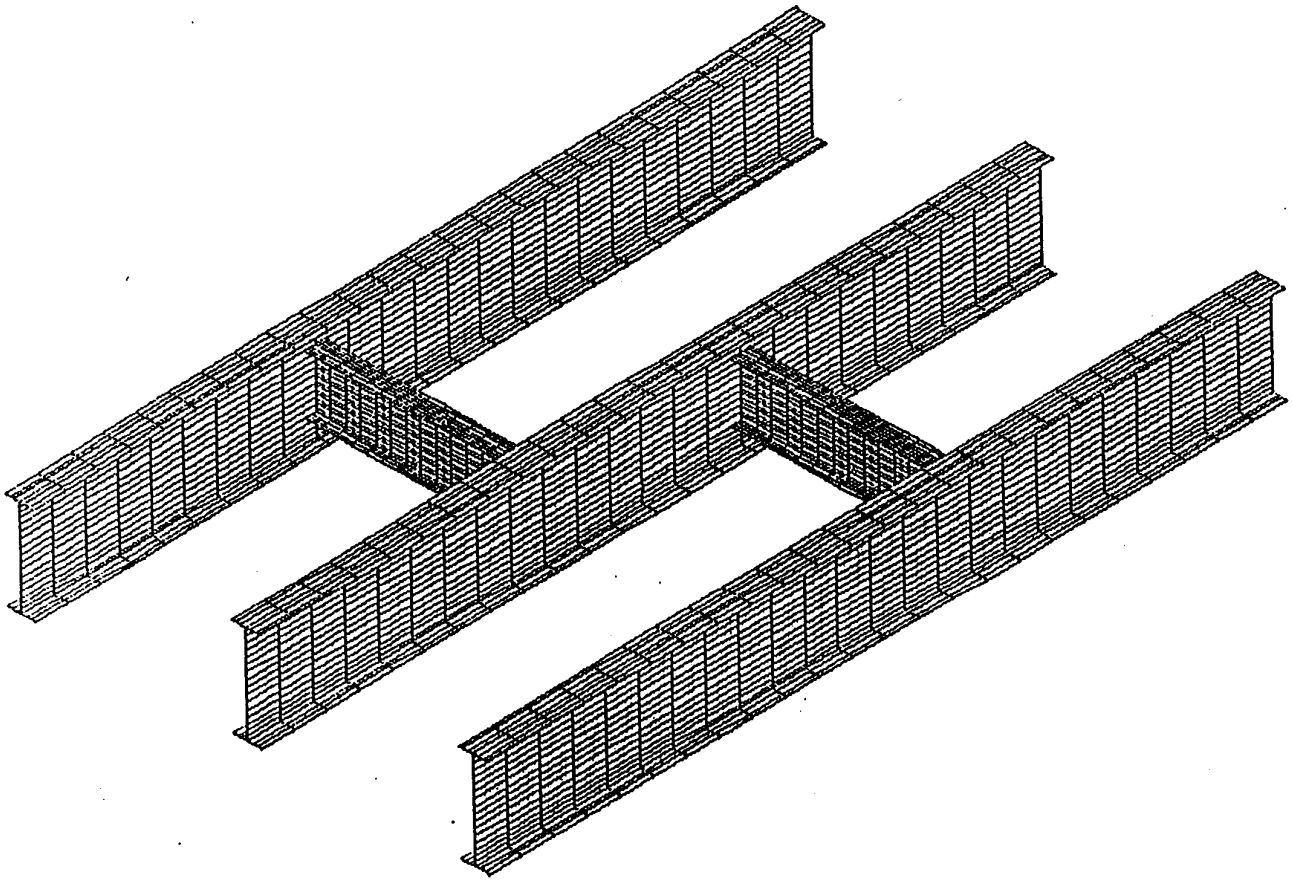

Figure 6.1 Global finite element mesh for stagger diaphragm configuration

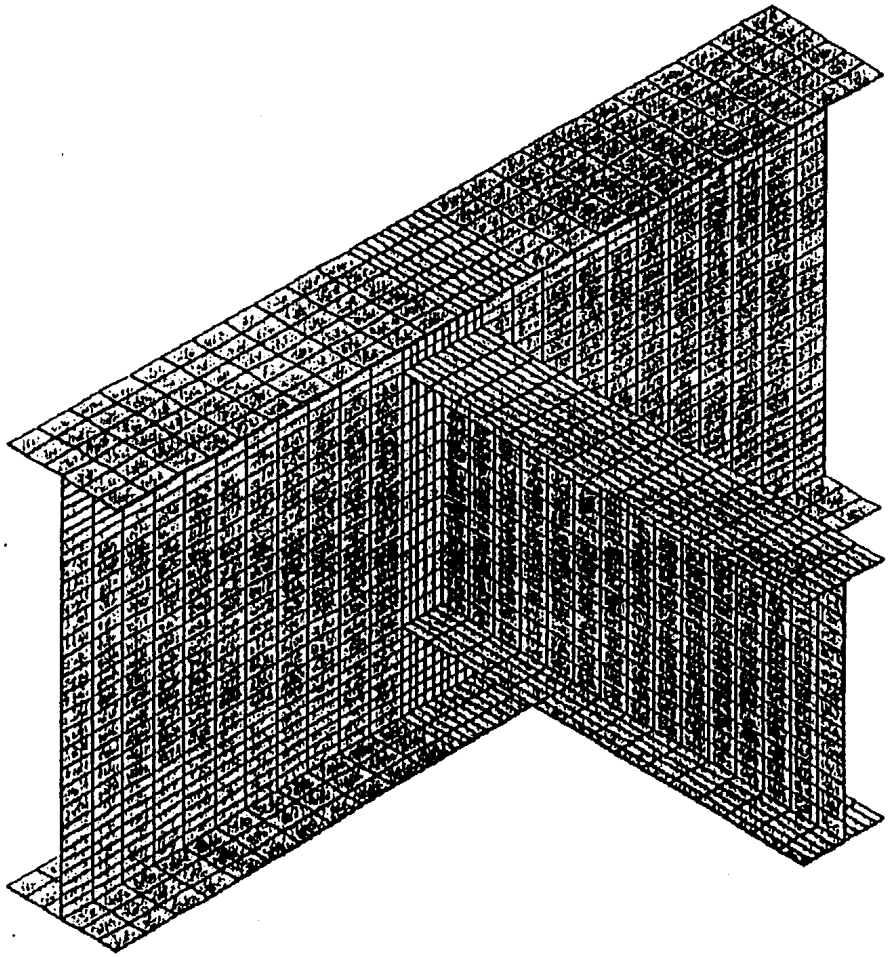

Figure 6.2 Submodel finite element mesh for stagger diaphragm configuration

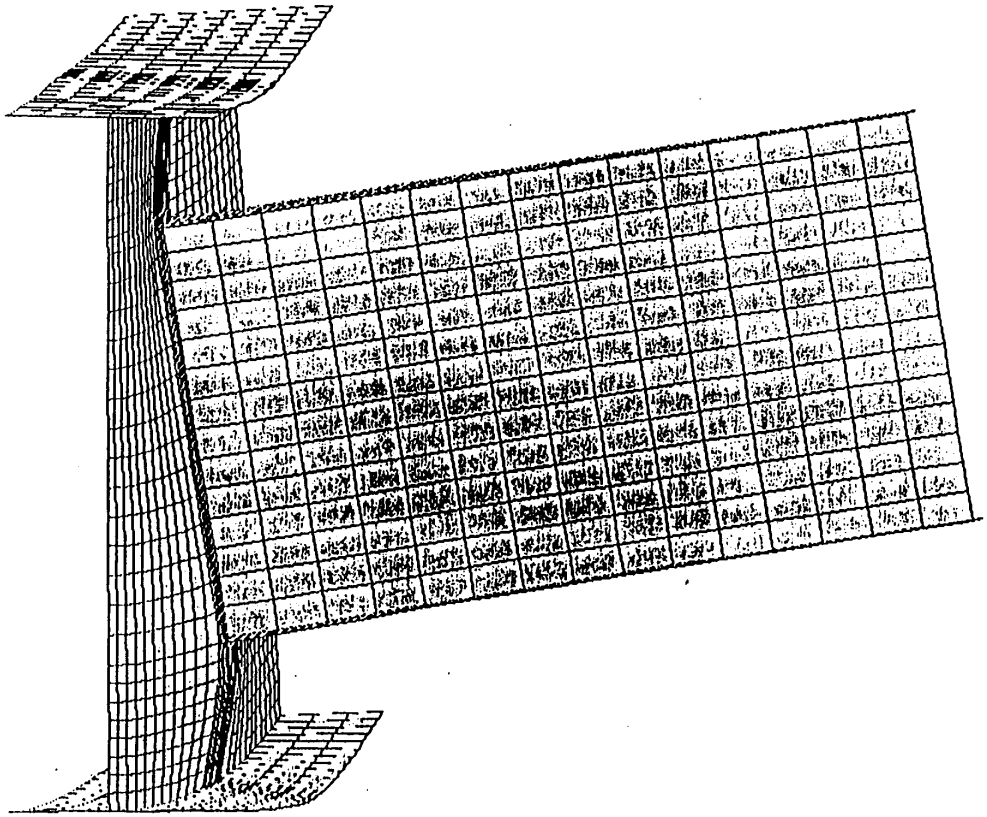

Figure 6.3 Deformed shape for SC(50) – Magnification 50X

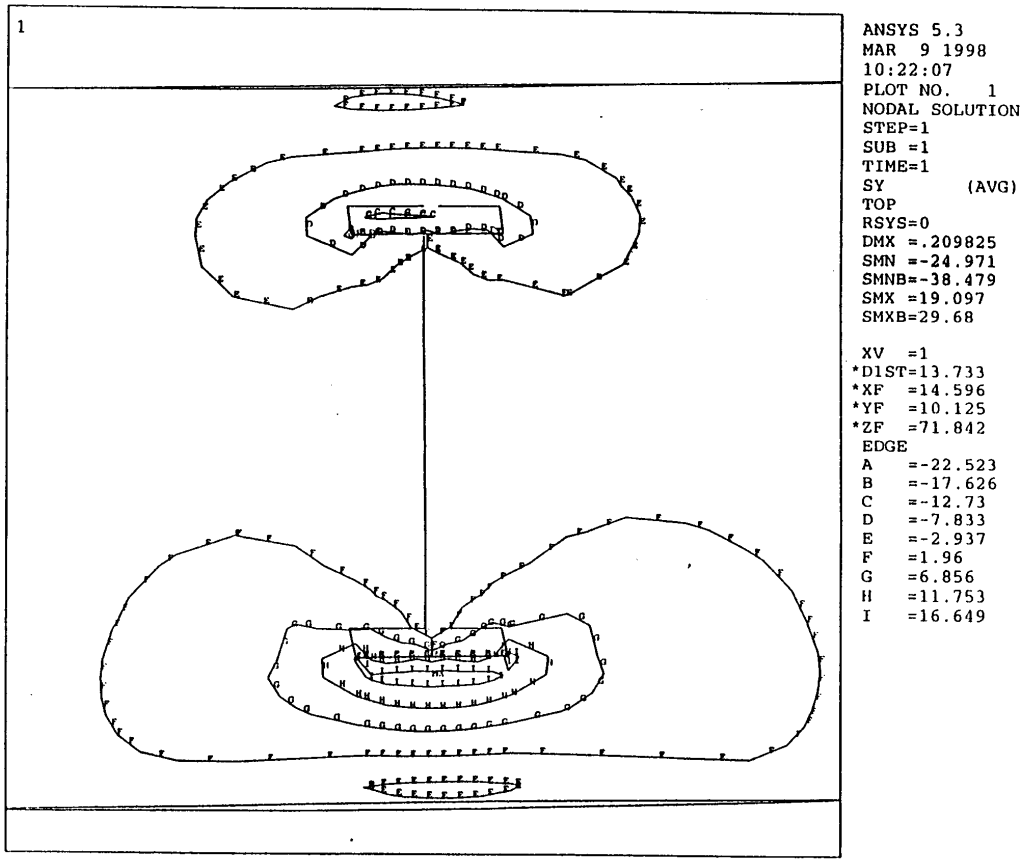

Figure 6.4 Out-of-plane stress contours for SC(50)

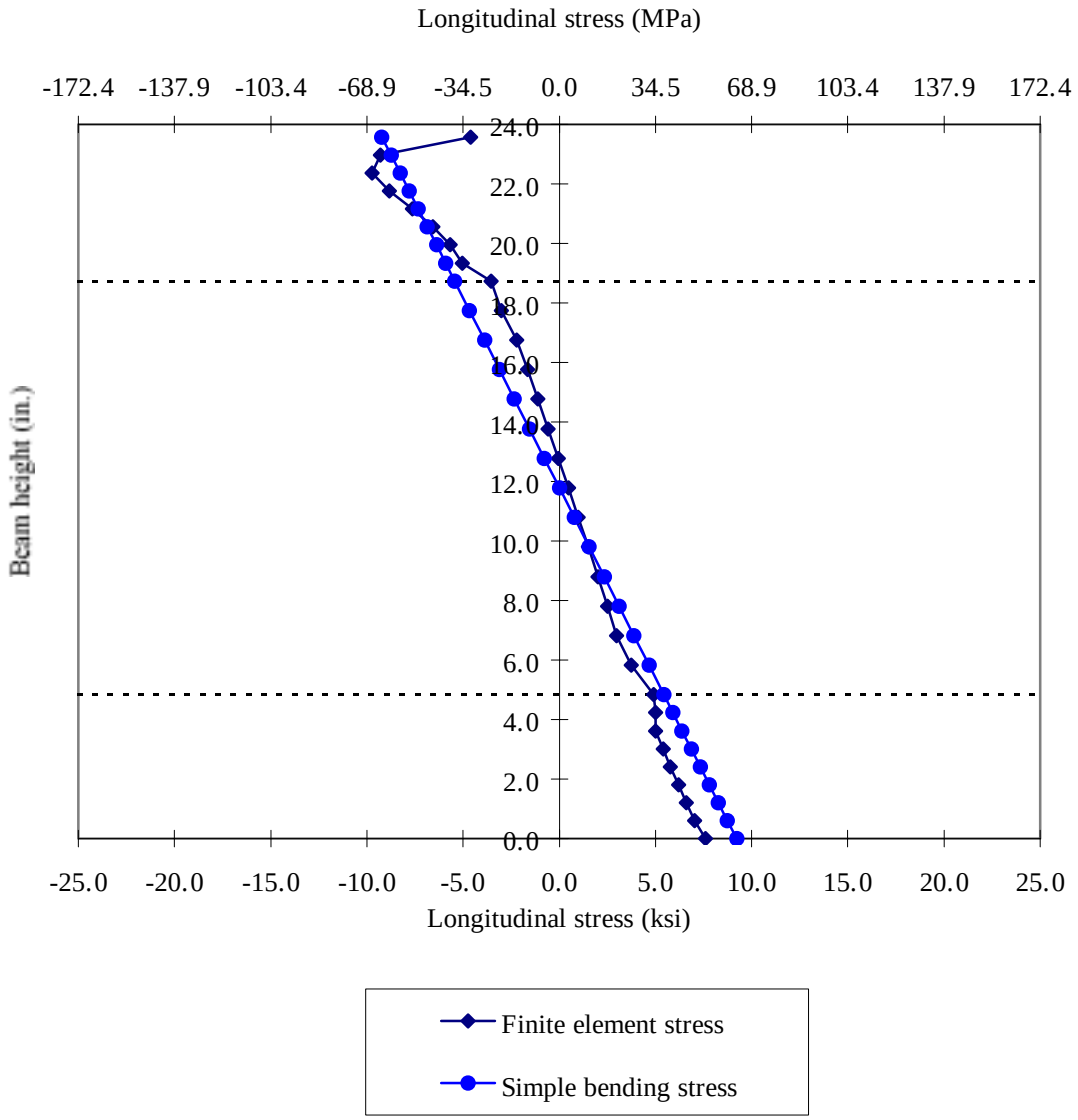

Note: 1 in. = 25.4 mm

Figure 6.5 NS(33) Stress distribution

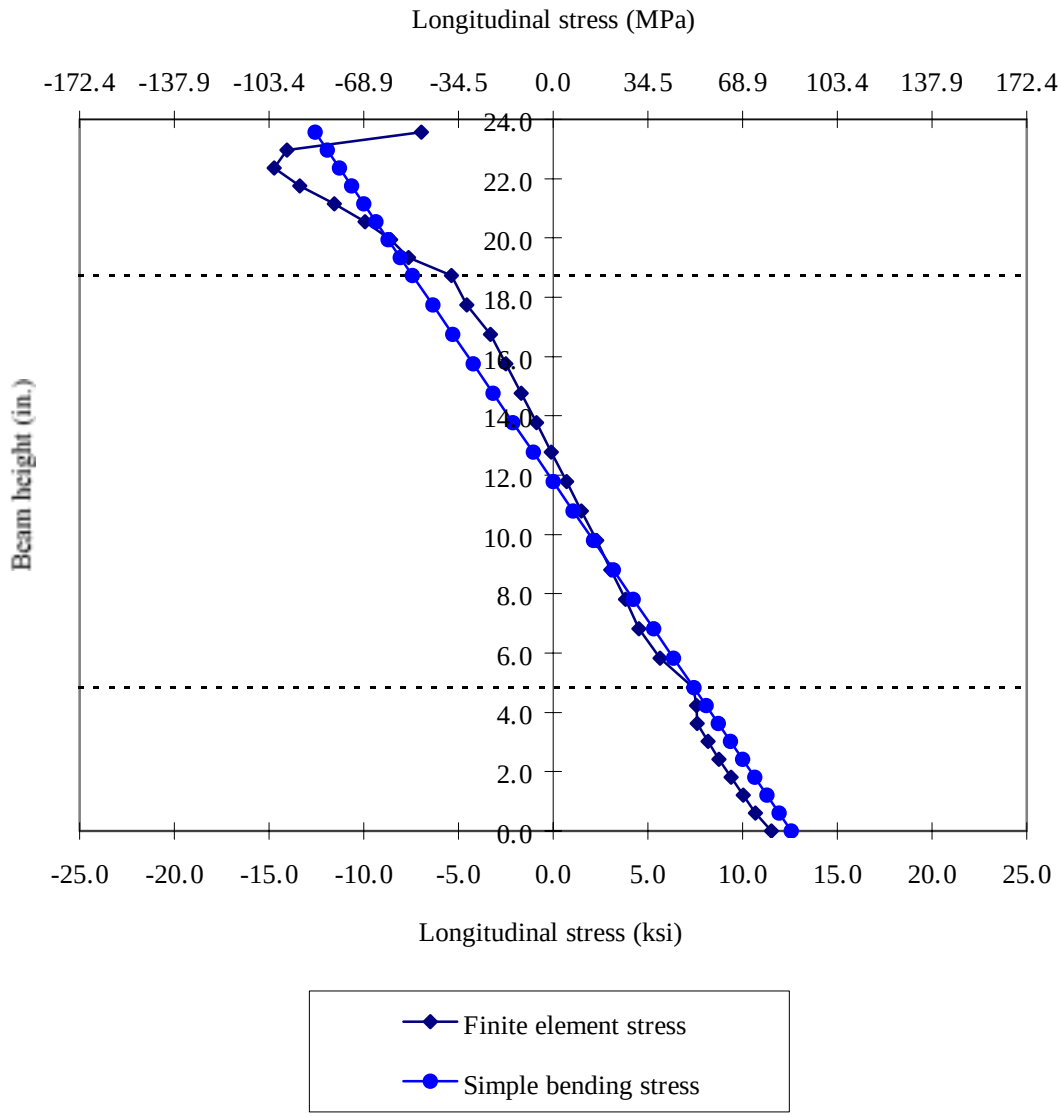

Note: 1 in. = 25.4 mm

Figure 6.6 NS(50) Stress distribution

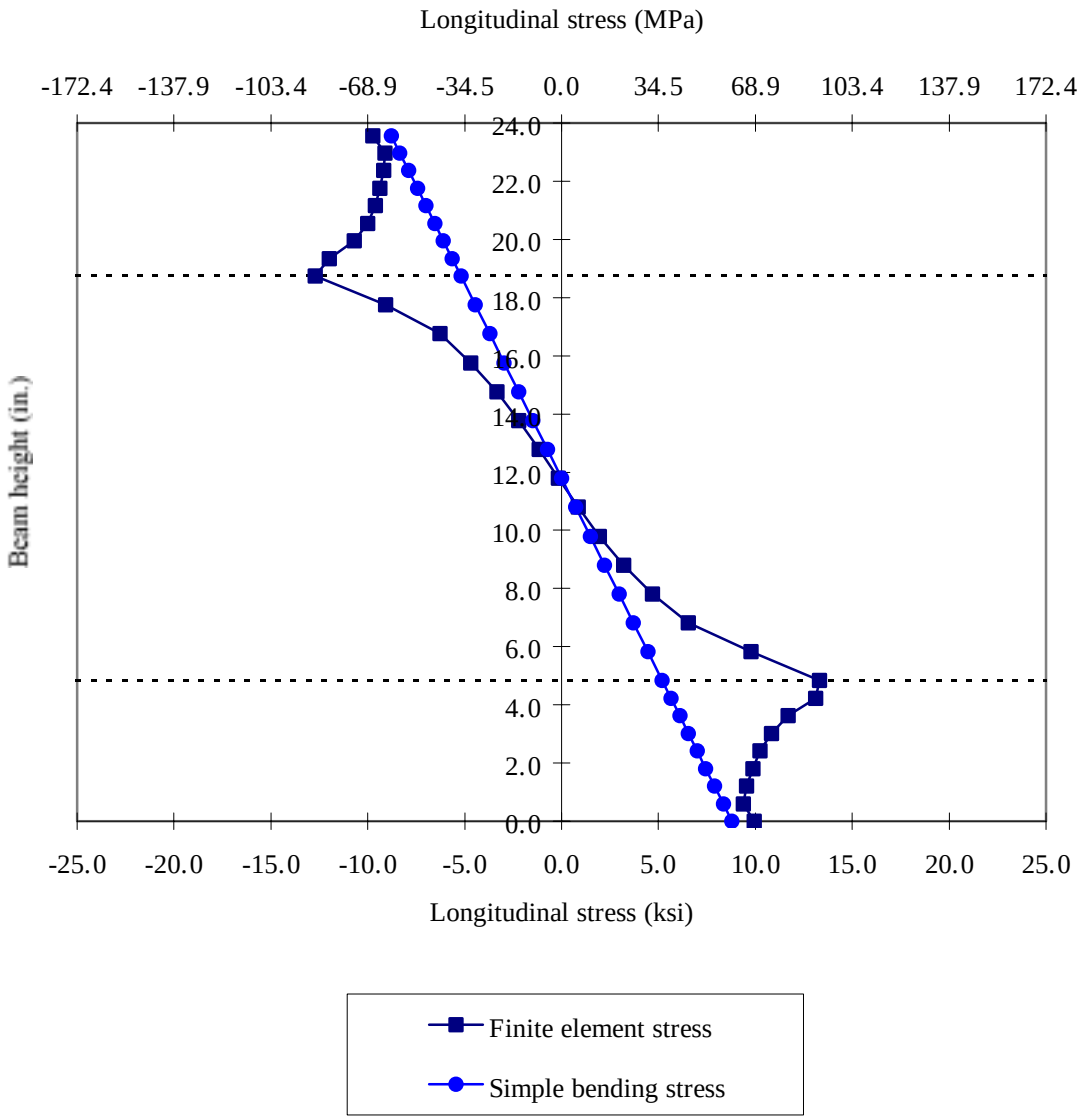

Note: 1 in. = 25.4 mm

Figure 6.7 SC(33) Stress distribution

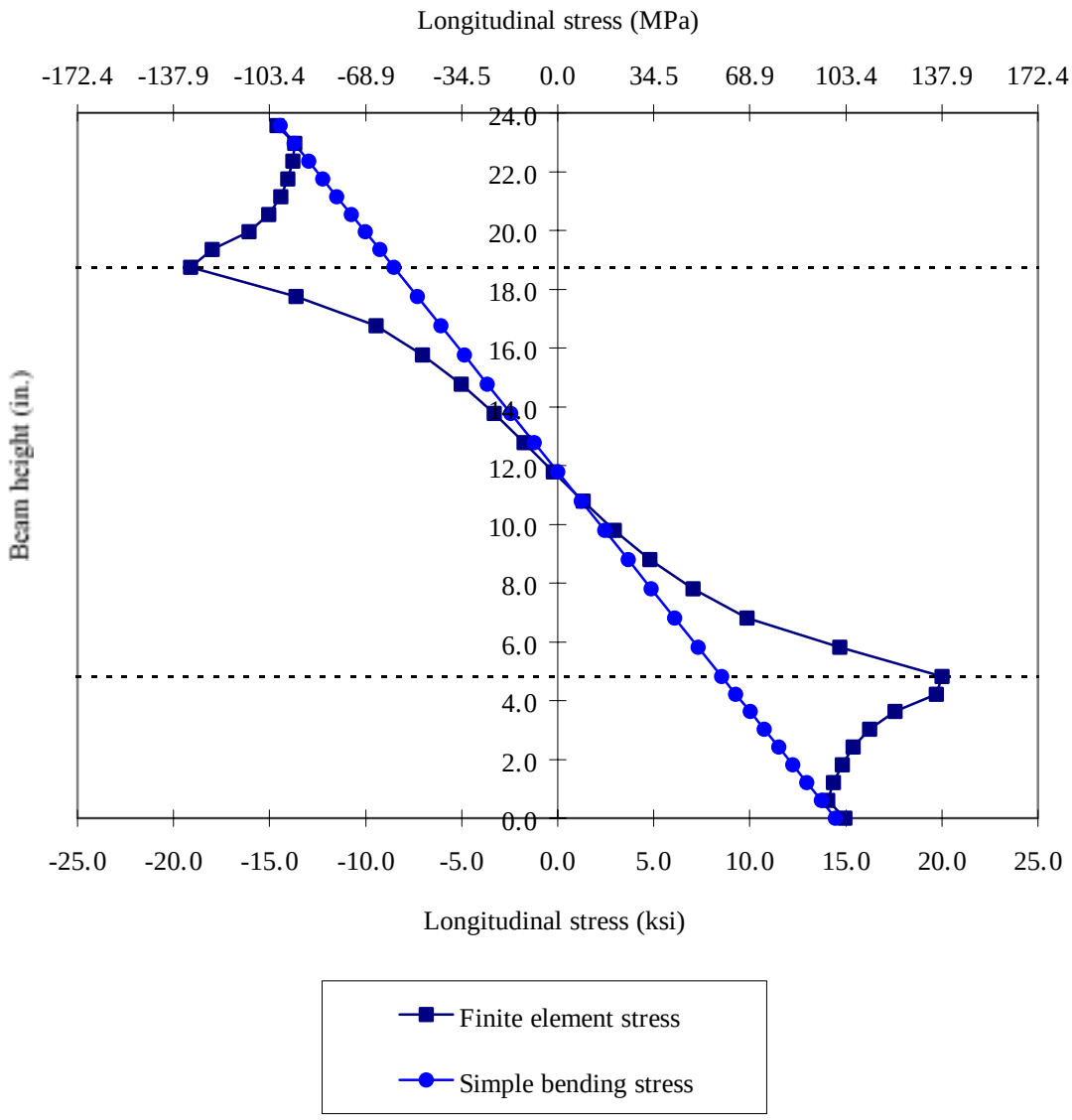

Note: 1 in. = 25.4 mm

Figure 6.8 SC(50) Stress distribution

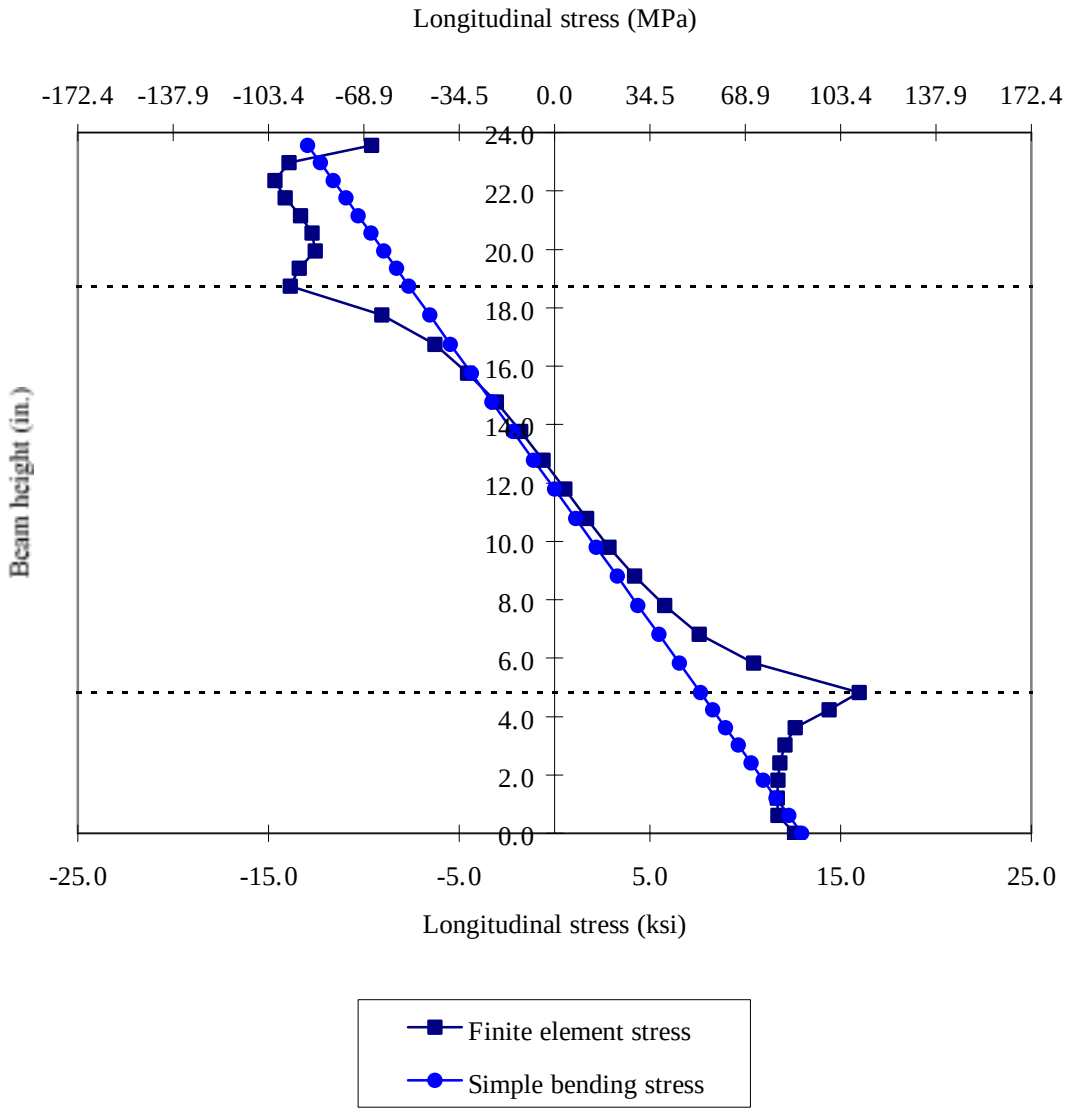

Note: 1 in. = 25.4 mm

Figure 6.9 SL(33) Stress distribution

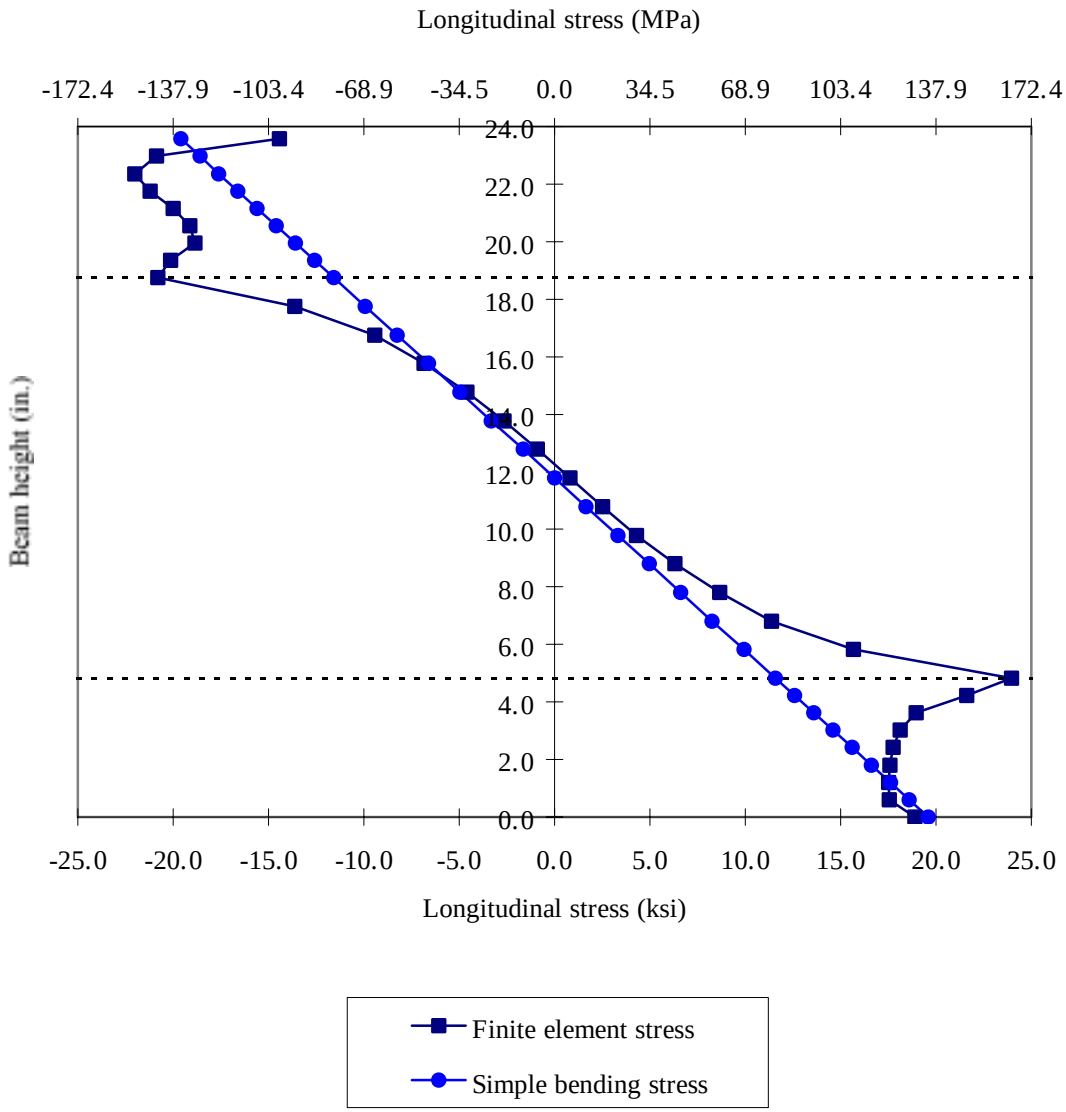

Note: 1 in. = 25.4 mm

Figure 6.10 SL(50) Stress distribution

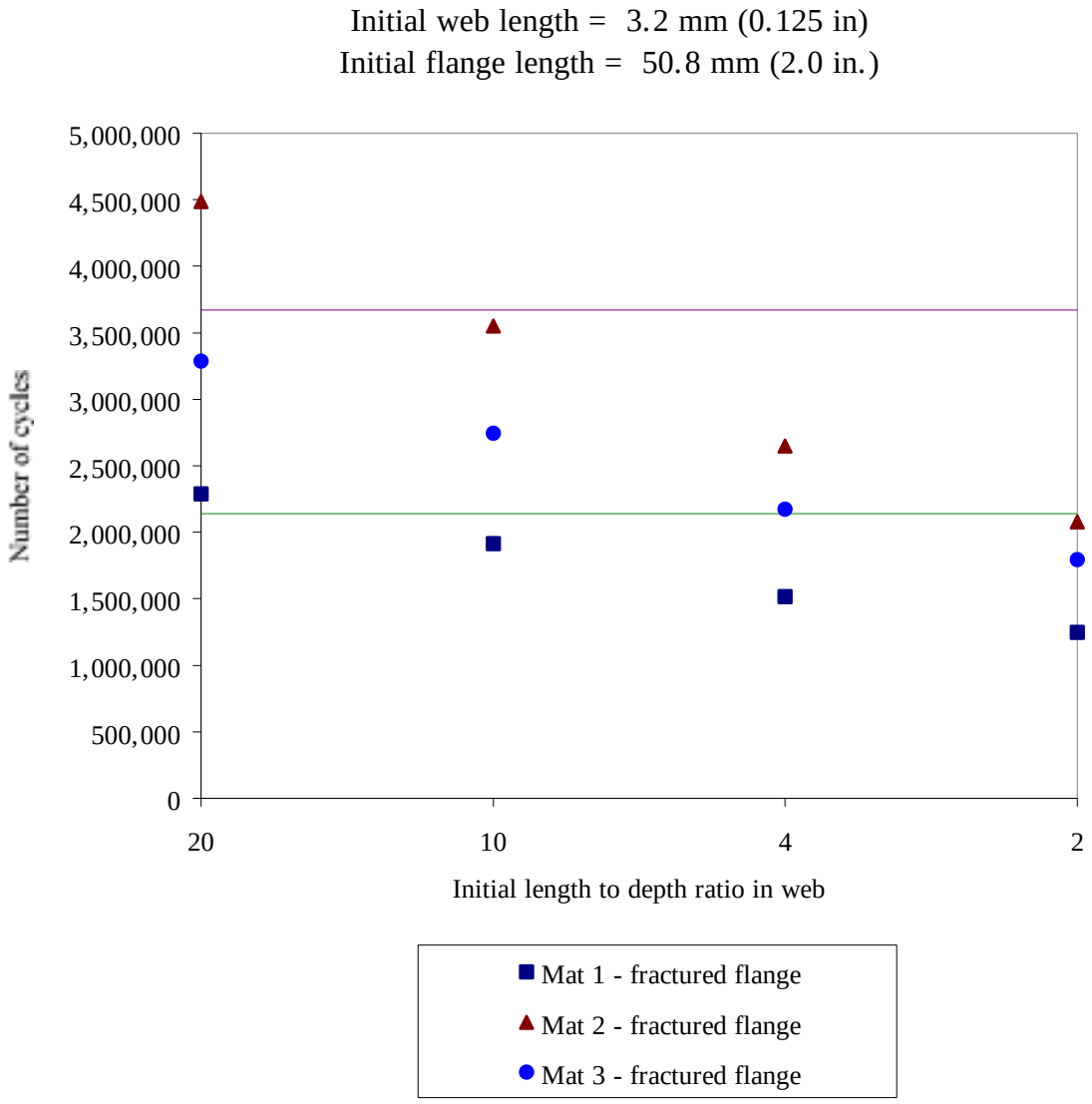

Figure 6.11 Fractured flange comparison for staggered diaphragms and:
initial web crack length = 3.2 mm (0.125 in.),
applied load = 222 kN (50 kip),
flange depth to length ratio: 1/4

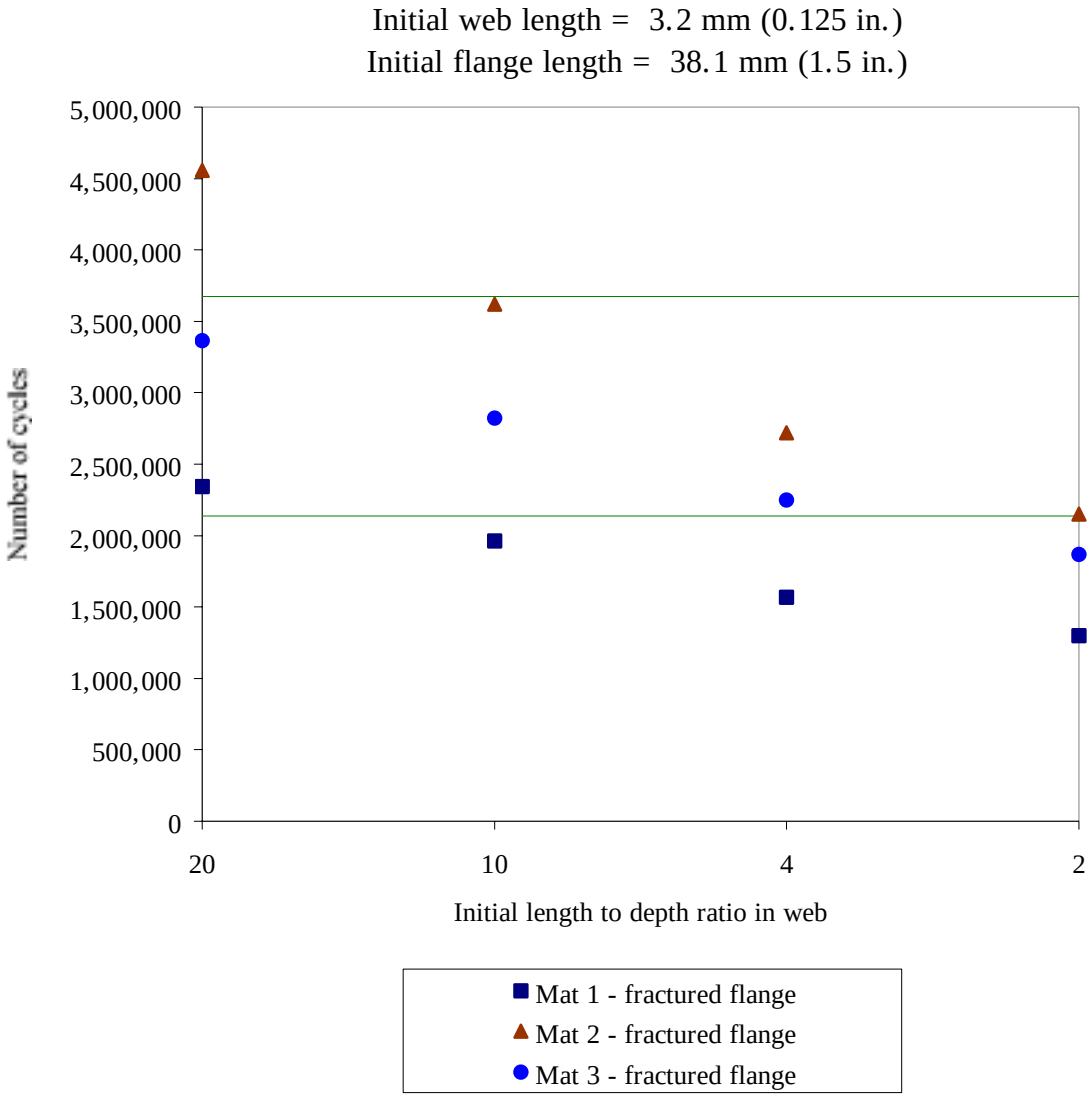

Figure 6.12 Fractured flange comparison for staggered diaphragms and:
initial web crack length = 3.2 mm (0.125 in.),
applied load = 222 kN (50 kip),
flange depth to length ratio: 1/3

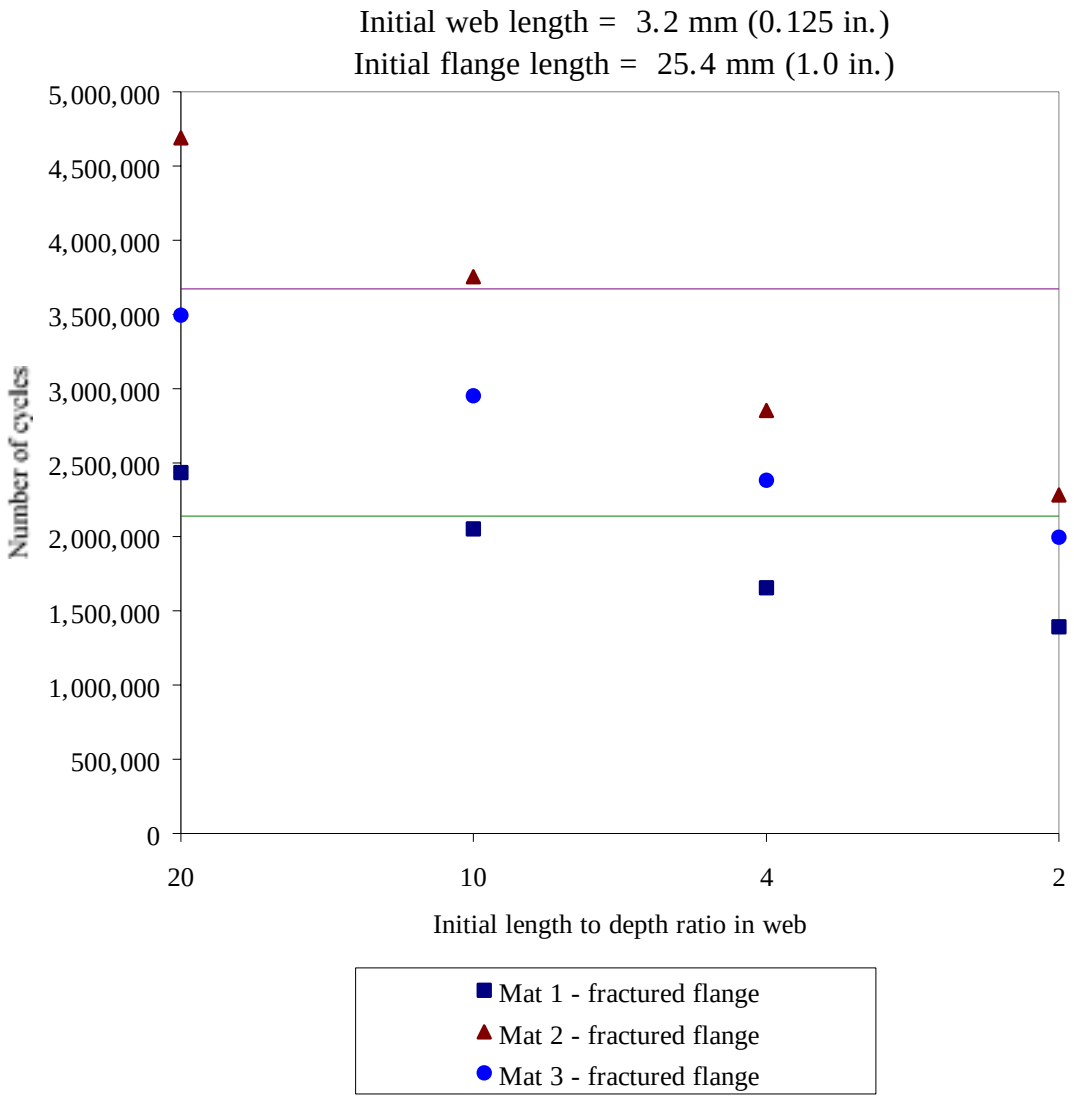

Figure 6.13 Fractured flange comparison for staggered diaphragms and:
initial web crack length = 3.2 mm (0.125 in.),
applied load = 222 kN (50 kip),
flange depth to length ratio: 1/2

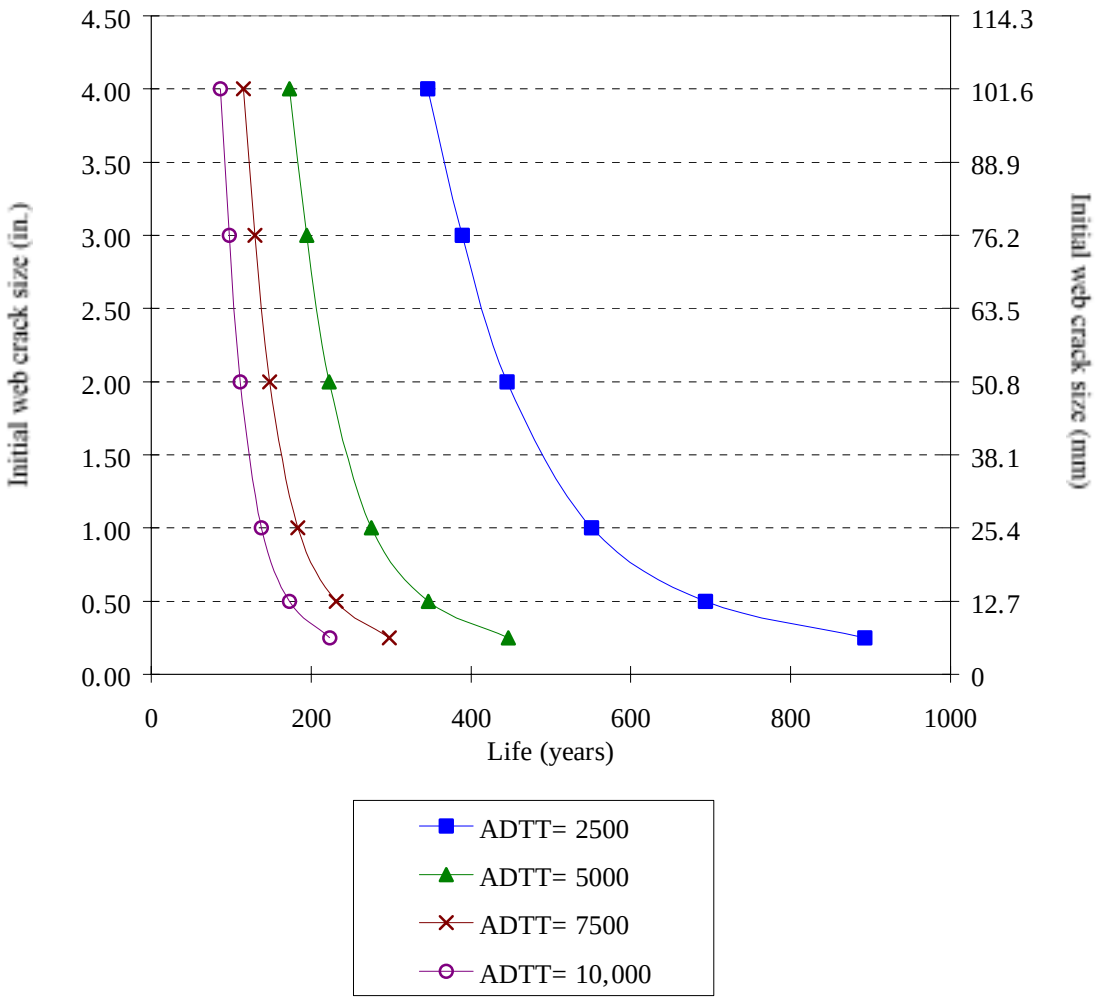

Figure 6.14 Life of W36x160 bridge member

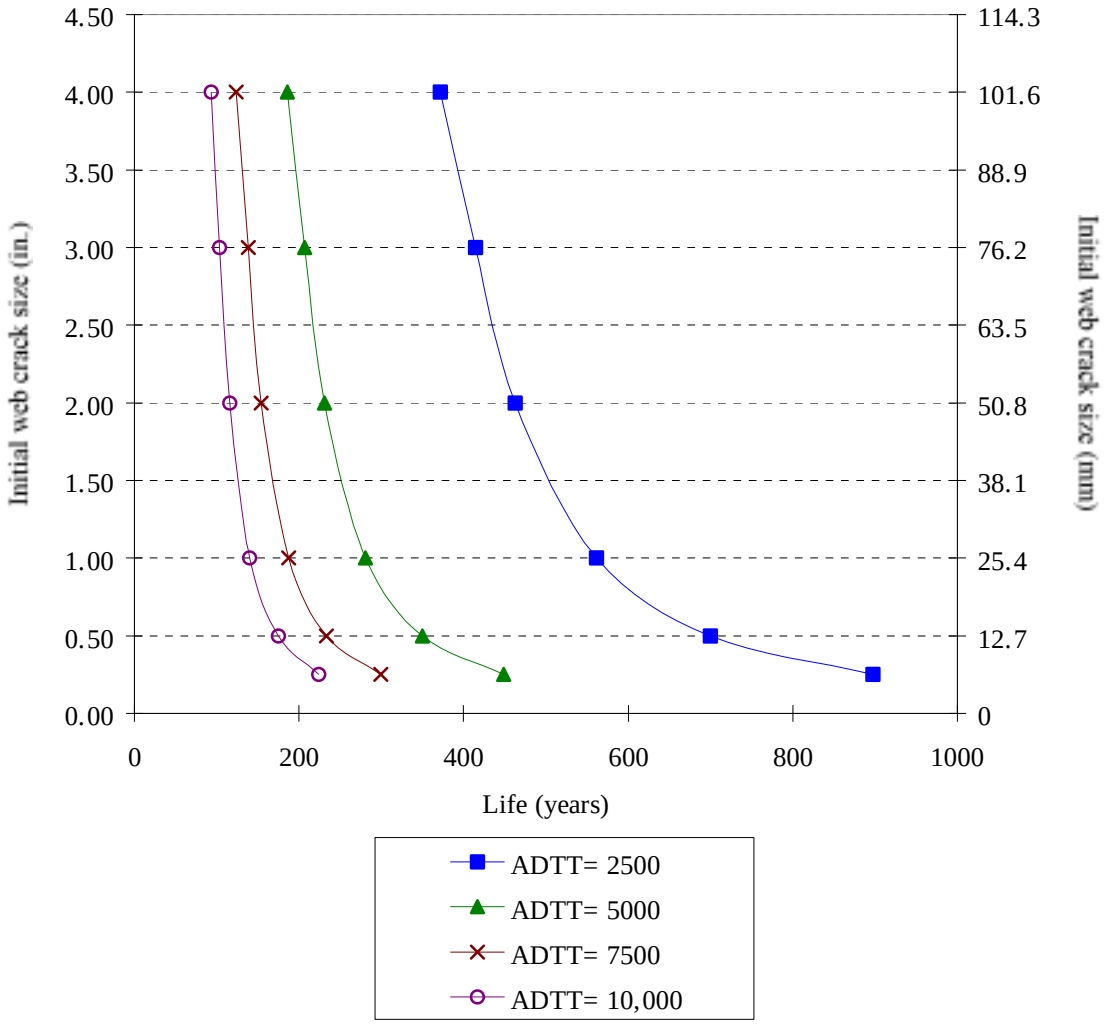

Figure 6.15 Life of W33x130 bridge member

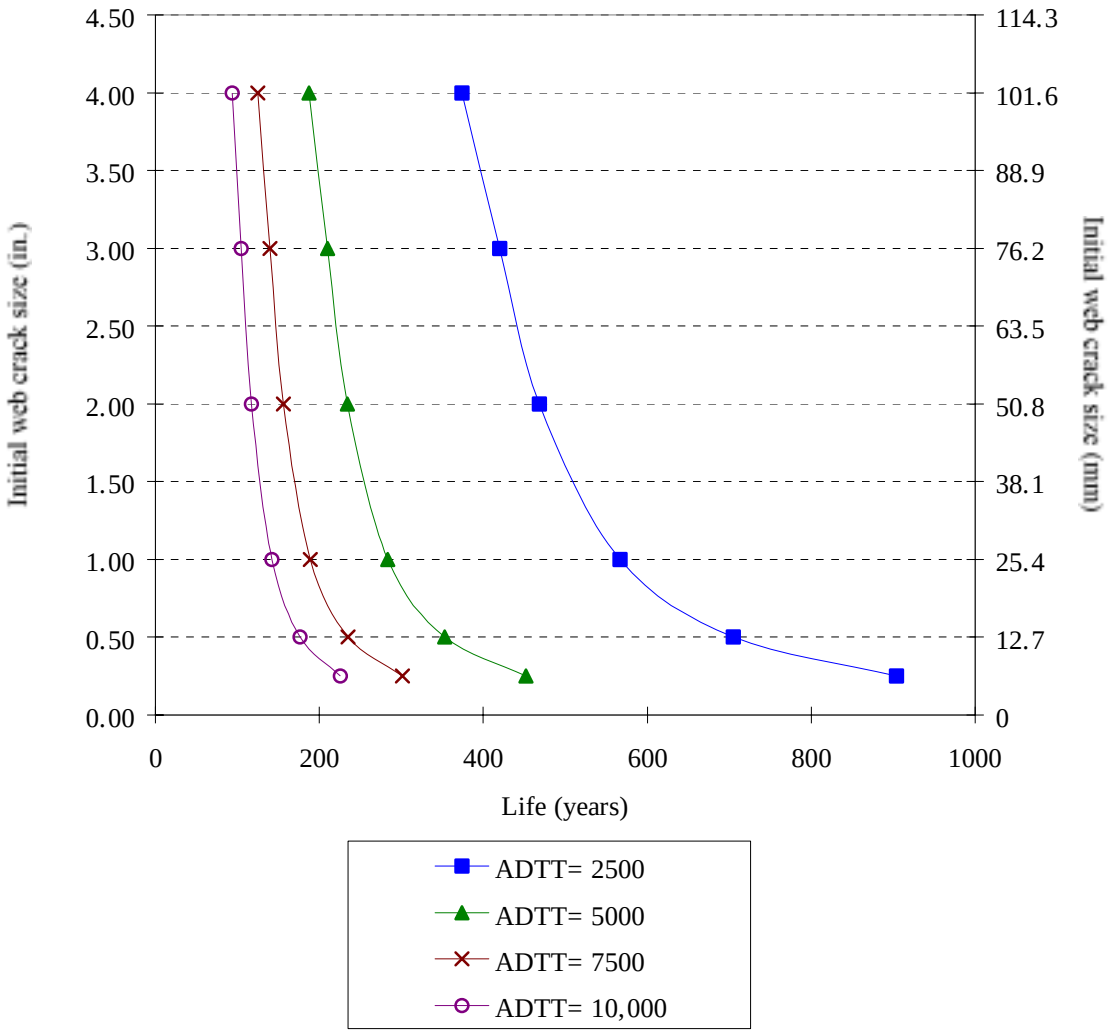

Figure 6.16 Life of W30x116 bridge member

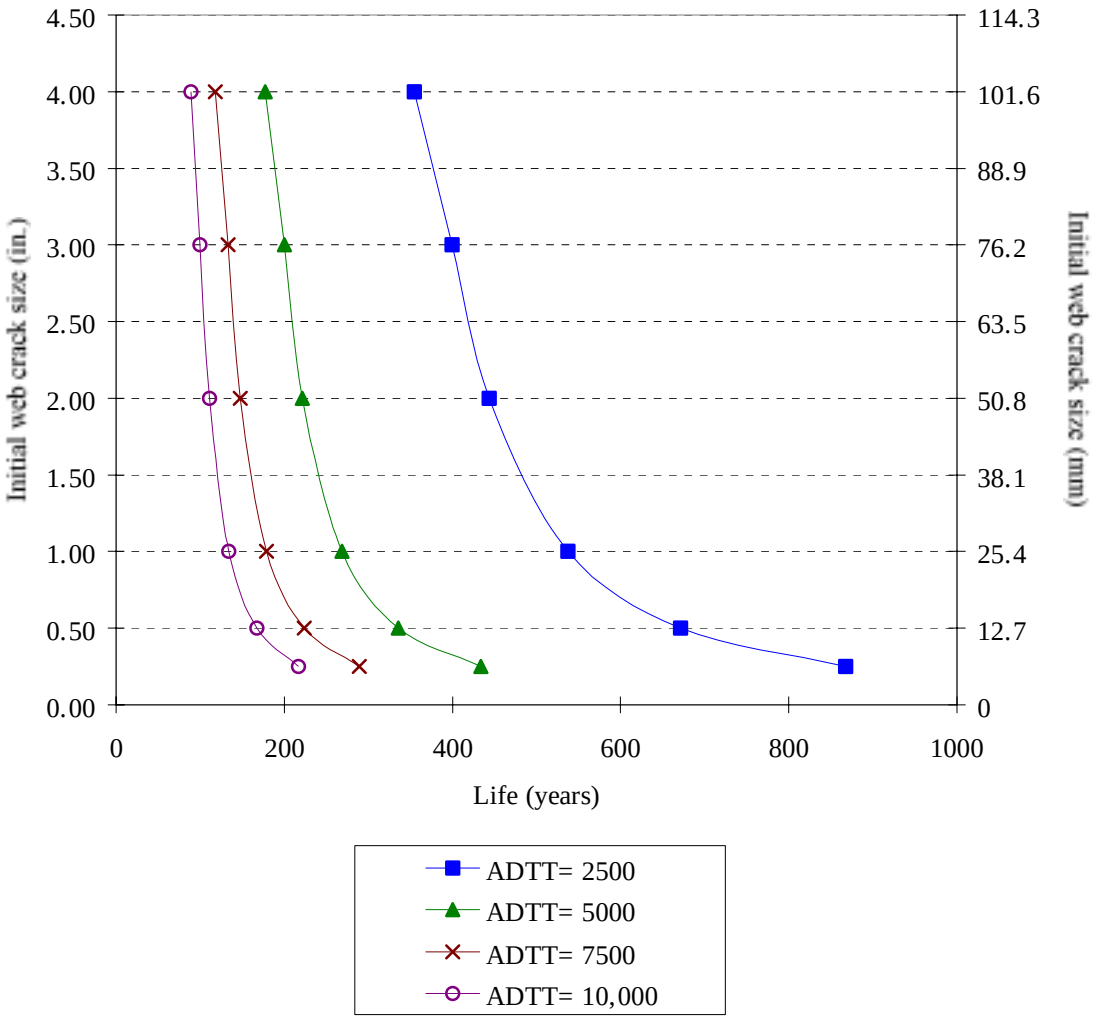

Figure 6.17 Life of W27x102 bridge member

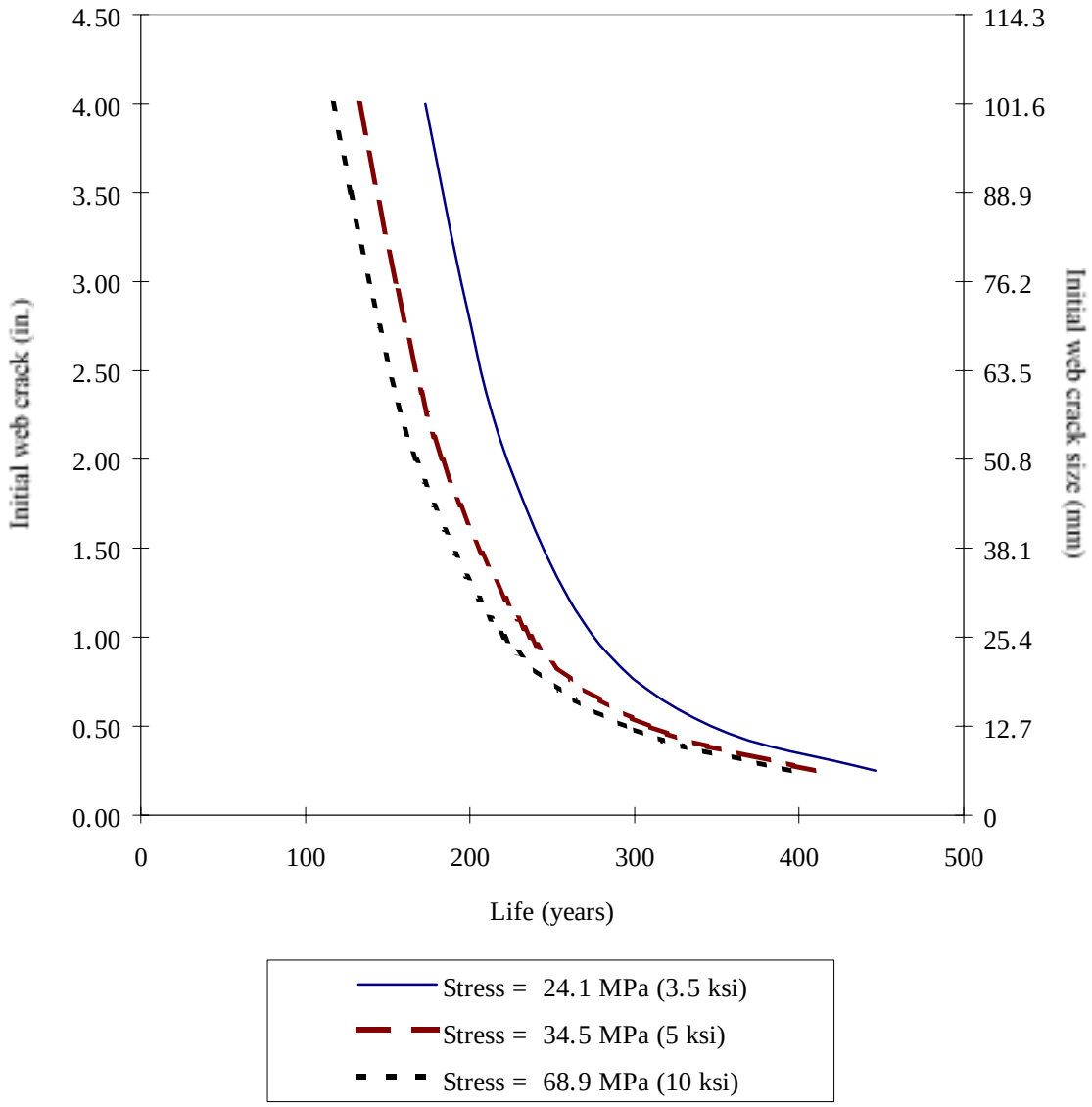

Figure 6.18 Life of W36x160 bridge member for varying stresses and ADTT=5,000

CHAPTER 7

CONCLUSIONS AND RECOMMENDATIONS

7.1 Summary and Conclusions

The fatigue strength of beams with a welded diaphragm-to-beam connection was investigated. Nine steel beams, with each beam having two welded diaphragm connections, were tested under constant amplitude cycling. Two diaphragm configurations were examined: one with diaphragms positioned back-to-back and one with staggered diaphragms. Three beams were repaired with one of the following methods: removing the diaphragm and drilling holes at the beam crack tips, removing the diaphragm and peening the bottom flange weld toes, and leaving the diaphragm in place and peening the bottom flange weld toes. In addition to the experimental tests, an analytical model was developed to predict the crack propagation life of cracked bridge beam members with the welded diaphragm connection.

Based upon the experimental test results and analytical predictions, the following conclusions can be made:

1. Web and flange welds connecting the diaphragms to the beam fractured in the non-staggered diaphragm arrangement. No welds fractured for the staggered diaphragm configuration.

2. The diaphragms positioned back-to-back had higher bending strains than the staggered diaphragms before the welded connection fractured. After one of the welded connections fractured, the bending strains in the nonstaggered diaphragms were similar to the staggered diaphragms which had little strain.
3. Horizontal cracks developed in the beam webs for the back-to-back diaphragm setup but did not affect the fatigue strength of the beam.
4. Beam cracks perpendicular to the stress field occurred at the toe of the bottom flange connection welds in staggered diaphragm cases and eventually fractured the beam tension flange. Beam cracks developed at this location for nonstaggered diaphragms after some of the web and flange connection welds fractured.
5. When the beam tension flange fractured at a diaphragm location, the flange splice plates, which were installed to repair the fatigue damage, were effective in carrying the flange force for a significant number of cycles.
6. Peening the bottom flange weld toes before beam cracks developed was effective in substantially increasing the fatigue life of the beam member. No cracks were detected in the beams that had been retrofitted by peening of the bottom flange weld toes.
7. It is not necessary to remove the entire diaphragm for an effective retrofit.
8. Drilling holes at the beam crack tips does arrest the crack growth. The holes should be sized based on the stress level in the beam and the effective crack length.

9. The stresses measured and computed on typical highway bridge structures are quite low and typically fall below the endurance limit. Hence, the diaphragm detail should be relatively fatigue proof for typical loadings.
10. The experimental lives of the diaphragm details fall between the AASHTO Category C and Category D design lives. The experimental lives were long even with a large applied load.

7.2 Implementation

The following suggestions are made as ways for INDOT to implement the results of the report to improve the performance of highway bridge members with the welded diaphragm connection.

1. Crack initiation that is detrimental and will eventually lead to failure of a simply supported beam member is most likely to occur in the beam web at the toe of a lower flange connection weld. It is recommended that the welded connections in the maximum positive moment regions be closely examined at the lower flange welds; the upper flange welds should be examined for connections in the negative moment regions (near the piers of continuous structures).
2. If fatigue crack initiation is to be avoided, then air hammer peening of the lower flange weld toes can be performed to extend the fatigue life for beams that have not developed cracks. However, the stresses in the bridge members are often quite low and crack initiation is not likely, especially if peening has been performed.

3. If a beam web crack is detected at the toe of a lower or upper diaphragm flange weld, the crack dimensions should be determined. The fatigue propagation program should then be used to estimate the time to propagate the crack to a specified length for a given load history and ADTT. Since the welded connection was widely used on highway bridges in Indiana, the program can be used to determine an appropriate repair schedule. Although a crack may be present in a beam member, the stresses are often quite low such that rapid crack growth is not likely to occur and an immediate repair is often not necessary.
4. In order to repair a beam member that has developed cracks, holes should be drilled at the beam crack tips to arrest crack growth. The holes should be ground smooth so no sharp edges are present for crack re-initiation. It is important that the crack tip is contained within the drilled hole, otherwise the hole may accelerate crack propagation. The holes should be sized according to the stress level and the effective crack length.
5. The diaphragm should not be removed during beam repair. Flame cutting operations may inadvertently result in some damage to the primary beam member. If it is necessary to remove the diaphragm (due to a completely fractured welded connection), then engineers should be present to supervise the repair. However, diaphragm members are important because they act as lateral bracing for the longitudinal beam members during bridge deck replacement and they help to distribute lateral loads.

7.3 Future Research Needs

The current study has shown that the fatigue life of the welded diaphragm-to-beam connection exceeds the design life of the bridge. The current study focused on the behavior of bridge members with traffic crossing the bridge. However, an increasing number of bridge members are hit by tractor-trailers that exceed the clearance limit for overpass bridges. The impact from the trailer traveling at highway speeds is substantial. Since the transverse diaphragms connect the longitudinal members, the impact is transmitted through the system. This impact force could cause the welded connections to fracture and beam cracks to initiate at the lower flange welds in multiple connection locations. If a crack is already present in the beam member, the impact force could increase the crack propagation rate. Additional tests are needed to determine the effect the impact load would have on the fatigue behavior of the welded connection.

LIST OF REFERENCES

Albrecht, P., Brown, W.P. and Wright, W.J. 1992. "Analysis of Fatigue Cracking in I-64 Bridges over Maury River and Kerr's Creek, Rockbridge County, Virginia."

Albrecht, P. and Yamada, K. 1977. "Rapid Calculation of Stress Intensity Factors." *Journal of the Structural Division. ASCE.* vol. 103. No. ST2: 377-390.

American Association of State Highway and Transportation Officials. 1996. *Standard Specifications for Highway Bridges.* Sixteenth edition. Washington, D.C.

American Association of State Highway and Transportation Officials. 1990. *Guide Specifications for Fatigue Design of Steel Bridges.* Washington, D.C.

American Welding Society. 1994. *Structural Welding Code – Steel, ANSI/AWS D1.1-94.* Fourteenth edition.

ANSYS. 1996. Swanson Analysis Systems, Inc. version 5.3. General Purpose Finite Element Program. Houston, PA.

Barsom, J.M. and Rolfe, S.T. 1987. *Fracture and Fatigue Control in Structures: Applications of Fracture Mechanics.* Second edition. Prentice-Hall, Inc. New Jersey.

Canna, T. 1996. "Field Evaluation of Bridge Diaphragm Members with Welded Connections." Master's Thesis. Purdue University.

Castiglioni, C., Fisher, J. and Yen, B. 1988. "Evaluation of Cracking at Cross Diaphragms of a Multigirder Steel Bridge." *Journal of Constructional Steel Research.* vol. 9. no. 2: 95-110.

Fisher, J.W. 1984. *Fatigue and Fracture in Steel Bridges.* John Wiley and Sons. New York.

Fisher, J.W., Barthelemy, B.M., Mertz, D.R. and Edinger, J.A. 1980. "Fatigue Behavior of Full-Scale Welded Bridge Attachments." *NCHRP 227.* Washington, D.C.

Fisher, J., Fisher, T. and Kostem, C. 1979. "Displacement-Induced Fatigue Cracks." *Engineering Structures.* vol. 25. no. 5: 252-257.

Fisher, J.W., Hausammann, H., Sullivan, M.D. and Pense, A.W. 1979. "Detection and Repair of Fatigue Damage in Welded Highway Bridges." *NCHRP Report 206.* Washington, D.C.

Fisher, J.W., Jim, J., Wagner, D.C. and Yen, B.T. 1990. "Distortion Induced Fatigue Cracking in Steel Bridges." *NCHRP Report 336.* Washington, D.C.

Fisher, J.W., Kaufmann, E.J., Kostem, C.N., Lee, J.J., Moser, D., Papavizas, P.G. and Yen, B.T. 1987. *Deformation Induced Cracking in Steel Girder Bridges and Retrofit Guidelines - Final Report.* FHWA-PA-86-030+83-21.

Fisher, J.W., Nussbaumer, A., Keating, P.B., and Yen, B.T. 1993. "Resistance of Welded Details Under Variable Amplitude Long-Life Fatigue Loading." *NCHRP Report 354.* Washington, D.C.

Fisher, J., Pense, A., and Roberts, R. 1977. "Evaluation of Fracture of Lafayette Street Bridge." *Journal of Structural Division, ASCE.* vol. 103 no. ST7: 1339-1357.

Fisher, J.W., Yen, B.T. and Daniels, J.H. 1976. "Fatigue Damage in the Lehigh Canal Bridge From Displacement-Induced Secondary Stresses." *Transportation Research Record 607*: 56-62.

Fisher, J.W., Yen, B.T., Kaufmann, E.J., Ma, Z.Z. and Fisher, T.A. 1995. "Crack Evaluation and Repair of Cantilever Bracket Tie Plates of Edison Bridge." *Proceedings - Fourth International Bridge Conference.* San Francisco, CA: 15-25.

Fisher, J.W., Yen, B.T. and Wagner, D.C. 1987. "Review of Field Measurements for Distortion-Induced Fatigue Cracking in Steel Bridges." *Transportation Research Record 1118*: 49-55.

Grider, A.S. 1998. "Fatigue Behavior of Welded Diaphragm-to-Beam Connections." Ph.D. Thesis. Purdue University.

Keating, P.B. and Fisher, J.W. 1987. "Fatigue Behavior of Variable Loaded Bridge Details Near the Fatigue Limit." *Transportation Research Record 1118*: 56-64.

Kennedy, J.B., and Grace, N.F. 1983. "Load Distribution in Continuous Bridges." *Canadian Journal of Civil Engineering.* vol. 10. no. 3: 384-395.

Kennedy, J.B., Grace, N.F. and Soliman, M. 1989. "Welded- versus Bolted-Steel I-Diaphragms in Composite Bridges." *Journal of Structural Engineering.* vol. 115. no. 2: 417-432.

Kulicki, J. and Mertz, D. 1987. "Case Studies of Displacement-Induced Fatigue." *Proceedings of the Sessions of Structures Congress '87 Related to Materials and Member Behavior*. Duane S. Ellifrit ed.: 660-675.

Kulicki, J.M., Murphy, R.E., Mertz, D.R. and Fisher, J.W. 1986. "Fatigue Cracking on I-79 Bridges in West Virginia." *Proceedings - 3rd Annual International Bridge Conference*, Pittsburgh, PA: 93-102.

Lai, L. 1996. "Fatigue Cracks at Stringer-Floorbeam Connections." *Proceedings of Structures Congress XIV*. Chicago, IL: 483-490.

Lee, J.J. 1987. "Fatigue Strength of Steel Bridge Girders with Distortion-Induced Stresses." Ph.D. Thesis. Lehigh University.

Mertz, D. 1984. "Displacement-Induced Fatigue Cracking in Welded Steel Bridges." Ph.D. Thesis. Lehigh University.

Newman, J.C. and Raju, I.S. 1981. "An Empirical Stress-Intensity Factor Equation for the Surface Crack." *Engineering Fracture Mechanics*. vol. 15. no. 1-2: 185-192.

Nowak, A.S., Laman, J.A. and Nassif, H. 1994. *Effect of Truck Loading on Bridges*. Research Report UMCE 94-22. Department of Civil and Environmental Engineering, University of Michigan, Ann Arbor, Michigan.

Pullaro, J.J. 1990. "Retrofit of Cracked Welded Steel Bridge Girders." *Extending the Life of Bridges, ASTM STP 1100*. G. W. Maupin, Jr., B. C. Brown, and A. G. Lichtenstein, Eds. American Society for Testing and Materials, Philadelphia, PA: 18-31.

SAP90. 1990. Computers and Structures, Inc. Structural Analysis Program. Berkeley, CA.

SAP2000. 1996. Computers and Structures, Inc. version 6.0. Structural Analysis Program. Berkeley, CA.

Stallings, J. M. and Cousins, T.E. 1997. "Fatigue Cracking in Bolted Diaphragm Connections." *Proceeding-ASCE Structures Congress XV*. Portland, OR: 36-40.

Wilson, P., Duncan III, R. and Fisher, J. 1989. "Repair of Fatigue Cracks in Steel Box Girder Bridges." *Public Works*. vol. 120 no. 4.: 40-41.

Wright, W., Nelson, R. and Chase, S. 1991. "I-64 over Maury River Analysis of Fatigue Retrofit Procedures." Turner Fairbank Highway Research Center, McLean, Virginia.

Yamada, K. and Hirt, M.A. 1982. "Fatigue Crack Propagation from Fillet Weld Toes." *Journal of the Structural Division*, ASCE, vol. 108, no. ST7: 1526-1540.

Zwerneman, F., West, A. and Lim, K. 1993. "Fatigue Damage to Steel Bridge Diaphragms." *ASCE Journal of Performance of Constructed Facilities*. vol. 7 no. 4: 207-224.

Zwerneman, F., West, A. and Lim, K. 1989. *Fatigue Damage to Steel Bridge Diaphragms*. FHWA/OK 89(10).

APPENDIX A

MATERIAL PROPERTIES

APPENDIX A

MATERIAL PROPERTIES

This section contains the properties of materials used in the experimental tests. According to the manufacturer, no tests are required of the 3.2 mm (0.125 in.) welding electrode used to make the welded diaphragm-to-beam connection. The American Welding Society (1994) requirements for this electrode type are provided in Table A.1.

The test beams were from three different heats of ASTM A572 Gr. 50 steel and the diaphragms were all from the same heat of ASTM A572 Gr. 50 steel. The chemical composition of the heats as provided by the manufacturer is given in Table A.2 and the mechanical properties are given in Table A.3. Tension coupon tests were performed according to ASTM A370 in order to check the supplied mechanical properties. Four coupons were tested for each heat of steel: two from the web and two from the flange. The coupons were cut from the steel beams upon completion of a test and were taken from low-stress regions near the end of the beam (but not over the support). The coupons were tested in a 979 kN (220 kip) MTS servo-hydraulic testing machine in order to obtain the yield strength, ultimate stress, modulus of elasticity, and the percent elongation. Figures A.1 to A.16 contain the tension coupon results for the heats of steel used in the experimental tests.

Table A.1 AWS Requirements for Mechanical Properties of E6010 Weld Electrodes

Property	E6010 Electrode Requirements
Tensile Strength (psi)	62,000 min.
Yield Strength (psi)	50,000 min.
Elongation, % in 2 in.	22 min.
Hardness, Rockwell B	Not required
Impact Properties (Charpy V-notch), ft-lbs. at –20 °F	20 min.

Table A.2 Chemical Composition of Steel

(a) W24x55 Test Beams

Chemical	Heat Number			ASTM Max. Heat Limits
	58882	89782	181N340	
C	0.08	0.16	0.20	0.23
Mn	0.85	0.80	1.20	1.35
P	0.015	0.012	0.011	0.04
S	0.04	0.029	0.025	0.05
Si	0.10	0.23	0.05	0.40
Cu	0.31	0.22	0.05	--
Ni	0.10	0.11	0.02	--
Cr	0.09	0.19	0.05	--
Mo	0.02	0.041	0.01	--
V	0.02	--	0.046	--
Nb	0.006	--	0.001	--

(b) W 14x26 Diaphragms

Chemical	Heat Number	ASTM Max. Heat Limits
	76692	
C	0.13	0.23
Mn	0.80	1.35
P	0.018	0.04
S	0.032	0.05
Si	0.24	0.40
Cu	0.17	--
Ni	0.10	--
Cr	0.22	--
Mo	0.35	--
V	0.26	--
Nb	--	--

Note: All values given in percent weight

Table A.3 Mechanical Properties of Steel

(a) W24x55 Test Beams

Heat No.	Material	Yield Strength (MPa) *(ksi)*	Ultimate Stress (MPa) *(ksi)*	Young's Modulus (MPa) *(ksi)*	% Elongation*
58882	Web	337.8 *(49.0)*	449.5 *(65.2)*	211,407 *(30,662)*	28.9
58882	Web	344.7 *(50.0)*	466.8 *(67.7)*	212,972 *(30,889)*	29.7
58882	Flange	344.7 *(50.0)*	457.1 *(66.3)*	214,896 *(31,168)*	21.1
58882	Flange	360.6 *(52.3)*	465.4 *(67.5)*	217,060 *(31,482)*	25.8
58882	Manufacturer	368.9 *(53.5)*	486.1 *(70.5)*	--	29.0
89782	Web	398.5 *(57.8)*	534.3 *(77.5)*	252,210 *(36,580)*	--
89782	Web	389.6 *(56.5)*	510.9 *(74.1)*	214,896 *(31,168)*	26.6
89782	Flange	379.2 *(55.0)*	503.3 *(73.0)*	205,871 *(29,859)*	--
89782	Flange	362.0 *(52.5)*	499.2 *(72.4)*	201,616 *(29,242)*	--
89782	Manufacturer	368.2 *(53.4)*	507.5 *(73.6)*	--	24.2
181N340	Web	402.0 *(58.3)*	535.0 *(77.6)*	204,050 *(29,595)*	25.0
181N340	Web	408.9 *(59.3)*	535.7 *(77.7)*	200,058 *(29,016)*	25.8
181N340	Flange	402.0 *(58.3)*	555.7 *(80.6)*	206,884 *(30,006)*	22.5
181N340	Flange	390.2 *(56.6)*	548.8 *(79.6)*	201,603 *(29,240)*	24.0
181N340	Manufacturer	410.2 *(59.5)*	548.1 *(79.5)*	--	27.0
ASTM Limits		344.7 *(50.0)*	448.2 *(65.0)*	--	18.0

(b) W 14x26 Diaphragms

Heat No.	Material	Yield Strength (MPa) *(ksi)*	Ultimate Stress (MPa) *(ksi)*	Young's Modulus (MPa) *(ksi)*	% Elongation*
76692	Web	393.0 *(57.0)*	534.3 *(77.5)*	208,325 *(30,215)*	25.8
76692	Web	379.2 *(55.0)*	523.3 *(75.9)*	236,717 *(34,333)*	24.0
76692	Flange	347.5 *(50.4)*	487.5 *(70.7)*	197,383 *(28,628)*	25.0
76692	Flange	358.5 *(52.0)*	500.6 *(72.6)*	196,790 *(28,542)*	21.9
76692	Manufacturer	386.8 *(56.1)*	517.8 *(75.1)*	--	20.3
ASTM Limits		344.7 *(50.0)*	448.2 *(65.0)*	--	18.0

* Based on 203 mm (8 in.) gage length

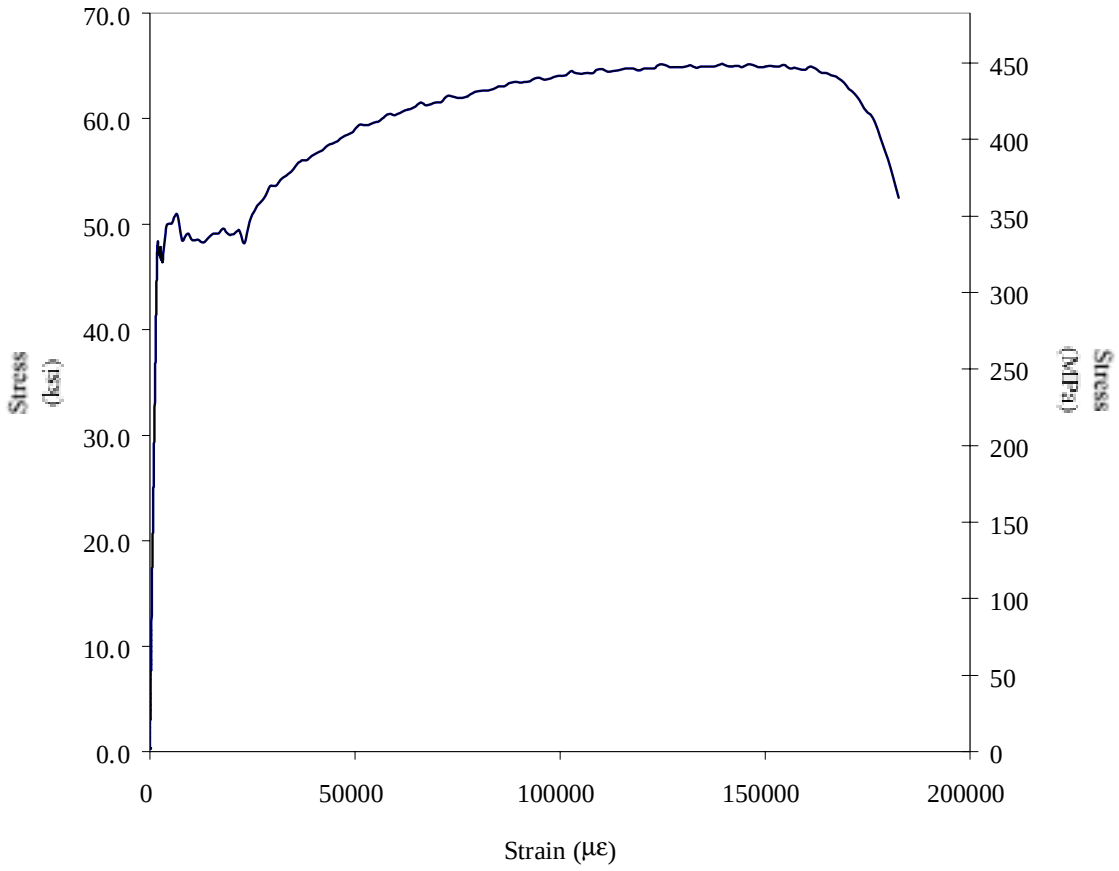

Figure A.1 Heat no. 58882 beam web tension coupon 1

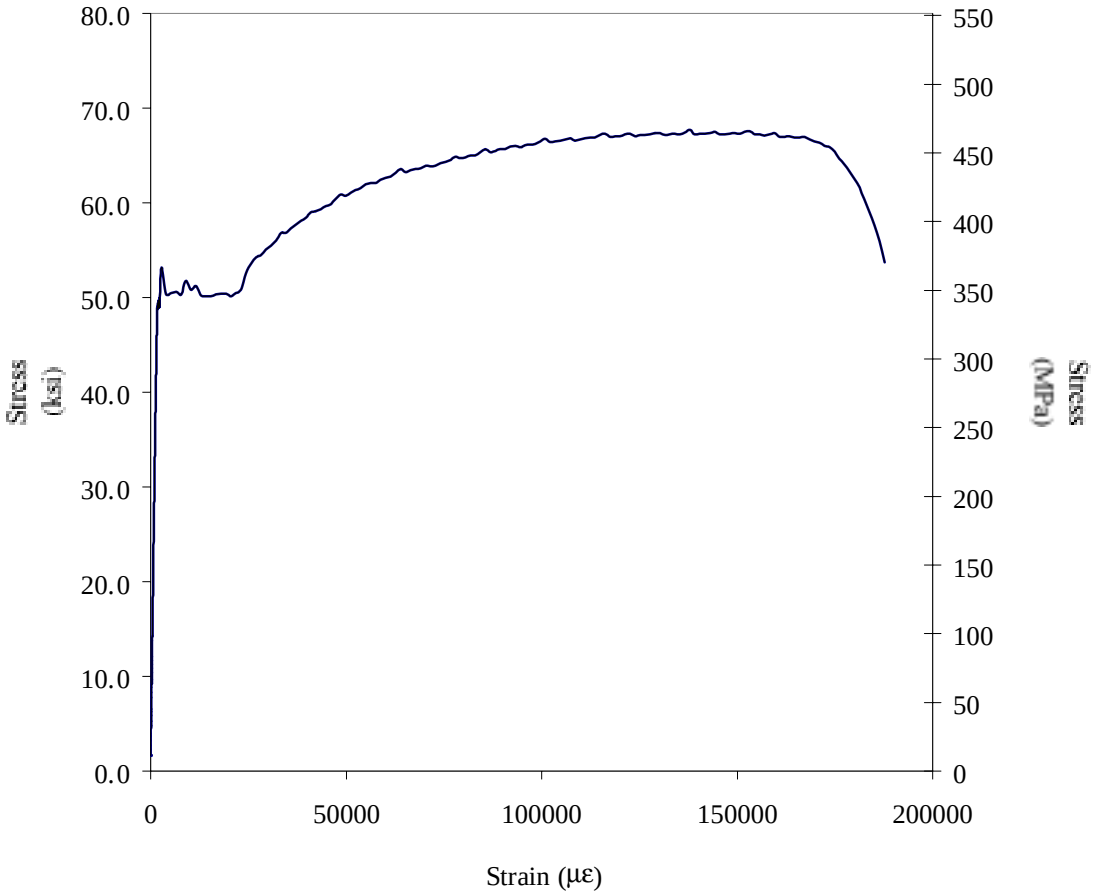

Figure A.2 Heat no. 58882 beam web tension coupon 2

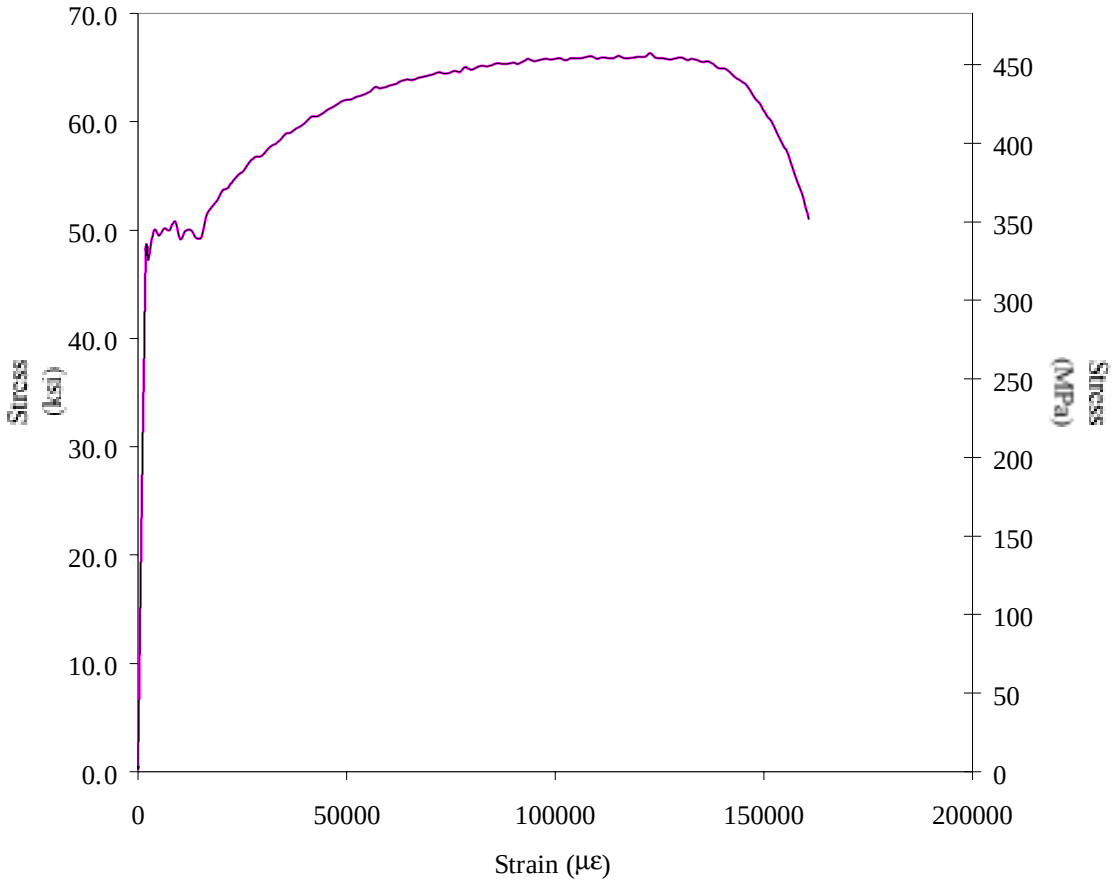

Figure A.3 Heat no. 58882 beam flange tension coupon 1

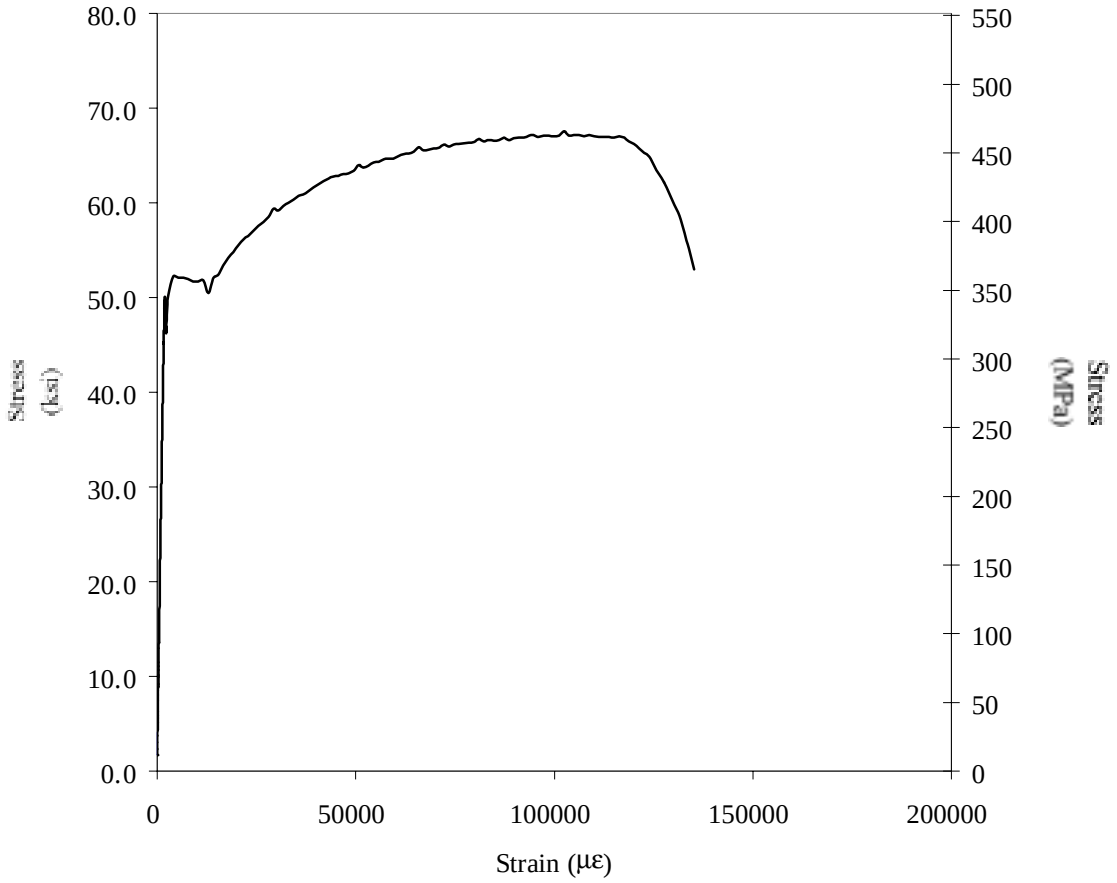

Figure A.4 Heat no. 58882 beam flange tension coupon 2

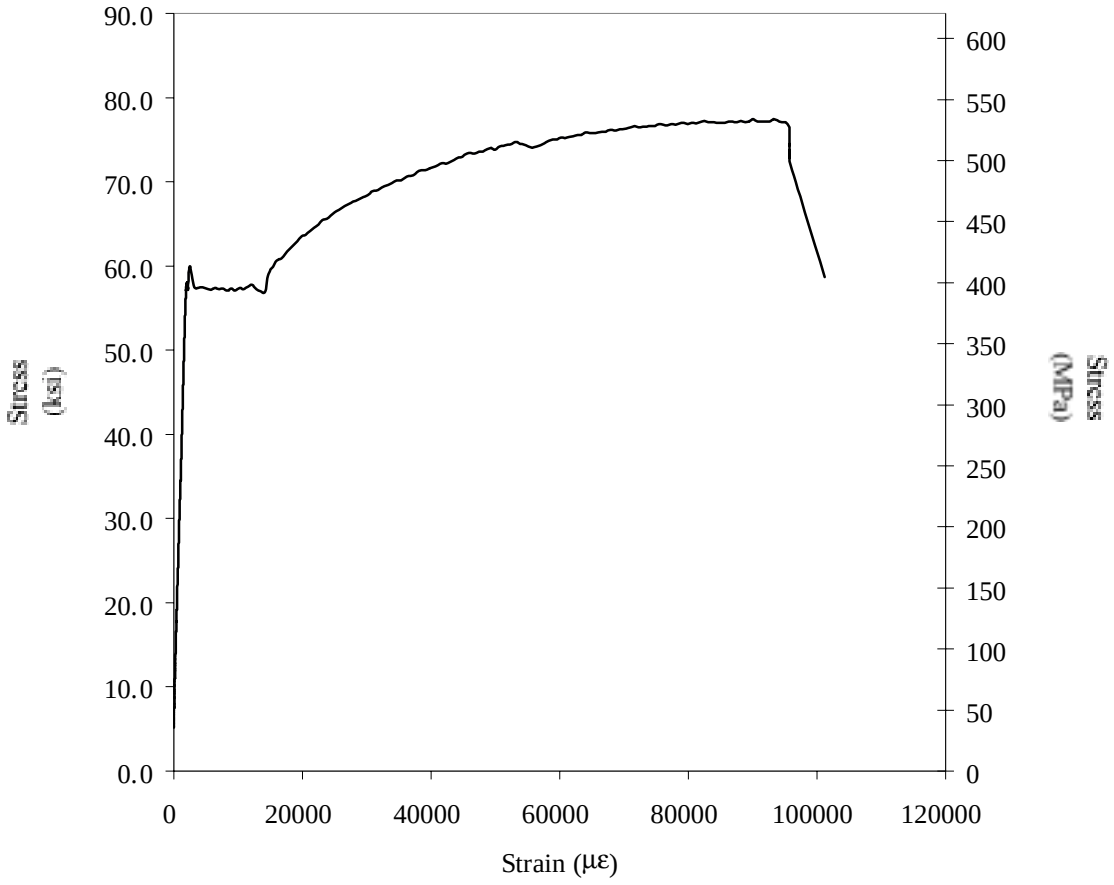

Figure A.5 Heat no. 89782 beam web tension coupon 1

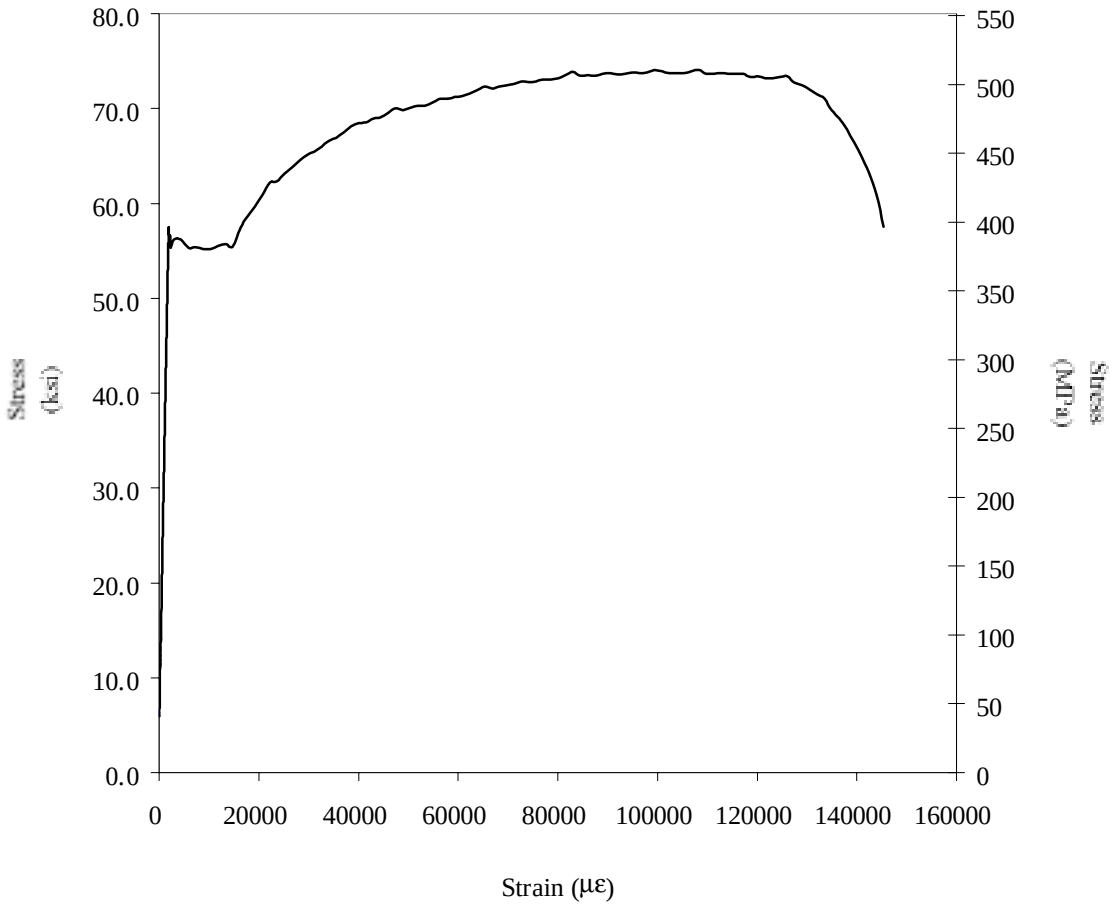

Figure A.6 Heat no. 89782 beam web tension coupon 2

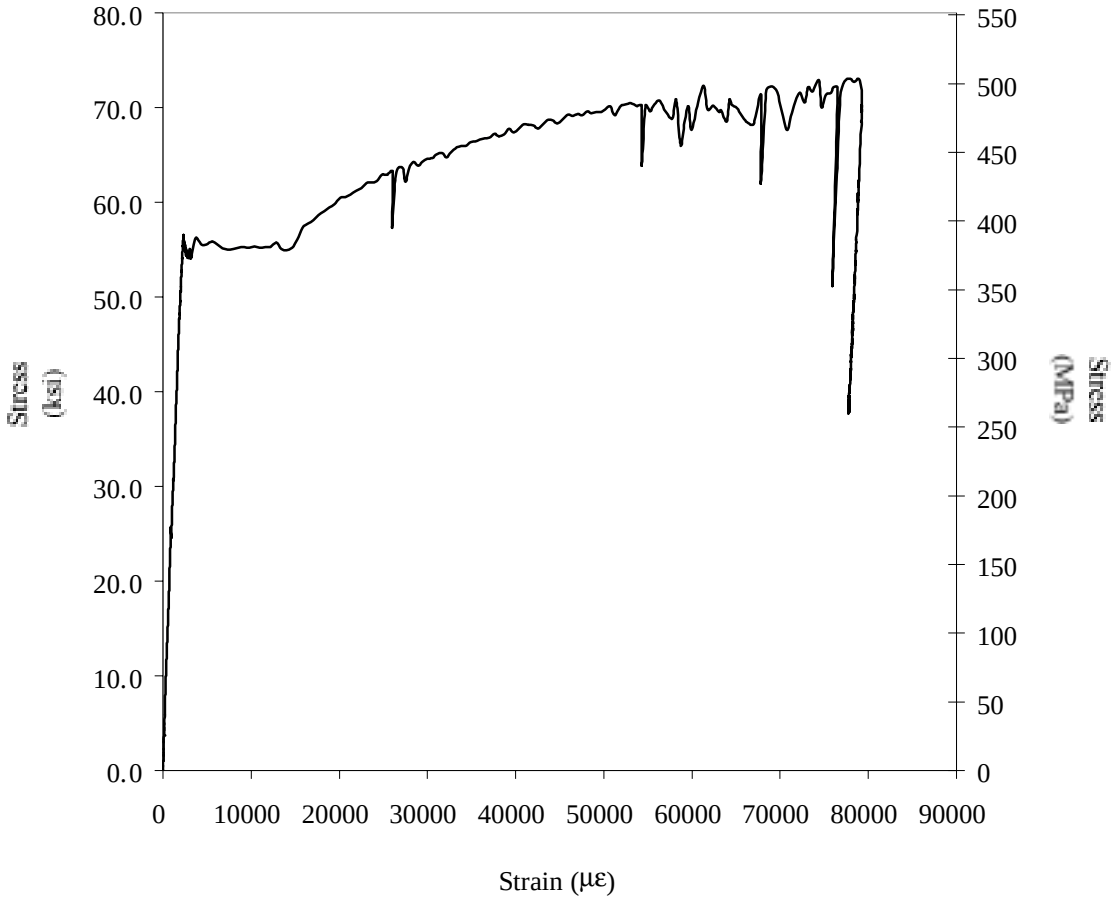

Figure A.7 Heat no. 89782 beam flange tension coupon 1

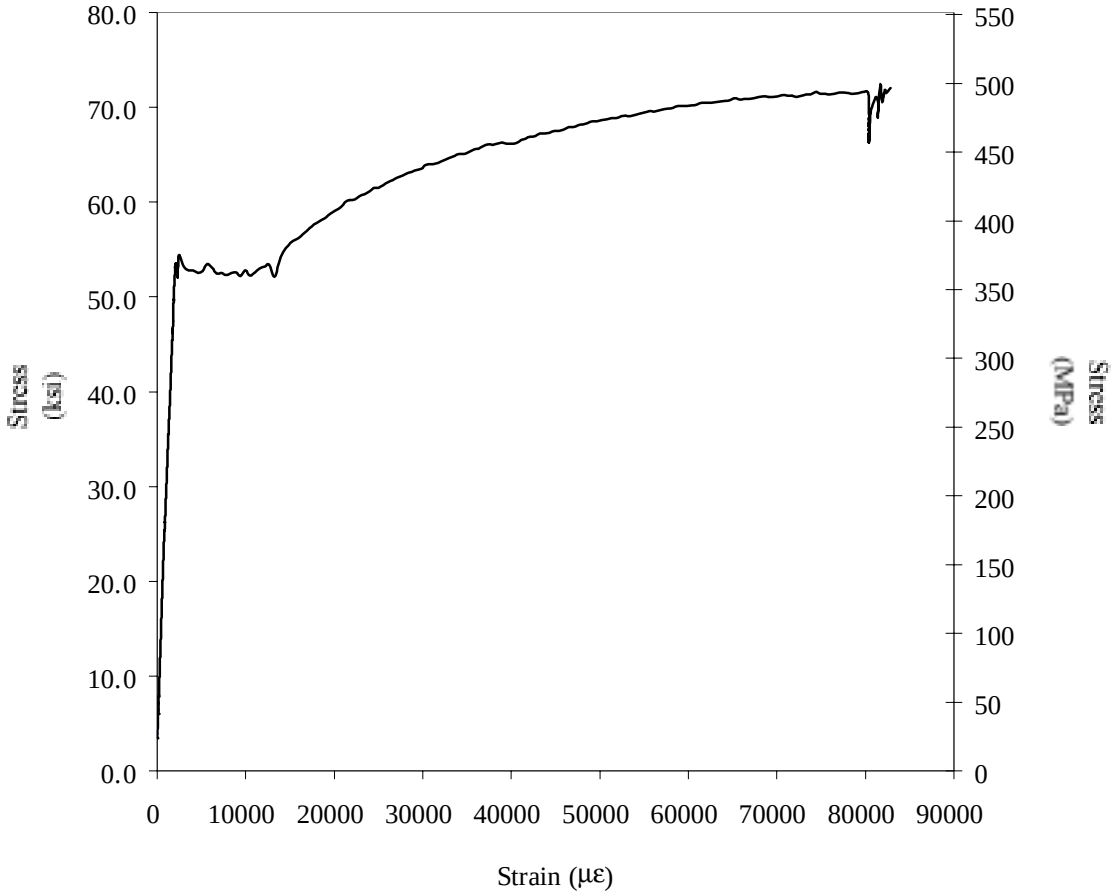

Figure A.8 Heat no. 89782 beam flange tension coupon 2

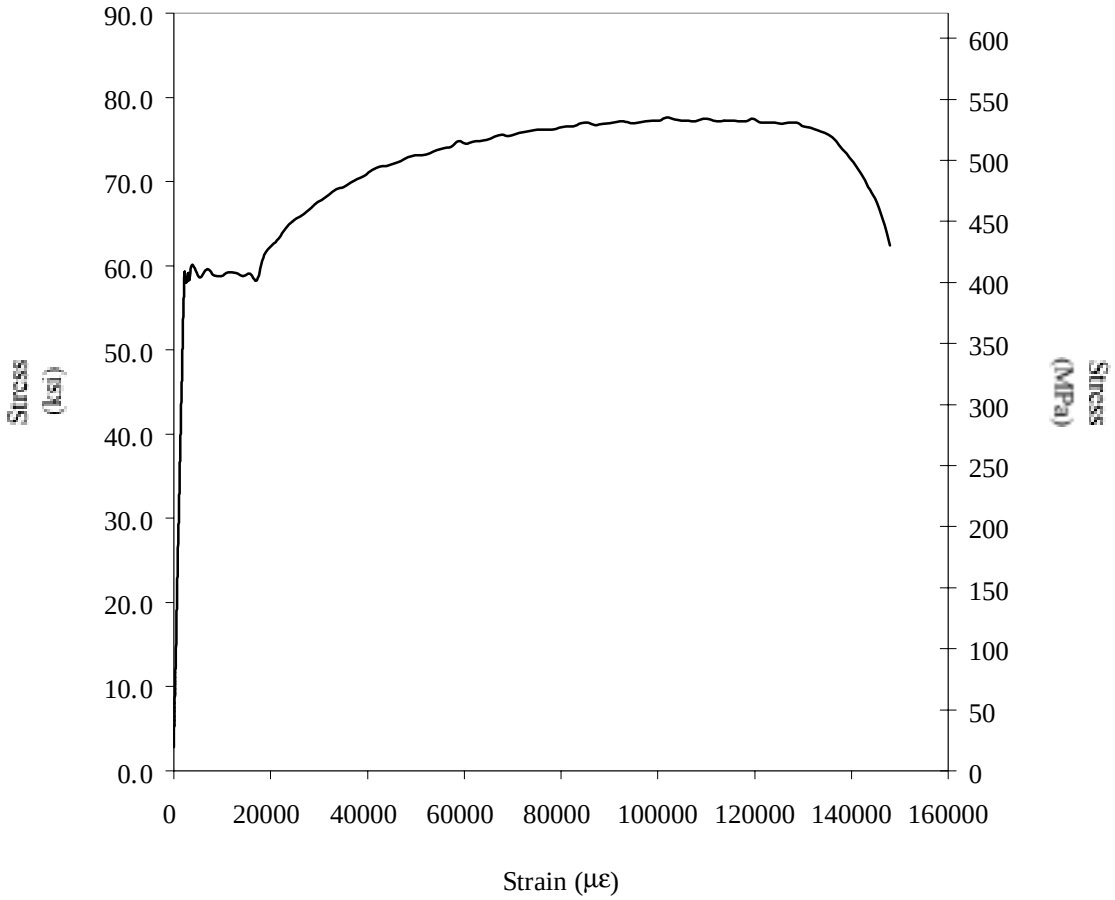

Figure A.9 Heat no. 181N340 beam web tension coupon 1

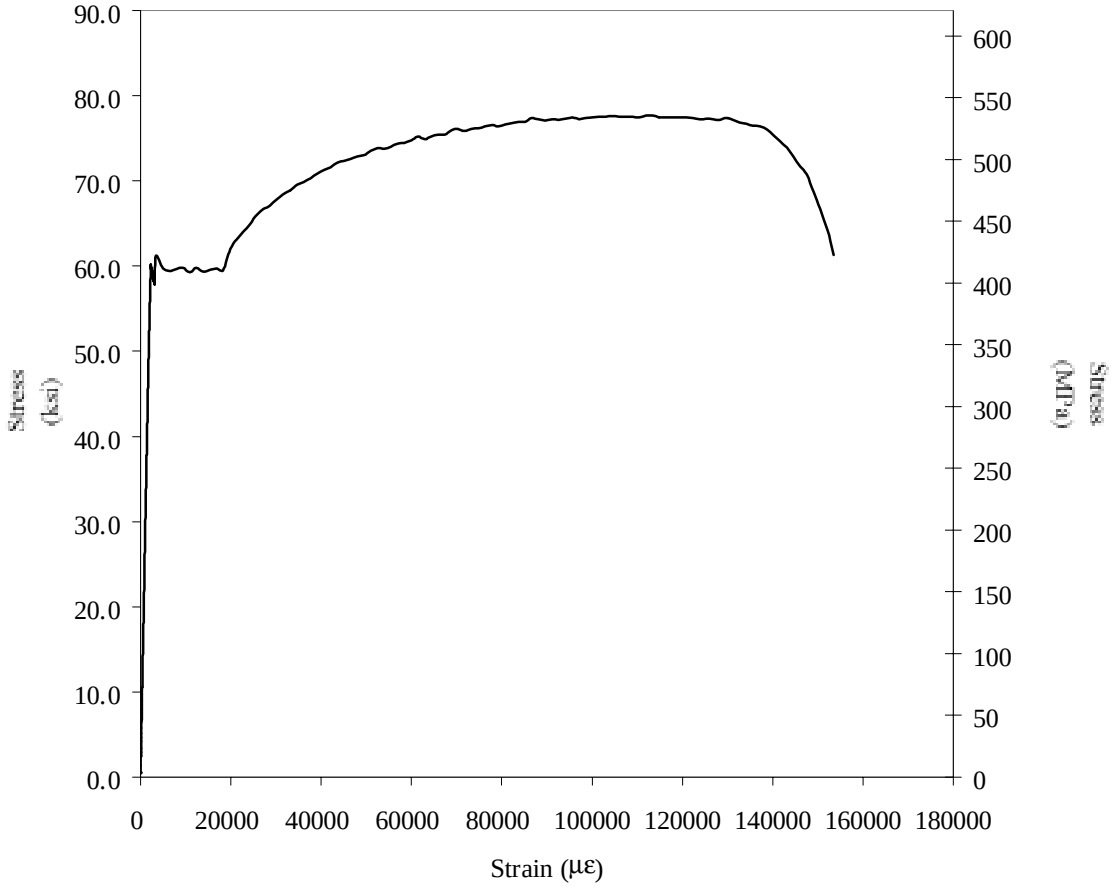

Figure A.10 Heat no. 181N340 beam web tension coupon 2

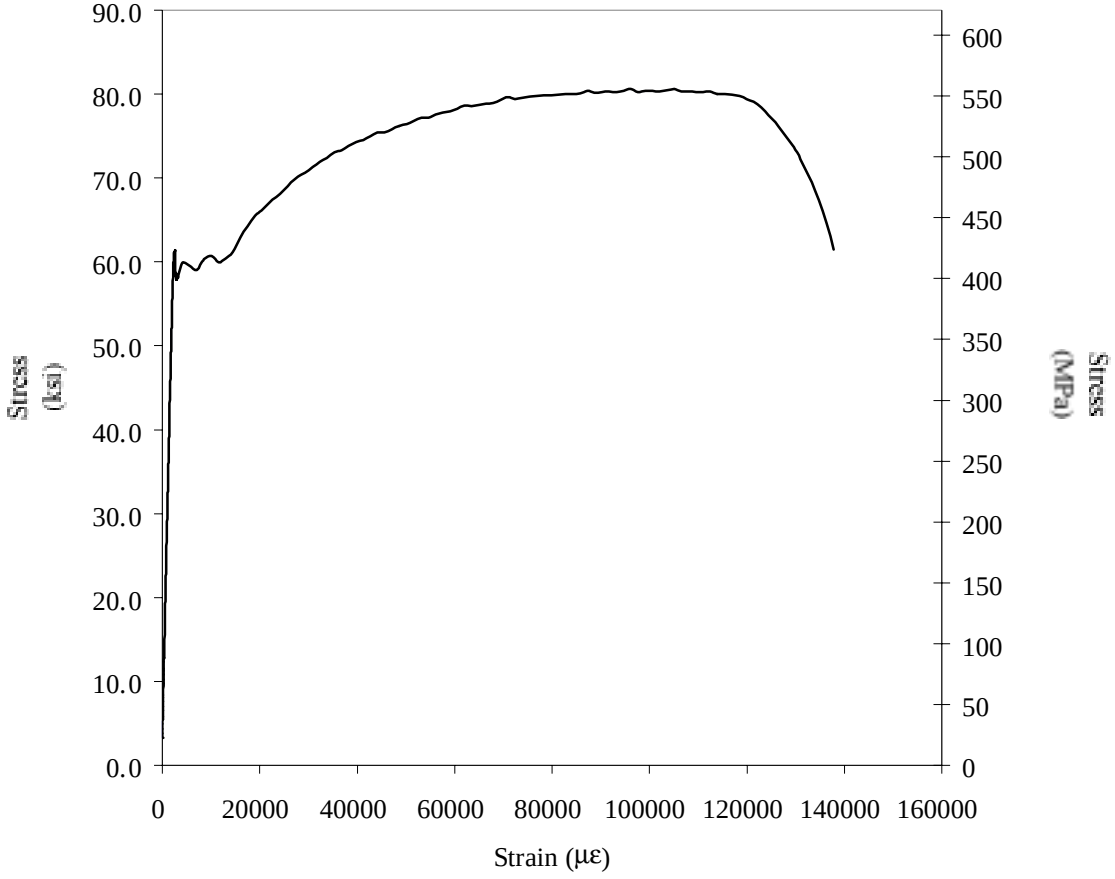

Figure A.11 Heat no. 181N340 beam flange tension coupon 1

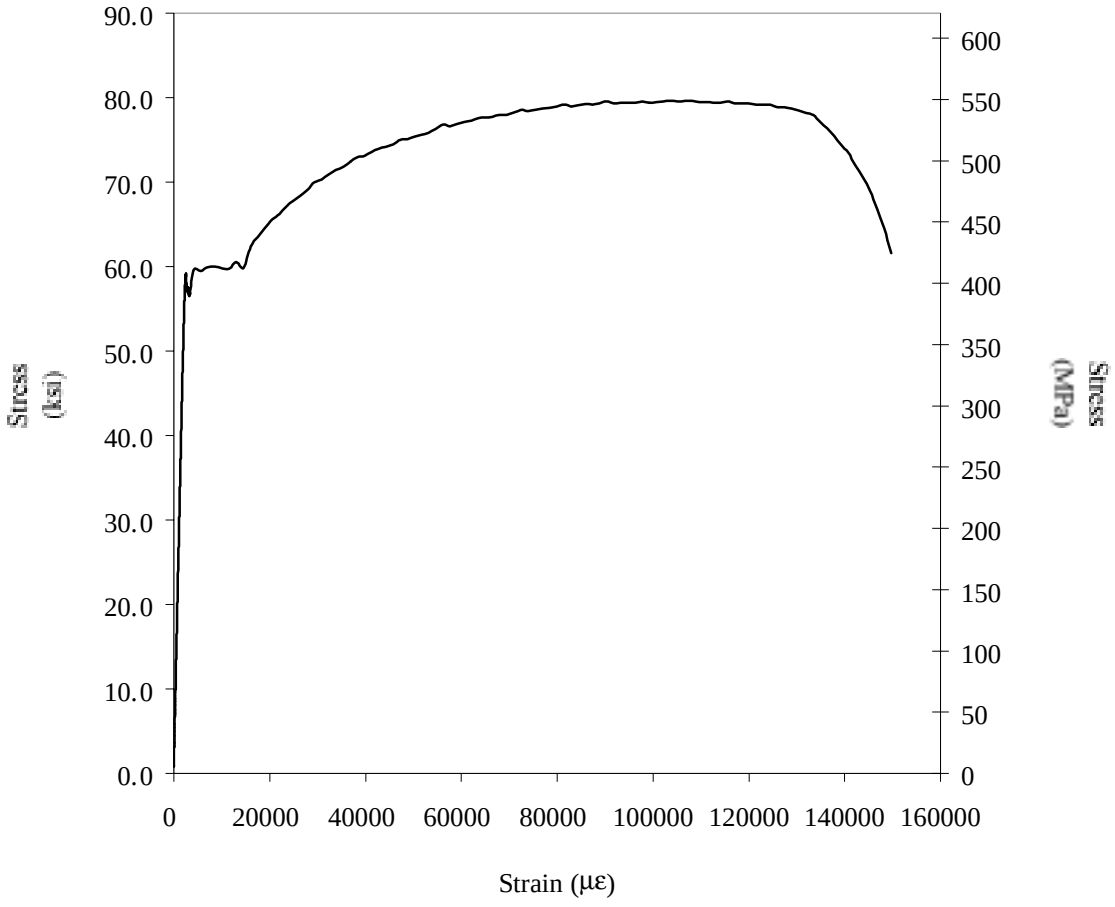

Figure A.12 Heat no. 181N340 beam flange tension coupon 2

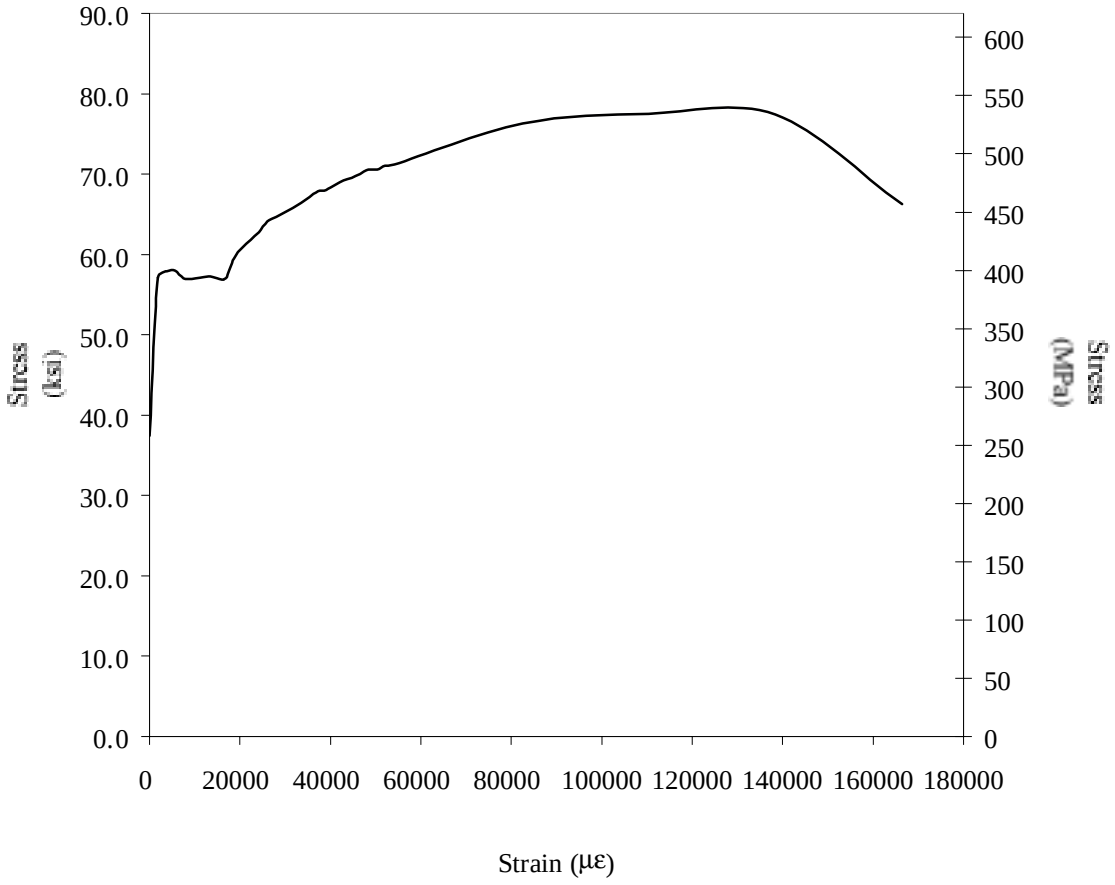

Figure A.13 Heat no. 76692 diaphragm web tension coupon 1

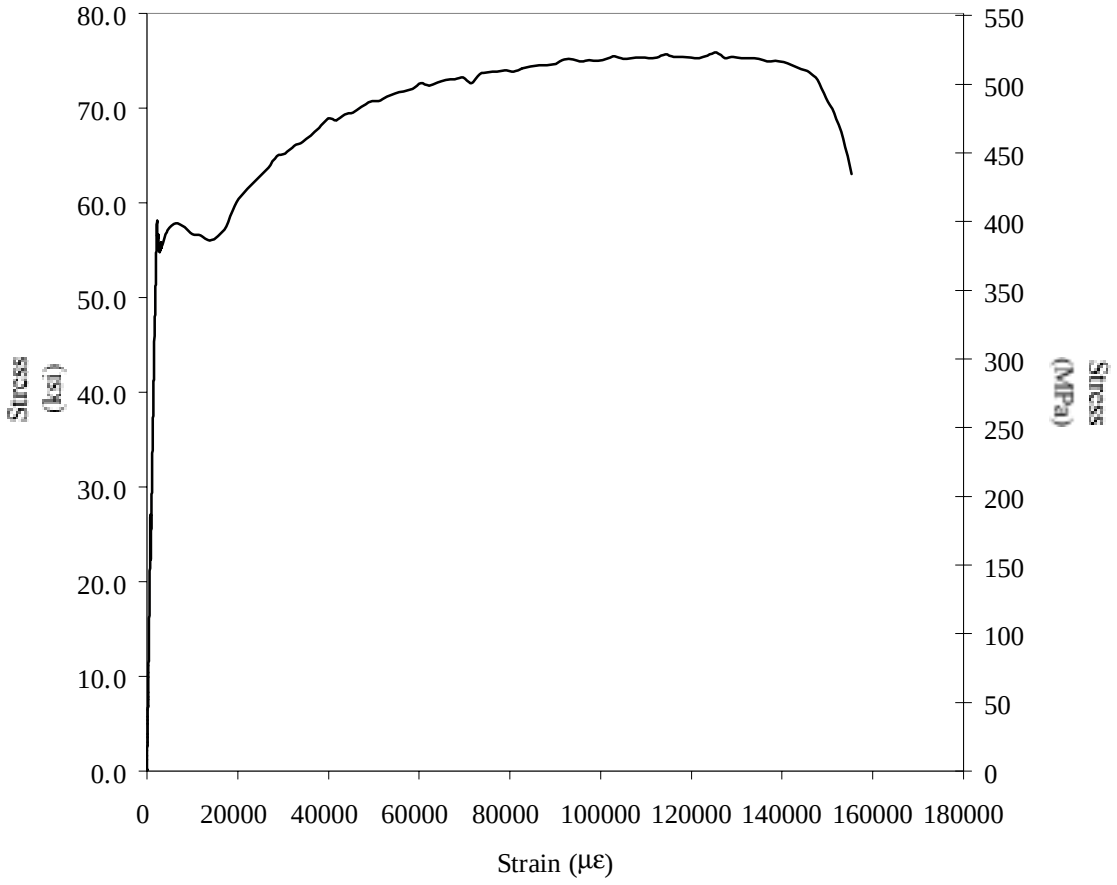

Figure A.14 Heat no. 76692 diaphragm web tension coupon 2

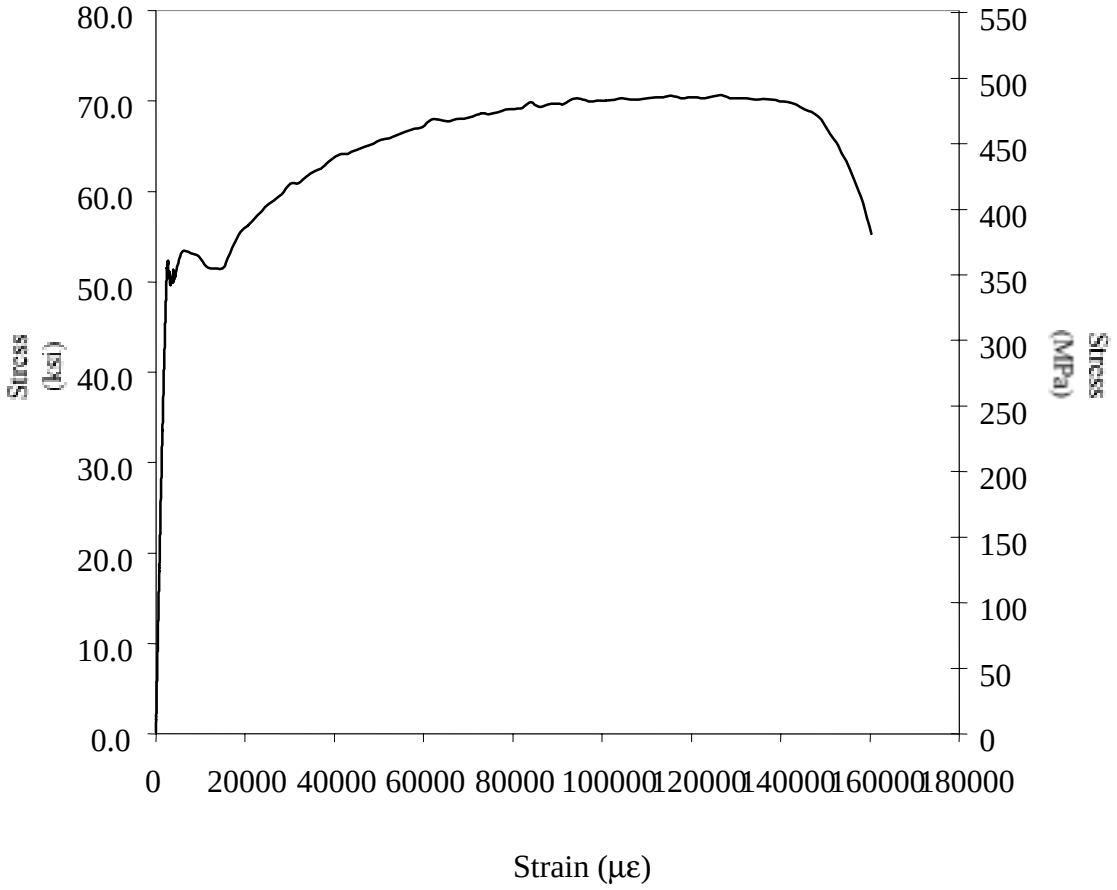

Figure A.15 Heat no. 76692 diaphragm flange tension coupon 1

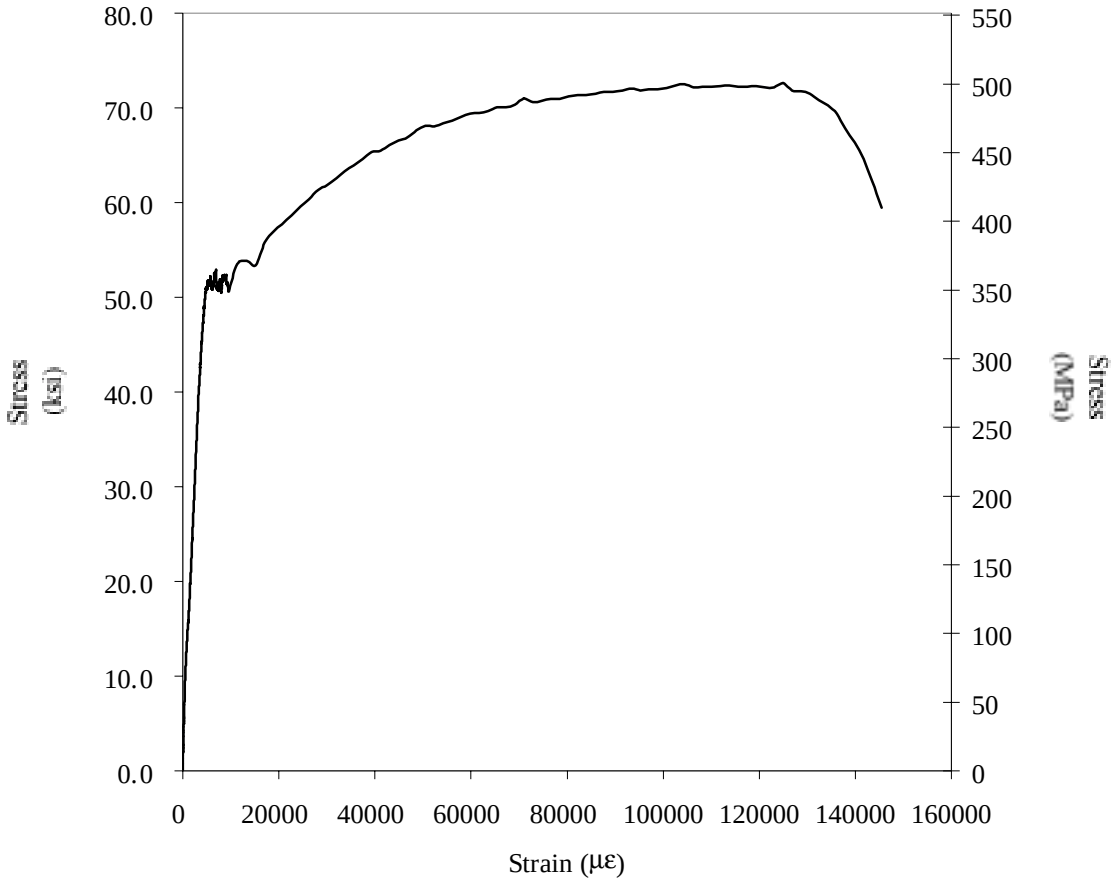

Figure A.16 Heat no. 76692 diaphragm flange tension coupon 2

APPENDIX B

EXPERIMENTAL WELD MEASUREMENTS

APPENDIX B

EXPERIMENTAL WELD MEASUREMENTS

This section contains the weld measurements for each of the welded diaphragm-to-beam connections in the experimental tests. Weld and spacing lengths are included. The measurements were made using a six-inch metal ruler. All dimensions are presented in inches since it was the unit of measurement. The measurements have not been converted to mm.

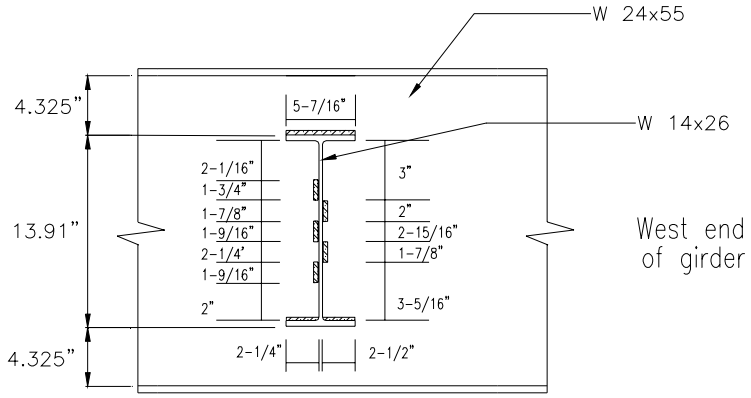

(a) North connection

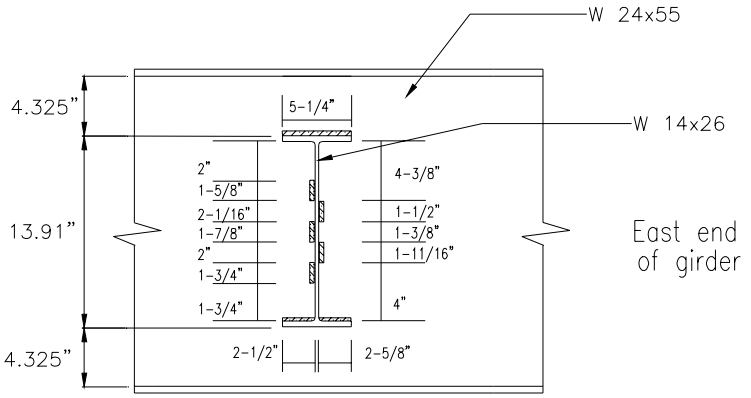

(b) South connection

Figure B.1 NS-NR(30) Welded connection

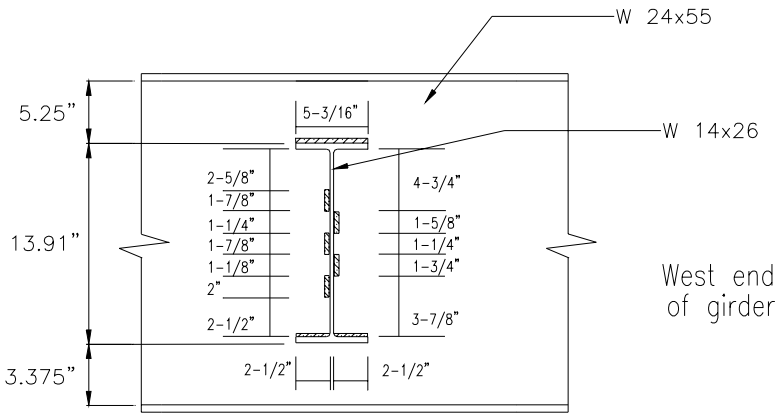

(a) North connection

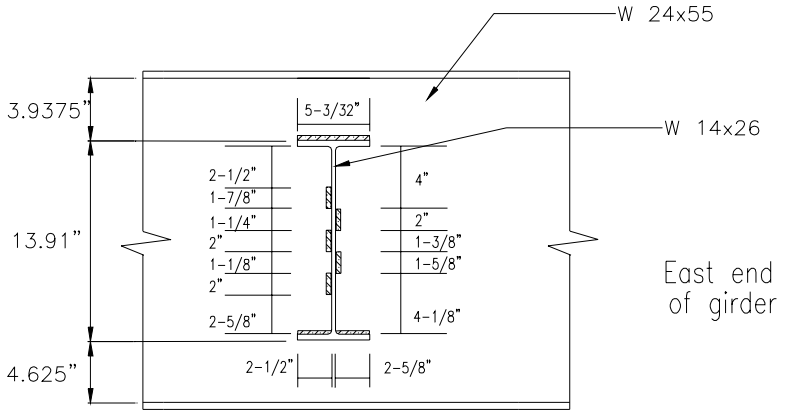

(b) South connection

Figure B.2 NS-NR(45) #1 Welded connection

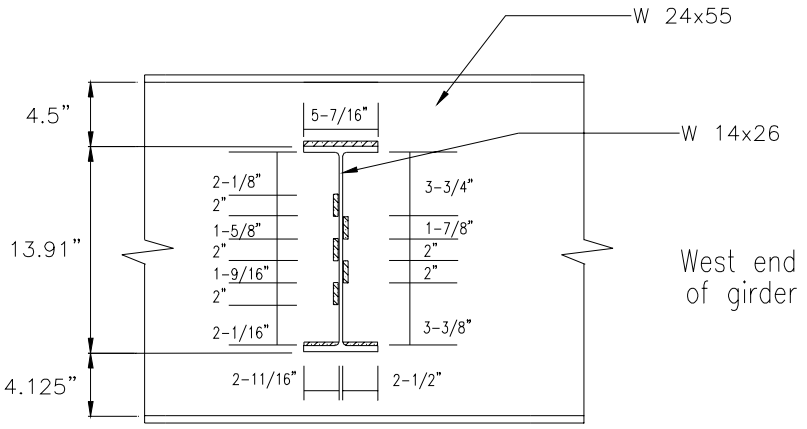

(a) North connection

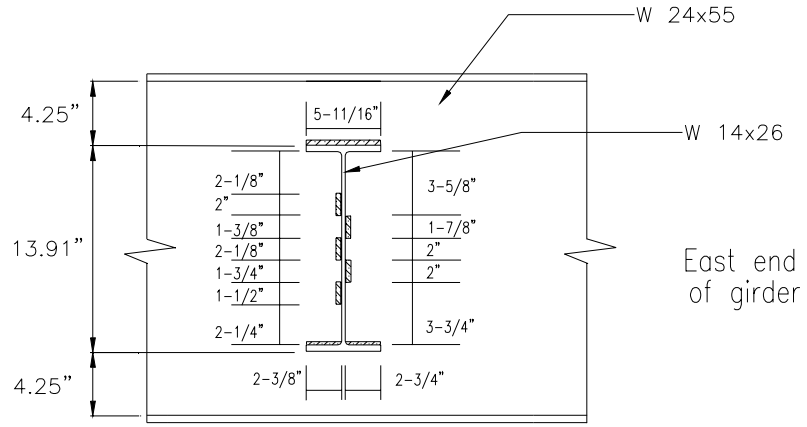

(b) South connection

Figure B.3 NS-NR(45) #2 Welded connection

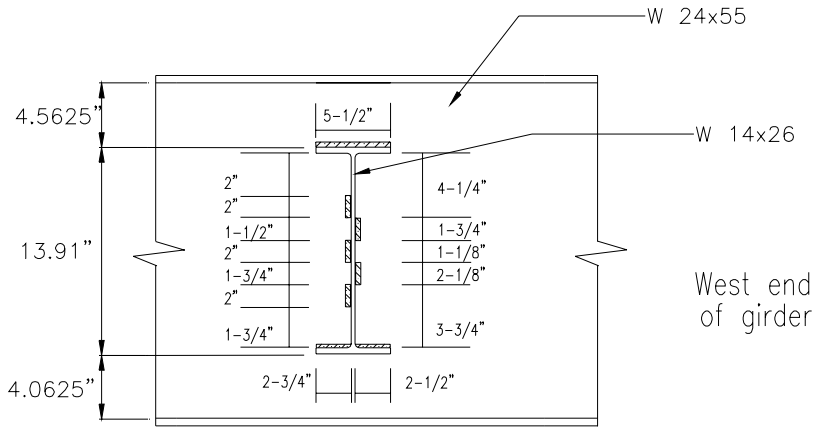

(a) North connection

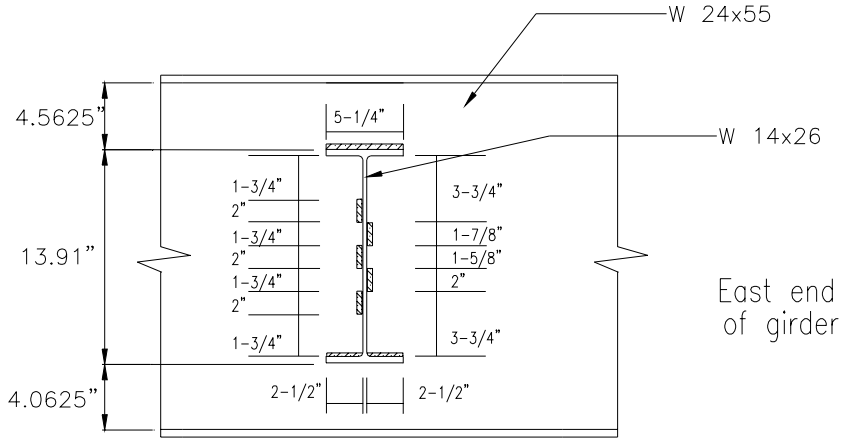

(b) South connection

Figure B.4 NS-FP(45) Welded connection

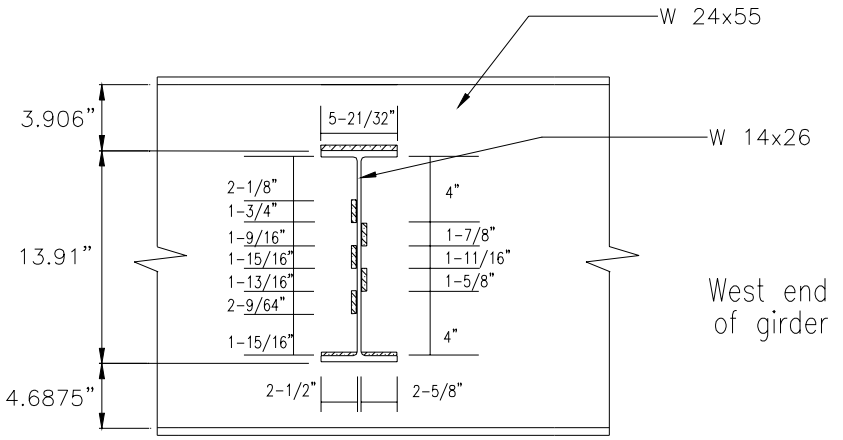

(a) North connection

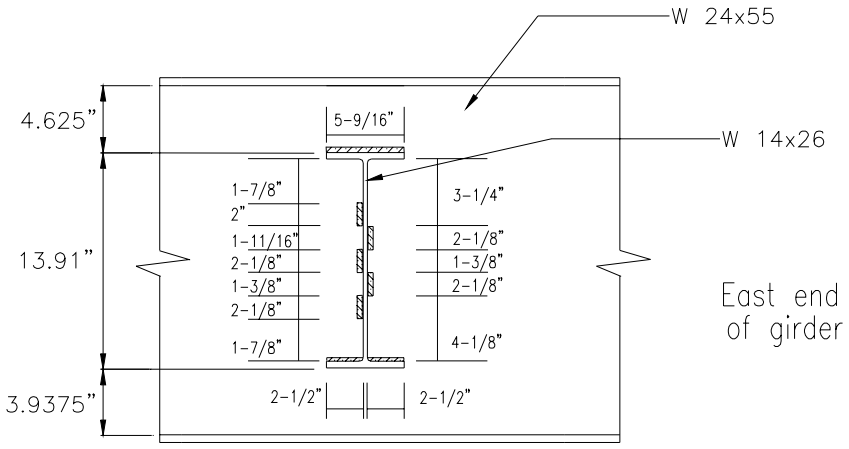

(b) South connection

Figure B.5 SC-NR(30) Welded connection

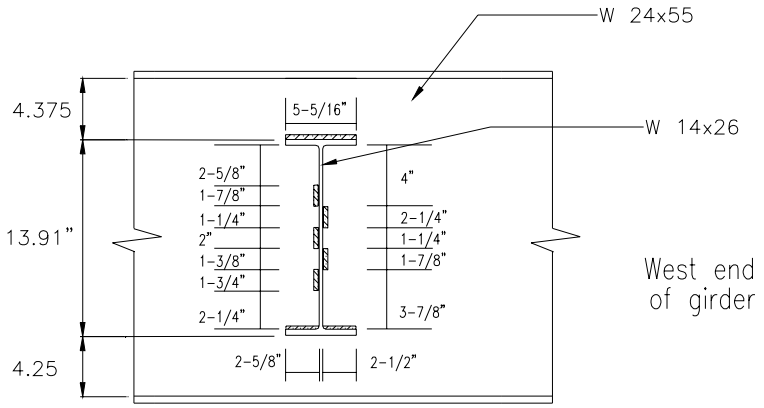

(a) North connection

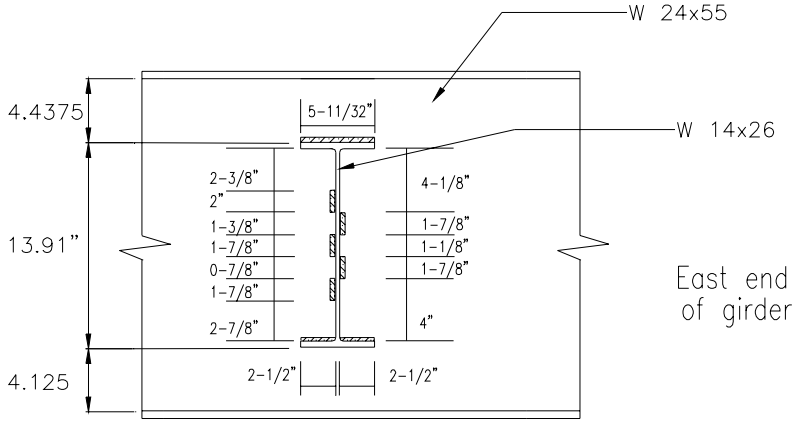

(b) South connection

Figure B.6 SC-NR(45) Welded connection

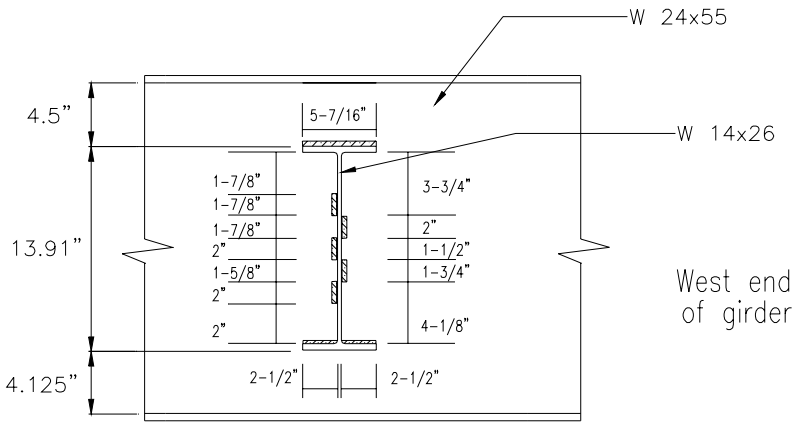

(a) North connection

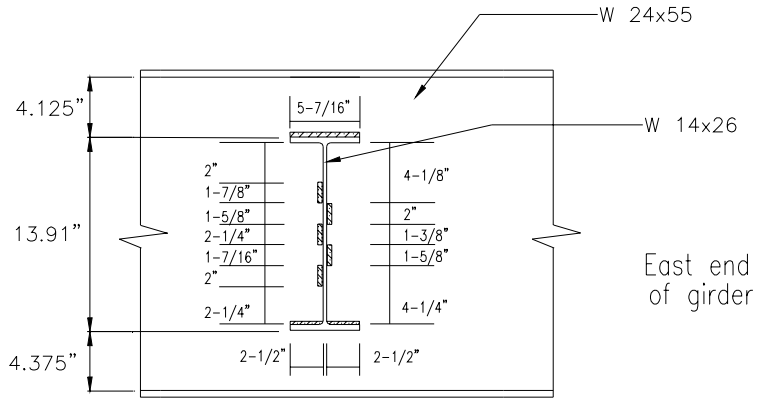

(b) South connection

Figure B.7 SL-NR(45) Welded connection

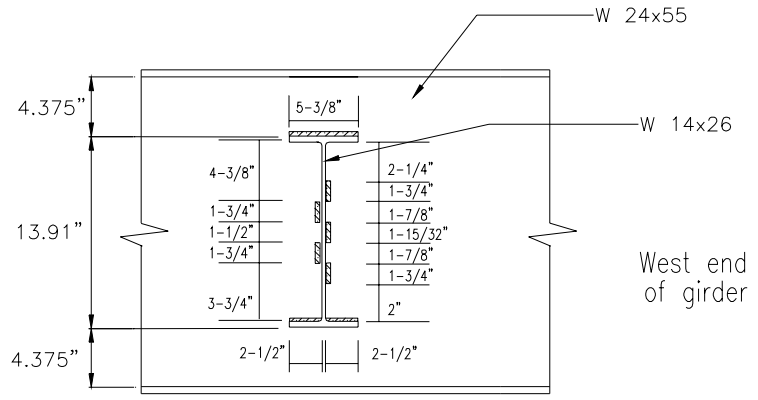

(a) North connection

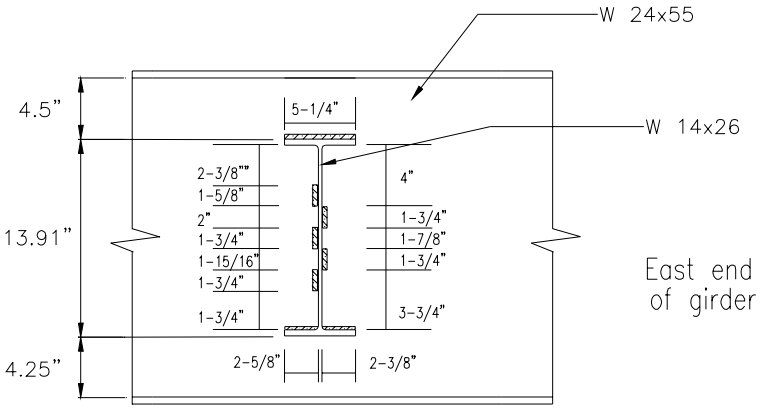

(b) South connection

Figure B.8 SC-FH(45) Welded connection

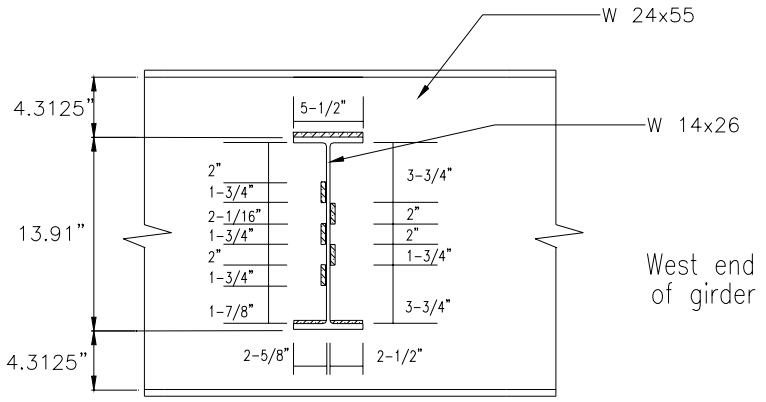

(a) North connection

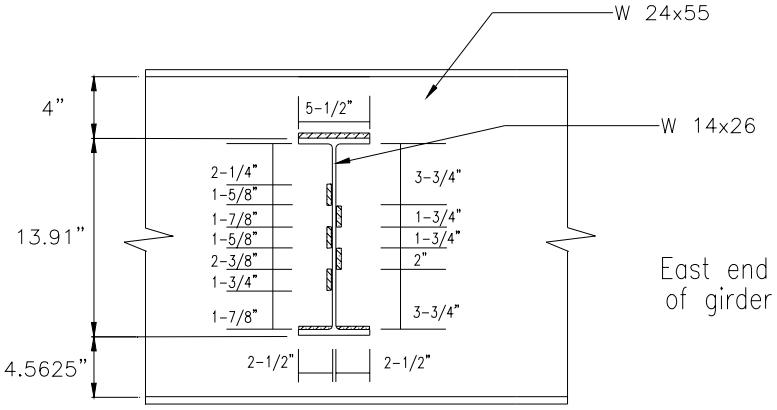

(b) South connection

Figure B.9 SC-LP(45) Welded connection

APPENDIX C

CRACK SIZE AND NUMBER OF CYCLES

APPENDIX C

CRACK SIZE AND NUMBER OF CYCLES

This appendix contains a description of the beam crack sizes measured during the experimental tests and the number of loading cycles applied. A detailed discussion of this information was presented in Chapter 4. Table C.1 presents the crack size at detection and at the end of the test along with the corresponding number of loading cycles. Notes made during the test are also included.

Table C.1 Crack Size and Loading Cycles

Specimen	Connection	Detectable Crack Size (in)		Final Crack Size (in)		Number of Loading Cycles (Thousands)		Notes
		East	West	East	West	Crack Detection	End of Test	
NS-NR(30)	North	3/8”	1/2”	2-7/8”	3-5/8”	3,007	8,000	By 1,640,844 cycles all of the web welds were severed. At 6,184,200 cycles the bottom flange welds severed. The beam cracks remained horizontal.
	South	1”	3/4”	2”	1-3/8”	3,007	8,000	By 1,640,844 cycles the bottom flange welds and 3 of the 5 web welds were severed. The beam cracks remained horizontal.
NS-NR(45)	North	3/4”	1/8”	10-3/8”	3-1/8”	1,704	5,660	At 1,704,800 cycles a 1-5/8” horizontal crac at the top flange weld was detected. At end of test horizontal crack was 9-3/8”. East crack was at base of beam fillet.
	South	--	--	--	--	--	5,660	By 32,000 cycles the bottom flange welds and all web welds were severed.

Table C.1 Crack Size and Loading Cycles, continued

Specimen	Connection	Detectable Crack Size (in)		Final Crack Size (in)		Number of Loading Cycles (Thousands)		Notes
		East	West	East	West	Crack Detection	End of Test	
NS-NR(45)	North	1/4”	--	3-5/8”	--	2,430	6,000	A 5-3/8” horizontal crack at welded top flange was detected at 1,747,500 cycles. At end of test crack was 8”.
	South	--	--	--	--	--	--	Web welds and bottom flange welds were severed by 18,380 cycles. At 1,500,000 cycles top flange weld was severed.
NS-FP(45)	North	--	--	--	--	--	4,474	Top and bottom flange weld areas were peened at 385,300 cycles under 5,000 lb. applied load.
	South	--	--	--	--	--	4,474	Top and bottom flange weld areas were peened at 385,300 cycles under 5,000 lb. applied load
SC-NR(30)	North	1-5/8”	--	5-3/4”	--	3,555	8,790	
	South	--	2-5/8”	--	12-1/4”	3,555	8,790	Crack fractured tension flange at 8,790,046 cycles.

Table C.1 Crack Size and Loading Cycles, continued

Specimen	Connection	Detectable Crack Size (in)		Final Crack Size (in)		Number of Loading Cycles (Thousands)		Notes
		East	West	East	West	Crack Detection	End of Test	
SC-NR(45)	North	1/8”	--	11-7/8”	--	510	4,182	Crack fractured tension flange at 2,649,537 cycles. Crack was repaired with 1/2 inch splice plates and hole was drilled at beam crack tip.
	South	--	1/8”	--	11-1/4”	358	4,182	Crack fractured tension flange at 4,182,467 cycles.
SL-NR(45)	North	1/8”	1/8”	2”	3-7/8”	849	6,550	Diaphragm was located under load.
	South	2”	1/4”	2”	1/4”	4,138	6,550	Diaphragm was 4 feet from applied load. East crack was detected at 5,545,900 cycles.
SC-FH(45)	North	3/8”	3/8”	3/8”	2-1/4”	1,570	6,000	West crack was detected at 2,186,400 cycles.
	South	1/4”	1/2”	1-7/8”	2-3/8”	1,032	6,000	West crack was repaired at 1,785,100 cycles by drilling holes at beam crack tips and removing diaphragm.

Table C.1 Crack Size and Loading Cycles, continued

Specimen	Connection	Detectable Crack Size (in)		Final Crack Size (in)		Number of Loading Cycles (Thousands)		Notes
		East	West	East	West	Crack Detection	End of Test	
SC-LP(45)	North	--	--	--	--	--	4,947	Bottom flange weld area was peened at both connections at 385,300 cycles with 5,000 lb. applied load. At 3,904,500 cycles a 1/8” crack was detected at toe of East bottom flange weld.
	South	--	1/8”	--	--	385	4,947	Bottom flange weld area was peened at both connections at 385,300 cycles with 5,000 lb. applied load. At 1,419,300 cycles a 1/8” crack was detected at toe of West bottom flange weld and a 3/4” crack was detected in East bottom flange weld. West crack was 3/8” and East crack was 1-1/8” at end of test.

APPENDIX D

EXPERIMENTAL MEASUREMENTS

APPENDIX D

EXPERIMENTAL MEASUREMENTS

The static measurements from the experimental tests are included here. During the experimental tests, selected surface strains were measured on the beams and diaphragms for all tests. For the tests conducted using the 1468 kN (330 kip) actuator, load cell readings at each end of the test beam were gathered as well as deflection measurements of the test beam and outside beams. The following tests were performed in the 1468 kN test bay: NS-NR(30), SC-NR(30), SC-NR(45), SL-NR(45), SC-FH(45), and SC-LP(45).

For the three tests in which repairs were performed, NS-FP(45), SC-FH(45), and SC-LP(45), the vertical dashed line on the summary graph represents the time of repair.

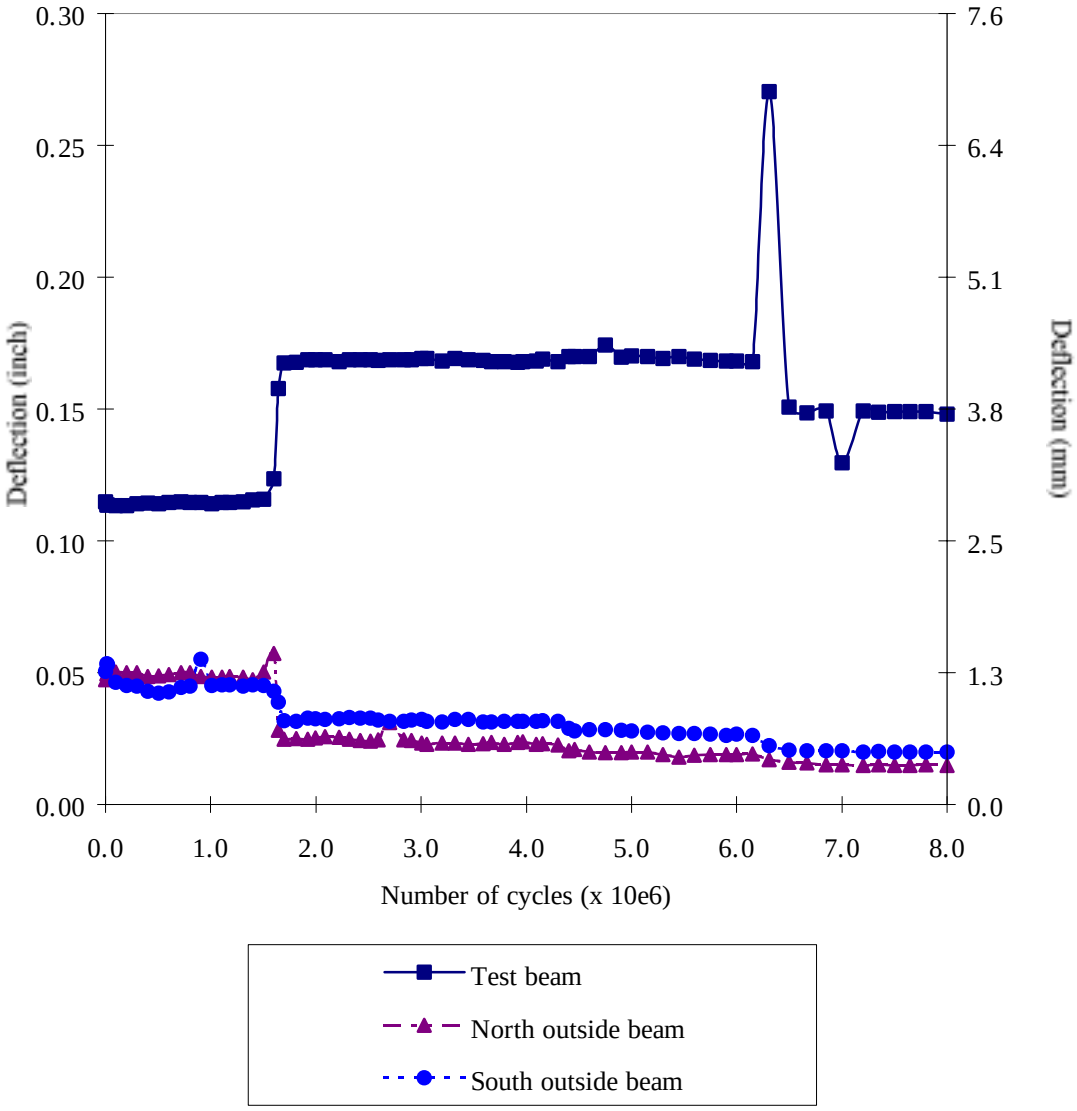

Figure D.1 Deflection measurements for NS-NR(30)

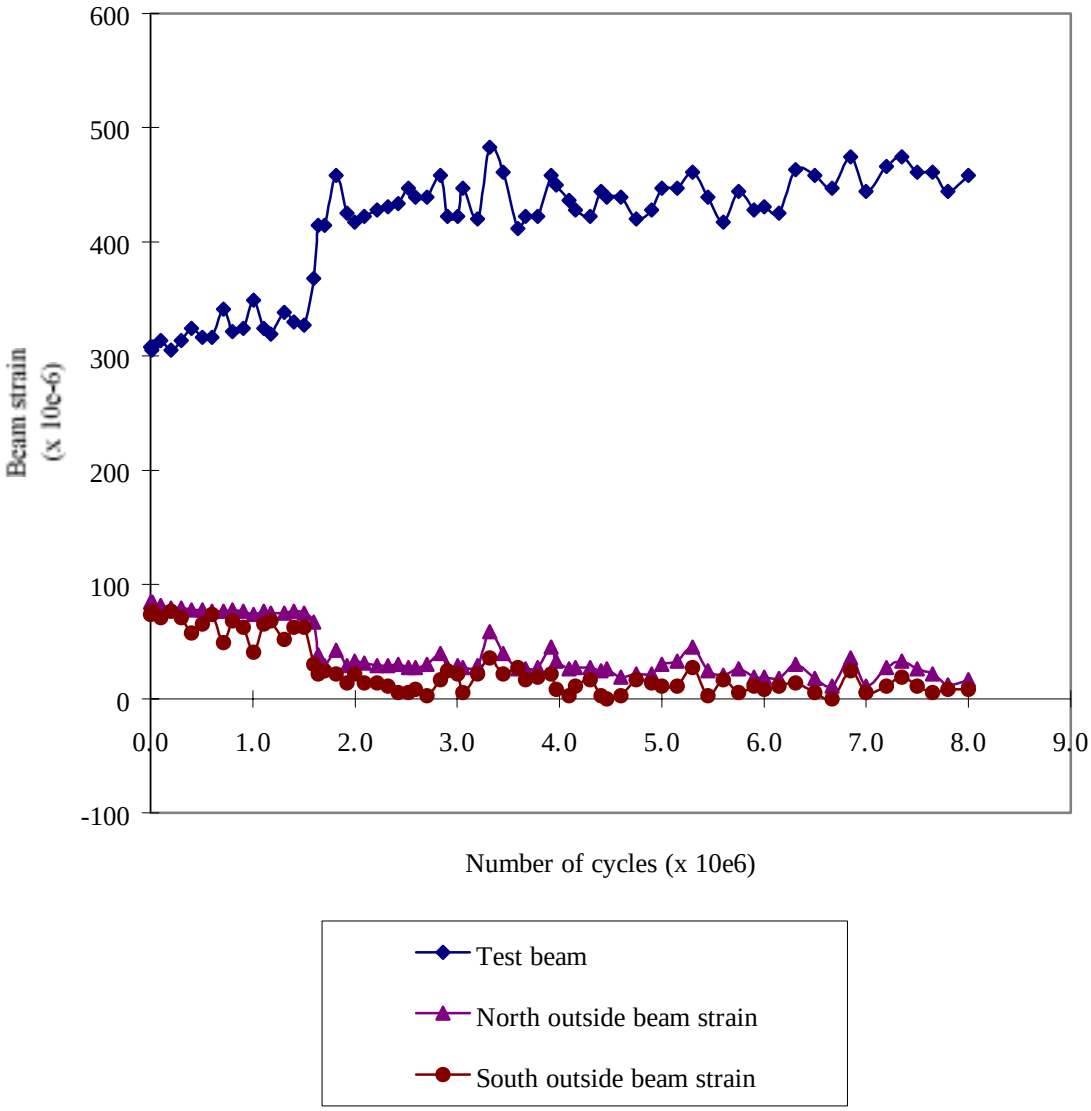

Figure D.2 Longitudinal beam strain measurements for NS-NR(30)

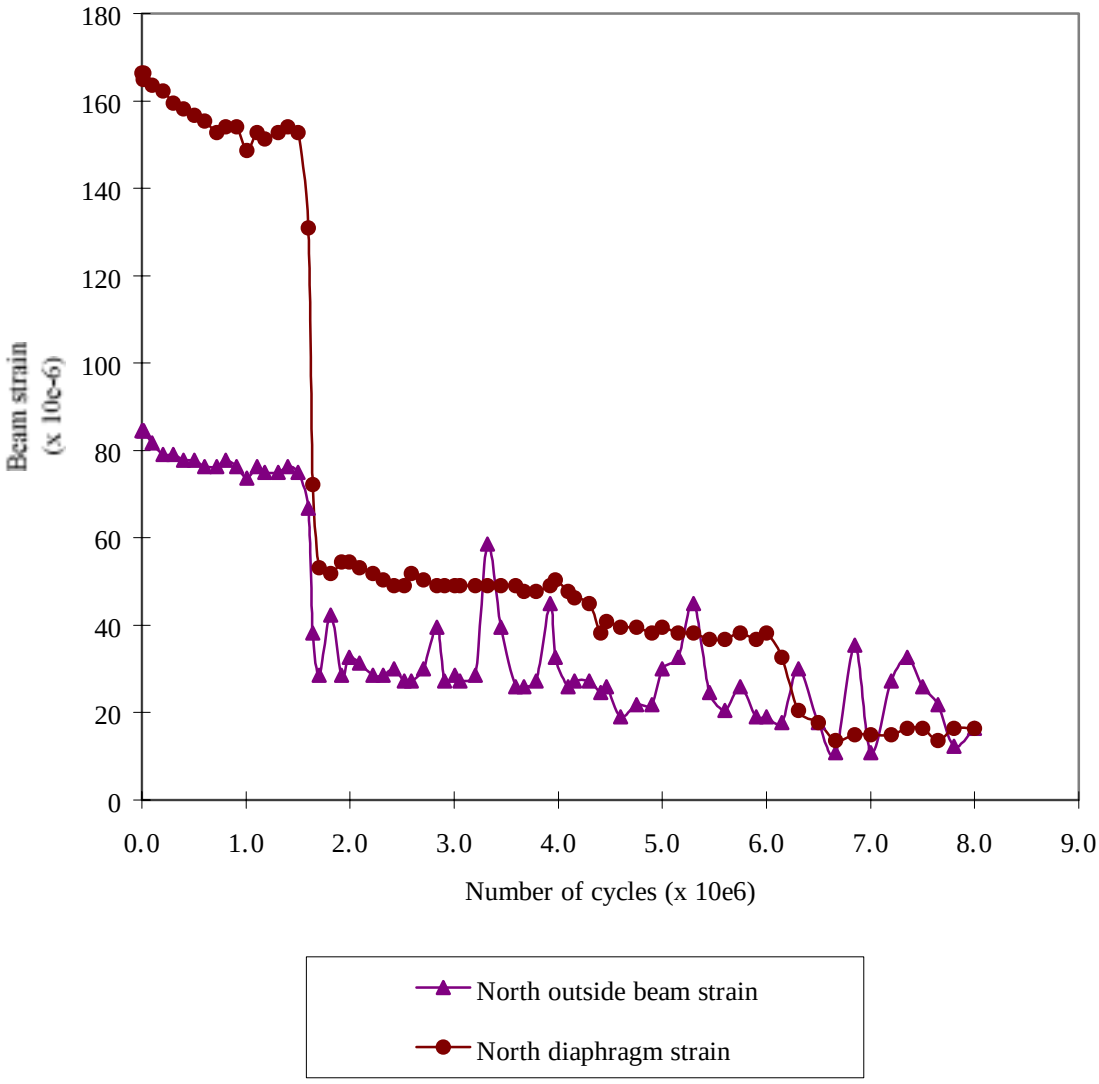

Figure D.3 North outside beam and diaphragm measurements for NS-NR(30)

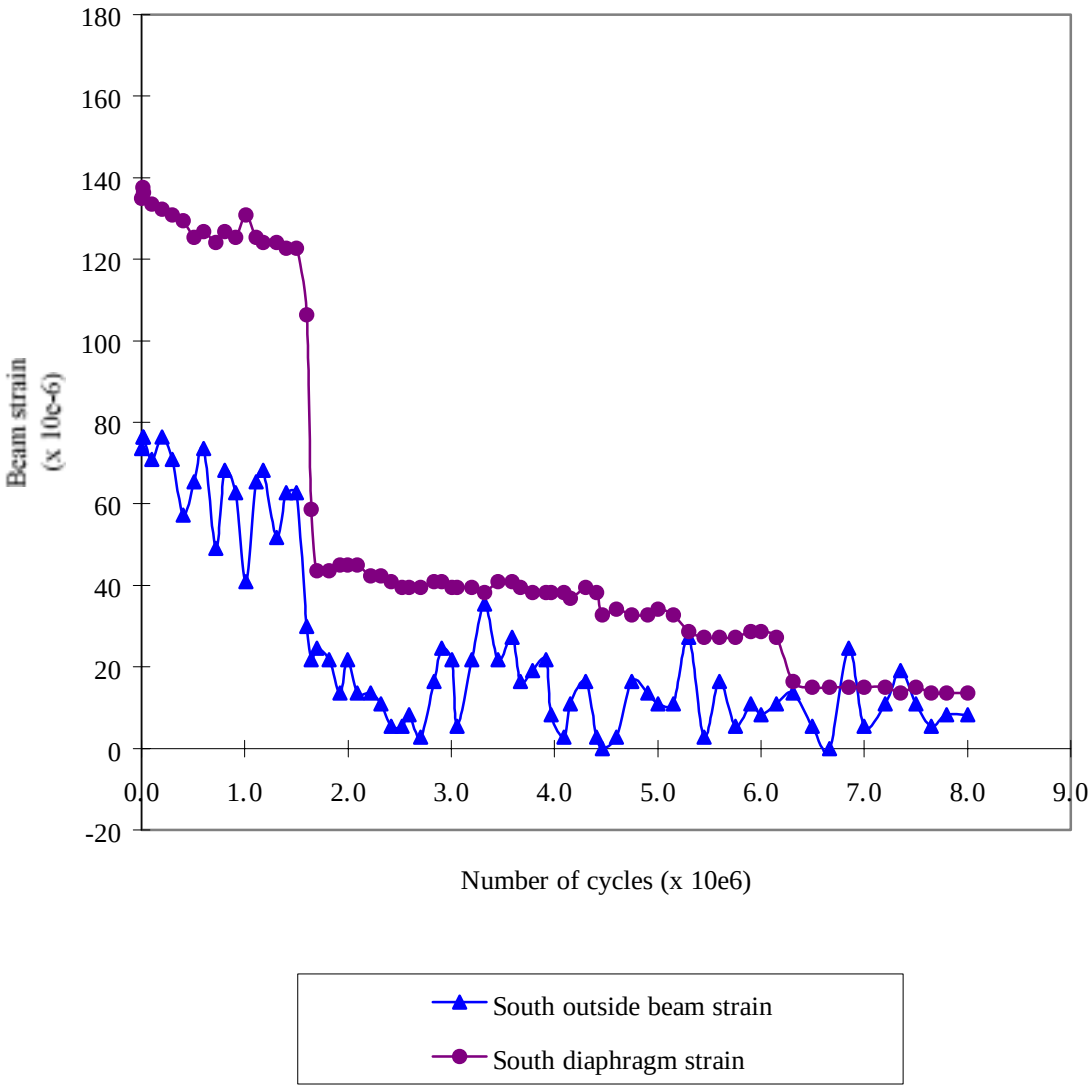

Figure D.4 South outside beam and diaphragm measurements for NS-NR(30)

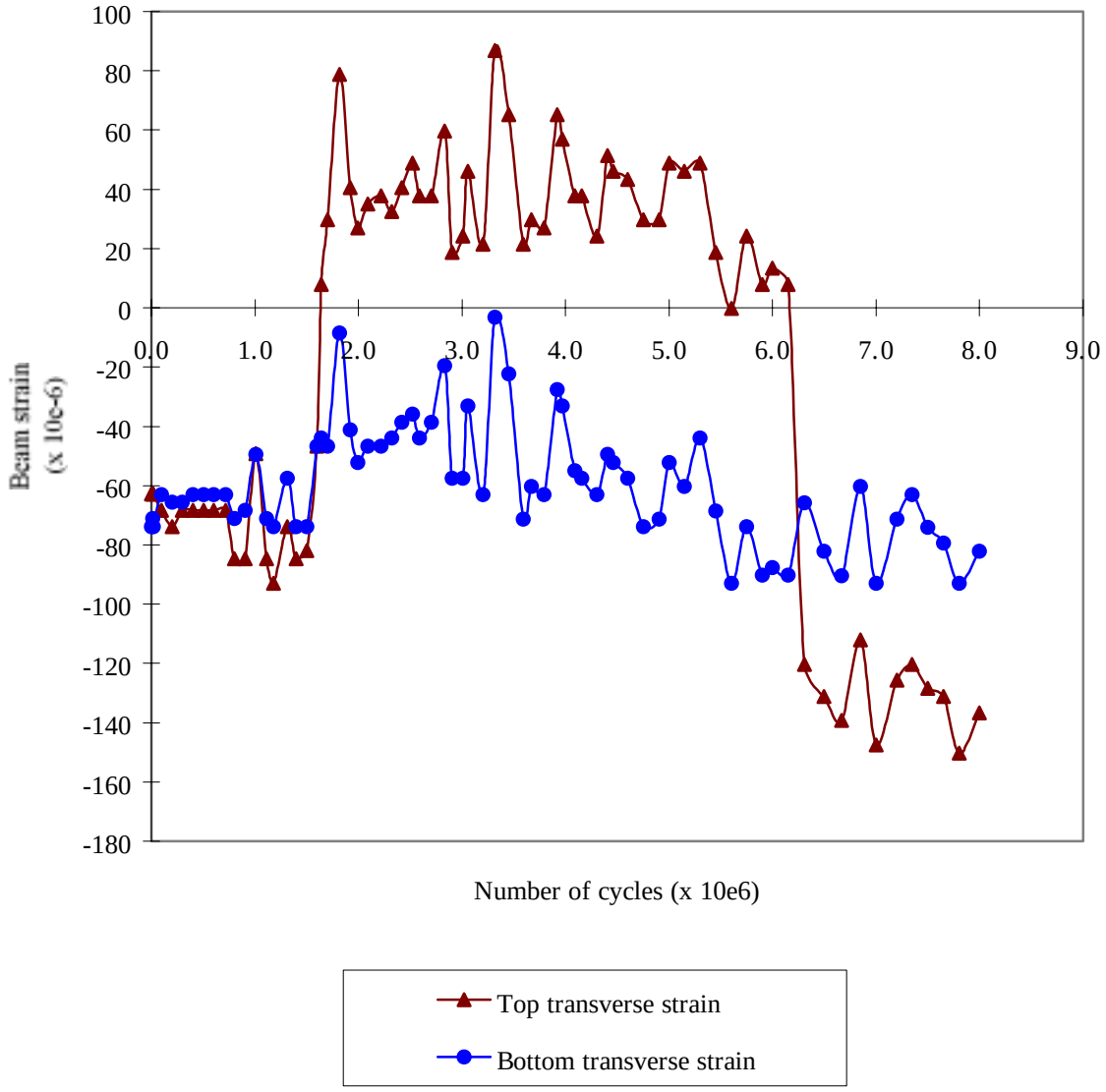

Figure D.5 Transverse beam strains in web gap region at north diaphragm for NS-NR(30)

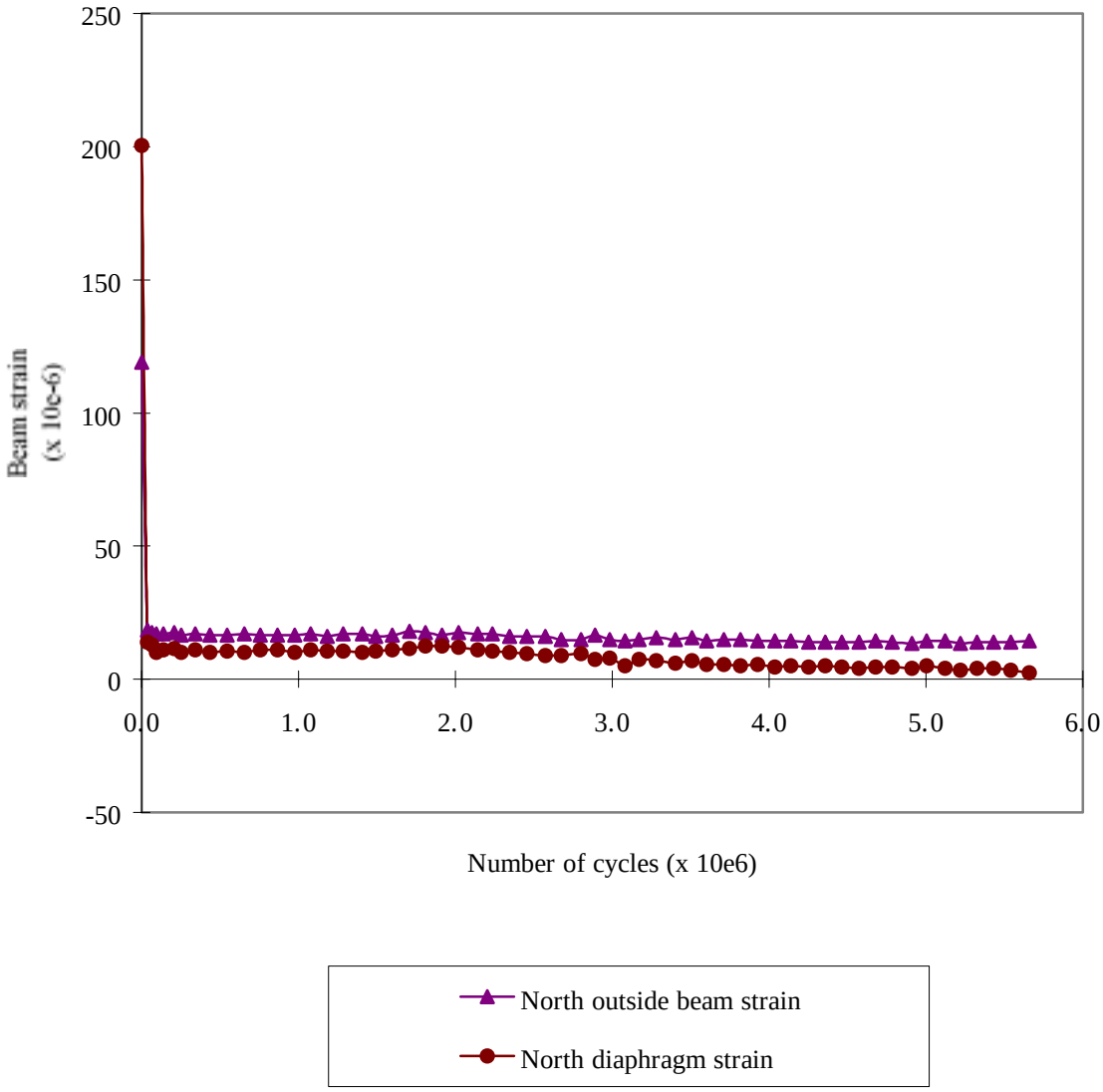

Figure D.6 North outside beam and diaphragm measurements for NS-NR(45) #1

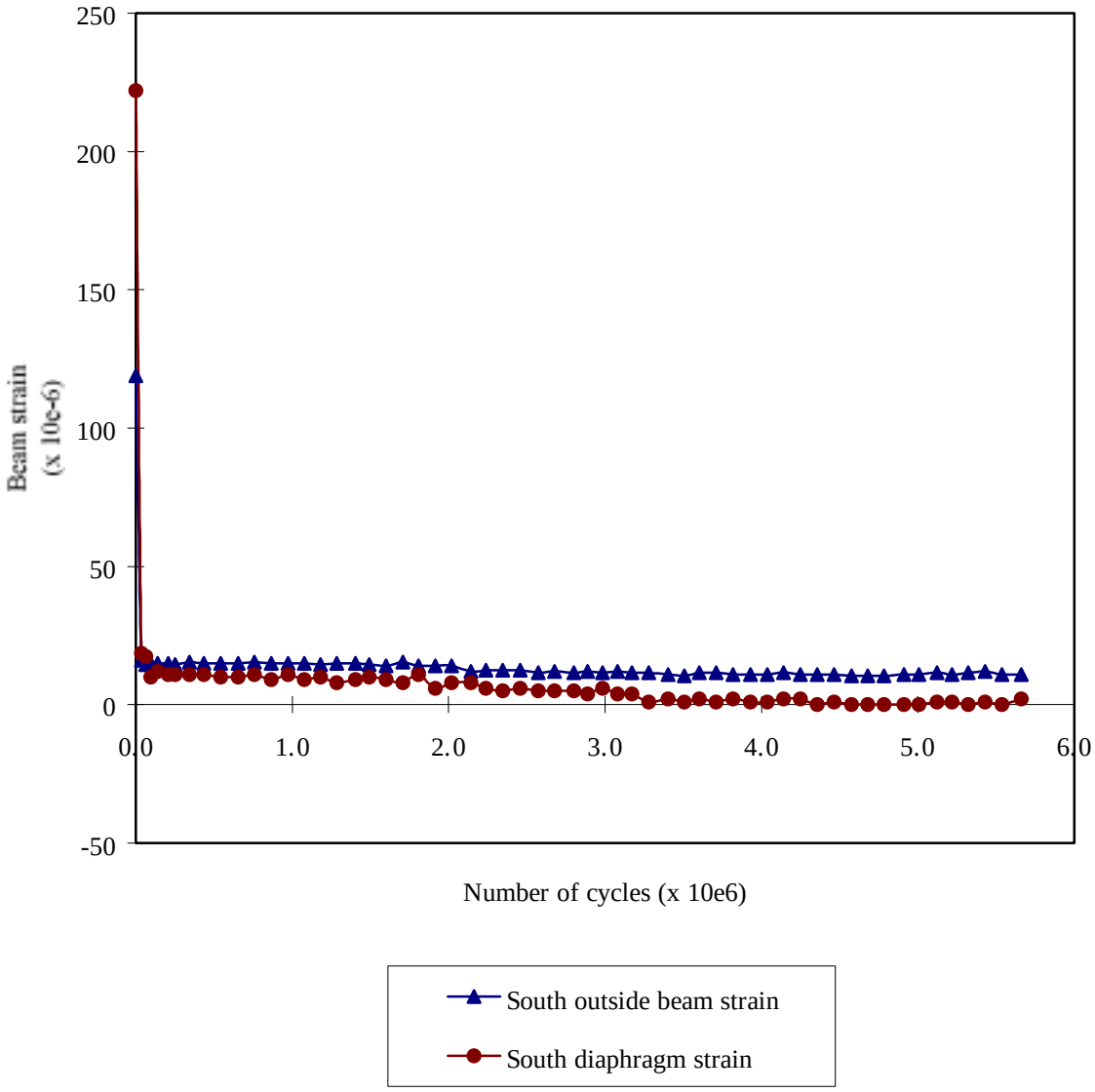

Figure D.7 South outside beam and diaphragm measurements for NS-NR(45) #1

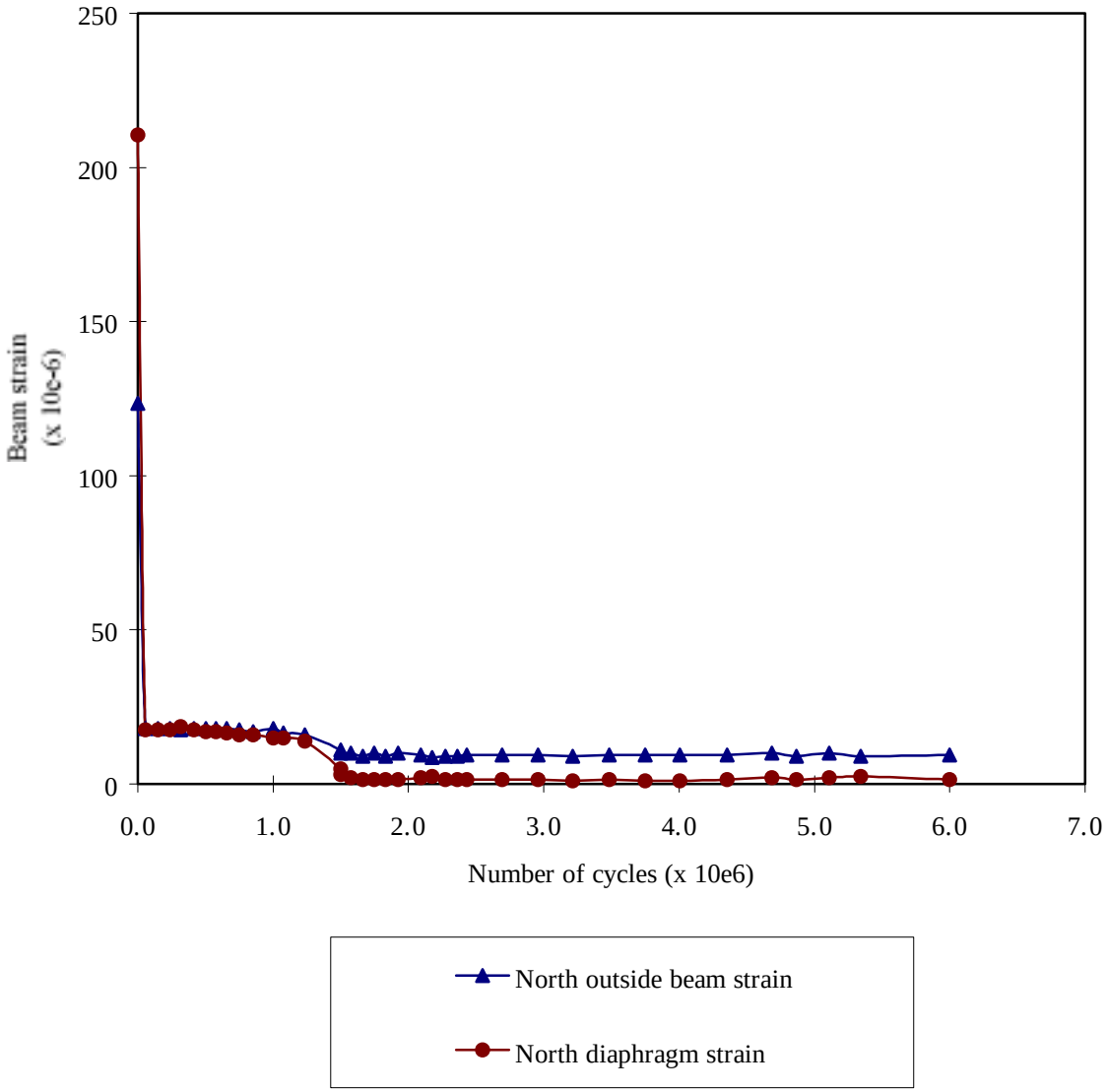

Figure D.8 North outside beam and diaphragm measurements for NS-NR(45) #2

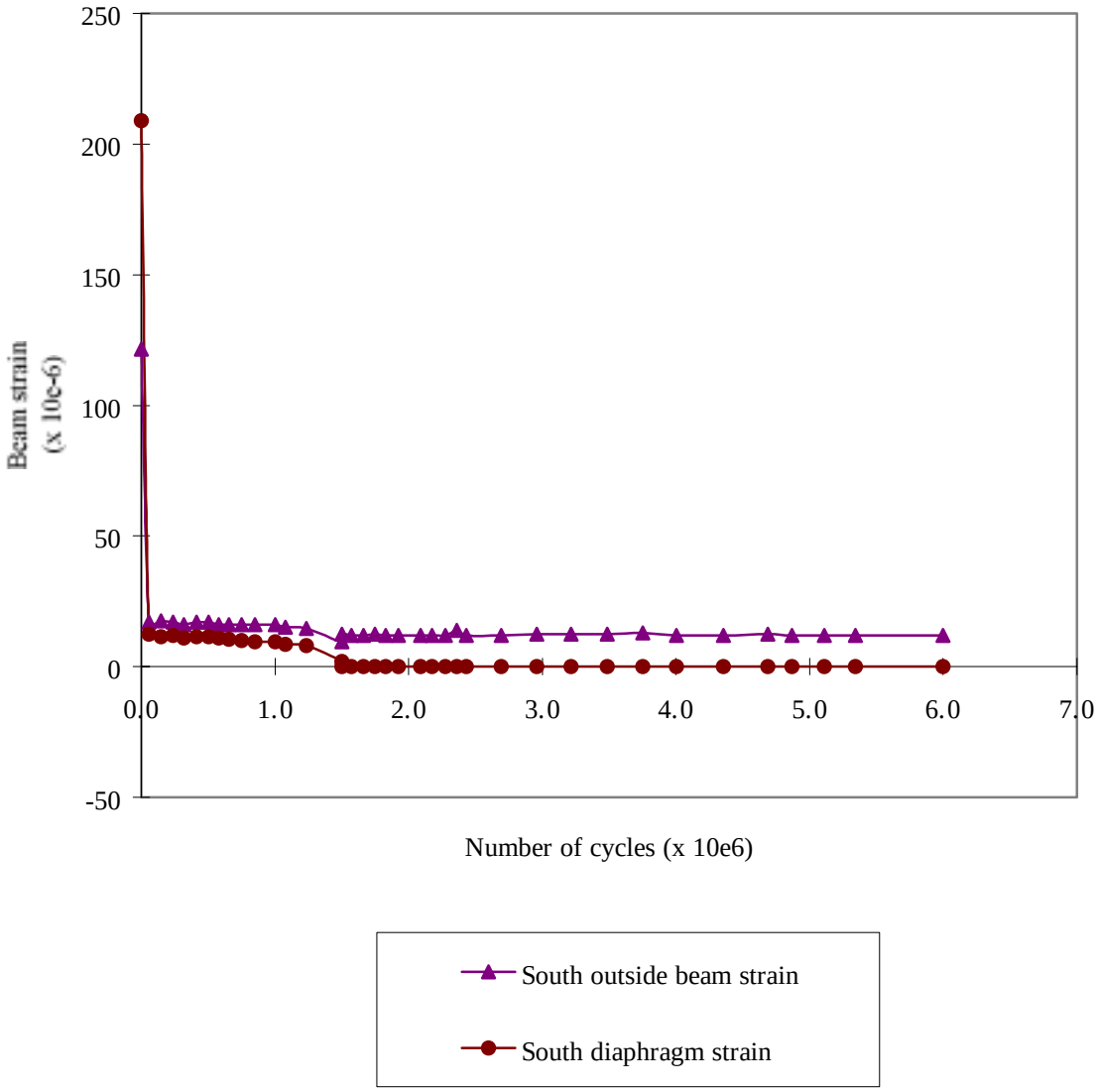

Figure D.9 South outside beam and diaphragm measurements for NS-NR(45) #2

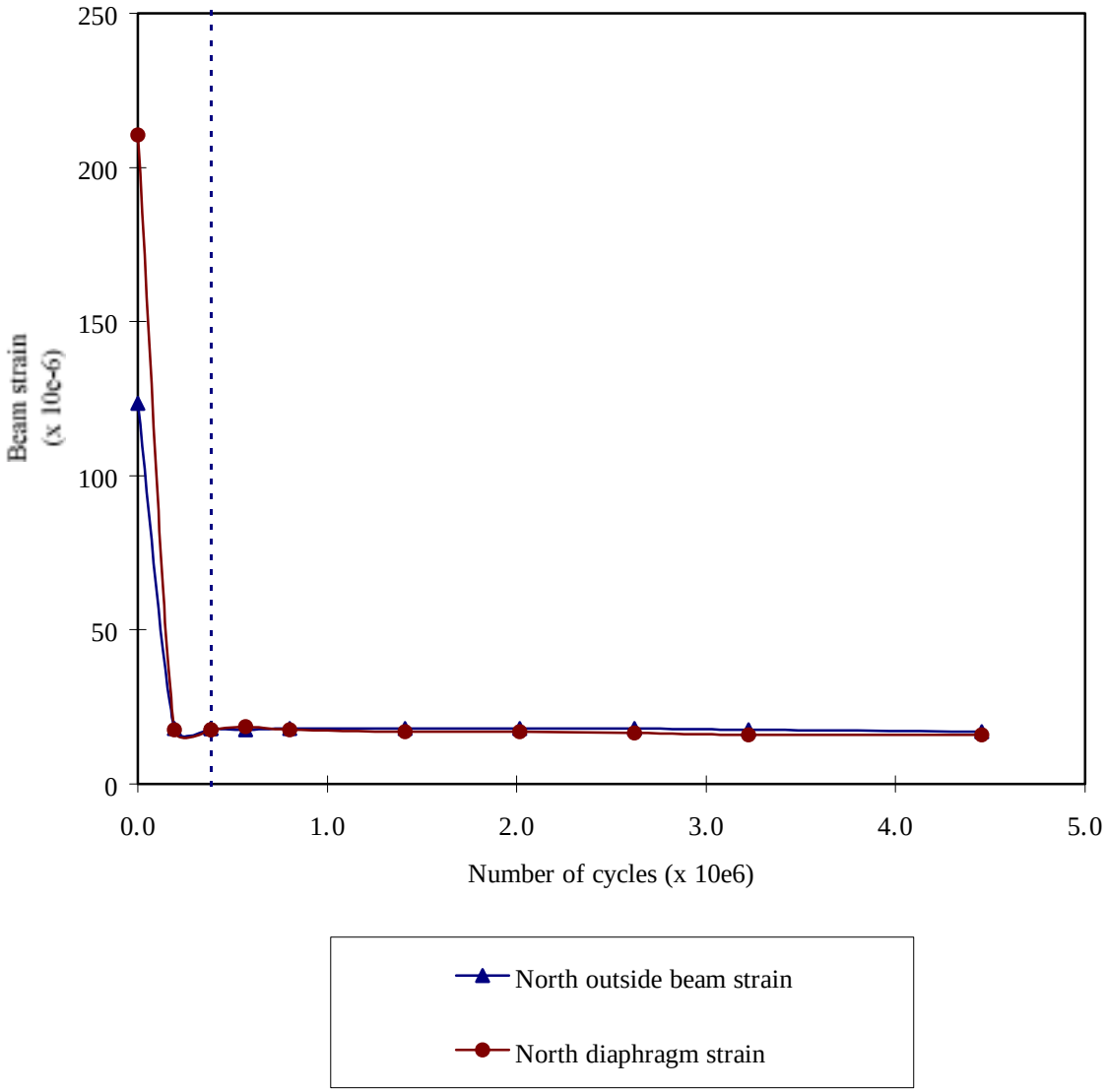

Figure D.10 North outside beam and diaphragm measurements for NS-FP(45)

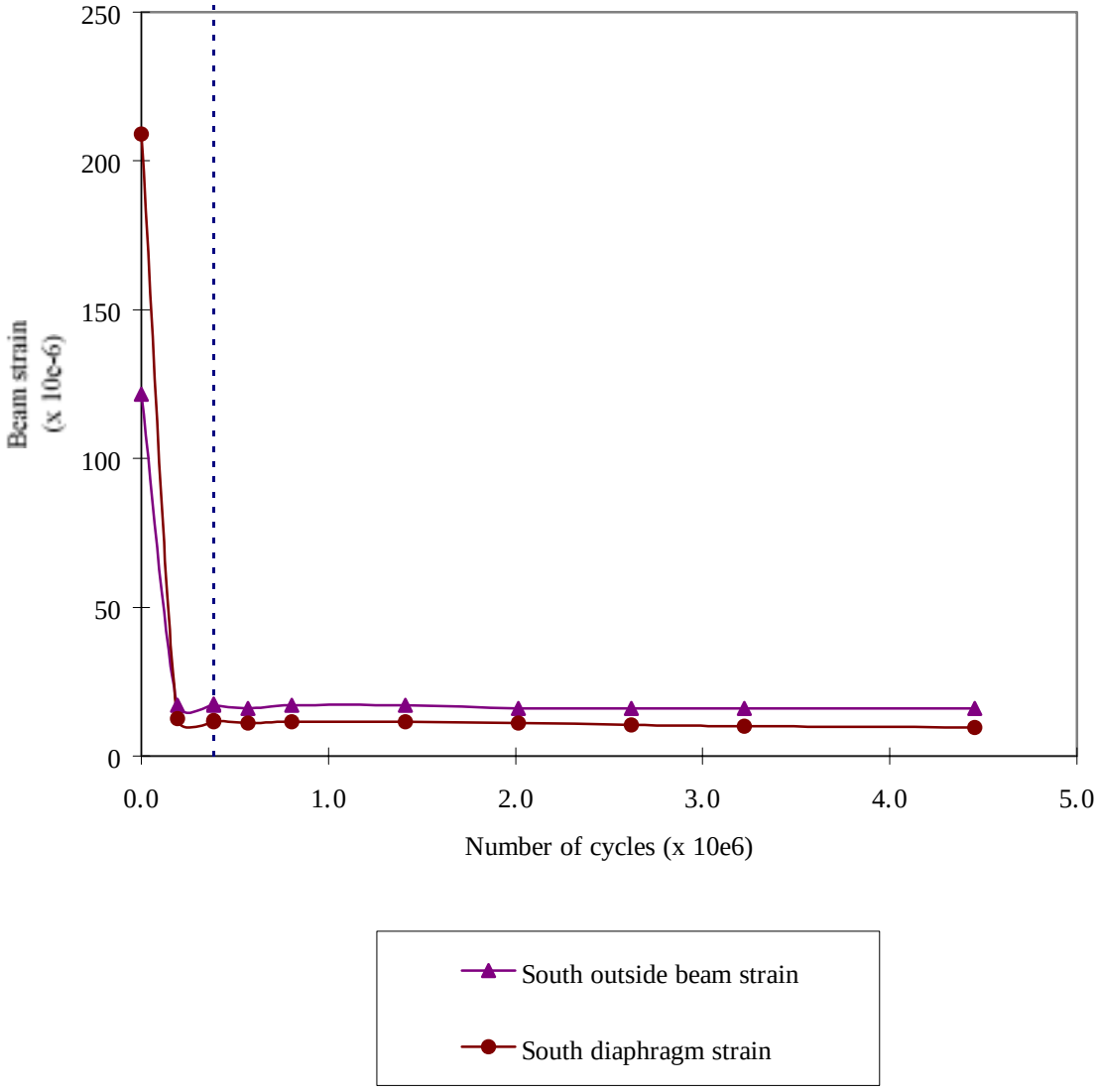

Figure D.11 South outside beam and diaphragm measurements for NS-FP(45)

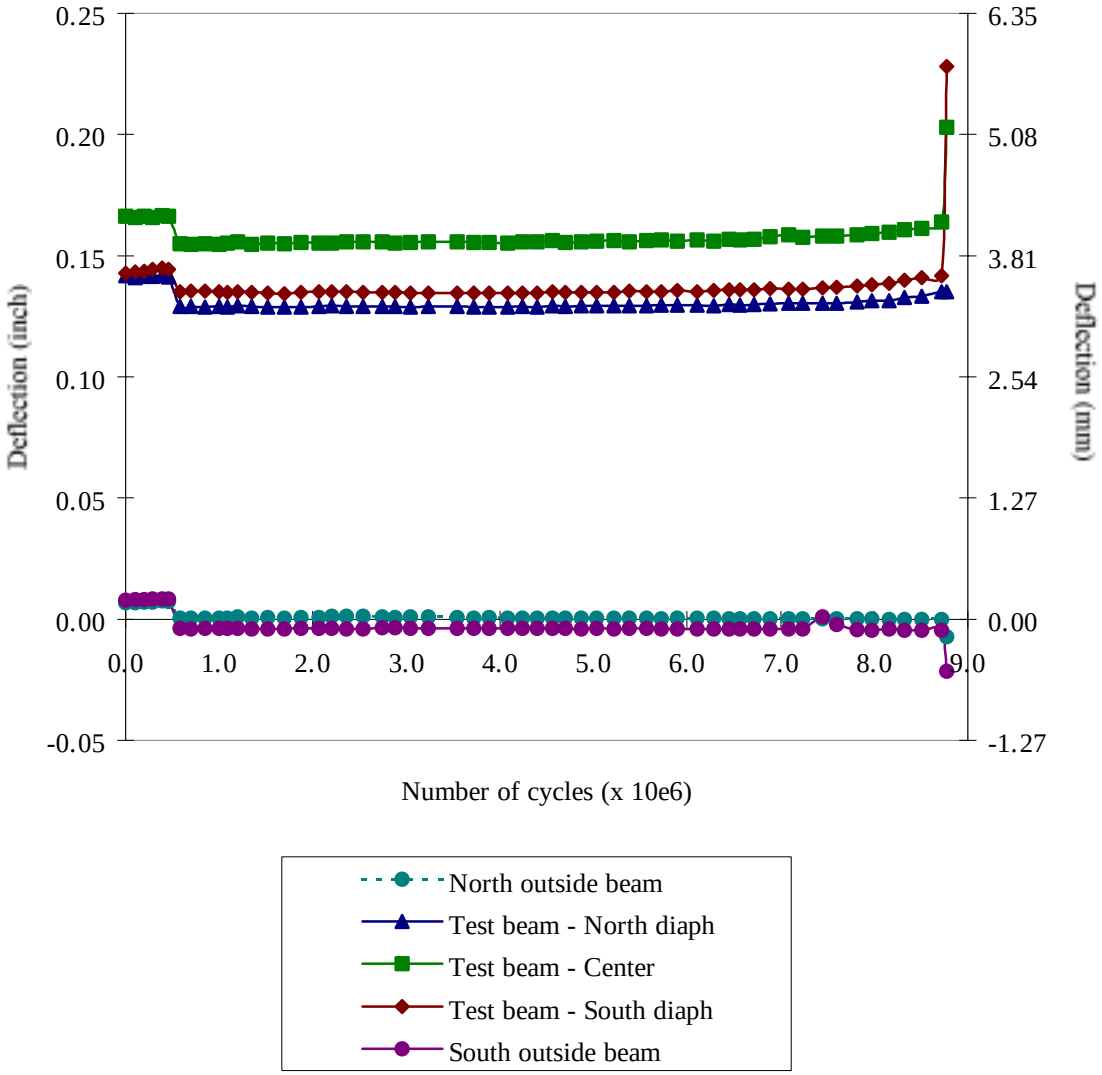

Figure D.12 Deflection measurements for SC-NR(30)

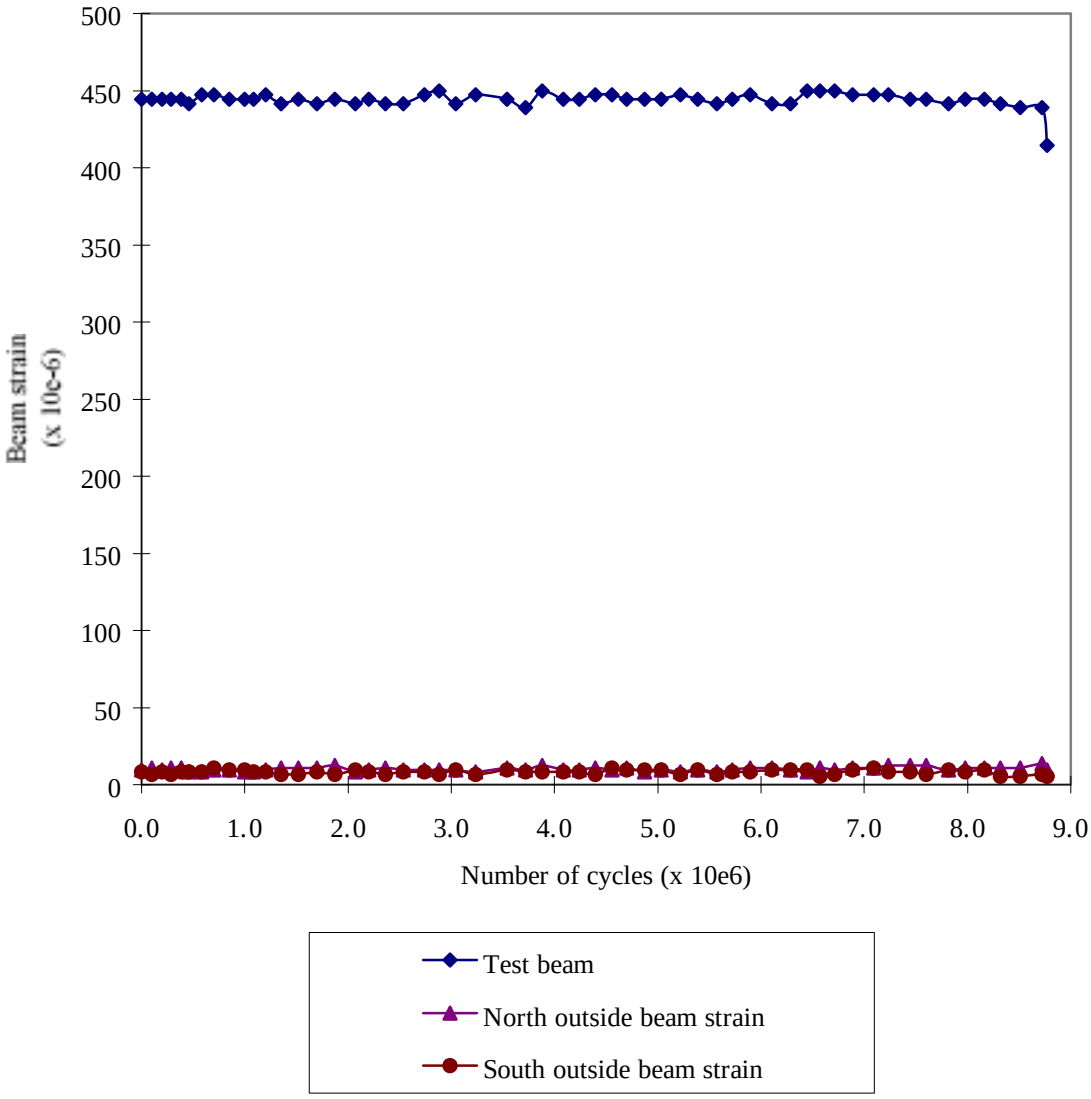

Figure D.13 Longitudinal beam strain measurements for SC-NR(30)

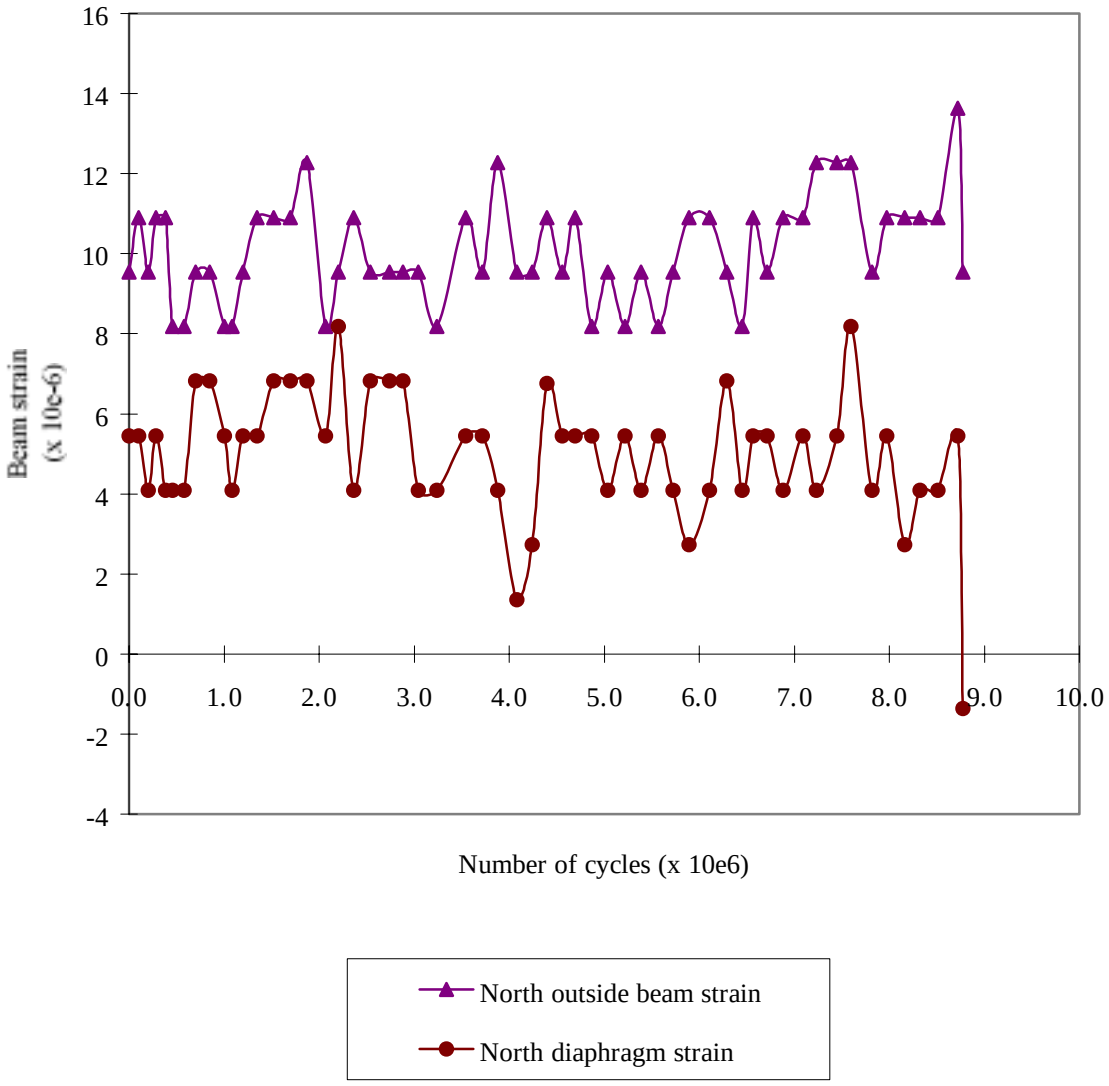

Figure D.14 North outside beam and diaphragm measurements for SC-NR(30)

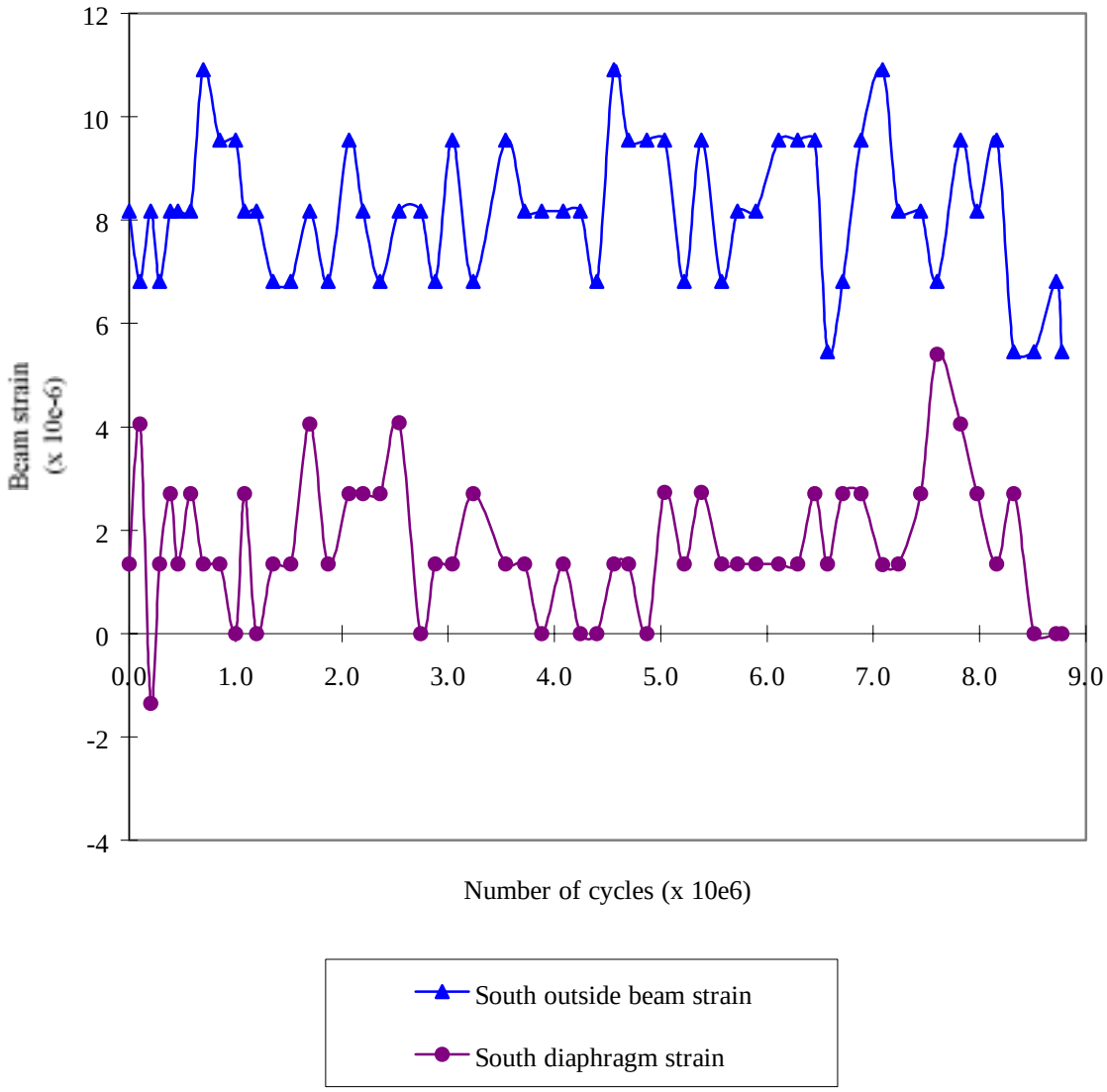

Figure D.15 South outside beam and diaphragm measurements for SC-NR(30)

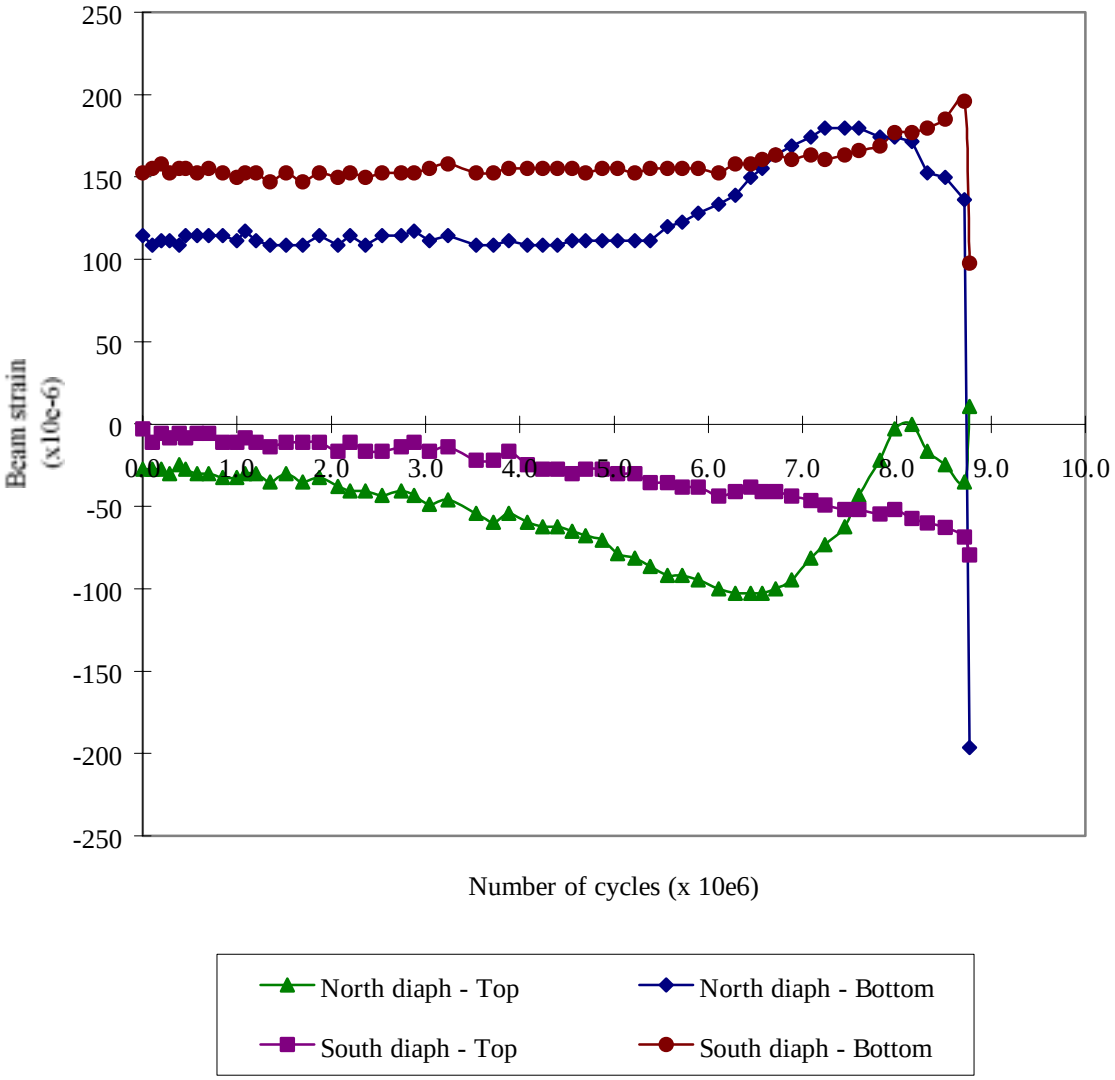

Figure D.16 Transverse beam strains in web gap regions at north and south diaphragms for SC-NR(30)

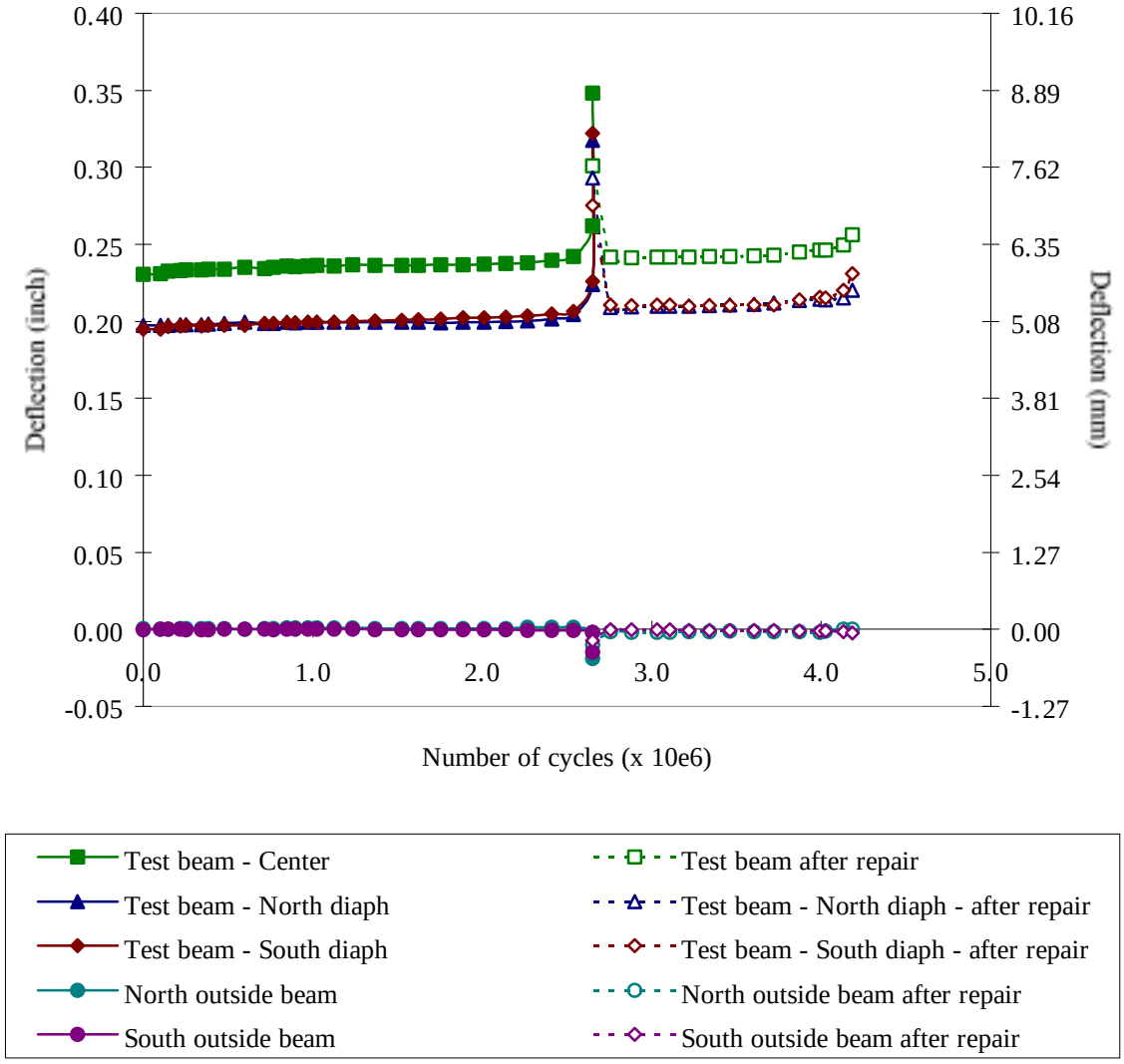

Figure D.17 Deflection measurements for SC-NR(45)

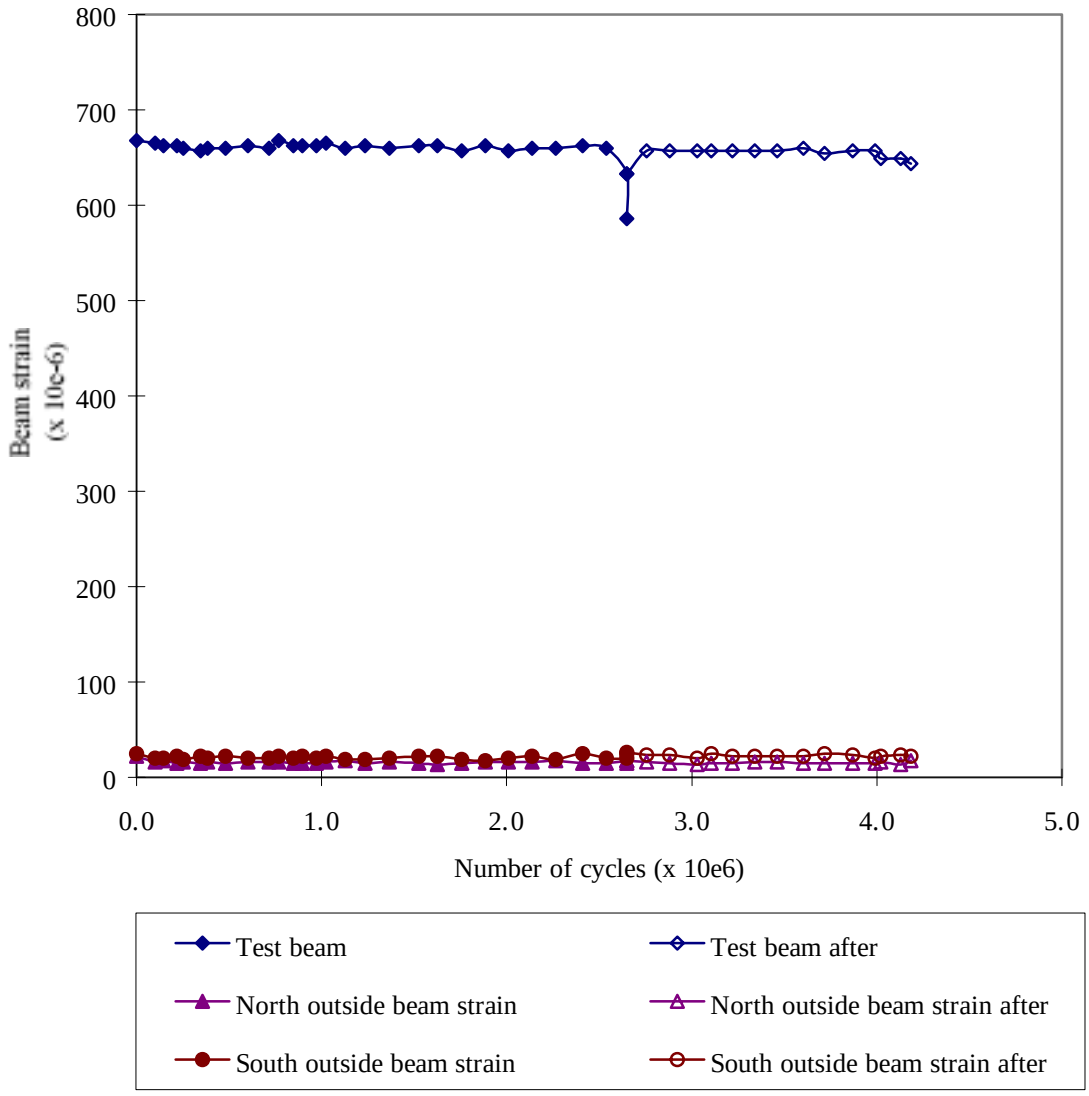

Figure D.18 Longitudinal beam strain measurements for SC-NR(45)

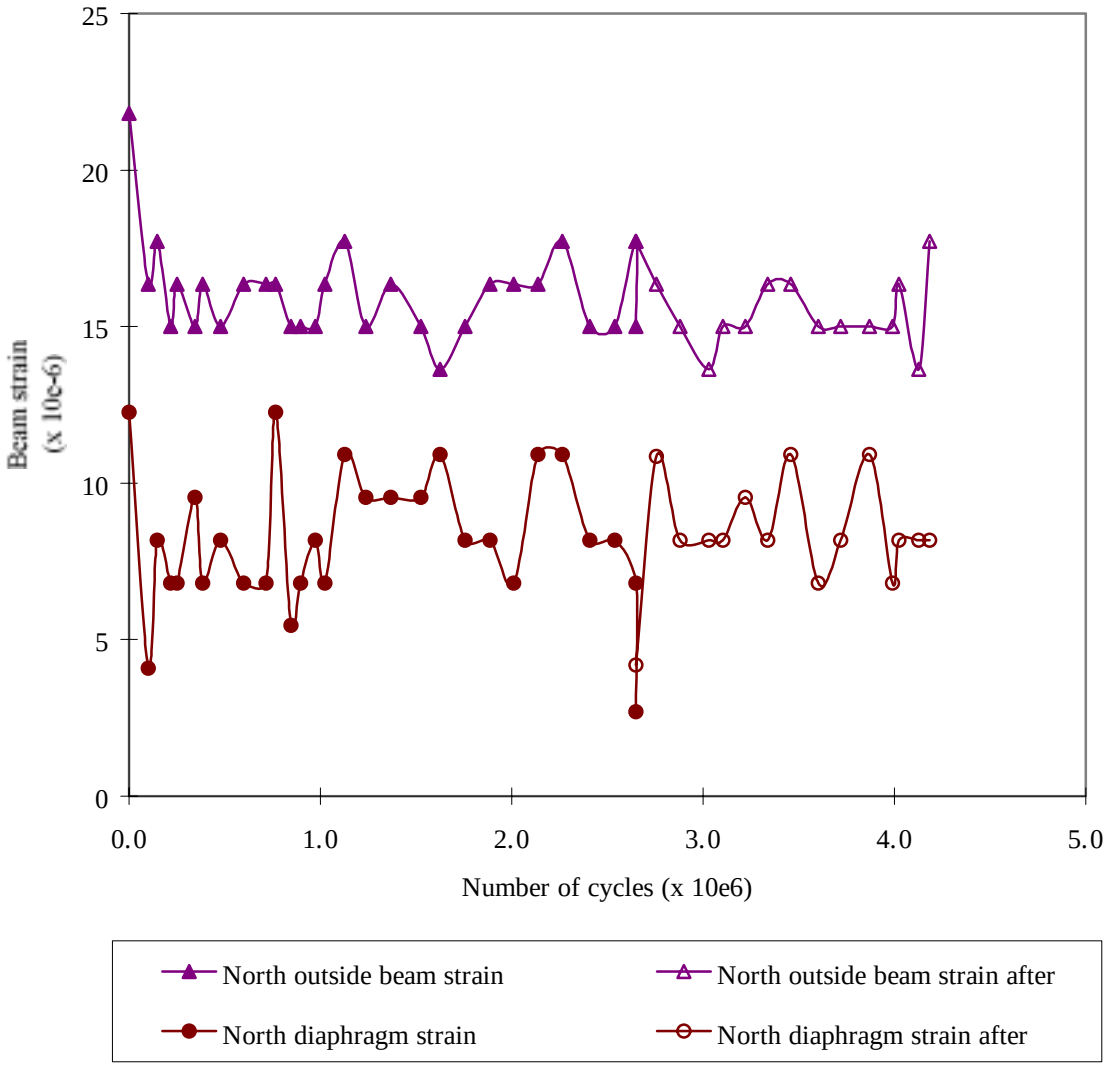

Figure D.19 North outside beam and diaphragm measurements for SC-NR(45)

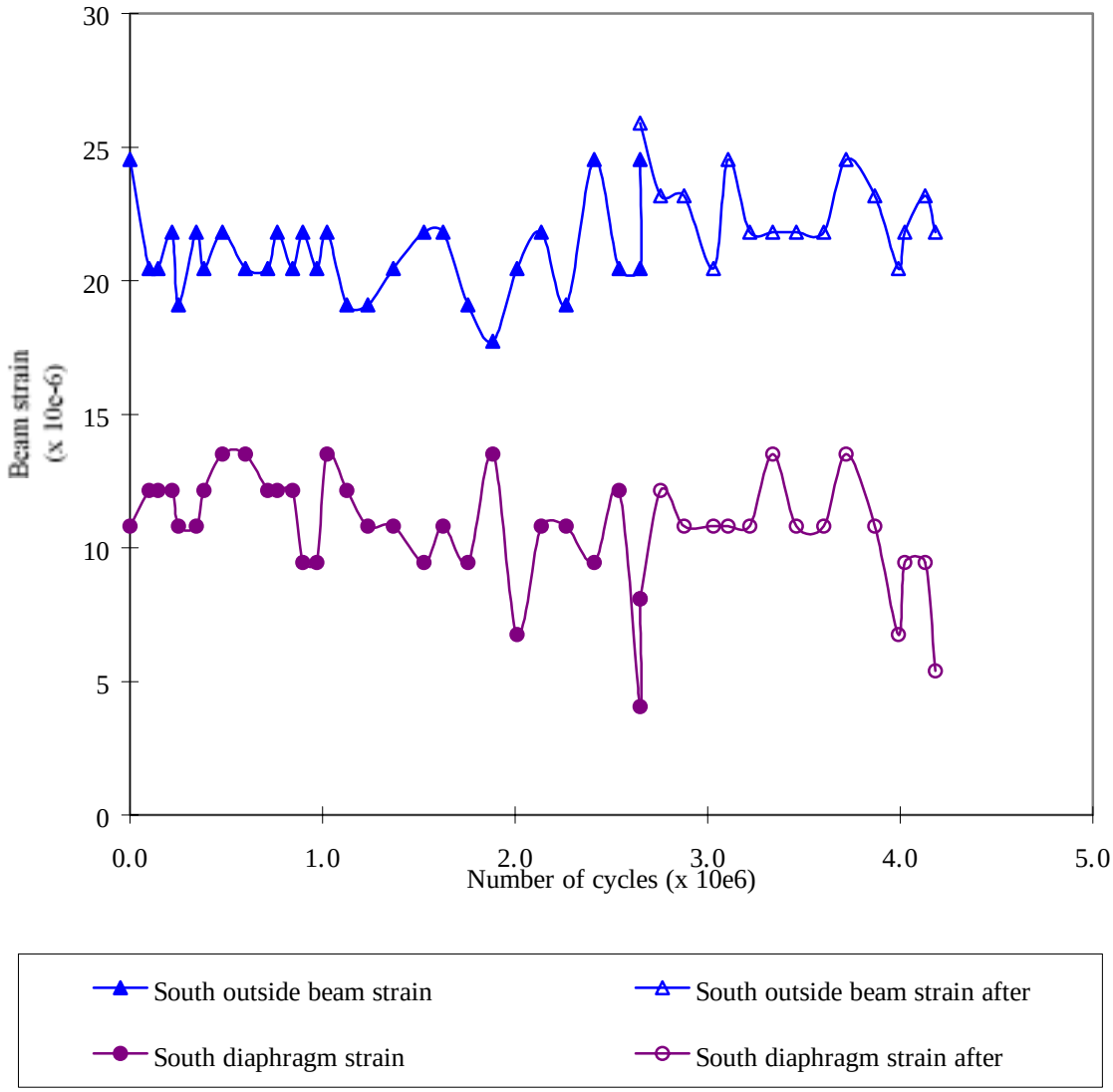

D.20 South outside beam and diaphragm measurements for SC-NR(45)

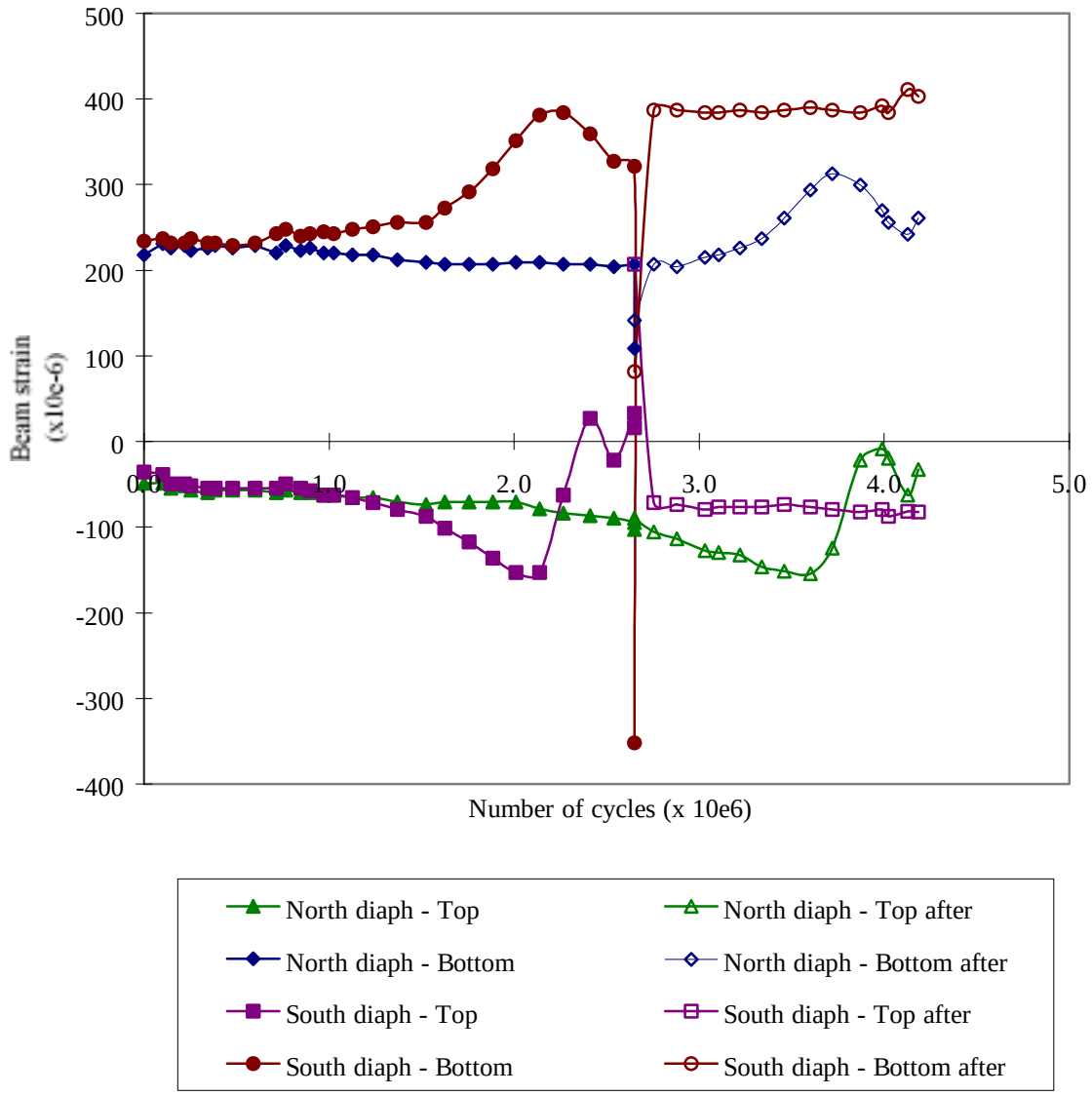

Figure D.21 Transverse beam strains in web gap regions at north and south diaphragms for SC-NR(45)

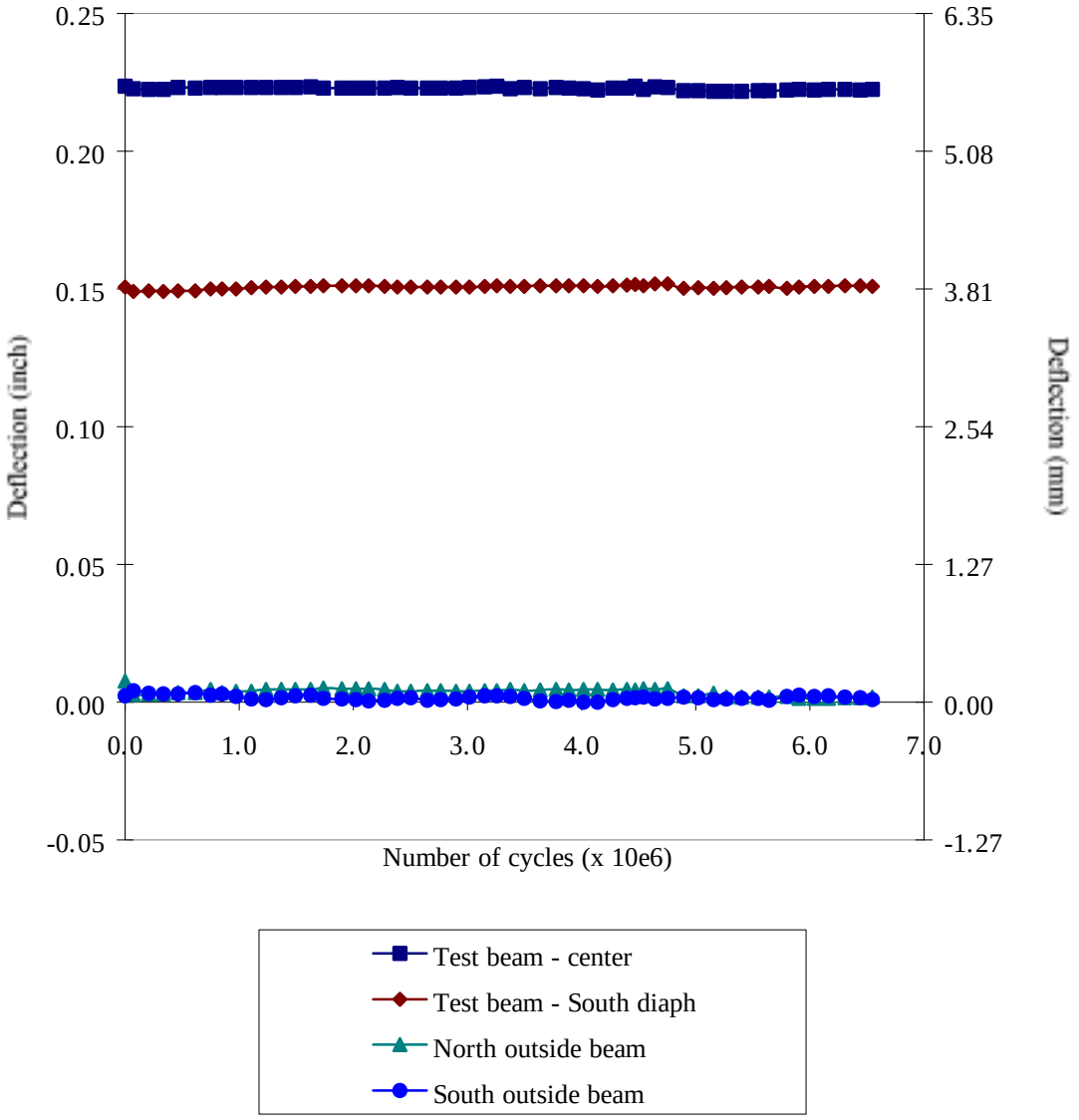

Figure D.22 Deflection measurements for SL-NR(45)

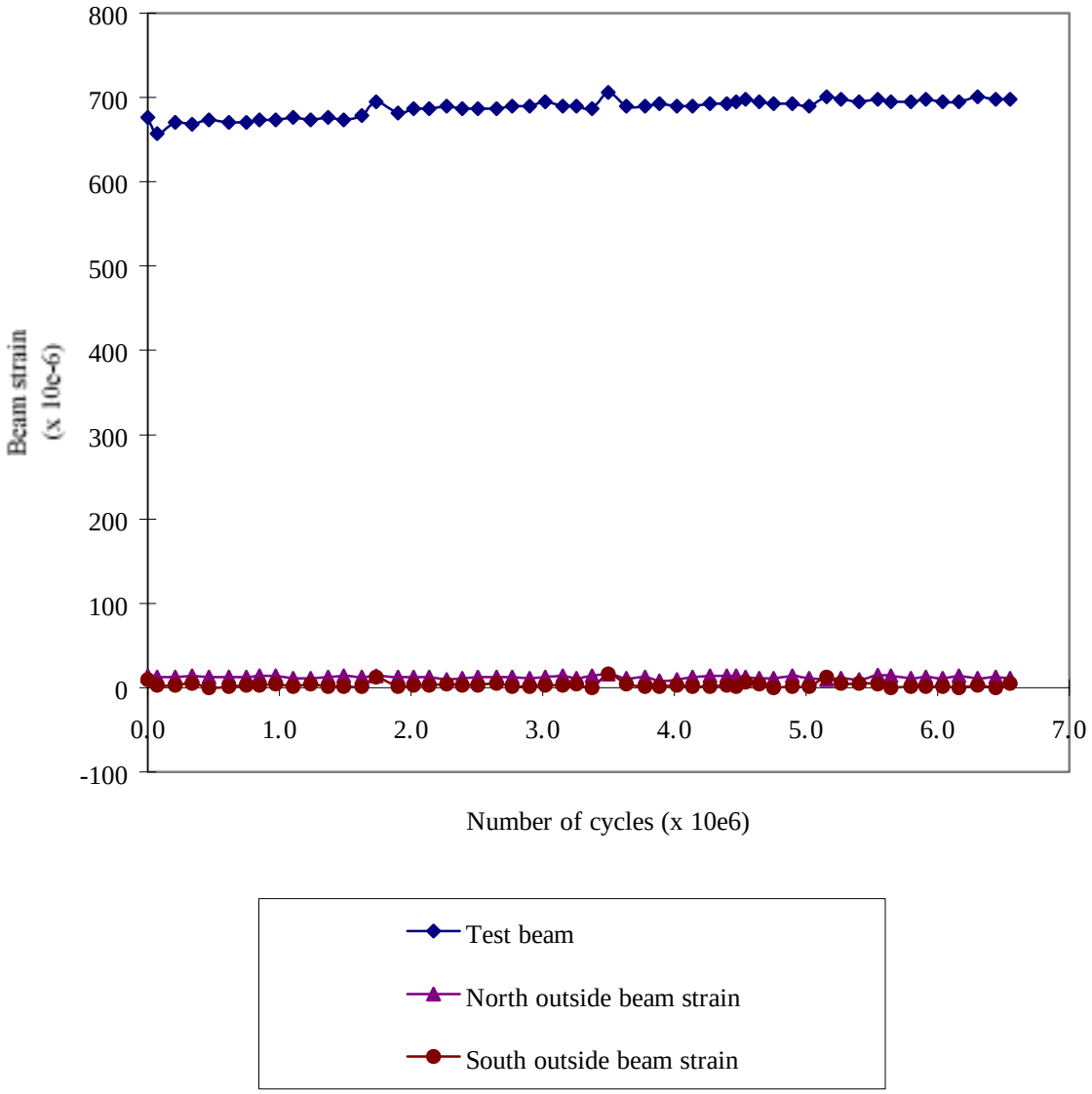

Figure D.23 Longitudinal beam strain measurements for SL-NR(45)

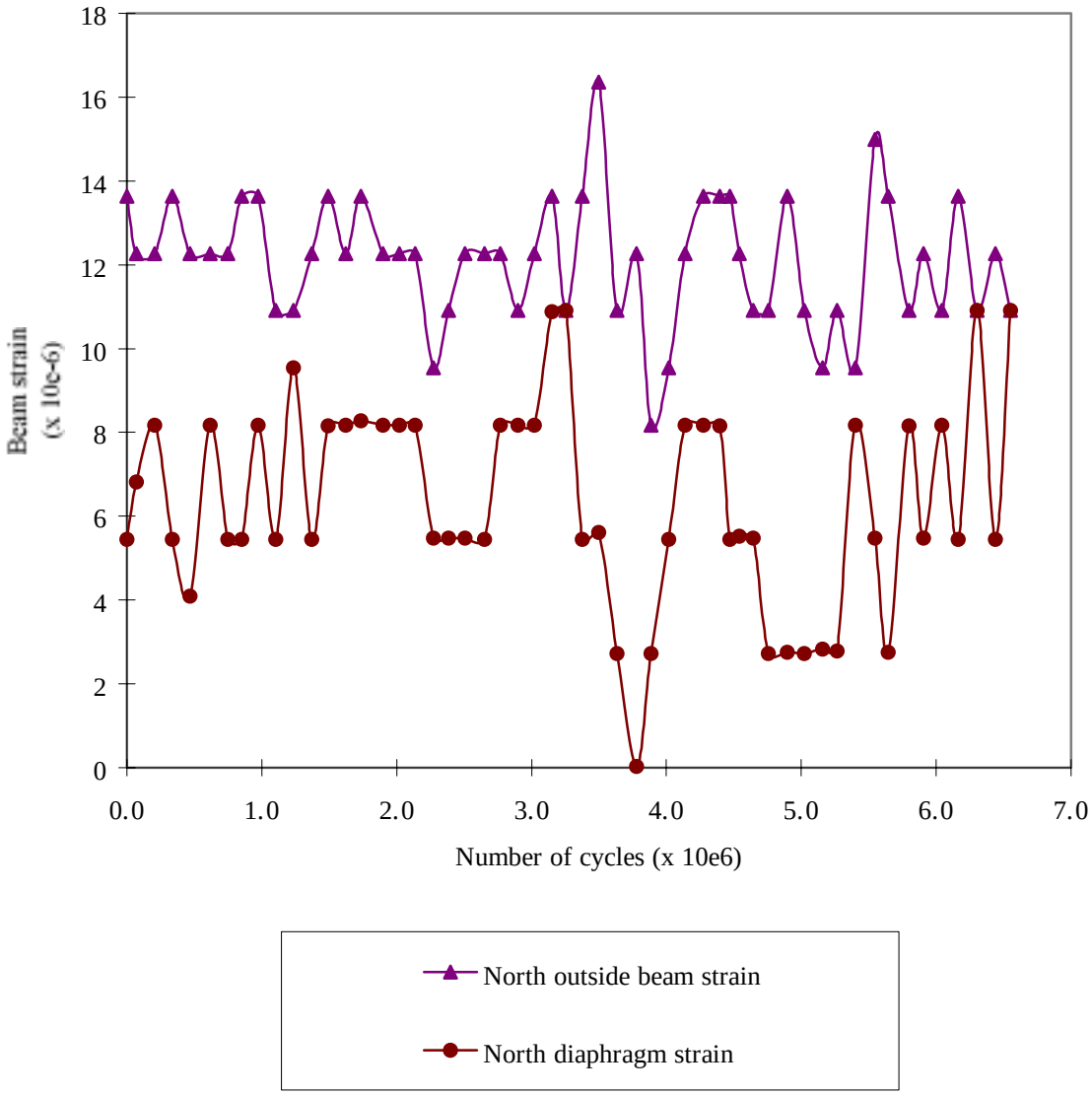

Figure D.24 North outside beam and diaphragm measurements for SL-NR(45)

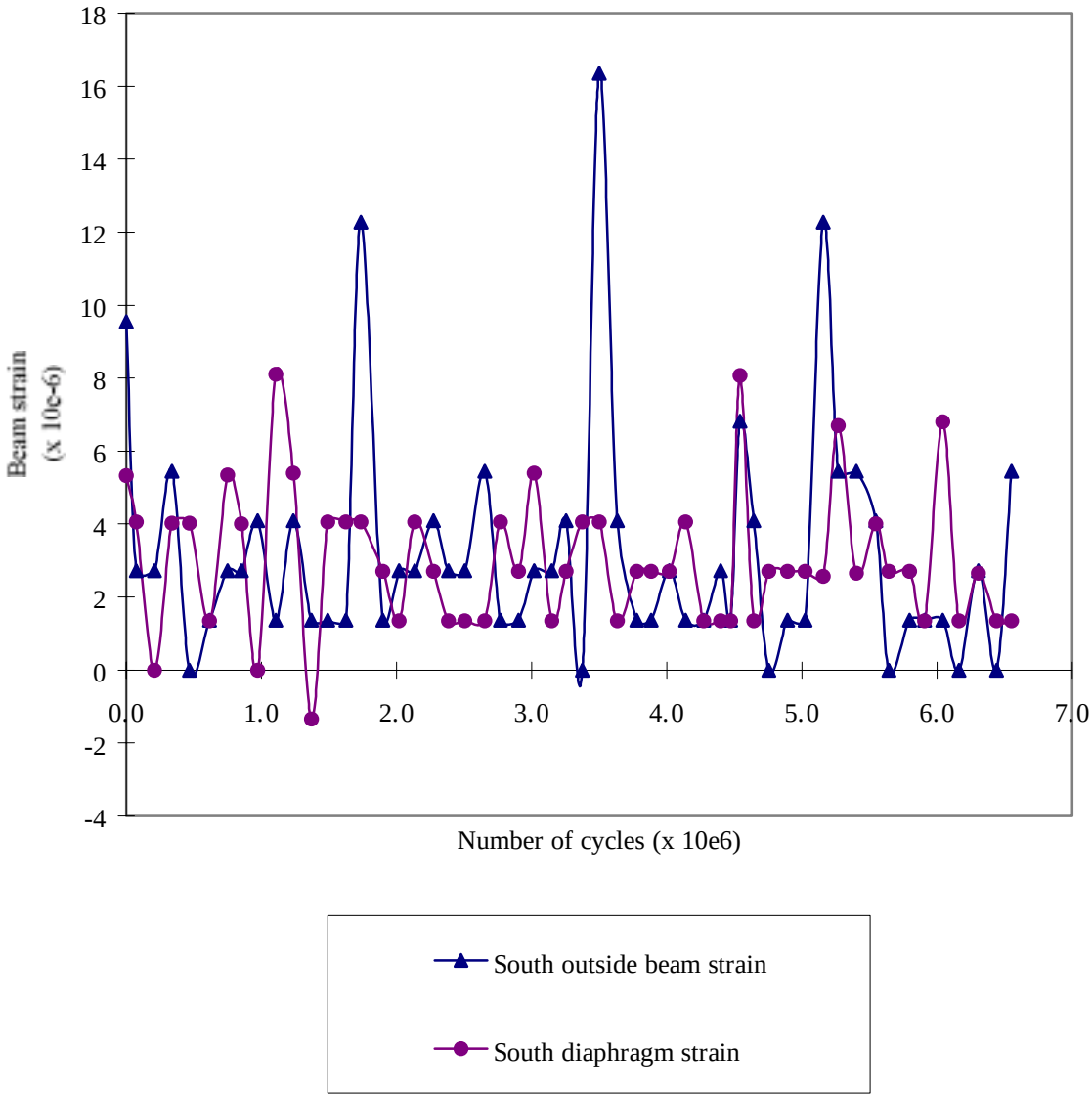

Figure D.25 South outside beam and diaphragm measurements for SL-NR(45)

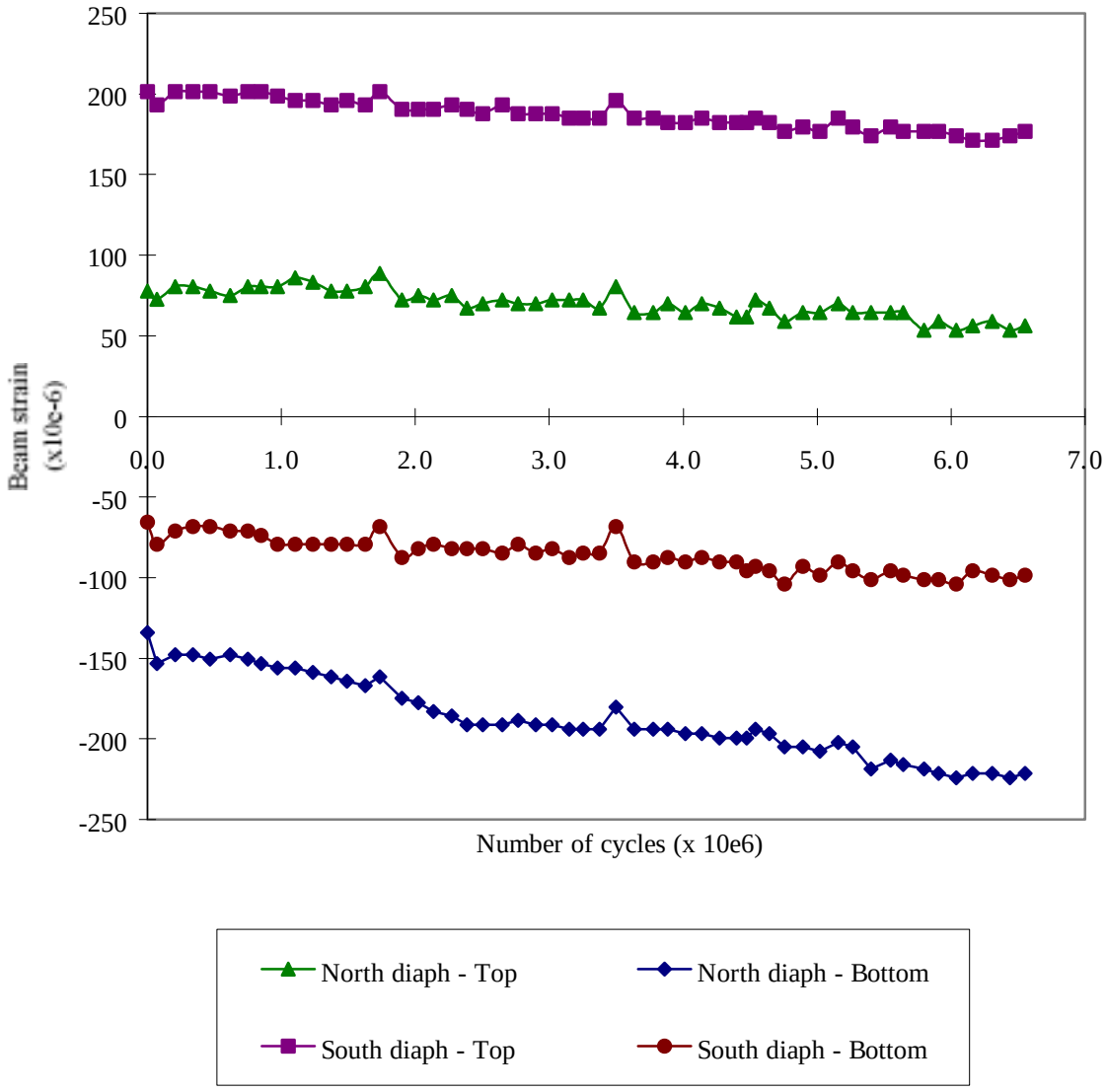

Figure D.26 Transverse beam strains in web gap regions at north and south diaphragms for SL-NR(45)

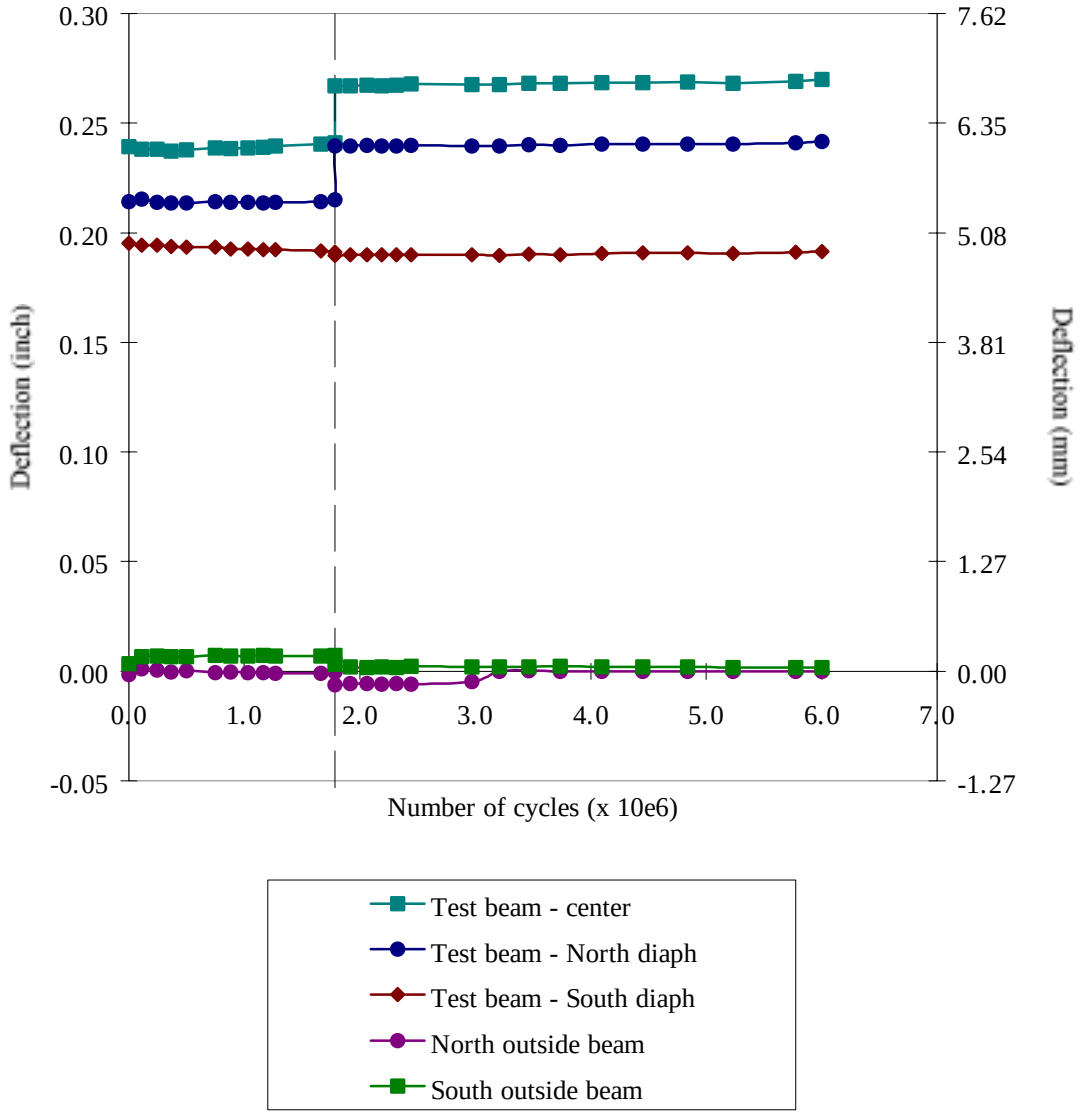

Figure D.27 Deflection measurements for SC-FH(45)

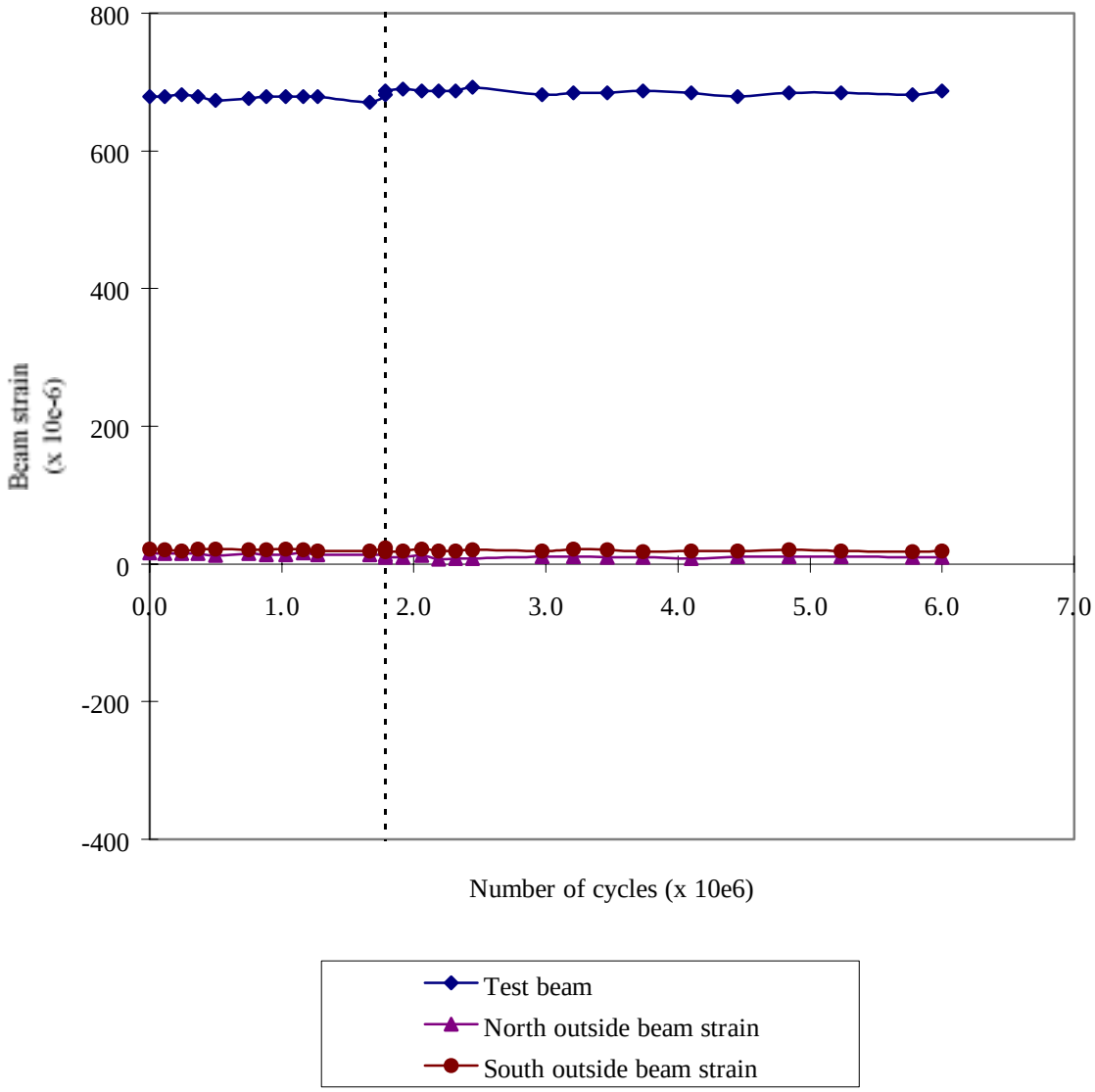

Figure D.28 Longitudinal beam strain measurements for SC-FH(45)

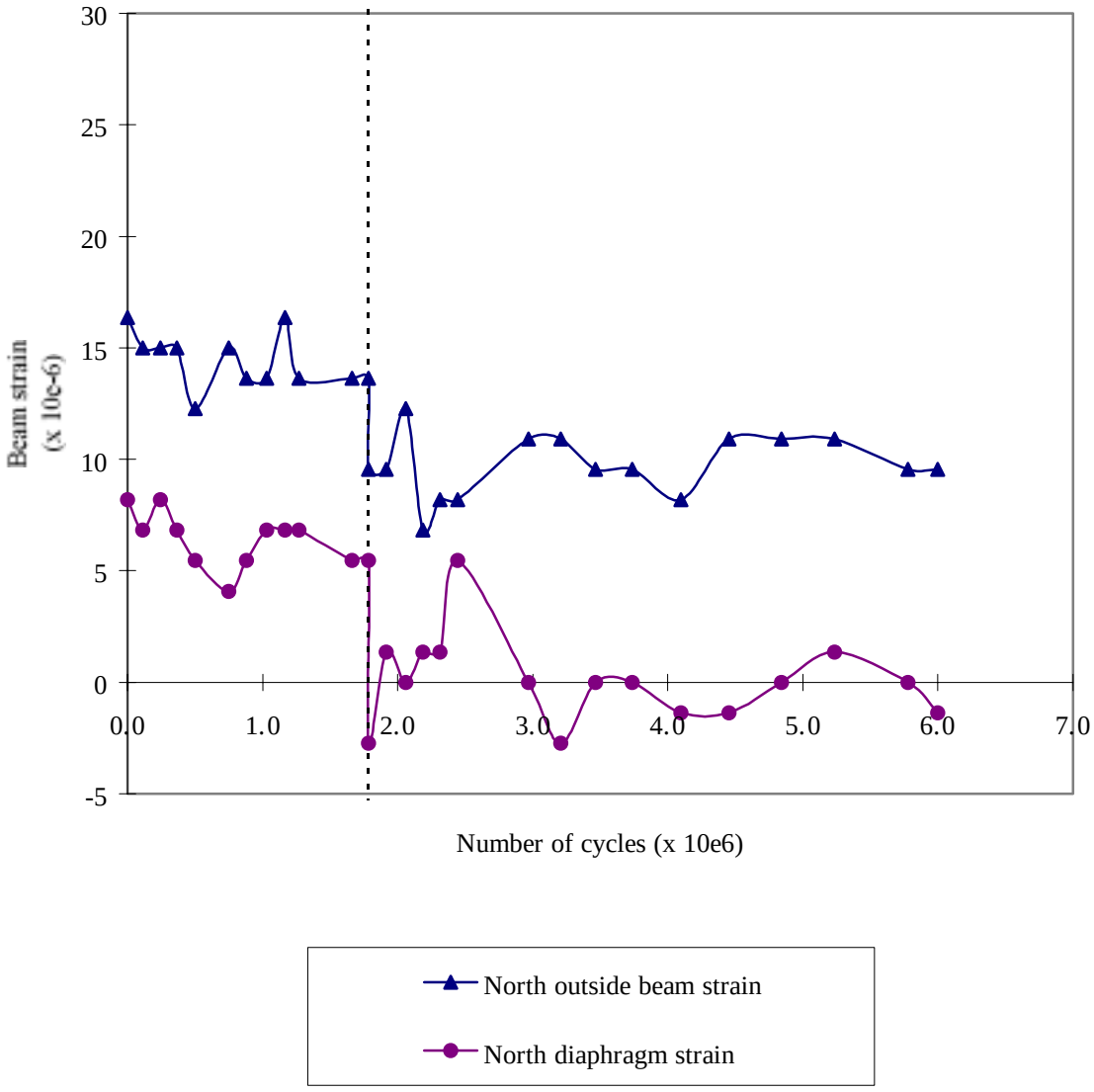

Figure D.29 North outside beam and diaphragm measurements for SC-FH(45)

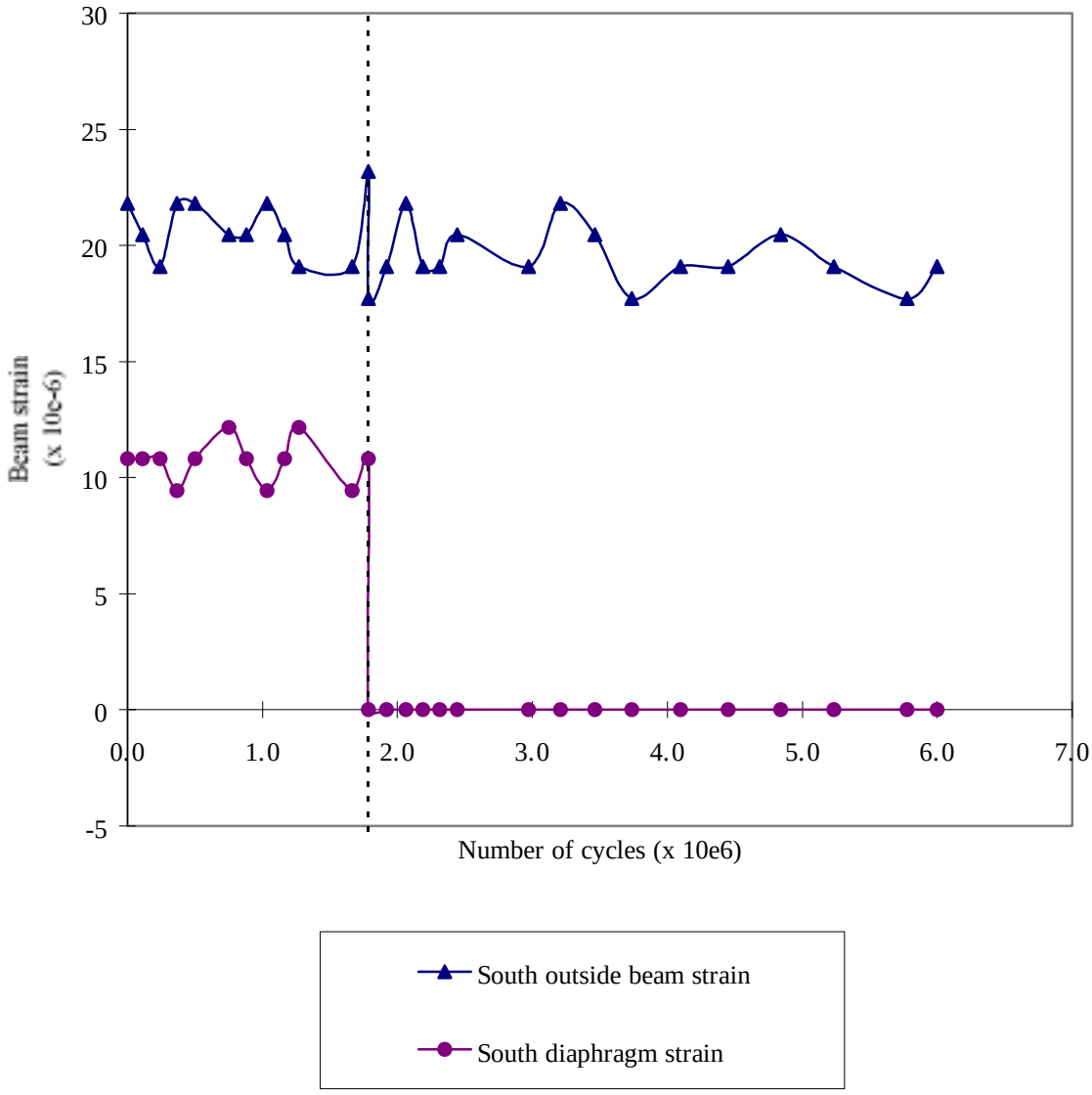

Figure D.30 South outside beam and diaphragm measurements for SC-FH(45)

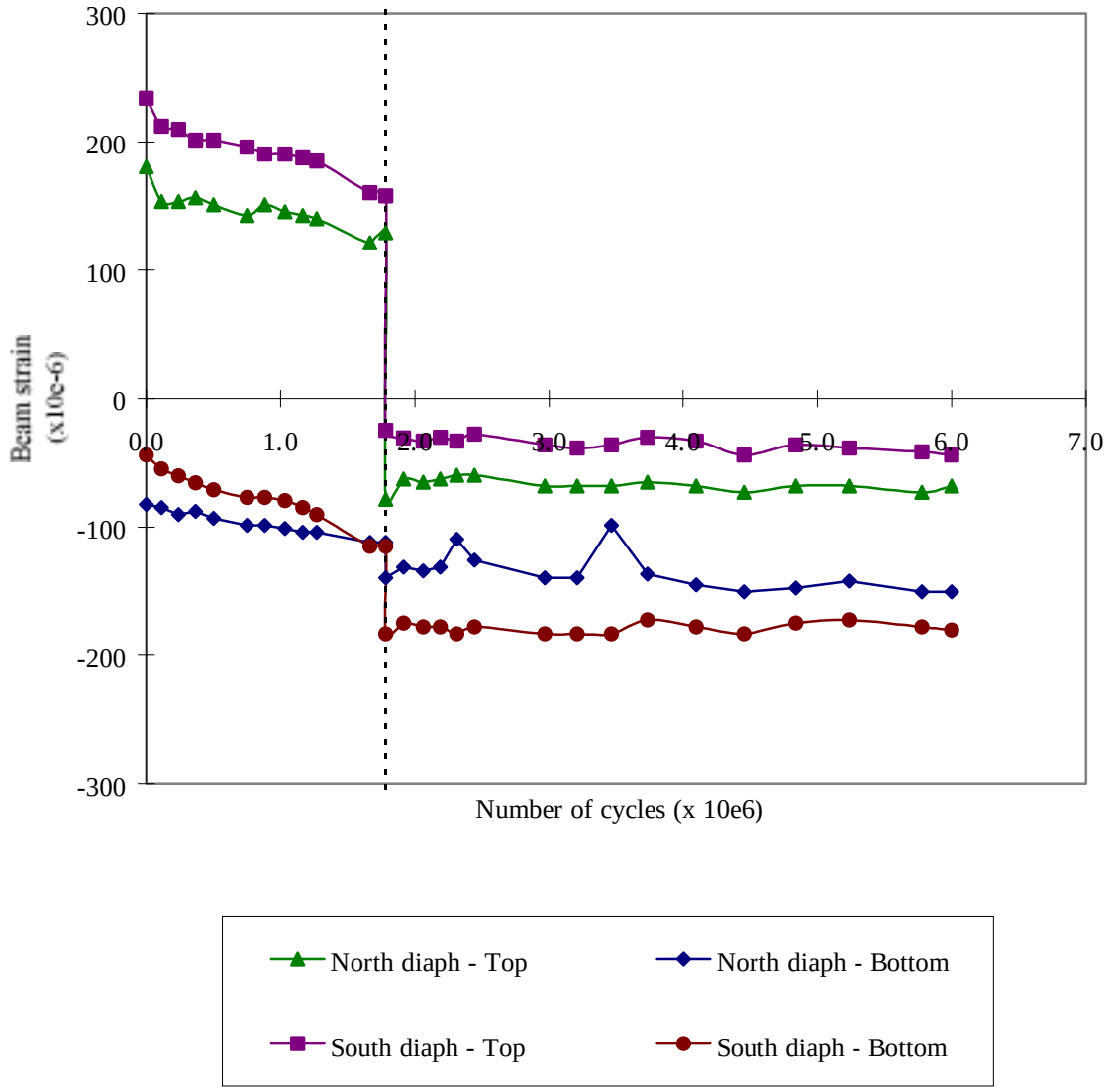

Figure D.31 Transverse beam strains in web gap regions at north and south diaphragms for SC-FH(45)

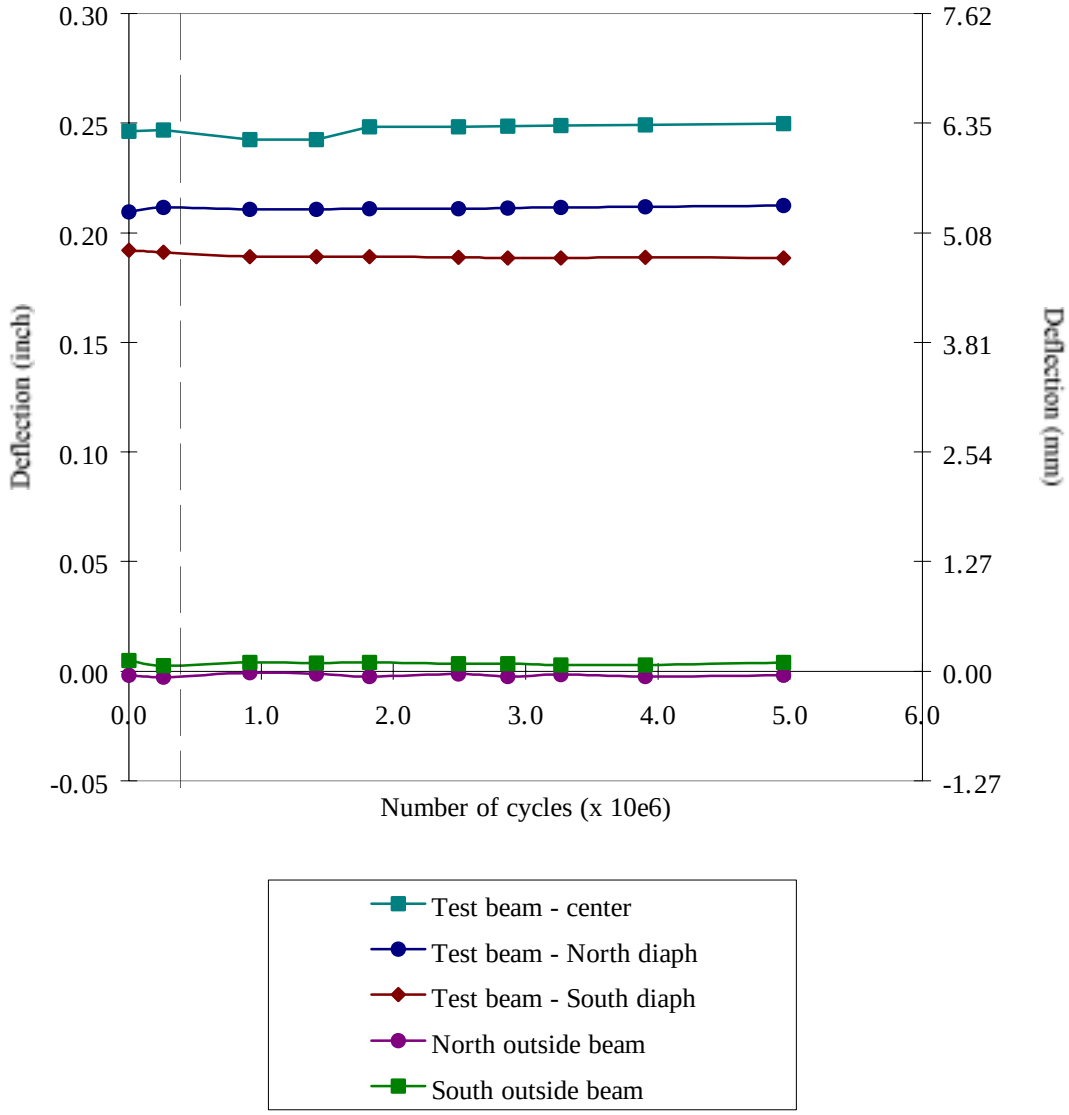

Figure D.32 Deflection measurements for SC-LP(45)

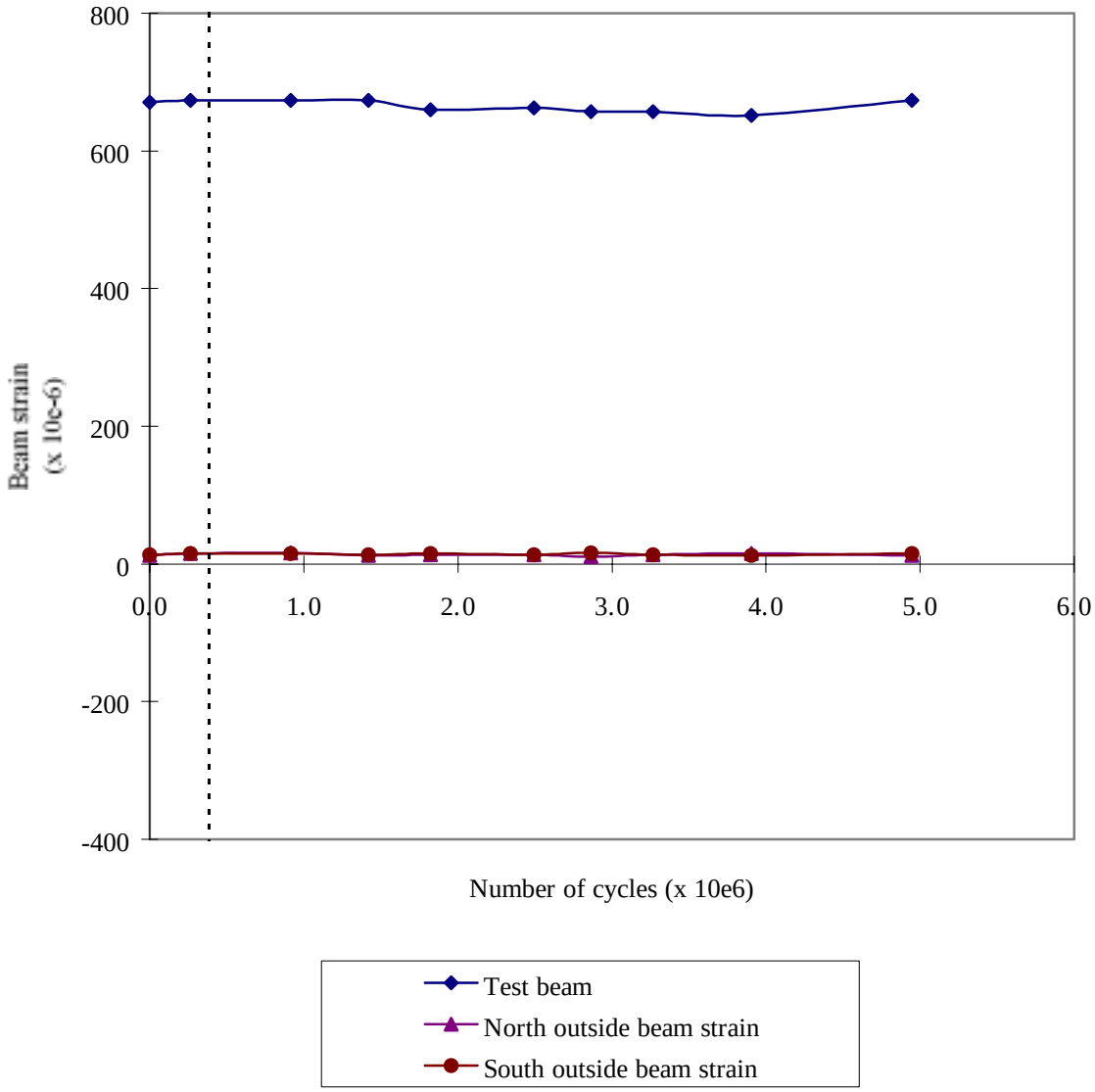

Figure D.33 Longitudinal beam strain measurements for SC-LP(45)

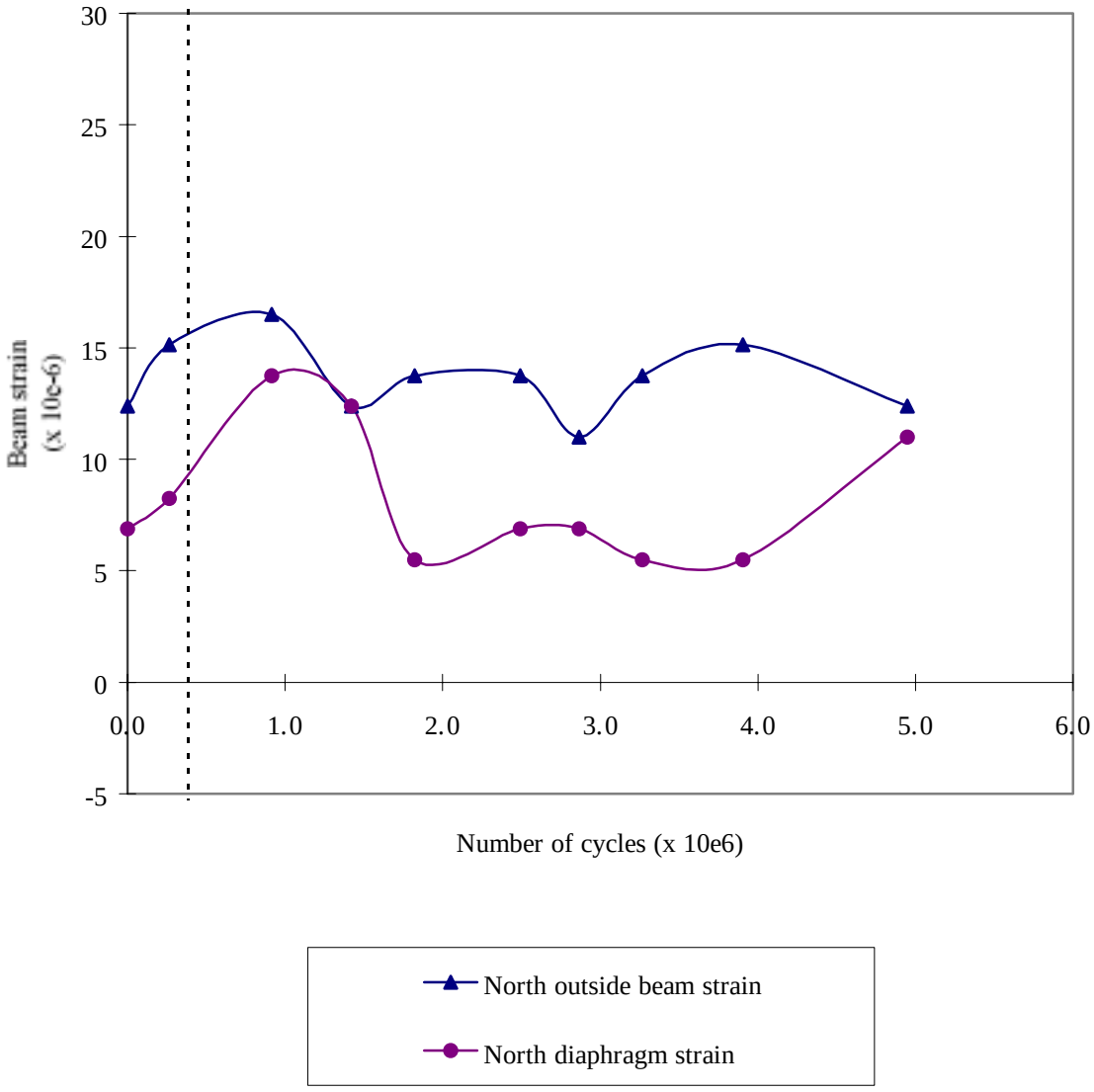

Figure D.34 North outside beam and diaphragm measurements for SC-LP(45)

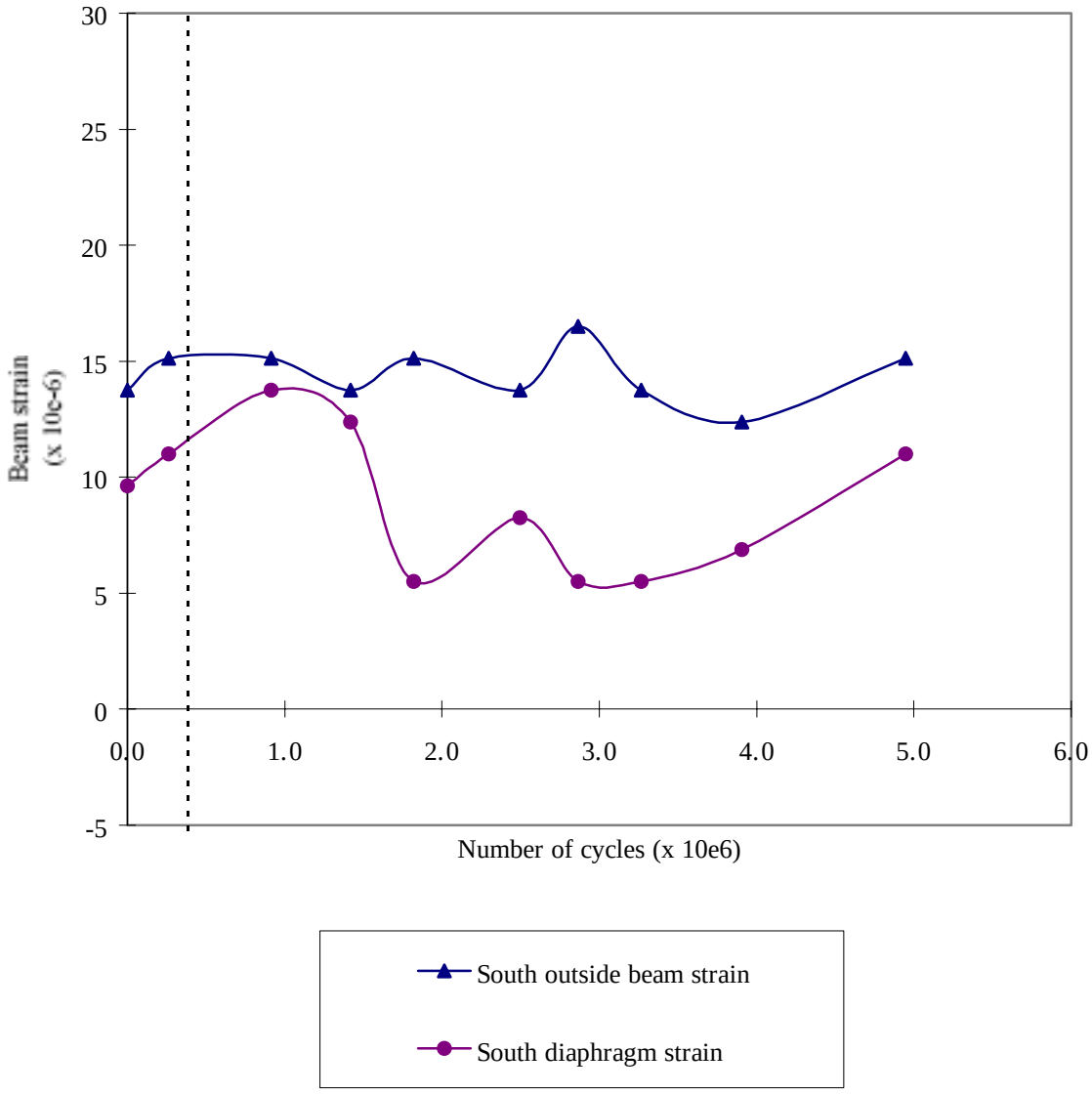

Figure D.35 South outside beam and diaphragm measurements for SC-LP(45)

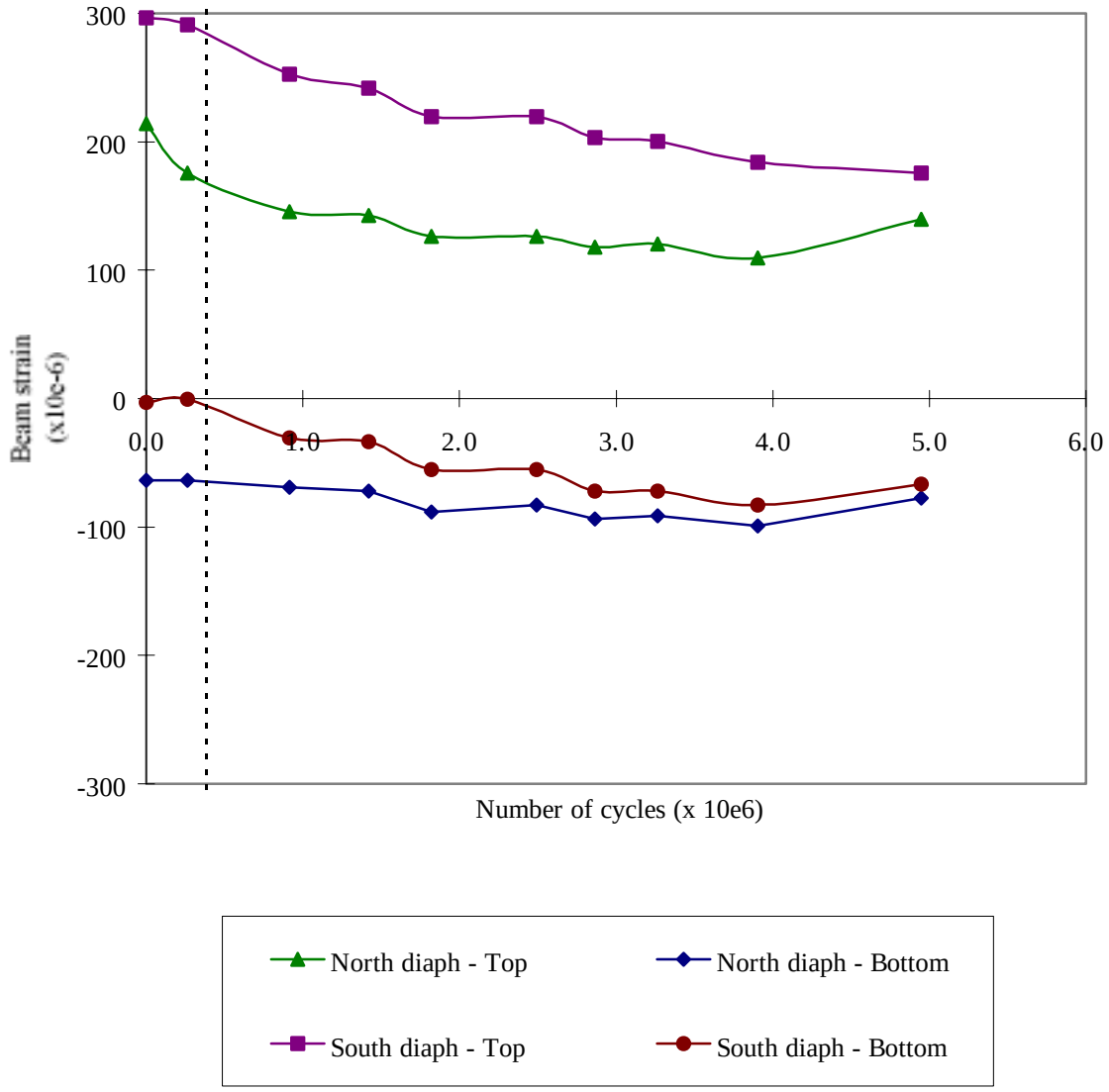

Figure D.36 Transverse beam strains in web gap regions at north and south diaphragms for SC-LP(45)

APPENDIX E

CRACK PROPAGATION PROGRAM

APPENDIX E

CRACK PROPAGATION PROGRAM

E.1 Introduction

This section contains the crack propagation program which was developed to calculate the propagation life for cracked steel beams with the welded diaphragm connection. The program was written in FORTRAN. Also contained in this section are examples for the input files for beams subjected to constant stress as well as a load histogram. The corresponding output is also included.

E.2 Propagation Program

```
c
c             Crack Propagation Program
c for Intermittently Welded Diaphragm-to-Beam Connection
c           with Elliptical Surface Crack
c
c                  by
c               Amy S. Grider

          program crack
          real n
          dimension weight(100), stress(100), freq(100), rlife(100)
          open (5, file='data.inp')
          open (4, file='input.out')
          open (7, file='life.out')


c Define variables

c bd = beam depth (in)
c bbf = beam flange width (in)
c btf = beam flange thickness (in)
c btw = beam web thickness (in)

c dd = diaphragm depth (in)

c stagger = flag for stagger condition
c           = NS for no stagger diaphragms
c           = S for stagger diaphragms
c amount = flag for diaphragm stagger
```

```
c          = 0 for no stagger diaphragms
c          = 1 for stagger diaphragms
c scase = flag for stress condition
c       = cs for constant stress
c       = hist for histogram

c cp = applied axle load (kip)
c cst = stress range at extreme fiber of beam at diaphragm location (ksi)
c st = stress level at crack tip (ksi)
c fest = stress at crack tip from finite element results (ksi)
c bst = bending stress at crack tip (ksi)

c stwt = stress corresponding to truck axle weight input (ksi)
c wt = truck axle weight (kip)
c adtt = average daily truck traffic
c weight(100) = array of truck axle weight (kip)
c stress(100) = array of stress from truck axle weight (ksi)
c freq(100) = array of frequency for truck axle weight

c ai = initial web crack depth (in)
c a = web crack depth (in)
c da = change in web crack depth (in)
c twoci = total initial crack length (in)
c ccrit = crack length to repair (in)
c cup= crack length above diaphragm flange (in)
c cdown = crack length below diaphragm flange (in)
c dc = change in web crack length (in)
c c = half web crack length (in)
c twoc = total web crack length (in)
c cfl = half flange crack width (in)
c dcfl = change in flange crack width (in)
c twocfl = total flange crack width (in)
c afl = flange crack depth (in)
c dafl = change in flange crack depth (in)

c fg = geometric correction factor
c dk = delta K at crack tip
c gro = growth rate for web crack
c grofl = growth rate for flange crack

c ic = flag for web fracture criteria
c id = flag for flange fracture criteria
c ip = flag for point on elliptical crack
c inc = step increment

c n = number of cycles
c ni = cycle interval for geometric correction factor
c dn = change in number of cycles for crack growth
c hlife = histogram life in number of cycles
c ylife = histogram life in number of years

c pc = material constant used in Paris equation
c rm = material constant used in Paris equation
c mc = flag for material constants used in Paris equation
c rkc = material fracture toughness (ksi*in**0.5)
```

```
c Format statements
800     format (a4)
850      format (f5.3)
2000    format (/,2x, 'Crack Propagation Program')
2100    format (/,5x, 'Stagger condition = ', a4)
2150    format (/,5x, 'Wheel load = ', f6.3, 1x, 'kip')
2200    format (/,5x, 'Beam depth = ', f6.3, 1x, 'in')
2250     format (/,5x, 'Beam flange width = ',f6.3, 1x, 'in')
2300    format (/,5x, 'Beam flange thickness = ', f5.3, 1x, 'in')
2400    format (/,5x, 'Beam web thickness = ', f5.3, 1x, 'in')
2500    format (/,5x, 'Diaphragm depth = ', f6.3, 1x, 'in')
2600    format (/,5x, 'Initial crack depth = ', f5.3, 1x, 'in')
2700    format (/,5x, 'Initial crack length = ', f5.3, 1x, 'in')
2800    format (/,5x, 'Crack length for repair = ', f5.2, 1x, 'in')
2900    format (/,5x, 'Stress range at extreme fiber of beam = ',
     *  f6.3, 1x, 'ksi')
2950     format (/,5x, 'Fracture toughness = ',f9.5,1x,'ksi*in**0.5')
3000     format (/,5x, 'ADTT = ',f8.0)
3100    format (/,4x,'Inc.',5x, 'No. of cycles', 5x, 'Crack length',5x,
     *  'Crack depth')
3140     format (2x,'Crack growth in flange')
3200    format (1x,i7, 5x f15.0, 7x, f5.3, 10x, f5.3)
3900    format (/,5x, 'Crack length equals crack length for repair')
4000    format (/,2x,'Ratio of crack depth to crack length exceeded')
4100    format (/,2x,'Crack depth exceeds web thickness')
4200    format (/,2x, 'Ratio of crack length to beam depth exceeded')
4250     format (/,2x, 'Stress intensity factor is larger than the
     *      fracture toughness',2x,'k=',f9.5)
4300     format (/,2x,'Crack length equals crack length for
     *      repair', 2x,'c=',f5.3)
4390     format (/,2x,'Crack is in tension flange')
4400     format (/,2x,'Tension flange fractured',2x,'c=',f5.3)
4450     format (2x,'Number of cycles = ',f15.0,/)
5000    format (/,2x,'Ratio of crack depth to crack length exceeded
     *      for flange growth')
5100    format (/,2x,'Crack depth exceeds flange thickness')
5200    format (/,2x, 'Ratio of crack length to beam flange width
     *       exceeded')
5300     format (/,2x,'Crack length equals crack length for
     *      repair', 2x,'c=',f5.3)
6100     format (/,1x,'Axle load',4x,'Stress',9x,'No. of cycles')
6150     format (4x,'(kip)',7x,'(ksi)')
6200     format (3x,f5.1,7x,f6.3,2x,f20.0)
6300     format (2x,'Number of years = ',f15.0)

c Read data
          read (5,800) scase
          read (5,*) amount
          read (5,*) bd, bbf, btf, btw
          read (5,*) dd
          read (5,*) ai, twoci, ccrit, rkc
          if (scase.eq.'cs') then
                    read (5,*) cst, wl, ni
                    read (5,*) mc
```

```
                if (mc .eq. 0) then
                        read (5,*) pc,rm
                endif
        else
                read (5,*) stwt, wt, adtt, ni
                read (5,*) mc,ml
                if (mc .eq. 0) then
                        read (5,*) pc, rm
                endif
                if (ml .eq. 0) then
                        read (5,*) rmean, stdev
                else
                        rmean=12.08
                        stdev=5.04
                endif
        endif
        if (amount .eq. 0.0) then
                stagger='NS'
        else
                stagger='S'
        endif


c Write data
        write (4, 2000)
        write (7, 2000)
        write (4, 2100) stagger
        if (scase .eq. 'cs') then
                write (4, 2150) wl
        endif
        write (4, 2200) bd
        write (4, 2250) bbf
        write (4, 2300) btf
        write (4, 2400) btw
        write (4, 2500) dd
        write (4, 2600) ai
        write (4, 2700) twoci
        write (4, 2800) ccrit
        if (scase .eq. 'cs') then
                write (4, 2900) cst
        else
                write (4,3000) adtt
        endif
        write (4, 2950) rkc

        if (scase .eq. 'cs') then
                write (7, 3100)
        else
                write (7,6100)
                write (7,6150)
        endif

c Initial conditions

        inc=0.
```

```
            n=0.
            hlife=0
            a=ai
            cup=twoci/2
            cdown=twoci/2
            twoc=cup+cdown
            ic=0
            id=0
            val=0
            afl=btf
            cfl=2.0*afl
            na=0
            ina=0
            if (scase .ne. 'hist') then
                  write (7,3200) inc,n,twoc,a
            endif
            if (mc .eq. 1) then
                  pc=3.6e-10
                  rm=3.
            else
                  if (mc .eq. 2) then
                        pc=1.0e-10
                        rm=3.3
                  else
                        if (mc .eq. 3) then
                              pc=2.507e-10
                              rm=3.
                        endif
                  endif
            endif

c Calculate stress array for truck histogram
            if (scase .eq. 'hist') then
                  call hstress (weight,stress,stwt,wt,freq,rmean,stdev)
            endif

c Initialize variables for truck histogram
            step=6
50          if (scase .eq. 'hist') then
                  sr=stress(step)
                  p=weight(step)/2
                  inc=0
                  n=0
                  a=ai
                  cup=twoci/2
                  cdown=twoci/2
                  twoc=cup+cdown
                  ic=0
                  id=0
                  afl=btf
                  cfl=2.0*afl
            endif

            if (scase .eq. 'cs') then
                  sr=cst
```

```
                p=wl
        endif

c Check if crack is through web thickness at start

        if (ai .ge. btw) then
                ic=2
                goto 200
        else
                goto 100
        endif

c Cycle by cycle calculations for elliptical web crack
c Point a of elliptical crack (through thickness)
100     continue
        c=twoc/2.
        ip=2
        call festress(amount,c,p,st)
        call stfaca(a,c,btw,bd,ip,st,dk)
        call growth(pc,rm,gro,dk)
        da=a/500.
        dn = da / gro

c Point c of elliptical crack (lengthwise)
        ip=1
        call stfaca(a,c,btw,bd,ip,st,dk)
        call growth(pc,rm,gro,dk)
        dc=dn*gro

c Update a,c,n
        a = a + da
        cup = cup + dc
        cdown = cdown + dc
        twoc = cup + cdown
        n = n + dn

        inc = inc + 1.
        if (scase .ne. 'hist') then
                if (inc/250*250 .eq. inc) then
                        write (7,3200) inc,n,twoc,a
                endif
        endif

c Check fracture criteria for elliptical crack
        call check(a,twoc,cdown,btw,bd,btf,dd,ccrit,dk,rkc,ic)

110     continue
        if (ic .eq. 0) goto 100
        if (ic. eq. 1) then
                if (scase .ne. 'hist') then
                write (7,3200) inc,n,twoc,a
                write (7,4000)
                write (7,4450) n
                endif
        endif
```

```
      if (ic .eq. 2) then
            if (scase .ne. 'hist') then
            write (7,3200) inc,n,twoc,a
            write (7,4100)
            write (7,4450) n
            endif
      endif
      if (ic .eq. 3) then
            if (scase .ne. 'hist') then
            write (7,3200) inc,n,twoc,a
            write (7,4200)
            write (7,4450) n
            endif
      endif
      if (ic .eq. 4) then
            if (scase .ne. 'hist') then
            write (7,3200) inc,n,twoc,a
            write (7,4300) twoc
            write (7,4450) n
            endif
      endif
      if (ic .eq. 5) then
            if (scase .ne. 'hist') then
            write (7,3200) inc,n,twoc,a
            write (7,4390)
            write (7,3140)
            write (7,3100)
            endif
            goto 400
      endif
      if (ic .eq. 6) then
            if (scase .ne. 'hist') then
            write (7,3200) inc,n,twoc,a
            write (7,4250) dk
            write (7,4450) n
            endif
      endif

      if (ic .eq. 2) then
            goto 200
      else
            goto 900
      endif

c Cycle by cycle calculations for crack through web thickness
200   continue
      ip=1
      c=twoc/2.

      call bstress(sr,c,bd,dd,st)
      call geo(amount,twoc,fg,ni,p,dd,bd,sr)
      call stfac1(twoc,bd,st,fg,dk)
      call growth(pc,rm,gro,dk)
      dc = c/500.
      dn = dc/gro
```

```
          if (cup .lt. bd/2-(bd/2-dd/2)) then
            cup = cup + dc
          else
            cup = bd/2-(bd/2-dd/2)
          endif

          cdown = cdown+dc
          twoc=cup+cdown
          n = n+dn
          inc = inc + 1.
          if (scase .ne. 'hist') then
                  if (inc/250*250 .eq. inc) then
                          write (7,3200) inc,n,twoc,a
                  endif
          endif

          call check1(twoc,cdown,bd,btf,dd,ccrit,dk,rkc,ic)
          if (ic .ne. 2) then
                  goto 110
          else
                  goto 200
          endif

c Cycle by cycle calculations for crack growing across flange
c thickness

400       continue
          id=2
c Crack in flange (through thickness)
          call astress(sr,bd,btf,astr)
          call flange(cfl,bbf,astr,pc,rm,grofl)
          dcfl=cfl/500
          dn=dcfl/grofl

c Update crack length
          cfl=cfl+dcfl
          twocfl=2*cfl
          n=n+dn

          inc=inc+1.
          if (scase .ne. 'hist') then
                  if (inc/250*250 .eq. inc) then
                          write (7,3200) inc,n,twocfl,afl
                  endif
          endif

          call flcheck2(twoc,cfl,bbf,bd,dd,ccrit,dkfl,rkc,id)
410       continue
          if (id .eq. 4) then
                  if (scase .ne. 'hist') then
                  write (7,3200) inc,n,twocfl,afl
                  write (7,5300) twoc
                  write (7,4450) n
                  endif
```

```
          endif
          if (id .eq. 5) then
                    if (scase .ne. 'hist') then
                    write (7,3200) inc,n,twocfl,afl
                    write (7,4400) twocfl
                    write (7,4450) n
                    endif
          endif
          if (id .eq. 6) then
                    if (scase .ne. 'hist') then
                    write (7,3200) inc,n,twocfl,afl
                    write (7,4400) dkfl
                    write (7,4450) n
                    endif
          endif

          if (id .eq. 2) then
                    goto 400
          else
                    goto 900
          endif

900     continue
          if (scase .eq. 'hist') then
                    rlife(step)=n
                    write (7,6200) weight(step),sr,rlife(step)
                    if (stress(step) .eq. stress (80)) then
                              goto 1000
                    else
                              step=step+2
                              goto 50
                    endif
          else
                    goto 1100
          endif

c Calculate life in years for ADTT
1000      continue
          do 1050 i=6,80,2
                    val=val+freq(i)/rlife(i)
1050      continue

          hlife=1/val
          ylife=hlife/(adtt*365)
          write (7,6300) ylife

          goto 1100

1100      continue
          stop
          end

c =================================================================
c                    SUBROUTINES
```

```
c Subroutine to calculate finite element stress
      subroutine festress(amount,c,p,st)
      if (amount .eq. 0.0) then
            stup=.234-.755*c+.282*c**2-.024*c**3
     *      +.142*p-.0215*c*p
            stdown=.443-.793*c+.258*c**2-.0207*c**3
     *      +.138*p+.0175*c*p
      else
            stup=2.42-3.086*c+.695*c**2-.0385*c**3
     *      +.343*p-.055*c*p
            stdown=.766-.499*c-.231*c**2+.074*c**3
     *      +.387*p-.025*c*p
      endif
      st=.5*(stup+stdown)
      return
      end

c Subroutine to calculate bending stress at middle of crack
      subroutine bstress(sr,c,bd,dd,st)
      stup=sr*(dd/2-c)/(bd/2)
      stdown=sr*(dd/2+c)/(bd/2)
      st=.5*(stup+stdown)
      return
      end

c Subroutine to calculate bending stress at point a of flange
      subroutine astress (sr,bd,btf,astr)
      str1 = sr*(bd/2-btf)/(bd/2)
      astr=0.5*(sr+str1)
      return
      end

c Subroutine to calculate geometric correction factor
c due to welded diaphragm
      subroutine geo(amount,twoc,fg,ni,p,dd,bd,sr)
      c=twoc/2.
      f2=0.
      do 100 k=1,ni
            bi=(k-1)/ni
            bi1=(k)/ni
            f1=asin(bi1)-asin(bi)
            call fgstr(amount,c,p,k,ni,fest,bst,sr,dd,bd)
            f2=f2 + f1*fest/bst

100   continue

      pi=4*atan(1.)
      fg = f2 * 2/pi
      return
      end

c Subroutine to calculate stress for geometric correction factor
      subroutine fgstr(amount,c,p,k,ni,fest,bst,sr,dd,bd)

      if (amount .eq. 0.0) then
```

```
                fest=.443-.793*(c/ni)*(k-1)+.258*((c/ni)*(k-1))**2
     *          -.0207*((c/ni)*(k-1))**3+.138*p+.0175*(c/ni)*(k-1)*p
        else
                fest=.766-.499*(c/ni)*(k-1)-.231*((c/ni)*(k-1))**2
     *          +.074*((c/ni)*(k-1))**3+.387*p-.025*(c/ni)*(k-1)*p
        endif
        bst=sr*(dd/2+(c/ni)*(k-1))/(bd/2)
        return
        end

c Subroutine to calculate stress intensity factor for elliptical
c surface crack growing through web thickness due to tension
        subroutine stfaca(a,c,btw,bd,ip,st,dk)
        fg=1.
        q = 1. + 1.464*(a/c)**1.65
        rm1 = 1.13 - 0.09*(a/c)
        rm2 = -0.54 + 0.89/(0.2 + a/c)
        rm3 = 0.5 - 1.0/(0.65 + a/c) + 14.*(1.-a/c)**24

        pi = 4 * atan(1.)
        if (ip .eq. 1) then
                phi=0.
        else
                phi = pi/2.
        endif

        g = 1. + (0.1+0.35*(a/btw)**2)*(1.-sin(phi))**2
        fphi = ( (a/c)**2 * (cos(phi))**2 + (sin(phi))**2)**0.25
        fw = ( 1. / cos ( (pi*c)/(bd/2) * sqrt(a/btw) ) )**0.5
        f = (rm1+ rm2*(a/btw)**2 + rm3*(a/btw)**4)*fphi*g*fw

        dk = fg*(st) * f * sqrt(pi*a/q)
        return
        end

c Subroutine to calculate stress intensity factor for crack through
c web thickness

        subroutine stfac1(twoc,bd,st,fg,dk)
        pi = 4. * atan(1.)
        c=twoc/2.
c       fw = sqrt( 1/cos( (pi*c) / (bd/2) ) )
        fw=sqrt( (bd/2)/(pi*c)*tan((pi*c)/(bd/2)))
        dk = fg * fw * st * sqrt(pi*c)
        return
        end

c Subroutine to calculate rate of growth for crack through
c flange thickness
        subroutine flange(cfl,bbf,astr,pc,rm,grofl)
        pi=4*atan(1.)
c       fwfl=sqrt(1/cos(pi*cfl/bbf))
        fwfl=sqrt( (bbf/(pi*cfl)) * tan(pi*cfl/bbf))
        fg=1.
        dkfl=astr*fwfl*fg*sqrt(pi*cfl)
```

```
      grofl=pc*(dkfl)**rm
      return
      end

c Subroutine to calculate rate of growth
      subroutine growth(pc,rm,gro,dk)
      gro = pc * (dk)**rm
      return
      end

c Subroutine to check fracture criteria for elliptical web crack
      subroutine check(a,twoc,cdown,btw,bd,btf,dd,ccrit,dk,rkc,ic)
      c=twoc/2.
      if (a/c .gt. 1.) goto 500
      if (a/btw .ge. 1.) goto 510
      if (c/(bd/2/2) .ge. 0.5) goto 520
      if (twoc .ge. ccrit) goto 530
      if ((cdown) .ge. (bd/2-dd/2)) goto 540
      if (dk .ge. rkc) goto 550
      goto 600

500   continue
      ic=1
      goto 600
510   continue
      ic=2
      goto 600
520   continue
      ic=3
      goto 600
530   continue
      ic=4
      goto 600
540   continue
      ic=5
      goto 600
550   continue
      ic=6
      goto 600
600   continue
      return
      end

c Subroutine to check fracture criteria for crack through web
c thickness
      subroutine check1(twoc,cdown,bd,btf,dd,ccrit,dk,rkc,ic)
      c=twoc/2.
      if (twoc .ge. ccrit) goto 530
      if ((cdown) .ge. (bd/2-dd/2)) goto 540
      if (dk .ge. rkc) goto 550
      goto 600

530   continue
      ic=4
      goto 600
```

```
540       continue
          ic=5
          goto 600
550       continue
          ic=6
          goto 600
600     continue
          return
          end

c Subroutine to check fracture criteria for crack through flange
c thickness
          subroutine flcheck2(twoc,cfl,bbf,bd,dd,ccrit,dkfl,rkc,id)
          if (twoc .ge. ccrit) goto 730
          if (2*cfl .ge. bbf) goto 740
          if (dkfl .ge. rkc) goto 750
          goto 800

730       continue
          id=4
          goto 800
740       continue
          id=5
          goto 800
750       continue
          id=6
          goto 800

800     continue

          return
          end

c Subroutine to calculate stress array for truck histogram
          subroutine hstress(weight,stress,stwt,wt,freq,rmean,stdev)
          dimension weight(100), stress(100), freq(100)

          pi=4*atan(1.)

          zeta=sqrt(alog(1+(stdev/rmean)**2))
          rlamb=alog(rmean)-.5*zeta**2

          m=80
          do 100 i=6,m,2
                    mid=(i+(i+2))/2
                    weight(i)=mid
                    stress(i)=weight(i)*stwt/wt
                    freq(i)=2*(1/(sqrt(2*pi)*zeta*weight(i))*exp((-.5*
     *    ( (alog(weight(i))-rlamb)/zeta)**2)))

100       continue
          return
          end
```

E.3 Input Parameters

The propagation program presented earlier requires an input file named “data.inp” in order to compute the propagation life. The input parameters are described in this section.

LINE 1 *scase*

scase ⇒ stress case

cs for constant stress

hist for histogram loading

LINE 2 *amount*

amount ⇒ amount of diaphragm stagger

0.0 for no stagger

1.0 for stagger diaphragm

LINE 3 *bd, bbf, btf, btw*

bd ⇒ beam depth (in.)

bbf ⇒ beam flange width (in.)

btf ⇒ beam flange thickness (in.)

btw ⇒ beam web thickness (in.)

LINE 4 *dd*

dd ⇒ diaphragm depth (in.)

LINE 5 *ai, twoci, ccrit, rkc*

ai ⇒ initial web crack depth (in.)

twoci ⇒ total initial web crack length (in.)

ccrit ⇒ crack length for repair (in.)

rkc ⇒ material fracture toughness (ksi*in$^{0.5}$)

LINE 6 *cst, wl, ni* **ONLY IF scase=“cs”**

stwt, wt, adtt, ni **ONLY IF scase="hist"**

cst ⇒ constant stress range at beam tension flange at diaphragm location (ksi)

wl ⇒ axle load that produces constant stress range (kip)

ni ⇒ number of segments for integration to obtain geometric concentration factor (suggested number =50)

stwt ⇒ stress range at beam tension flange at diaphragm location (ksi)

wt ⇒ axle load that produces input stress range (kip)

adtt ⇒ average daily truck traffic

LINE 7 *mc* **ONLY IF scase="cs"**

mc, ml **ONLY IF scase="hist"**

mc ⇒ 0 for user's defined values of C and m where

$$\frac{da}{dN} = C\left(\Delta K\right)^m$$

1 for conservative propagation estimates of ferrite-pearlite steels (Barsom and Rolfe 1987)

2 for average propagation estimates of ASTM A36 steel (Barsom and Rolfe 1987)

3 for average propagation estimates of ferrite-pearlite steels (Yamada and Hirt 1982)

ml ⇒ 0 for user's input mean axle weight and standard deviation of a truck load histogram

1 for mean axle weight and standard deviation values of truck load histogram from Michigan study (Nowak 1994)

LINE 8 *pc, rm* **ONLY IF "mc=0"**

pc ⇒ propagation model constant (refer to input in line 7)

rm ⇒ propagation model constant (refer to input in line 7)

LINE 9 *rmean, stdev* **ONLY IF "ml=0"**

rmean ⇒ mean axle weight of truck load histogram

stdev ⇒ standard deviation of truck axle loads of truck load histogram

E.4 Input Files

Input files for the fatigue life of a W24x55 beam with W14x26 staggered diaphragms are presented next. The initial crack has a depth of 0.25 in. and a length of 1.0 in. The beam is not repaired and the crack propagates to fracture of the beam tension flange.

The first input file corresponds to a constant applied stress range of 14.3 ksi at the beam tension flange at the diaphragm location. This stress is caused by a 50 kip axle load.

```
cs
1.0
23.57 7.005 0.505 0.395
13.91
0.25 1.0 20 150
14.3 50 50
2
```

The next input file corresponds to a truck histogram. An axle load of 32 kip causes a stress of 3.5 ksi at the beam tension flange at the diaphragm location. The average daily truck traffic is 1,000. The mean axle weight and standard deviation from the weigh-in-motion study performed in Michigan (Nowak 1994) is used to determine the truck histogram.

```
hist
1.0
23.57 7.005 0.505 0.395
13.91
0.25 1.0 20. 150.
```

```
3.5 32 1000 50
2 1
```

E.5 Output Files

The output for the input files listed earlier are shown here. The program writes the output to a file called "life.out." The constant stress output is provided first. The program calculates the web crack will be through the web thickness in 87,151 cycles. The crack will then reach the bottom of the beam at 433,448 cycles. The program estimates the tension flange will fracture at 563,200 cycles.

```
Crack Propagation Program

 Inc.    No. of cycles    Crack length    Crack depth
   0            0.          1.000          0.250
 229        87151.          1.304          0.395

Crack depth exceeds web thickness
Number of cycles =        87151.

 250        93861.          1.360          0.395
 500       171703.          2.240          0.395
 750       253632.          3.692          0.395
1000       351712.          6.084          0.395
1232       433448.          9.671          0.395

Crack is in tension flange
Crack growth in flange

 Inc.    No. of cycles    Crack length    Crack depth
1250       441273.          2.094          0.505
1500       524397.          3.451          0.505
1750       560889.          5.686          0.505
1855       563200.          7.014          0.505

Tension flange fractured  c=7.014
Number of cycles =        563200.
```

The output file for the truck histogram is printed next. For each mid-range axle weight, the cyclic life to fracture the tension flange is printed. For the given ADTT and

truck histogram the total life is then given in years. For the input file presented earlier, the program predicts a life of 1476 years for the given ADTT.

Crack Propagation Program

Axle load (kip)	Stress (ksi)	No. of cycles
7.0	0.766	35919392768.
9.0	0.984	5306099200.
11.0	1.203	1873826176.
13.0	1.422	901573056.
15.0	1.641	508075776.
17.0	1.859	315591040.
19.0	2.078	209576704.
21.0	2.297	146192480.
23.0	2.516	105924920.
25.0	2.734	79112944.
27.0	2.953	60575912.
29.0	3.172	47357456.
31.0	3.391	37684440.
33.0	3.609	30447936.
35.0	3.828	24930180.
37.0	4.047	20652422.
39.0	4.266	17287096.
41.0	4.484	14604873.
43.0	4.703	12442110.
45.0	4.922	10679796.
47.0	5.141	9230123.
49.0	5.359	8027288.
51.0	5.578	7021330.
53.0	5.797	6173948.
55.0	6.016	5455344.
57.0	6.234	4842197.
59.0	6.453	4316012.
61.0	6.672	3862066.
63.0	6.891	3468493.
65.0	7.109	3125682.
67.0	7.328	2825784.
69.0	7.547	2562365.
71.0	7.766	2330098.
73.0	7.984	2124554.
75.0	8.203	1942047.
77.0	8.422	1779467.
79.0	8.641	1634199.
81.0	8.859	1504022.
Number of years =		1476.